Role of KCNQ Potassium Channels in Control of Calcium Homeostasis in Vascular Smooth Muscle Cells

Yuan-Ming Tsai

Submitted in accordance with the requirements for the degree of

Doctor of Philosophy

University of Leeds

School of Biomedical Sciences

September 2020

The candidate confirms that the work submitted is his own and that appropriate credit has been given where reference has been made to the work of others.

Acknowledgements

I would like to express my sincerest gratitude and memories to my former supervisor Professor Chris Peers for giving me the opportunity to pursue a PhD study and for all the valuable advice, patience, and guidance from the very beginning. Although he is no longer with us, I always keep all his supporting and spirits in my mind. Most importantly, I do appreciate that Professor Nikita Gamper stepped in as my supervisor towards the end of my study. Without his continued support and encouragement, I would not have been able to produce this body of work. I acknowledge the support given to me by my second supervisor Professor Derek Steele and would like to thank Dr Karen E. Porter for the help in an academic matter.

Many thanks to past members in Peers lab who have all contributed to my development as a physician-scientist, in particular to Dr John Boyle, Dr Hayley Duckles, Dr Nishani Tania Hettiararchchi and Dr Moza Al-Owais; I thank them for teaching me techniques patiently. Also, thank you to previous/current Gamper lab members, Haixia Gao, Rosmaliza Ramli, Eleni Kyriakopoulou, Shihab Shah, Pierce Mullen, Frederick Jones and Stephen Milne for their assistance in all laboratory work and emotional support.

Especially, I would like to thank my beautiful wife Nana for everything she has done for me. To my lovely kids, Ruei-Ruei and Qiao-Qiao thank you for bringing me so much happiness. Thank you to all the wonderful friends I have become acquainted with in Leeds who made my PhD experience thoroughly enjoyable and unforgettable. Last but not least, I'm very grateful for my scholarship sponsor

Tri-Service General Hospital, National Defence Medical Centre and Medical Affairs Bureau, Taipei, Taiwan (R.O.C.).

Abstract

Voltage-gated Kv7 (or KCNQ) potassium channels control the activity of excitable cells, including vascular smooth muscle cells (VSMCs), by setting their resting membrane potential and controlling other excitability parameters. Calcium (Ca^{2+}) mediates excitation-contraction coupling in smooth muscle cells (SMCs), but until now the exact role of Kv7 channels in cytosolic Ca^{2+} dynamics in VSMCs have not been fully elucidated.

The Ca^{2+} imaging experiments presented herein show that both, direct (XE991) and G protein-coupled receptor mediated (vasopressin, AVP) Kv7 channel inhibition induced robust Ca^{2+} oscillations, which were significantly reduced in the presence of a Kv7 channel activator (retigabine), L- and T-type Ca^{2+} channel blockers (nifedipine and NNC 55-0396). Plasma membrane potential measured using FluoVolt demonstrated that both XE991 and AVP induced slow depolarisation followed by a burst of sharp spikes, which were temporally well-correlated with Ca^{2+} oscillations. Using the inhibitors of IP_3Rs (2-APB), RyRs (tetracaine) and phospholipase C (PLC; edelfosine), we found that PLC signalling is required for AVP-induced, but not XE991-induced Ca^{2+} oscillations.

Analysis of the Kv7 gene transcripts and protein levels identified Kv7.5 as the major Kv7 subunit expressed in rat VSMCs. *CACNA1C* (Cav1.2; L-type) and *CACNA1G* (Cav3.1; T-type) were the most abundant voltage-gated Ca^{2+} channel gene transcripts. Hypoxic treatment significantly reduced the expression of Kv7.5 and increased Cav3.2 T-type Ca^{2+} channels, and enhanced depolarisation-induced Ca^{2+} transients with prolonged and high-frequency Ca^{2+} oscillations.

These changes were orchestrated by the HIF-α transcriptional signalling pathway. Importantly, even with a reduced level of Kv7.5 expression, retigabine was still efficacious to stop AVP-induced Ca^{2+} oscillations.

AVP and XE991 induced a large increase of $[Ca^{2+}]_i$ in primary human internal mammary artery SMCs, which was also attenuated with retigabine and nifedipine. Interestingly, in saphenous vein SMCs, bradykinin-induced Ca^{2+} transients were not prevented by retigabine and nifedipine with some enhancement instead. Kv7.5 was found to be the predominant Kv7 subunit in human VSMCs as well.

This study establishes Kv7 channels as crucial regulators of Ca^{2+} signalling in VSMCs with Kv7.5 playing a dominant role. Retigabine or more selective activators of Kv7.5 may provide a clinically useful tool for the treatment of cardiovascular diseases, such as pulmonary hypertension.

Table of Contents

Publications

Yuan-Ming Tsai, Frederick Jones, Pierce Mullen, Karen E. Porter, Derek Steele, Chris Peers and Nikita Gamper. **Vascular Kv7 channels control intracellular Ca^{2+} dynamics in smooth muscle.** *Cell Calcium*. 2020. **92**:102283

Poster. Yuan-Ming Tsai, Derek Steele, Chris Peers and Nikita Gamper. **Role of KCNQ Potassium Channels in the Control of Ca^{2+} Signalling in Vascular Smooth Muscle Cells.** International Kv7 Channels Symposium 2019, Naples, Italy.

Poster (**Junior Travel Fellowship** from the European Calcium Society for in relation to this work)**.** Yuan-Ming Tsai, John Boyle, Nikita Gamper and Chris Peers. **KCNQ potassium channels control calcium homeostasis in vascular smooth muscle cells.** 2018 International Meeting of the European Calcium Society, Hamburg, Germany.

This thesis builds on the findings of the publications mentioned above. Posters presented were produced from data generated during this study.

List of Figures

List of Tables

Abbreviations

AM	Acetoxymethyl
ARNT	Aryl Hydrocarbon Receptor Nuclear Translocator
AUC	Area Under the Curve
AVP	Arginine Vasopressin
bHLH–PAS	Basic Helix-Loop-Helix–Per-Arnt-Sim
BK_{Ca}	Large-Conductance Ca^{2+}-Activated K^+ Channel
Ca^{2+}	Calcium
$[Ca^{2+}]_i$	Intracellular Calcium Concentration
CABG	Coronary Artery Bypass Grafting
CACC	Ca^{2+}-Activated Cl^- Channel
CaM	Calmodulin
cAMP	Cyclic AMP
Cav	Voltage-Gated Ca^{2+}
CICR	Ca^{2+}-Induced Ca^{2+} Release
CO	Carbon Monoxide
CPI-17	Protein Kinase C-Potentiated Phosphatase Inhibitor Protein-17
DAG	Diacylglycerol
DMEM	Dulbecco's Modified Eagle Medium
DMOG	Dimethyloxalylglycine
E_m	Membrane Potential
ER	Endoplasmic Reticulum
FBS	Fetal Bovine Serum
FIH	Factor-Inhibiting Hypoxia-Inducible Factor Protein
GPCR	G Protein-Coupled Receptor
HIF	Hypoxia-Inducible Factor
HPRT1	Hypoxanthine Phosphoribosyltransferase 1
HRE	Hypoxia Response Element
HVA	High-Voltage-Activated
IMA	Internal Mammary Artery
IP_3	Inositol 1,4,5-trisphosphate
IP_3R	Inositol 1,4,5-trisphosphate Receptor
K^+	Potassium

KCa	Ca^{2+}-Activated K^{+}
Kv	Voltage-Dependent Potassium
LDL	Low-Density Lipoprotein
LOX-1	Lectin-like Oxidised LDL Receptors Type-1
LVA	Low-Voltage-Activated
MCU	Mitochondrial-Calcium-Uniporter
MLC20	20-kDa Regulatory Myosin Light Chain
MLCK	Myosin Light Chain Kinase
NCX	Na^{+}/Ca^{2+} Exchanger
NO	Nitric Oxide
NOS	Nitric Oxide Synthase
ODDD	Oxygen-Dependent Degradation Domain
oxLDL	Oxidised Low-Density Lipoprotein
PAH	Pulmonary Arterial Hypertension
PASMC	Pulmonary Arterial Smooth Muscle Cell
PBS	Phosphate Buffered Saline
PD	Pore Domain
PHD	Prolyl Hydroxylase Domain
PIP_2	Phosphatidylinositol 4,5-bisphosphate
PKA	Protein Kinase A
PKC	Protein Kinase C
PLC	Phospholipase C
PMCA	Plasma Membrane Ca^{2+} ATPase
PVAT	Perivascular Adipose Tissue
RNA	Ribonucleic Acid
ROCC	Receptor-Operated Ca^{2+} Channel
ROCK	Rho-Associated Protein Kinase
ROS	Reactive Oxygen Species
RT-PCR	Real-Time Polymerase Chain Reaction
R.U.	Ratio Units
RyR	Ryanodine Receptor
SERCA	Sarco/Endoplasmic Reticulum Ca^{2+}-ATPase
SMC	Smooth Muscle Cell
SOCC	Store-Operated Ca^{2+} Channel

SOCE	Store-Operated Ca^{2+} Entry
SR	Sarcoplasmic Reticulum
SV	Saphenous Vein
SVR	Systemic Vascular Resistance
TAD	Transactivation Domain
TRP	Transient Receptor Potential Channel
TRPC	Transient Receptor Potential-Canonical Channel
VEGF	Vascular Endothelial Growth Factor
VGCC	Voltage-Gated Ca^{2+} Channel
VHL	Von Hippel-Lindau
VSD	Voltage-Sensing Domain
VSM	Vascular Smooth Muscle
VSMC	Vascular Smooth Muscle Cell

Chapter 1

Introduction

1.1 Thesis outline

This thesis investigates the role of the Kv7 (KCNQ) potassium channels in the control over intracellular calcium concentration ($[Ca^{2+}]_i$) in vascular smooth muscle cells (VSMCs). Specifically, this study analyses the expression of the Kv7 subunit in VSMCs and explores pathways and ion channels responsible for Ca^{2+} homeostasis downstream of Kv7 channel inhibition. We focus on how direct pharmacological block and G protein-coupled receptor (GPCR) mediated Kv7 channel inhibition regulate $[Ca^{2+}]_i$ through modulating the activity of voltage-gated Ca^{2+} channels (VGCCs) in rat and human VSMCs in normoxic and under hypoxic conditions.

This thesis will begin with a general introduction that reviews areas central to this project. These are:

(1) Role of the cardiovascular system and regulation of vascular tone

(2) Overview of calcium (Ca^{2+}) signalling and the role of VGCCs in VSMCs

(3) Overview of Kv7 channels and their role in VSMCs

(4) Disorders of vascular remodelling

(5) Overview of hypoxia and its role in VSMCs

A section about methods and materials will then outline the experimental techniques and chemicals used in this project. Following the methods description, there are three results chapters. Finally, a general discussion section summarises the work, highlights issues raised by the project findings and explores potential future work.

1.2 Cardiovascular system

The cardiovascular system is a circulatory system which is vital to maintain blood pressure and regulate the blood distribution in different organs and tissues in order to meet the demand of the body in different environments. It is an organ system comprising three basic parts: heart (as a pump), blood (as a carrier) and blood vessels (as elastic tubes), which integrate to circulate oxygen, hormones, and nutrients through the body for the survival of the cells. The pulmonary circulation carries deoxygenated blood away from the right ventricle to the lungs and returns oxygenated blood to the left heart, which is the portion of the circulatory system (Figure 1.1). Within this system, vessels play an essential role in the control of blood pressure, delivery of oxygen and regulation of blood distribution to meet the demand of the different organs and tissues in different conditions (Jacob et al., 2016; Mayet and Hughes, 2003).

The organ vasculature starting from the main organ artery connects to the aorta is classified into the arteries (high-pressure), capillaries and veins (low-pressure), returning blood to the heart. The walls of arteries and veins consist of three distinct layers: tunica intima, tunica media and tunica externa (tunica adventitia).

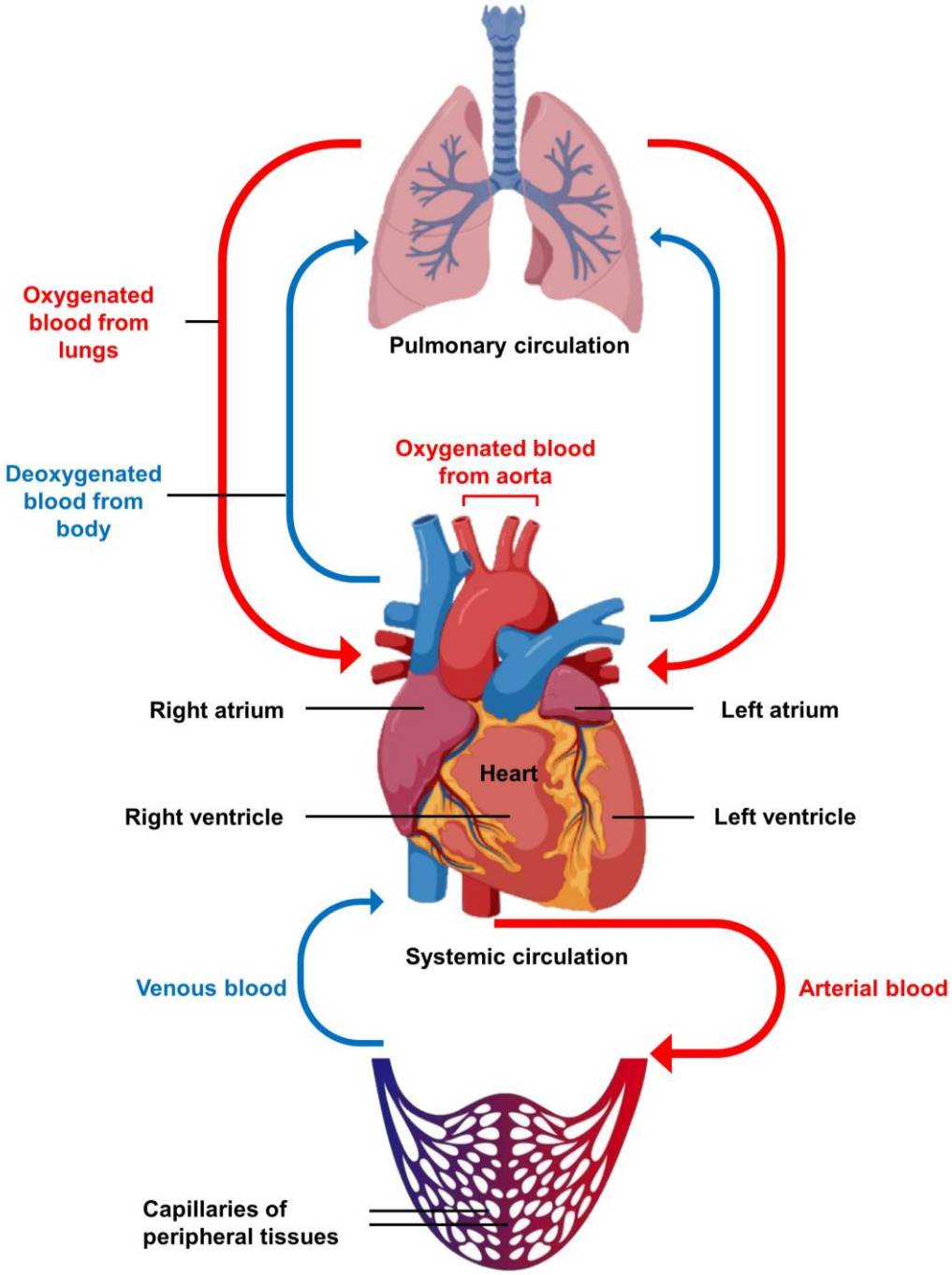

Figure 1.1 Illustration of the circulation system. The cardiovascular system is composed of systemic circulation (the circuit through the rest of the body to provide oxygenated blood) and pulmonary circulation (the circuit through the lungs where blood is oxygenated). Adapted from “Anatomy & Clinical” by BioRender.com (2020). Retrieved from https://app.biorender.com/biorender-templates

Endothelial cells are located in the tunica intima and smooth muscle cells (SMCs) are the major cell type of the tunica media. SMCs and elastic tissue are predominant in arteries, whereas connective tissue with elastic fibres mainly consists of a tunica media layer in veins. Tunica externa is the outermost layer of a vessel, and the elastic membrane exists between each tunica (Figure 1.2). Due to both cellular and fibrous composition and lower SMCs tone, the walls of veins are generally less stiff than those of arteries. The smooth muscle tone of the arteries has been attributed to mechanical autoregulation of blood flow in a way that an increase in blood pressure is directly linked to an increase in VSMCs tone to keep blood flow to the vital organs (brain, heart, kidney, liver) (Bayliss, 1902). The contractility of VSMCs at the medial layer of the blood vessel wall responds to chemical, electrical and mechanical signals to maintain basal vascular tone, which is a key element of vessel function that determines the diameter of vessels and induces the resistance to blood flow (Cribbs, 2006). The other principal effectors of arterial resistance can be classified as 1) neurovegetative control (adrenergic, cholinergic and non-adrenergic/cholinergic), 2) humoral- and tissue-generated mediators (angiotensin II, vasopressin, bradykinin and natriuretic acid), 3) local metabolic regulation (oxygen, pH, potassium ion concentration), and 4) shear stress (nitric oxide (NO) release) (Jacob et al., 2016).

Systemic vascular resistance (SVR) is the amount of force exerted on circulating blood by the vasculature of the body, which is generated primarily by arterial resistance. Three main factors determine the SVR: the length of the vessels, the diameter of the vessels, and the viscosity of the blood. SVR plays a vital role in the maintenance of the mean arterial pressure. The relationships between the

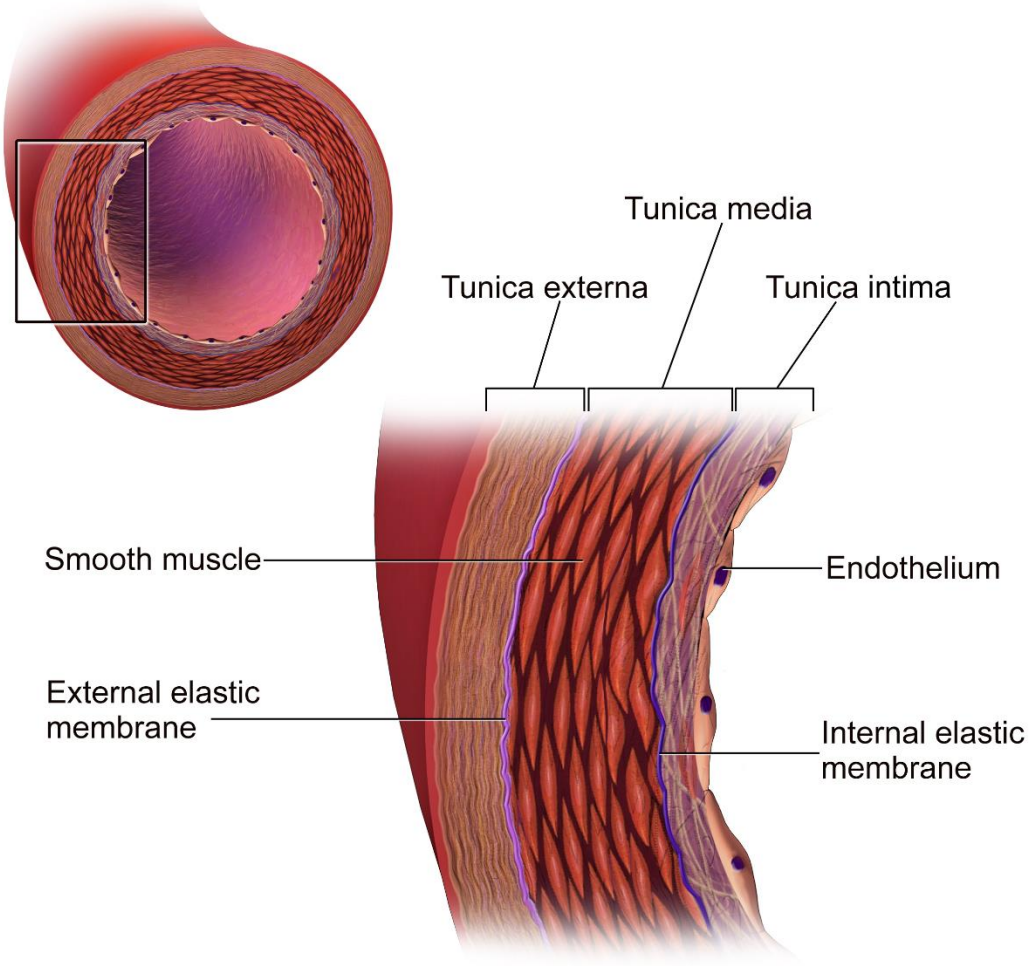

Figure 1.2 Structure of an artery wall. The typical wall of an artery is the tri-laminar structure from the innermost layer to the outermost layer can be divided into tunica intima (endothelial cells), tunica media (VSMCs) and tunica externa (connective tissue) (Blausen.com staff, 2014).

cardiac output, the volume of blood pumped by the heart per minute and SVR are expressed as follows,

Mean arterial pressure = cardiac output x SVR.

Accordingly, abnormal regulation of vascular tone plays a central role in the pathogenesis of hypertension and cardiovascular diseases (Mayet and Hughes, 2003).

1.3 Regulation of vascular tone

The excitation-contraction coupling in vascular smooth muscle (VSM) is a response to the increased $[Ca^{2+}]_i$ to modulate vascular diameter. Stimulation could be caused by vasoactive peptides (such as endothelin-1 and angiotensin II) and neurohumoral stimuli (such as phenylephrine and acetylcholine), which results in the rapid rise in $[Ca^{2+}]_i$ via signalling cascades resulting in Ca^{2+} influx through the VGCCs and Ca^{2+} release from the intracellular stores. The Ca^{2+} diffuses to the contractile machinery and binds to cytosolic protein calmodulin (CaM). The Ca^{2+}-CaM complex can bind and induce a conformational change in myosin light chain kinase (MLCK), resulting in it converted from an inactive to an active state (Hilgers and Webb, 2005). Activation of MLCK causes phosphorylation at serine residue 19 of the 20-kDa regulatory myosin light chain (MLC20) to enable the cross-bridge formation with adjacent actin filaments. Phosphorylation of MLC20 increases its actin-activated ATPase activity. Interaction between myosin and actin cause ATP hydrolysis, which generates myosin-actin cross-bridge cycling and vascular constriction (Deng et al., 2012). In contrast, relaxation of VSM occurs as a result of decreased $[Ca^{2+}]_i$, which causes dissociation of the Ca^{2+}-CaM complexes, subsequently reduces MLC20

phosphorylation or dephosphorylation of MLC20 by myosin light chain phosphatase (MLCP) leads to VSMCs relaxation (Khalil et al., 1987; Khalil and Vanbreemen, 1988).

However, the Ca^{2+}-dependent MLC20 phosphorylation is not the only step in the excitation-contraction coupling, which is targeted during the regulation of vascular tone. Several hormones and growth factors can bind to specific GPCRs on the plasma membrane to result in the activation of phospholipase C (PLC) followed by the hydrolysis of phosphatidylinositol 4,5-bisphosphate (PIP_2) to produce the diacylglycerol (DAG) and inositol 1,4,5-trisphosphate (IP_3). DAG can further activate protein kinase C (PKC) and its downstream signalling while IP_3 can bind to the IP_3Rs. The latter event subsequently leads to Ca^{2+} release from the ER and a recruitment of neighbouring RyRs, leading to an increase in cytosolic Ca^{2+} concentration, thereby resulting in cell contraction (Gordienko and Bolton, 2002).

DAG serves as a second messenger to activate protein kinase C (PKC). For instance, activation of PKC has also been suggested to cause VSM contraction (Salamanca and Khalil, 2005). PKC is a kinase which phosphorylates the PKC-potentiated phosphatase inhibitor protein-17 (CPI-17) to increase MLC phosphorylation which, in turn, causes VSM contraction (Woodsome et al., 2001). PKC also activates a cascade of protein kinases leading to the phosphorylation of the actin-binding proteins CaP and CaD, an increase of actin-myosin interaction, and VSM contraction (Liu and Khalil, 2018). In addition, PKC can affect VSM contraction through regulation of ion channels, pumps, Ca^{2+}

sensitisation of the contractile proteins, and activation of Ca^{2+} independent contraction pathways (Figure 1.3). There are also additional signalling cascades regulating VSM contractility; for instance, some GPCR agonists engage small GTP-binding protein RhoA, which activates Rho-associated coiled-coil protein kinase or Rho-kinase protein kinase (ROCK) and increase the MLC20 phosphorylation to promote vascular contraction (Hilgers and Webb, 2005; Liu and Khalil, 2018). Furthermore, similar to $[Ca^{2+}]_i$, reactive oxygen species (ROS; i.e. the superoxide, hydrogen peroxide, and hydroxyl radical) are increasingly recognised as the critical messenger molecules in VSMCs (Jin and Berk, 2004) (Figure 1.3).

Mitochondria are an important source of ROS within most mammalian cells. Generation of ROS mainly takes place at the electron transport chain located on the inner mitochondrial membrane by enzymes, the NADPH oxidases (Noxs). These enzymes transfer electrons across the biological membrane and generate ROS from oxygen, of which Nox1, 2, 4, and 5 are expressed and functionally active in human VSMCs (Touyz and Briones, 2011). Vascular ROS effects are mediated through redox-sensitive signalling pathways to regulate protein kinases, phosphatases, actin, actin-binding proteins, myosin and the contractile machinery (Fedorova et al., 2010). The production of intracellular ROS and oxidative stress have been implicated in the pathogenesis of the cardiovascular disease, in part by promoting VSM proliferation (Jin and Berk, 2004). Overall, VSMCs are highly differentiated and normally maintain a contractile state which is regulated by Ca^{2+}-dependent and Ca^{2+}-independent pathways, Ca^{2+} channels and many other signalling cascades ((Touyz et al., 2018); schematised in Figure 1.3).

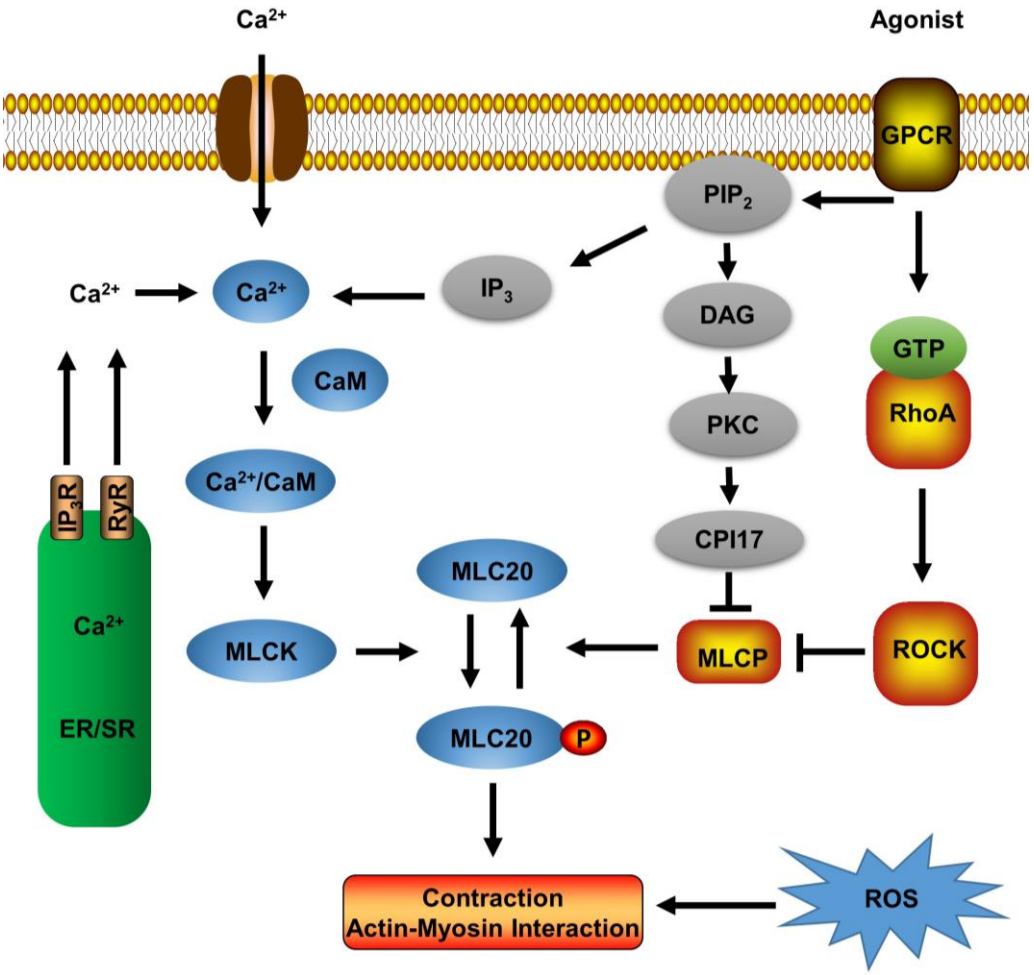

Figure 1.3 Overview of Ca^{2+} pathways regulating vascular tone. A rise in $[Ca^{2+}]_i$ initiates the contractile response, including i) a Ca^{2+}-CaM interaction, ii) the MLCK activation to iii) initiate phosphorylation of the MLC20 and therefore, contraction and cell migration (left part). Agonists that bind to the GPCR in the VSMC's plasma membrane can induce hydrolysis of PIP_2 into IP_3 and DAG, which activate PKC to phosphorylate the CPI-17 (middle part) and activate the RhoA/Rho-kinase signalling pathway (right part). Both of these effects (middle and right part) inhibit the MLCP and result in sustained vascular contraction.

CaM: calmodulin; CPI-17: PKC-potentiated phosphatase inhibitor protein-17; DAG: diacylglycerol; ER/SR: endoplasmic and sarcoplasmic reticulum; IP_3: inositol 1,4,5-trisphosphate; MLCP: myosin light chain phosphatase; PIP_2: phosphatidylinositol 4,5-bisphosphate; PKC: protein kinase C; RyR: ryanodine receptor; ROS: reactive oxygen species

1.4 Ca^{2+} signalling in the vascular system

Ca^{2+} is an important, ubiquitous intracellular messenger. It has different functions in various cell types and controls cellular processes as diverse as gene transcription, muscle contraction and cell proliferation (Kuhr et al., 2012). In the vascular system, the mechanisms involved in the alteration of $[Ca^{2+}]_i$ levels within VSMCs play crucial roles in regulating vasoconstriction and dilation, hence the blood flow. Ca^{2+} concentrations throughout any given tissue are not uniform. The extracellular milieu (e.g. plasma) contains about 1-2 mM Ca^{2+} (Hughes, 1995). $[Ca^{2+}]$ is also high in the lumen of the endoplasmic reticulum (ER)/ sarcoplasmic reticulum (SR) around 500 μM, whereas it is low in the cytosolic space at 100-300 nM (Zhang and Trebak, 2011). The lower $[Ca^{2+}]_i$ indicates that the opening of Ca^{2+} channels (either in the plasma membrane or in the ER/SR) would cause Ca^{2+} flux into the cytosol and elevate $[Ca^{2+}]_i$, which plays a physiological and pharmacological role in the regulation of VSMCs function (Bootman et al., 2001).

Multiple counteracting processes can regulate $[Ca^{2+}]_i$ to make cytosolic Ca^{2+} increase or decrease (Berridge et al., 2000). When cells are at rest, $[Ca^{2+}]_i$ is the range of 100 nM. If cells encounter some stimulations such as depolarisation, mechanical deformation or hormone activation, global $[Ca^{2+}]_i$ can rise up to about 1 μM (Bootman et al., 2001), or even higher in some specific locations, such as microdomains. Ca^{2+} enters the cytosol via Ca^{2+} entry and Ca^{2+} release channels. The concentration gradient requires a balance with Ca^{2+} extrusion to the extracellular space or re-sequestering into intracellular stores within VSMCs. Different cell types express various combinations of channels that lead to the variability in the characteristics of Ca^{2+} signalling. Figure 1.4 summarised some

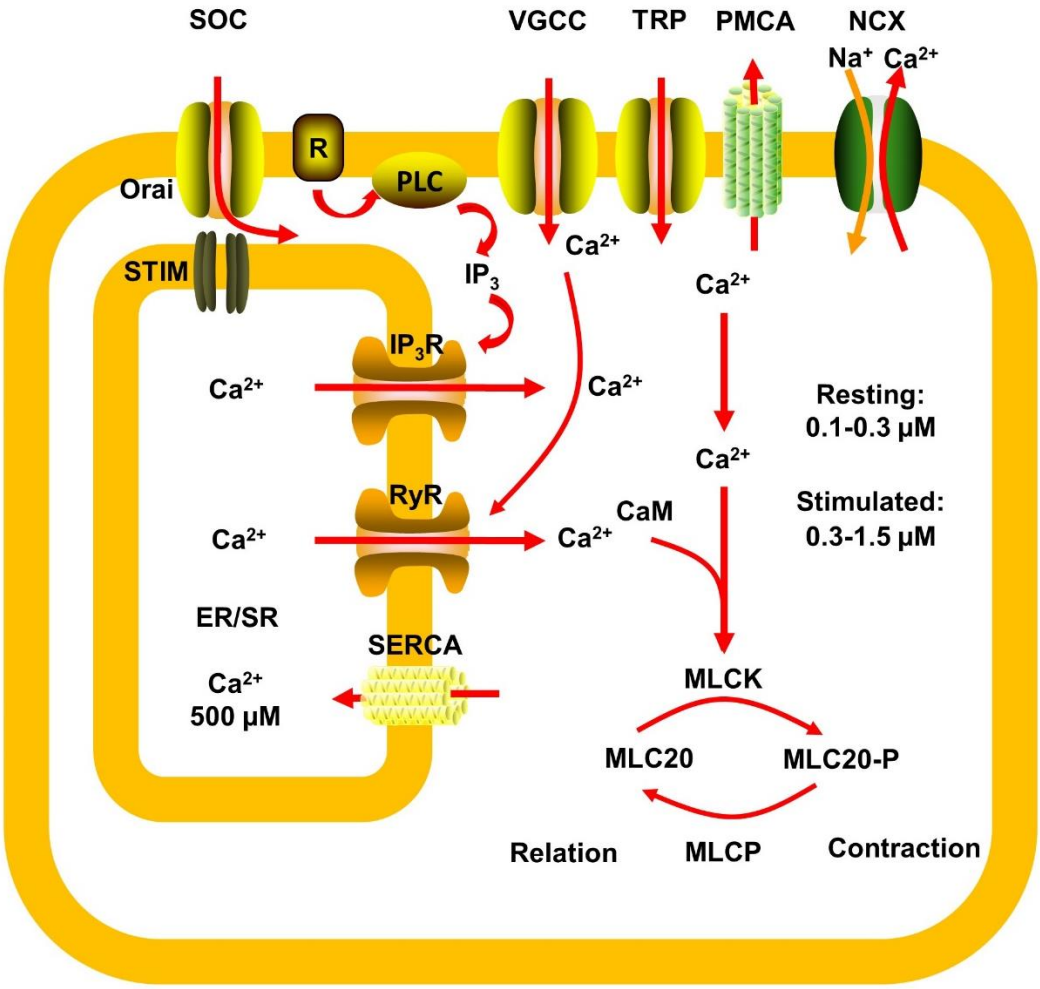

Figure 1.4 Ca^{2+} handling mechanisms in vascular smooth muscle cells. Schematic representation of the interplay of ion channels and transporters directly involved in the Ca^{2+} homeostasis and vascular contractility. The entry of Ca^{2+} to the cytosol is mediated by VGCC, TRP, IP_3R, RyR and store-operated Orai channels that are activated by STIM protein. Removal of Ca^{2+} is achieved by the SERCA, PMCA and NCX.

VGCC: voltage-gated Ca^{2+} channel; TRP: transient receptor potential channel; IP_3R: inositol 1,4,5-trisphosphate receptor; RyR: ryanodine receptor; SERCA: sarco/endoplasmic reticulum Ca^{2+}-ATPase; PMCA: plasma membrane Ca^{2+} ATPase; NCX: Na^+/Ca^{2+} exchanger

important mechanisms that were shown to coordinate a dynamic control of Ca^{2+} homeostasis in VSMCs.

1.4.1 Intracellular Ca^{2+} release and uptake mechanisms

Ca^{2+} release channels located on the ER/SR membrane of VSMCs play important roles in vascular reactivity and cellular excitability. Two major types of Ca^{2+} release channels in VSMCs are inositol 1,4,5-trisphosphate receptor (IP_3R) and ryanodine receptor (RyR). IP_3Rs are ubiquitously expressed Ca^{2+} release channel localised to the ER/SR membrane in mammalian tissues (Narayanan et al., 2012; Nixon et al., 1994). Although mitochondria also play a role in storing and buffering Ca^{2+}, the ER/SR is the main store to release Ca^{2+} via activation of IP_3Rs and RyRs to increase $[Ca^{2+}]_i$.

1.4.1.1 IP_3 receptors (IP_3Rs) and generation of IP_3

IP_3Rs consist of four membrane-spanning subunits surrounding the central ion permeation pore. So far, three subtypes (IP_3R1, IP_3R2, IP_3R3) have been reported (Narayanan et al., 2012). The expression patterns are distinct, and all three subtypes have been found in VSM from aorta, mesenteric and cerebral arteries. IP_3Rs consists of NH_2-terminus containing a suppressor domain, which inhibits IP_3 binding activity and determines different IP_3-binding affinity for each subtype. An IP_3-binding core domain is required for specific IP_3 binding. Both the suppressor domain and the IP_3-binding core domain are often referred to as the IP_3-binding domain, which confers regulation by Ca^{2+} and ATP and interacts with Transient Receptor Potential-Canonical (TRPC) channels (Iwai et al., 2007; Gao, 2017). The COOH-terminus is the channel domain, which is suggested to contribute to IP_3Rs tetramerisation which, in turn, results in the opening of the

pore to allow Ca^{2+} into the cytoplasm (Uchida et al., 2003). However, the expression of the three IP_3R isoforms can have a tissue- and development-specific manner. For example, high levels of IP_3R2 and IP_3R3 have been found in proliferating VSMCs. IP_3R3 is high in neonatal smooth muscle, but its level decreases during vascular development (Tasker et al., 2000). The IP_3-binding affinity of different IP_3R subtypes has been found as follows, IP_3R2> IP_3R1> IP_3R3 (Gao, 2017). Thus, the diversity of the subtype expression and subcellular localisation can contribute to the complexity of IP_3, Ca^{2+} and proteins interaction to influence $[Ca^{2+}]_i$.

Many vasoactive molecules can stimulate GPCRs to produce IP_3 via the hydrolysis of PIP_2 by PLC, which can diffuse rapidly to bind IP_3R on the ER/SR. Activation of IP_3R leads to the conformation change in IP_3R, thus allowing the Ca^{2+} to enter the cytoplasm (Allbritton et al., 1992). Although IP_3 can activate IP_3R to increase $[Ca^{2+}]_i$ levels, the opening status is also affected by the Ca^{2+} concentration. Higher Ca^{2+} concentration (>1 μM) inhibits IP_3R opening, whereas modest increased concentration (0.5-1 μM) can enhance the opening (Bootman et al., 2001). The Ca^{2+} release activity of the IP_3R in VSMCs can be modulated by IP_3, $[Ca^{2+}]_i$, ATP, protein kinases, and ROS to influence the diverse Ca^{2+} signalling in cellular responses (Narayanan et al., 2012; Foskett et al., 2007).

1.4.1.2 Ryanodine receptors (RyRs)

RyRs are functionally and structurally analogous to IP_3Rs. They are expressed mainly in excitable cells, such as neurons and muscle (Bennett et al., 1996) and normally closed at low $[Ca^{2+}]_i$ (100–200 nM) and activated at 1-10 μM Ca^{2+} concentration (Bezprozvanny et al., 1993). RyRs form homotetramers comprising

four 565 kDa subunits (Zalk et al., 2015). Three isoforms (RyR1-RyR3) have been identified in mammalian tissues (Lanner et al., 2010), with RyR1 predominantly in skeletal muscle cells, RyR2 in the heart and RyR3 in the brain. RyR1 are responsible for releasing Ca^{2+} in skeletal muscles, whereas RyR2 are activated following depolarisation in cardiac muscle (Bootman et al., 2001). All RyR isoforms have been detected in VSMCs, but there are significant regional differences in the expression of RyR isoforms. Expression of RyR2 was found predominantly in rat aorta, cerebral arteries, pulmonary arteries and murine skeletal muscle resistance arteries and arterioles (Yang et al., 2005; Vaithianathan et al., 2010; Westcott et al., 2012). Like IP_3Rs, the expression of the RyR isoforms also may change during proliferation with the loss of RyR3, indicating the varied roles of the RyR isoforms in proliferating SMCs (Vallot et al., 2000).

The opening of RyRs forms the elementary Ca^{2+} signal, "Ca^{2+} spark", in cardiac cells and many other cell types to contribute to the global increase in $[Ca^{2+}]_i$ for contraction (Cheng et al., 1993). RyRs can be activated by caffeine to induce Ca^{2+} release from intracellular stores and increase the frequency of Ca^{2+} sparks in VSMCs (Jagger et al., 2000). Ca^{2+} sparks control the contraction and relaxation in VSMCs. Therefore, pharmacological blockers, such as tetracaine, have been used to investigate the function of RyRs in $[Ca^{2+}]_i$ in VSMCs (Ghosh et al., 2017). In addition, RyRs can sense the Ca^{2+} concentrations in ER/SR stores. If the ER is overloaded with Ca^{2+}, RyRs can also become sufficiently sensitive to open in response to the ER Ca^{2+} change (Tykocki et al., 2017).

1.4.1.3 SER Ca^{2+} ATPases (SERCA)

Within VSMCs, maintaining Ca^{2+} homeostasis under basal condition is critical to relax pre-constricted vessels. One of the main sites for dynamic control of $[Ca^{2+}]_i$ is at sarcoplasmic/endoplasmic reticulum calcium ATPases (SERCA), which sequester Ca^{2+} into intracellular stores. Ca^{2+} is transported against a concentration gradient from the cytoplasm to regulate the relaxation of muscle cells and cardiac contractility at a ratio of two Ca^{2+} ions for every hydrolysed ATP molecule (Liu and Khalil, 2018). Molecular cloning studies have revealed that three genes (*ATP2A1-3*) encode SERCA1-3 pumps, each with different physiological functions (Wu et al., 2001). SERCA1 is mainly expressed in skeletal muscles. SERCA2 is ubiquitously expressed, with two major splice variants in cardiac muscle, neuronal cells (SERCA2a) and in all cell types (SERCA2b), which can transport Ca^{2+} from the cytosol into the ER/SR lumen to maintain low cytosolic Ca^{2+} concentration (Vangheluwe et al., 2005). SERCA2b is the predominant protein (> 90%), followed by SERCA2a and SERCA3 in VSMCs (Wu et al., 2001). SERCA activity has a very direct and dynamic effect on the regulation of Ca^{2+} signalling to influence the constriction of VSMCs. In addition, studies have shown that the expression of SERCA2a is either absent or highly downregulated in highly proliferating VSMCs, however, increased expression of SERCA2b and IP_3Rs-evoked Ca^{2+} signals in proliferating VSMCs suggests the expression and activity of SERCA2 is a potent regulator of the abnormal Ca^{2+} dynamics in cell proliferation (Vallot et al., 2000; Lipskaia et al., 2005).

1.4.1.4 Mitochondria

Mitochondria act as another major Ca^{2+} buffering organelle (Poburko et al., 2004). In addition to ER/SR, mitochondria also accumulate high luminal $[Ca^{2+}]$

and have also been receiving substantial attention as an organelle involved in the regulation of $[Ca^{2+}]_i$ (Berridge et al., 2000). Previous studies have demonstrated that mitochondria physiology can change the VSMCs phenotype to induce vascular diseases (Nguyen et al., 2018). Mitochondria can sequester cytosolic Ca^{2+} via high-speed mitochondrial-calcium-uniporter (MCU) and release their stored Ca^{2+} by a Na^+-dependent exchanger with a significantly slower rate than the uniporter (Bootman et al., 2001). However, ER/SR is the primary Ca^{2+} storage site under physiological conditions, and mitochondria uptake Ca^{2+} only when $[Ca^{2+}]_i$ increases to abnormally high levels (Liu and Khalil, 2018). Inhibition of mitochondrial Ca^{2+} uptake reduces the amplitude but increase the frequency of agonist-induced Ca^{2+} oscillations in VSMCs (Swärd et al., 2002). Mitochondria participate in intracellular Ca^{2+} signals between Ca^{2+} entry and ER/SR refilling in VSMCs (Poburko et al., 2009). Recently, mitochondrial Ca^{2+}/calmodulin-dependent kinase II in the mitochondrial matrix in VSMC have been reported to be a regulator of mitochondrial Ca^{2+} uptake via MCU, thereby controlling mitochondrial ROS release and VSMC remodelling and migration (Nguyen et al., 2018). Mitochondria play a vital role in intracellular Ca^{2+} signalling under pathological conditions when the Ca^{2+} overload occurs and threatens cell viability.

1.4.2 Ca^{2+} entry mechanisms

VSMCs utilise several different types of Ca^{2+} influx channels, including the VGCCs, receptor-operated Ca^{2+} channels (ROCCs) and store-operated Ca^{2+} channels (SOCCs) (Berridge et al., 2000). Ca^{2+} entry happens through VGCCs as a result of membrane depolarisation. However, ROCCs, activated by agonists

acting on a range of GPCRs, and SOCCs, activated by depleting the Ca^{2+} stores within the ER/SR, are non-voltage-gated channels.

Ca^{2+} can enter intracellular spaces via ROCCs which are activated by the binding of agonists to the extracellular domain of the channel. The term ROCCs is not commonly used now, and these channels are more commonly referred to by their corresponding ion channel family; these channels are mostly transient receptor potential (TRP) channels (Martinsen et al., 2014). TRP channels have been considered to play a major role in receptor-induced Ca^{2+} entry in many cell types. There are six subfamilies in TRP channels: TRPA (ankyrin), TRPC (canonical), TRPM (melastatin), TRPML (mucolipin), TRPP (polycystin) and TRPV (vanilloid). Multiple TRP channels are expressed in VSMCs and contribute to the regulation of contraction and development of myogenic tone. Once activated by external ligands, GPCRs, or physical stimuli, the influx of cations through TRP channels can cause depolarisation of the membrane potential (E_m) (Earley and Brayden, 2015).

Most TRP channels are permeable to Ca^{2+}, whereas TRPM4 and TRPM5 are impermeable to Ca^{2+} and activated by intracellular Ca^{2+} (Earley and Brayden, 2015). TRPC channels are more abundantly expressed in VSMCs and play a major role in receptor-induced Ca^{2+} entry (Ghosh et al., 2017). TRPC channels have been suggested to encode ROCCs and SOCCs, based on their participation in Ca^{2+} entry routes which activated downstream of GPCR and receptor tyrosine kinases that activate PLC (TRPC3, TRPC6, and TRPC7) or secondary to internal Ca^{2+} stores depletion that induces Ca^{2+} entering through the highly Ca^{2+}-selective channels (TRPC1, TRPC4 and TRPC5) (Earley and Brayden, 2015).

Store-operated Ca^{2+} entry (SOCE) or capacitative Ca^{2+} entry is an ubiquitous Ca^{2+} entry pathway via the activation of SOCCs in response to the depletion of intracellular Ca^{2+} stores (ER/SR) (e.g. following GPCRs stimulation and IP_3 release or through RyRs activation (Zhang and Trebak, 2011)). The opening of SOCCs can also be induced by pharmacological agents or physiological Ca^{2+} mobilisation. The best characterised, physiological and pathological store-operated Ca^{2+} current is the Ca^{2+} release-activated Ca^{2+} current (I_{CRAC}) (Hoth and Penner, 1992). Following decades-long investigations aimed at revealing the molecular identity of I_{CRAC}, the major protein components of the SOCE pathway were identified as the Ca^{2+} sensor protein STIM1 and the Ca^{2+} channel protein Orai1. STIM1 is an ER-localised protein; store depletion of Ca^{2+} causes unbinding of Ca^{2+} from the luminal EF-hands containing N-terminal domains of STIM1; this, in turn, results in the migration of STIM1 to the ER-PM junctions and the extension of its cytosolic C-terminal domains across the ER-PM space. The C-terminal domain of STIM1 interact with plasma-membrane-localised, pore-forming subunit, Orai1, causing it to cluster and activate to induce Ca^{2+} entry (Roos et al., 2005; Zhang et al., 2005).

Although it is clearly established that Orai1 protein forms the CRAC channel, some studies have reported that TRPC channels are required for SOCE with the involvement of Orai1 proteins in making up the store-operated channel (Cheng et al., 2011). A role for TRPC proteins in forming SOCE complex and activation by STIM1 remains an open question (Yuan et al., 2009). The SOCCs are recognised to be important in replenishing internal Ca^{2+} stores and may represent an essential contributor to the pathophysiology of cardiovascular diseases (Giachini et al., 2012).

1.4.3 Ca^{2+} extrusion mechanisms

The plasma membrane contains two systems for extrusion of the cytosolic Ca^{2+} to the extracellular space to regulate Ca^{2+} homeostasis. One is the high-affinity, low-capacity Ca^{2+}-ATPase (plasma membrane Ca^{2+} ATPase (PMCA)), and the other is the low affinity, high capacity Na^{+}/Ca^{2+} exchanger (NCX) (Brini and Carafoli, 2011). The PMCA pump belongs to the family of P-type ATPases, which operates with 1:1 Ca^{2+}/ATP hydrolysed. There are four PMCA isoforms encoded by four genes (*ATP2B1-4*) have been identified. PMCA1 and PMCA4 are expressed in most tissues, whereas PMCA2 and PMCA3 are found in the brain, striated muscle and the mammary gland (Brini and Carafoli, 2009; Brini and Carafoli, 2011). PMCA maintain the basal cytosolic Ca^{2+} level at ~100 nM and the Ca^{2+} transients generated by cell stimulation around ~1 μM range. Importantly, PMCA4 is essential for regulating Ca^{2+} homeostasis in all cells and modulating the contractility in vascular or bladder SMCs and excitation-contraction coupling of the heart through its interaction with neuronal nitric oxide synthase (nNOS) (Okunande et al., 2004; Schuh et al., 2001).

NCX mediates Ca^{2+} extrusion by using the electrochemical gradient, which couples the extrusion of 1 Ca^{2+} ion with the influx of 3 Na^{+} ions. Three isoforms of the NCX family have been identified (NCX1-3); NCX1 is ubiquitously expressed in the heart and VSMCs, whereas NCX2 and NCX3 are restricted to brain and skeletal muscle (Szewczyk et al., 2007; Brini and Carafoli, 2011). The relative proportion of NCX and PMCA varies in different cell types; it has been reported that NCX plays a significant role in vascular diseases such as hypertension (Blaustein and Hamlyn, 1984).

1.5 Voltage-gated Ca^{2+} (Cav) channels

Excitable cells such as neurons and SMCs express large numbers of VGCCs, which are activated by membrane depolarisation and mediate Ca^{2+} influx in response to the action potential. Ca^{2+} entering through VGCCs can serve as the second messenger of electric signalling to influence many cellular responses. They display vast diversities of electrophysiological properties. In cardiac, smooth and skeletal muscle cells, activation of Ca^{2+} channels can initiate the contraction by increasing $[Ca^{2+}]_i$ and directly/indirectly activating the secondary mechanism called Ca^{2+}-induced Ca^{2+} release (CICR) by RyRs in the SR. In neurons, VGCCs can induce synaptic transmission (Catterall, 2011). The initial discovery of this channel type dates back to 1953, and by now, several major groups of VGCC have been identified, including L-, P/Q-, N-, R- and T-type Ca^{2+} channels (Catterall, 2011) (Table 1.1).

Due to the gating specificity and pharmacology, different types of VGCCs have their own different characteristics. For instance, L-type Ca^{2+} channels have slow voltage-dependent inactivation, long-lasting current and large-conductance (Tsien et al., 1988). In comparison to L-type Ca^{2+} channels, T-type Ca^{2+} channels have transient current due to fast inactivation at strong depolarisation and small single-channel conductance (Nowycky et al., 1985). L- and T-type Ca^{2+} channels are recorded in a wide range of cell types, whereas P/Q-, N-, and R-type Ca^{2+} channels are found mostly in neurons (Catterall, 2011).

Table 1.1 Overview of voltage-gated Ca^{2+} channels

Group	Physiological name	α1 subunit	Protein	Gene	Activation potential (mV)	$V_{1/2}$ (mV)	Inactivation kinetics	Reference
HVA	L	α1S	Cav1.1	*CACNA1S*	-10 to -50	8-14	Slow	Gurkoff et al., 2017; Kuo et al., 2011; Hering et al., 2008
	L	α1C	Cav1.2	*CACNA1C*		-15		
	L	α1D	Cav1.3	*CACNA1D*		-18		
	L	α1F	Cav1.4	*CACNA1F*		-2.5~-12		
	P/Q	α1A	Cav2.1	*CACNA1A*	-50	-5~-11	Slow to Intermediate	
	N	α1B	Cav2.2	*CACNA1B*	-20	8	Intermediate	
	R	α1E	Cav2.3	*CACNA1E*	-25 to -40	3.5	Vary fast	
LVA	T	α1G	Cav3.1	*CACNA1G*	-70	-29	Fast	
	T	α1H	Cav3.2	*CACNA1H*		-31		
	T	α1I	Cav3.3	*CACNA1I*		-25		

$V_{1/2}$ represents the half-maximal activation voltage

1.5.1 Structure-function relationships of Cav channels

Ca^{2+} channels are complexes of α1, α2, β, γ, and δ subunits, and the key determinant of the Cav subtype is defined by its α1 subunit (170-240 kDa), which is responsible for the channel properties and may associate with other (auxiliary) subunits in various combinations. The α1 subunit is a protein of approximately 2000 amino acid sequence to arrange into four domains (I–IV), which each made up of six transmembrane segments (S1–S6) (Catterall, 2011). The S1-S4 forms the voltage sensor to open the ion pore. A key feature is the charged S4 segment which can control voltage-dependent activation. The S4 segment slides upwards when cells encounter depolarisation to open the VGCC channels. In contrast, the S4 segment moves downwards to close channels upon repolarisation. A membrane-associated loop located between transmembrane S5 and S6 segments provides the pore region of the channel (Bezanilla, 2008) (Figure 1.5).

Until now, three structurally and functionally distinct Ca^{2+} channel families (Cav1, Cav2, Cav3) have been grouped based on the different types of Ca^{2+} currents, which are primarily defined by different α1 subunits (Ertel et al., 2000). High-voltage-activated (HVA) channels include: L-type (Cav1.1-1.4), P/Q-type (Cav2.1), N-type (Cav2.2) and R-type (Cav2.3) Ca^{2+} channels. Low-voltage-activated (LVA) channels are T-type (Cav3.1-3.3) Ca^{2+} channels (Perez-Reyes et al., 1998; Ertel et al., 2000). In relations to the smooth muscle, two VGCC families have been shown to play the most important roles: L- and T-type Ca^{2+} channels.

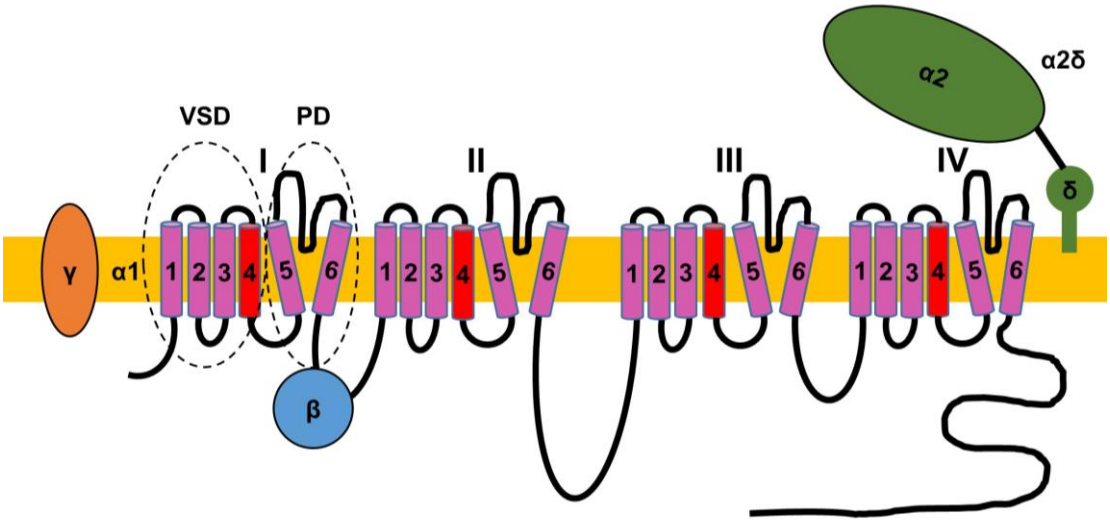

Figure 1.5 Subunit composition of voltage-gated Ca^{2+} channel. The α1 is the pore-forming subunit which contains voltage-sensing and -gating mechanisms. There are four homologous domains (I–IV), each containing six transmembrane segments (S1–S6) in α1 subunit. The α2δ and β subunits enhance expression and modulate the voltage dependence and gating kinetics of VGCCs.

VGCC: voltage-gated Ca^{2+} channel; VSD: voltage-sensing domain; PD: pore domain

1.5.2 L-type Ca^{2+} channels

L-type Ca^{2+} channels are the dihydropyridine-sensitive channels with a major role in the regulation of the myogenic tone of VSM (Amberg and Navedo, 2013; Nelson et al., 1990). The α1 subunits of L-type Ca^{2+} channels play a critical role in vascular function and modulation of the myogenic tone and arterial pressure (Catterall, 2011). The β subunit is a cytoplasmic protein that resides on the intercellular side between domains I and II to interact with other regions on Ca^{2+} channel α1 subunits. Four β subunits genes have been identified, and β3 is predominant in VSMCs (Kharade et al., 2013). In addition, co-expression of α2δ subunit with different α1 and β subunits was shown to produce distinct gating profiles and current densities (Klugbauer et al., 1999).

The hallmark characteristic of arterioles is rhythmic oscillations which depend on Ca^{2+} influx through L-type VGCCs. Hence, vasoconstrictor agonists that act through GPCRs causing contraction of VSMCs can be inhibited by L-type VGCC blockers. In arterial SMCs, Cav1.2 channel is localised to Ca^{2+} microdomain regions (Ca^{2+} sparklet sites) to contribute to local and global $[Ca^{2+}]_i$ under physiological conditions. PKC can modulate Cav 1.2 VGCCs via AKAP150 (Navedo et al., 2008), resulting in high activity Cav 1.2-Ca^{2+} sparklets that appear to significantly contribute to the increase of Ca^{2+} influx and myogenic tone in arterial SMCs (Amberg et al., 2007; Navedo et al., 2008). In some vascular SMCs, after sensing membrane depolarisation, L-type Ca^{2+} channels activate the GPCR-PLC-IP_3 pathway to induce release of Ca^{2+} from internal stores through IP_3Rs and amplify the process of CICR by RyRs (Fernández-Tenorio et al., 2010; del Valle-Rodríguez et al., 2003). Thus, L-type VGCCs have the potential to impact VSM function during physiological and pathological conditions.

1.5.3 T-type Ca^{2+} channels

T-type Ca^{2+} channels provide a route for Ca^{2+} influx, which influence numerous physiological effects (Catterall, 2011). Three types of T-type Ca^{2+} channels (Cav3.1, Cav3.2 and Cav3.3) have been identified, which are formed by different α1 subunits (α1G, α1H and α1I, respectively; Table 1.1). T-type Ca^{2+} channels do not require auxiliary β, α2δ, or γ subunits for functional assembly (Perez-Reyes, 2006). T-type Ca^{2+} channels have a very negative threshold activation voltage (~-60 mV) and can be opened by weak depolarisation. Upon depolarisation, T-type Ca^{2+} channels exhibit fast opening and closing and inactivate rapidly. A fast inactivation stops the ionic flux of Ca^{2+} in tens of milliseconds. A vital feature of T-type Ca^{2+} channels is the so called 'window current', which is produced under basal conditions and is due to the overlap of voltage-dependent activation and steady-state inactivation curves (Perez-Reyes, 2003) (Figure 1.6). Consequently, T-type Ca^{2+} channels can facilitate a window current which influence $[Ca^{2+}]_i$ at resting E_m via a proportion of active and not fully inactivated channels (Capiod, 2011).

T-type Ca^{2+} channels are present throughout the body, including the heart, kidneys, smooth muscle, nervous system and endocrine organs. Whilst Cav3.3 channel expression is generally restricted to the nervous system, Cav3.1 and Cav3.2 are prominently found in cardiac and smooth muscle (Catterall et al., 2005). The voltage dependence of channel inactivation and recovery from inactivation varies between the three T-type Ca^{2+} channel subtypes. Among three isoforms, Cav3.1 has the fastest inactivation and Cav3.2 has the slowest recovery from inactivation (Klöckner et al., 1999; Perez-Reyes, 2003).

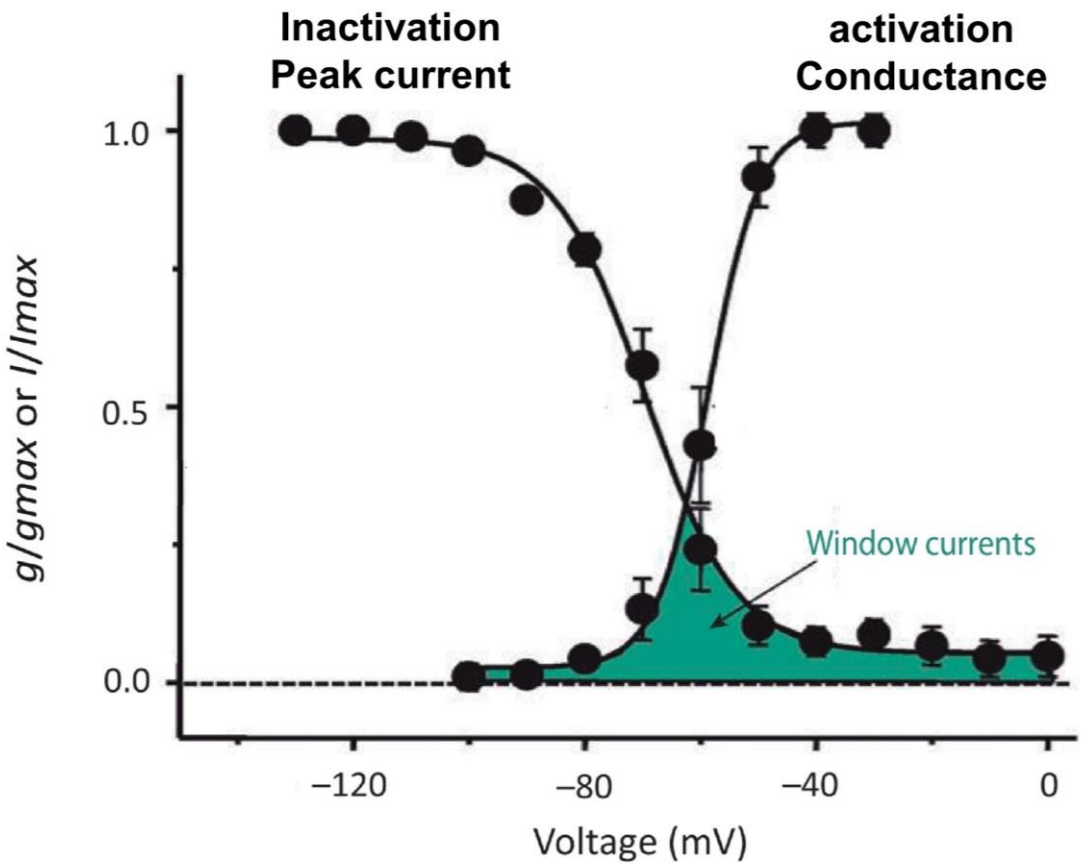

Figure 1.6 Voltage dependence of activation/inactivation of T-type Ca^{2+} channels. T-type Ca^{2+} channels operate in a subthreshold voltage range, with an overlap of the activation and inactivation curves which gives rise to a window current (indicated in green), a voltage range where T-type Ca^{2+} channels can be active tonically. Adapted from (Visa et al., 2019).

The elucidation of functional roles for Ca^{2+} channels has been significantly facilitated by the availability of relatively selective channel blockers, e.g. dihydropyridines, such as nifedipine for Cav1 L-type Ca^{2+} channels. However, until recently, specific contributions of T-type Ca^{2+} channels have been difficult to assess because there was a lack of specific blockers to block the different subtypes. Ni^{2+} has been classically considered a T-type Ca^{2+} channel blocker (Senatore and Spafford, 2015), but it also produced discrete blocking events to L-type Ca^{2+} channels (Winegar et al., 1991). Mibefradil, originally named Ro 40-5967 and previously licensed as an anti-hypertensive drug, is used to block T-type Ca^{2+} channels, but it also blocks other channel types, such as Na^{+} and other Ca^{2+} channels (Senatore and Spafford, 2015). NNC55-0396 is a structural analogue of mibefradil which is considerably more stable and selective to T-type Ca^{2+} channels without much effect on HVA channels (Li et al., 2005). Recently, the new generation of T-type Ca^{2+} channel pharmacology emerged, these compounds include Z944 (Tringham et al., 2012) and TTA-A2/P2 (Kraus et al., 2010); these compounds are much more selective towards T-type channels, which makes possible more specific interrogation of their functional roles.

Recent findings indicated the role of T-type Ca^{2+} channels in VSM physiology and vascular reactivity, which is related to the vascular tone, SMC contraction and proliferation (Perez-Reyes, 2003). Cav3.1 and Cav3.2 T-type Ca^{2+} channels have been found in VSMCs in human and many other species. Although Cav3.1 and Cav3.2 were shown to be involved in maintenance of myogenic tone in skeletal muscle resistance arteries (VanBavel et al., 2002), Cav3.1 channel was related to the pressure-induced constriction, whereas Cav3.2 was found responsible for the artery relaxation, owing to the negative feedback by modulating the RyR-BK_{Ca}

(large-conductance Ca^{2+}-activated K^+ channel) axis (Harraz et al., 2014). The functional role of T-type VGCCs in regulating vascular tone remains controversial, though. T-type Ca^{2+} channels can also be modulated by protein kinase pathways to modulate VSM function and the myogenic response (Harraz and Welsh, 2013). Some results showed that the activation of the Rho-kinase/ROCK pathway activation resulted in an inhibition of the Cav3.1 channel (Iftinca et al., 2007). In addition, the Cav3.2 channel can be selectively inhibited by Zn^{2+} via the unique extracellular binding site at the DII (Perez-Reyes and Lee, 2014) and ascorbate because of their unique sensitivity to redox modulators (Nelson et al., 2007).

T-type Ca^{2+} channels are essential for the physiological roles of rapid oscillatory activity in cellular responses, which mediate rebound burst firing, especially in the sinoatrial node to general heartbeats (Mangoni et al., 2006) and the thalamocortical circuit to control the transition between awake and sleep states (Lee et al., 2004). However, It has been increasingly clear that T-type Ca^{2+} channels are more than just contributors to pacemaker rhythms in the brain and heart as these are also important to the neuronal firing, epilepsy, nociception, hypertension, cell proliferation, gene expression, hormone secretion, and cancer growth (Perez-Reyes, 2003).

1.6 Kv7/KCNQ channels

The voltage-dependent potassium (Kv) channels are vital determinants of the resting E_m in SMCs and other cell types (Yuan, 1995; Evans et al., 1996). The Kv channels superfamily expressed in mammalian tissues is very diverse. There are twelve known Kv channel subfamilies (Kv1-Kv12) (Wulff et al., 2009). Several

vascular diseases such as hypertension, diabetes and atherosclerosis are associated with the abnormal function or expression of Kv channels in the vasculature (Cox, 2005). To date, the functional roles of several Kv channels in VSM have been examined, especially these belonging to the Kv1 and Kv2 families (Stott et al., 2014). Kv1.3-1.5 channels participate in VSMCs proliferation and vascular remodelling (Zhang and Gutterman, 2019). Kv2.1 form heteromeric channels with Kv9.3, which may involve pulmonary arterial hypertension (Patel et al., 1997). In addition, the upregulation of Kv6.3 and its co-expression with Kv2 channels appear to account for hypertension development. Although Kv3 and Kv4 expressions have been reported in VSMCs, there is little evidence for the regulation of vascular tone (reviewed in (Jackson, 2018)).

The family of the Kv7 channels has recently been brought to the picture as another important vascular K^+ channel type (Mackie and Byron, 2008; Greenwood and Ohya, 2009; Ng et al., 2011). These channels have been widely investigated in the nervous system, inner ear and heart, where these demonstrate a number of important physiological functions (Jentsch, 2000; Robbins, 2001). Most research has focussed on the role in cardiac (Kv7.1) and neuronal (Kv7.2-7.5) systems. Mutation of Kv7.1 can induce fatal cardiac arrhythmia (hereditary long QT syndrome) owing to the delayed cardiac repolarisation (Barhanin et al., 1996). Genetic alterations in Kv7.2 and Kv7.3 have been reported to result in benign familial neonatal seizures (Wuttke et al., 2005; Maljevic and Lerche, 2014). Defects in Kv7.4 leads to the early onset of non-syndromic hearing loss, and the expression was believed to be limited to the inner ear (Kubisch et al., 1999). It has been identified that Kv7 channels play critical roles in the membrane excitability of neurones (Marrion, 1997; Robbins,

2001). Although various groups have provided evidence of the functional importance of Kv7 channels in VSM (Mani et al., 2016; Stott et al., 2014; Brueggemann et al., 2014), the exact mechanisms of Kv7 physiological regulation or function in VSMCs are still incompletely understood.

1.6.1 Structure-function relationships of Kv7 channels

Kv7 channels, like other Kv channels, are assembled as a complex of four pore-forming α-subunits. Each of these subunits consists of six transmembrane spanning domains (S1-S6), with the cytoplasmic localisation of the NH_2 and COOH regions. The S1-S4 region forms the voltage-sensing domain (VSD), whereas the linker region between the S5-S6 region forms the K^+-selective pore (Soldovieri et al., 2011) (Figure 1.7). The S4 domain contains four to six positively charged arginine residues. The environment around the S4 segment is critical for its ability to participate in charge movement, necessary for gating the pore (Soldovieri et al., 2011; Wulff et al., 2009; Borjesson and Elinder, 2008). Five subtypes (Kv7.1-Kv7.5), encoded by the genes *KCNQ1-5*, have been identified in Kv7 family (Gutman et al., 2003). Kv7.2, Kv7.4 and Kv7.5 can form functional homotetramers or heterotetramers with Kv7.3 (Howard et al., 2007) to display different biophysical properties in cells (Mani et al., 2016).

Several Kv7 channels depend on the accessory proteins (KCNE β-subunit) to fulfil a variety of physiological functions, and the best known is the KCNE1 modulation of Kv7.1 in the cardiomyocytes (Morin and Kobertz, 2008). The other β-subunits, KCNE2-5, also can regulate Kv7 channels expression and function (Haick and Byron, 2016). Moreover, the COOH-termini of Kv7 subunits carry

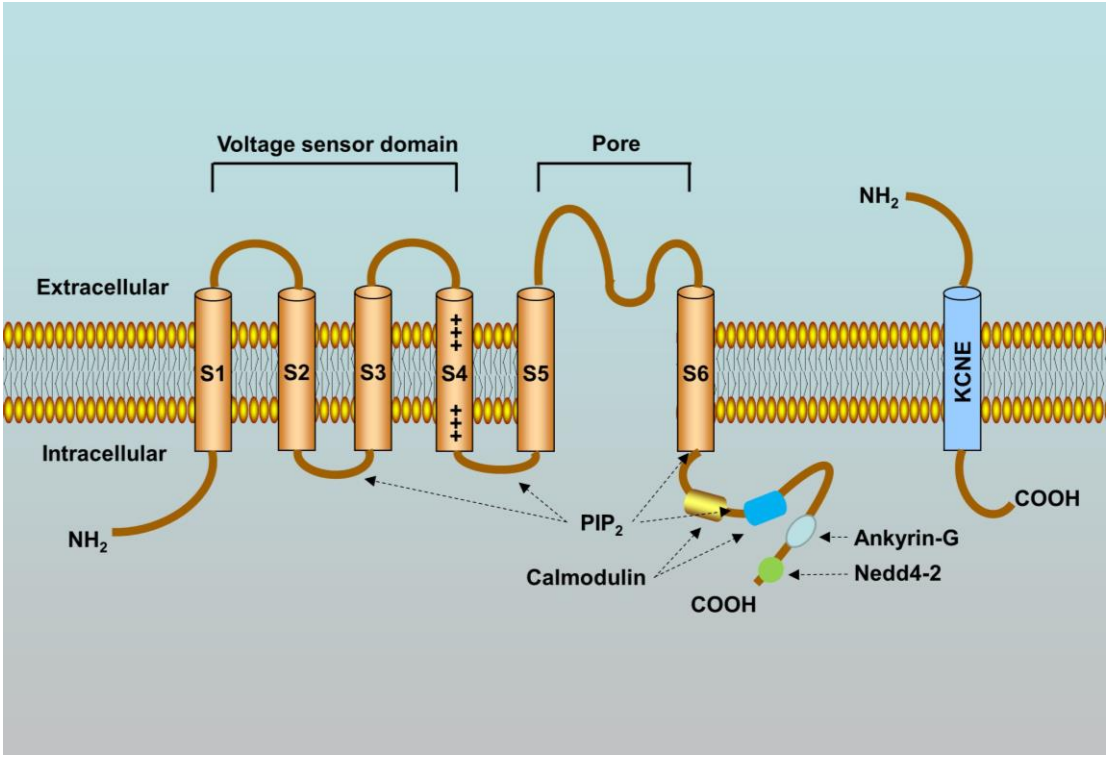

Figure 1.7 Schematic structure of Kv7 channel α-subunits. The α subunit of the Kv7 channel consists of six transmembrane spanning domains (S1–S6) with cytoplasmic NH_2- and COOH- terminal segments, S1-S4 is the voltage sensor domain with positively charged arginine residues in the S4 domain, and the single K^+-selective pore-loop domain is located between S5 and S6. KCNE is shown as a cylinder that represents the single transmembrane helix common to all KCNE family members. The location of the conserved interaction sites with calmodulin and PIP_2, with ankyrin-G in Kv7.2/3 and with ubiquitin-protein ligase Nedd4-2, are also shown.

PIP_2: phosphatidylinositol 4,5-bisphosphate

binding sites for various cytosolic regulatory molecules and accessory proteins, such as calmodulin, which regulate Kv7 channel trafficking, assembly and gating (Gamper et al., 2005; Tobelaim et al., 2017) and PIP_2, which is a co-factor necessary for channel activity (Gamper and Shapiro, 2007; Tobelaim et al., 2017) for the Kv7 channel open probability. Several other regulatory proteins interact with Kv7 C-terminal regions, including cytosolic-ubiquitin-protein ligase Nedd4-2, which regulates the membrane expression of Kv7.2/3, Kv7.3/5, and Kv7.1/KCNE1 heteromultimers (Ekberg et al., 2007; Jespersen et al., 2007) and Ankyrin-G, which targets Kv7.2/3 channels to axon initial segment and nodes of Ranvier in myelinated neurons (Pan et al., 2006).

Each Kv7 channel has a distinct expression pattern and function in each tissue type. Kv7.1 is restricted to peripheral epithelial and SMCs, as well as to cardiac myocytes, where it controls ventricular repolarisation (Barhanin et al., 1996; Sanguinetti et al., 1996). Kv7.2 - Kv7.5 are detected in the nervous system contributing to the M-current and the action potential in neurons (Delmas and Brown, 2005; Du and Gamper, 2013). Mutations in the Kv7.2 and Kv7.3 channels result in the development of encephalopathy and epilepsy in patients, exemplified by the familial neonatal seizures in humans. The Kv7 channels also play a central role in nociception. Loss of Kv7 activity or expression contributes to the initiation and propagation of the pain because of the role as a regulator of E_m in primary sensory afferents (Liu et al., 2010). Recently, Kv7 channels have been found in VSMCs (Ohya et al., 2003; Joshi et al., 2006; Brueggemann et al., 2007; Yeung et al., 2007) where these channels were reported to contribute to cell hyperpolarisation and the regulation of contractile functions of arteries. These findings suggest that the Kv7 channels might become a novel therapeutic target

for the treatment of disorders of the cardiovascular system (Ohya et al., 2003; Yeung et al., 2007; Fosmo and Skraastad, 2017).

1.6.2 Kv7 channels in vascular smooth muscle cells

Kv7 channels have been widely investigated in the nervous system and the heart (reviewed in (Delmas and Brown, 2005; Fosmo and Skraastad, 2017)). The first paper to show *Kcnq* gene expression in SMCs was the study by Ohya and colleagues, who reported *Kcnq1* expression in rat stomach SMCs (Ohya et al., 2002). In a follow up study, Ohya and colleagues identified that *Kcnq1* is abundantly expressed in murine portal vein myocytes (Ohya et al., 2003). Further studies showed that *Kcnq4* and *Kcnq5* were expressed in arterial SMCs from the murine aorta, carotid, femoral and mesenteric artery at levels equal to or higher than *Kcnq1* expression (Yeung et al., 2007; Brueggemann et al., 2007). *Kcnq1*, *Kcnq4*, and *Kcnq5* were also detected in rat mesenteric artery SMCs (Mackie et al., 2008). Similar results were also shown in rat pulmonary artery smooth muscle (PASMC), which expressed *Kcnq1*, *Kcnq4*, and *Kcnq5* subtypes, with *Kcnq4* mRNA being the most abundant (Joshi et al., 2009). After a series of studies, a consensus has been reached that VSMCs mostly express *Kcnq1*, *Kcnq4* and *Kcnq5*, while expression of *Kcnq2* and *Kcnq3* is negligible. (Greenwood and Ohya, 2009; Stott et al., 2014).

Most studies showed predominant expression of *Kcnq4*, followed by *Kcnq1* and *Kcnq5* (Yeung et al., 2007; Joshi et al., 2009; Ng et al., 2011; Zhong et al., 2010). *Kcnq5* was found at high expression levels in rat cerebral and mesenteric arteries (Brueggemann et al., 2014). Moreover, higher expression of *Kcnq1* and *Kcnq5* was noted in rat coronary artery (Morales-Cano et al., 2015). For human

vasculature, all *KCNQ* genes except the *KCNQ2* subtype were found in arteries from visceral adipose tissue and proximal mesenteric arteries (Ng et al., 2011). The expression of protein levels of Kv7.1, Kv7.4 and Kv7.5 was confirmed in rat aortic (Yeung et al., 2007), cerebral arterial myocytes (Zhong et al., 2010) and Kv7.4 protein in PASMCs (Joshi et al., 2009). Recently, the studies of the functional assembly of Kv7 channel protein subunits in VSMCs showed the existence of Kv7.4/Kv7.5 heterotetramers in mesenteric (Brueggemann et al., 2014) and cerebral artery myocytes (Chadha et al., 2014).

1.6.3 Regulation of Kv7 channels

Kv7 channels, as regulators of neuronal excitation, have been investigated with the use of activators or blockers. Inhibition of M-currents (currents produced by neuronal KCNQ channels) generally results in the increase of the excitability. Activation of GPCRs can suppress M-current and induce transient hyperexcitability in neurons (Delmas and Brown, 2005). Accordingly, the M-channel inhibitor, XE991, has been used increasingly to investigate the physiological and pathological roles of the Kv7 channels in both cell culture and animal experiments. XE991 and its close analogue, linopirdine, are reversible, state-dependent inhibitors that favour the activated state of the Kv7/KCNQ channels; all five Kv7 subunits are sensitive to these blockers (Chadha et al., 2014; Greene et al., 2017). Retigabine, a selective Kv7.2-7.5 channel activator, has been proven to be an effective anticonvulsant which activates Kv7 channels (except Kv7.1) by shifting the voltage-dependence of activation to hyperpolarised potentials to hold channels open and stabilise the resting E_m (Wuttke et al., 2005). In VSMCs, inhibition of Kv7 channels can increase vascular tone, while retigabine

can selectively relax constricted arteries (Tatulian et al., 2001; Joshi et al., 2009; Ng et al., 2011; Mani et al., 2011).

Kv7 channels act as effectors for some vasodilators and vasoconstrictors. For example, cyclic AMP (cAMP)/protein kinase A (PKA) mediated activation of Kv7 subunits can induce vasodilation (Mani et al., 2016). PKC dependent suppression of Kv7 channels in response to activation of GPCRs leads to vasoconstriction (Stott et al., 2014; Brueggemann et al., 2007). Accessory proteins, such as calmodulin and PIP_2, have been shown as modulators on Kv7 channels. Calmodulin can bind to the Kv7 C-terminus to form functional channels and interact with the low-affinity calmodulin-binding sites to reduce Kv7.2, Kv7.4 and Kv7.5 currents, whereas PIP_2 increases the activity of all Kv7 channels (Stott et al., 2014). Perivascular adipose tissue (PVAT) releases vasodilators to act through Kv7 channels. Hence, a deficiency in Kv7 channels correlated with the reduction of the anti-contractile effect of PVAT (Jackson, 2018).

1.6.4 The role of Kv7 channels in the excitability and resting E_m maintenance in excitable cells

Kv channels play an important role in Ca^{2+} signalling through their ability to maintain a negative E_m. They regulate the excitability of neurons and participate in the control of arteriolar tone and microvascular perfusion (Delmas and Brown, 2005; Tykocki et al., 2017). Their activity is predominately modulated by E_m, vasodilators and vasoconstrictors. Kv7 channels are directly activated by membrane depolarisation. Therefore, the opening of K^+ channels results in membrane hyperpolarisation and vasodilation, whereas closure of K^+ channels leads to membrane depolarisation and vasoconstriction. The Kv7 family has a

relatively negative threshold for activation at approximately -60 mV, as a result of which a fraction of these channels remains open at resting E_m. Hence, any depolarising influence will be opposed by the progressive opening of Kv7 channels to repolarise the membrane and prevent the activation of VGCCs, hence maintaining vascular tone (Stott et al., 2014; Nelson and Quayle, 1995).

Kv7.5 is highly expressed in skeletal and smooth muscle. The presence of native Kv7.5 has been reported as a sole source of K^+ conductance in the voltage range from -60 to +20 mV in VSMCs (Mani et al., 2016). Activation of Kv7.5 currents (half-maximal activation voltage ($V_{1/2}$), -46.7 ± 1.6 mV) was generally negative and faster than Kv7.2 (-37 mV), Kv7.4 (-11 mV), and Kv7.3/Kv7.5 (-35 mV) (Wang et al., 1998; Meritxell et al., 2009). However, the interaction with KCNE subunits can change the Kv7.5 channel gating: it takes seconds to fully activate the channel upon depolarisation, and the presence of KCNE1 shifts the $V_{1/2}$ to depolarised values (-42.2 ± 0.9 vs. -46.7 ± 1.6 mV) in Xenopus oocytes (Figure 1.8A, B). Likewise,, KCNE1 slowed the activation of Kv7.5 currents (the time constants of current activation, 129 ± 2 vs. 42 ± 3 ms) but increased the peak currents at +60 mV in HEK293 cells (Figure 1.8C, D) (Meritxell et al., 2009).

Importantly, many other ion channels expressed in the vasculature contribute to the regulation of $[Ca^{2+}]_i$. This includes multiple types of Kv channels (predominant Kv1.2, Kv1.5, Kv2.1) (Cox, 2005), inward-rectifier K^+ (K_{ir}) (Park et al., 2008), adenosine triphosphate (ATP)-dependent (K_{ATP}) (Brayden, 2002), Ca^{2+}-activated K^+ (K_{Ca}) (Köhler et al., 2010), two-pore K^+ (K_2P) (Wiedmann et al., 2016) channels, and Ca^{2+}-activated Cl^- channels (CaCC) (Kitamura and Yamazaki, 2001). These ion channels are also modulated by vasoconstrictors and

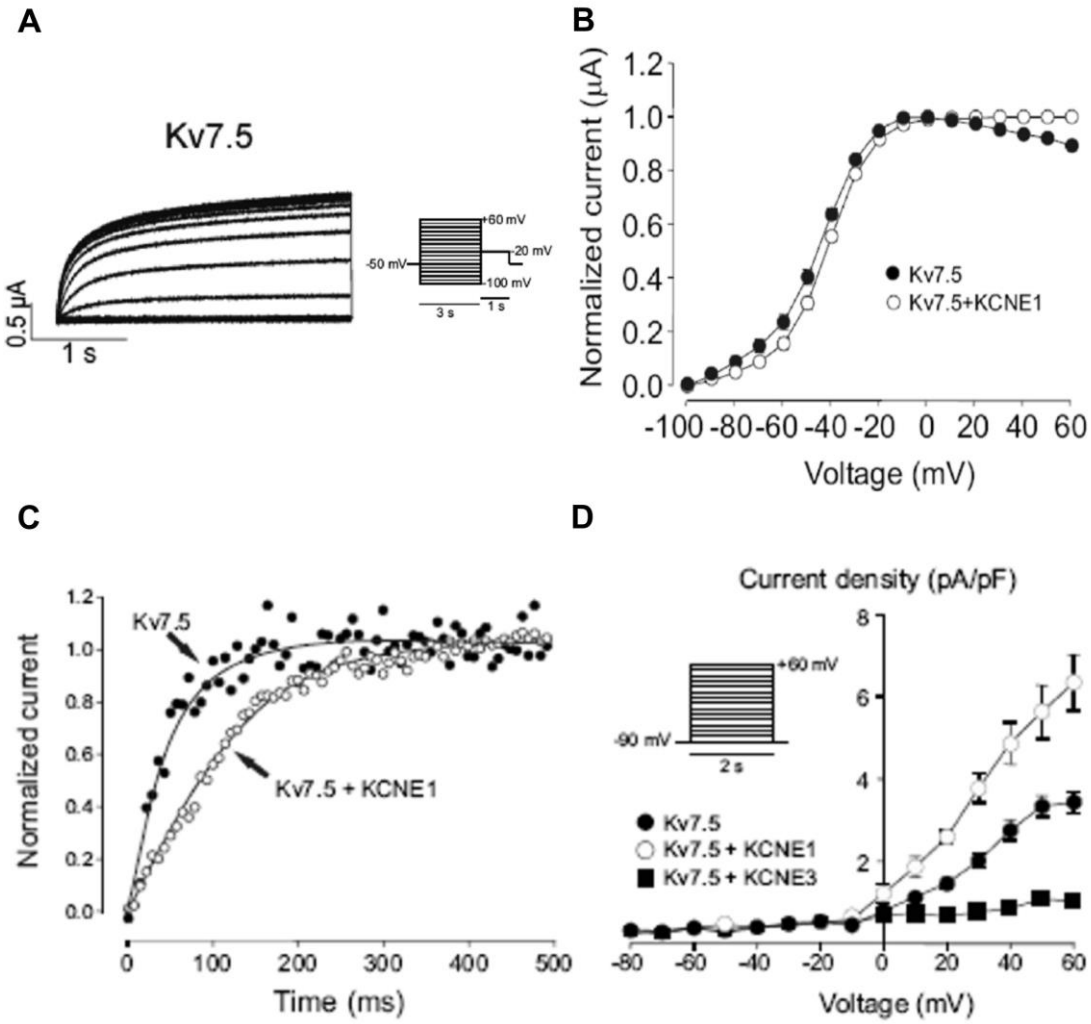

Figure 1.8 Interaction of KCNE1 with Kv7.5 in current kinetics. (**A**) Voltage clamp recording from Kv7.5/Xenopus oocytes. (**B**) I-V relationships in the presence of KCNE1 in Kv7.5/Xenopus oocytes. (**C**) Representative Kv7.5 currents in the absence or the presence of KCNE1 in Kv7.5/HEK293 cells. (**D**) I-V in the presence of KCNE1 and KCNE3 in Kv7.5/HEK293 cells. Adapted from (Meritxell et al., 2009)

vasodilators, contributing to all aspects of the regulation of vascular tone (Dogan et al., 2019), but these are outside of the scope of the current thesis.

1.7 Disorder of vascular remodelling

Cardiovascular disease is one of the top leading cause of death globally, which accounts for approximately 17.3 million deaths per year. The death number is estimated to increase to 23.6 million by 2030 (Benjamin et al., 2017). Stroke, heart attack, and ruptured aneurysms are the primary diseases to contribute to the high mortality rates up to 31% of all global deaths (Mozaffarian et al., 2016).

A central feature of cardiovascular disease is excessive VSMCs proliferation, which leads to vascular structural and functional changes in arteries. VSMCs typically exhibit a stable contractile phenotype to adapt to changes in the extravascular environment and local signalling molecules to maintain hemodynamic demands. However, in pathological conditions, such as restenosis, hypertension and atherosclerosis, these adaptive changes do not return to basal levels, which often leads to the VSMCs proliferation and increase of the vascular resistance. This process of maladaptive change is defined as vascular remodelling (Brown et al., 2018).

Several signalling pathways have been implicated in the pathophysiology of cardiovascular diseases. Many of the extrinsic factors that drive diseases seem to act through the Ca^{2+} signalling system. The mishandling of $[Ca^{2+}]_i$ is considered a crucial step in the pathogenesis of multiple vascular diseases and is associated with VSM ion channels regulation. Among other channels, Kv7 channels are well-

placed to play a strong role in the $[Ca^{2+}]_i$ modulation via the tight control of E_m, owing to their negative activation threshold and lack of inactivation. Thus, deficiency in Kv7 expression and/or activity may result in tonic depolarisation and Ca^{2+} overload. In broad agreement with this idea, mutations in the *KCNQ1* gene and a decrease in *KCNQ4* mRNA have been reported to increase the risk of hyperglycaemia, diabetes, and hypertension. Multiple studies indicated that Kv7 channel enhancement activation might function as a possible prevention and treatment of coronary artery disease, hypertension, diabetes, and their comorbidities (Chen et al., 2016; reviewed in (Mackie and Byron, 2008; Fosmo and Skraastad, 2017)). Since intracellular Ca^{2+} signals lead to the contraction in the vasculature (see section 1.3), the elucidation of physiological modulation of Ca^{2+} homeostasis can provide a prospective assessment of current and future research and pharmacological targets. The following section discusses the significance of pathological VSMCs proliferation within the development of the specific cardiovascular disease.

1.7.1 Atherosclerosis

Atherosclerosis is a complicated, chronic inflammatory disease, characterised by the pathologic process of atheromatous plaque of the arterial wall. The progression of atherosclerosis is related to plaque mass, intimal hyperplasia and arterial remodelling (Pasterkamp et al., 2000). It can be divided into three stages namely 1) the endothelial dysfunction, during this stage low-density lipoprotein (LDL) migrates into the sub-endothelial space to form oxidised LDL (oxLDL), ensuing an inflammatory cascade. 2) Plaque progression; at this stage, VSMCs migrate to the intima to proliferate, following the formation of a plaque and a fibrous cap. 3) Thrombosis and rupture of the plaque, which represents the

clinical complication of atherosclerosis (Lim and Park, 2014). Within the intima of arteries, oxLDL is thought to provide the initiation and progression of atherosclerosis. Lectin-like oxLDL receptors type-1 (LOX-1) is the major mediator of ox-LDL activity, which can trigger the proinflammatory signalling pathways in VSMCs (Sun and Chen, 2011). Proinflammatory cytokines, such as IL-1α, IL-1β, and TNF-α, can upregulate LOX-1 expression in VSMCs, causing advanced atherosclerotic lesions (Hofnagel et al., 2004). Also, LOX-1 activation promotes VSMCs to the proliferative and migratory phenotypes, even to the transformation of foam cells (Liu et al., 2014; Lim and Park, 2014). Endothelial injury and the release of inflammatory mediators from activated macrophages can also influence lesion formation and stimulate the migration and proliferation in VSMCs (Lusis, 2000). Plaque rupture and these series of reactions cause further devastating effects, such as stroke and myocardial infarction; therefore, the inhibition of excessive remodelling in VSMCs may have beneficial effects to prevent arterial occlusive diseases.

Atherosclerosis is a target for multiple pharmacological strategies to combat cardiovascular disease. Statins are therapeutically effective lipid-lowering drugs; current professional society guidelines recommend statin therapy in patients with the coronary arterial disease to reduce cardiovascular events and mortality (Gerhard-Herman et al., 2017; Aboyans et al., 2018; Harris et al., 2016). For example, pravastatin has been shown to downregulate LOX-1 expression in human VSMCs, reduce atherosclerotic lesions and decrease intimal media thickness (Hofnagel et al., 2006). Simvastatin was demonstrated to reduce the neointimal hyperplasia and proliferation in human VSMCs (Porter et al., 2002). As a number of these cellular and inflammatory processes are mediated by the

disruption in Ca^{2+} homeostasis, the potential roles of Ca^{2+} channel blockers have also been shown to significantly decrease atherosclerotic plaque burden and fibrous plaque content. The possible mechanism of this effect is the inhibition of the migration and proliferation in SMCs, which depends on the L-type VGCCs activity, but also decreased oxidative stress and vascular inflammation at atherosclerotic lesions (Yoshii et al., 2006; Eagleton et al., 2008). Accumulating evidence implicates a prominent role of endothelial dysfunction in the development of atherosclerosis and coronary arterial disease in diabetes (Morales-Cano et al., 2016). As changes in the Ca^{2+} transport mechanisms lead to cellular changes in atherogenesis, it has been proposed that Ca^{2+} channel antagonists may work in a synergistic fashion with other established treatments to effectively improve outcomes in patients who are at risk for or have established coronary artery disease (Mason, 2002). Moreover, as Kv7 activation limits Ca^{2+} influx through VGCC, selective activators of Kv7.4/7.5 may be useful for preventing or reducing angina pectoris episodes (Chen et al., 2016).

1.7.2 Hypertension

Hypertension is a risk factor for many chronic diseases, such as stroke, myocardial infarction, and heart failure. Pathophysiologically, hypertension often arises from increased vascular resistance and vascular remodelling, which involve changes to VSMCs in both large and small arteries (Touyz et al., 2018; Brown et al., 2018). These processes are regulated by complex, interacting systems to influence VSMCs through their highly plastic and dynamic features. Dynamic changes in excitation-contraction coupling largely depend on intracellular $[Ca^{2+}]_i$ signals, which orchestrate VSMC's responses to the mechanical, humoral, or neural stimuli (Touyz et al., 2018). In hypertension,

control of Ca^{2+} signalling is altered, which leads to an increase of $[Ca^{2+}]_i$, hypercontractile status, and vascular remodelling. Both systemic and pulmonary hypertension are linked to altered Ca^{2+} handling and vascular remodelling. VGCCs, TRP channels, and Na^+/Ca^{2+} exchanger are all related to the Ca^{2+} homeostasis and vascular dysfunction in hypertension (Goulopoulou and Webb, 2014). Moreover, increased expression of vascular SOCC complex, STIM1/Orai1, is also associated with augmented aortic contraction in hypertension (Giachini et al., 2012; Goulopoulou and Webb, 2014).

L-type Ca^{2+} channel blockers which target Cav1.2 L-type Ca^{2+} channels are well known to be effective in the regulation of blood pressure. T-type Ca^{2+} channels also have been linked to hypertension; hence, compared to selective L-type Ca^{2+} channels blockers, treatment with combined L- and T-type Ca^{2+} channels blockers has a beneficial effect on the high blood pressure and arterial stiffness in hypertension, indicating a significant vascular effect of T-type Ca^{2+} channels in hypertensive condition (Thuesen et al., 2017). Dysregulated Ca^{2+} homeostasis leads to the hypercontractile state and proliferative phenotype in VSMCs with the consequent vascular remodelling in hypertension. T-type Ca^{2+} channels might be of functional importance in hypertension because of a significant increase in the contribution of Cav3.1 and Cav3.2 T-type Ca^{2+} channels to vascular tone during augmented oxidative stress (Howitt et al., 2013; Thuesen et al., 2017) (see section 1.5.3).

1.7.3 Pulmonary arterial hypertension

Pulmonary arterial hypertension (PAH) is defined by a mean pulmonary artery pressure higher than 25 mmHg at rest. The initial classification in 1973 involved

only two categories: primary and secondary PAH, then was expanded into five major categories based on similar pathophysiology in 1998 and further revised to better group similar diseases in 2008. There are now five groups of pulmonary hypertension. Group 1 PAH is idiopathic and inherited, which is caused by drugs, toxins or conditions such as connective tissue disease, human immunodeficiency virus (HIV) infection, liver disease, congenital heart disease. Group 2 PAH is often associated with left heart diseases, such as mitral valve disease or long-term high blood pressure. Left heart disease is the most common cause of pulmonary hypertension. Group 3 PAH is related to lung problems and hypoxia, such as chronic obstructive pulmonary disease and interstitial lung disease, as well as sleep-related breathing disorders. Group 4 PAH is caused by blood clots in the lungs or general clotting disorders. Group 5 PAH is triggered by other disorders, such as sarcoidosis, vasculitis and tumours that press on the pulmonary arteries (Simonneau et al., 2009).

The pathogenesis of PAH is caused by pathologic vasoconstriction, followed by an increase in pulmonary vascular resistance. PAH is characterised by the proliferation and hypertrophy in endothelial cells and SMCs. Hypoxia, genetic defects, shear stress or inflammation, can lead to the remodelling of the vascular wall with a series of vascular contraction, proliferation and resistance to apoptosis, subsequent right ventricular hypertrophy (Cool et al., 2005). PASMCs contraction and proliferation directly influence the pulmonary vasoconstriction and vascular remodelling, respectively. The primary stimulus is often the increase of $[Ca^{2+}]_i$ which can trigger Ca^{2+}-dependent gene transcription in VSMCs (see below). Inhibition of the proliferation in PASMCs was found while removing the

extracellular Ca^{2+} and depleting the intracellular stored Ca^{2+} concentration (Golovina et al., 2001).

The elevation of $[Ca^{2+}]_i$ via the entry through the VGCCs and release from the intracellular Ca^{2+} stores (see section 1.4) in PASMCs activates signal transduction pathways to affect various gene expression, including these coding for TRP channels, Orai, STIM1, and Na^+/Ca^{2+} exchanger. The treatment of PAH is determined by risk stratification based on the severity of the disease. Containment of the disease aims to reduce vasoconstriction. Initial treatment with Ca^{2+} antagonists is only an option for a small cohort of PAH patients (< 5%) with the response to vasoreactivity testing during right heart catheterisation (Hoeper et al., 2017). Further investigation is warranted to identify additional mechanisms to target and reverse the vasoconstriction and structural remodelling by reducing PASMCs proliferation.

1.8 Hypoxia

Hypoxia is a condition in which the body is deprived of adequate oxygen supply at the tissue level. It can be classified as either generalised, affecting the whole body, or local, affecting a region of the body. Oxygen tensions vary widely across tissues. In the blood vessel system, arterial pO_2 is in the range of 75-100 mmHg (9.9-13.1% O_2) and venous pO_2 ranges 30-50 mmHg (3.9-5.6% O_2) (Injarabian et al., 2020). Many organs function normally at oxygen levels ranging between 19-70 mmHg (2-8% O_2), including the brain (21-47 mmHg), skeletal muscle (18-46 mmHg), and pulmonary artery (30-48 mmHg) (Ast and Mootha, 2019). Hypoxia is defined as a lower pO_2 (≤1% O_2), which results in reduced oxygen

availability at the tissue and cellular levels (Beaudry et al., 2016) and it causes a biological effect, for example, the accumulation of HIFα protein (Wenger. et al., 2015).

Regions of hypoxia (≤1% O_2) exists in arteries of hypertensive rodents and subjacent to atherosclerotic plaques. Hypoxia can lead to vasculogenesis, vascular remodelling and atherosclerosis (Ray et al., 2008). In the type I cells of the carotid body, neuroepithelial bodies in the lungs, and adrenal chromaffin cells, hypoxia inhibits Kv channels, leading to membrane depolarisation and Ca^{2+} entry through L-type Ca^{2+} channels (Weir and Olschewski, 2006). Responses to airway hypoxia are also associated with the depolarisation of SMCs in the pulmonary arteries and the reduction of the activity of the Kv channels. Therefore, Kv channels are important to the hypoxic depolarisation in PASMCs (Coppock et al., 2001).

Various studies have demonstrated that Kv1.2 (Wang et al., 1997; Hulme et al., 1999), Kv1.5 (Wang et al., 1997; Archer et al., 1998), Kv2.1 (Hulme et al., 1999; Archer et al., 1998; Patel et al., 1997), Kv3.1 (Patel et al., 1997) and Kv9.3 (Patel et al., 1997; Hulme et al., 1999) are potential candidates to form oxygen-sensitive channels in cells. Although Kv7 activators have been proposed to provide the therapeutic potential in hypoxia-induced pulmonary hypertension, there is an unclear understanding of how hypoxia regulates Kv7 channels in VSMCs (Sedivy et al., 2015).

1.8.1 Cellular responses to hypoxia

Oxygen is required to maintain normal cellular function in each cell, and the rate of oxygen consumption greatly varies depending on each tissue. When cells experience a reduction in oxygen availability (hypoxia), they will undergo a range of adaptive responses at transcriptional, translational or post-translational levels (Abe et al., 2017). These could be rapid changes in response to acute hypoxia (within seconds to minutes) or long terms changes in response to chronic hypoxia (over hours or days). Tissue hypoxia occurs in several cardiovascular disorders, including atherosclerosis, vascular remodelling and heart failure (Abe et al., 2017). Hypoxic pulmonary vasoconstriction is an important physiological phenomenon in which small pulmonary arteries constrict in the presence of alveolar hypoxia. It can cause major complications, such as pulmonary hypertension and cor pulmonale. Chronic or prolonged hypoxia results in the changes of the functional expression of ion channels, which may lead to the remodelling of excitability in some cell types (Peers, 2002). Cellular responses in the hypoxic environment can be mediated by transcription factors belonging to the hypoxia-inducible factor (HIF) family, HIF-1α and HIF-2α (Abe et al., 2017). For example, hypoxia enhanced Cav3.2 T-type Ca^{2+} channel gene expression via the HIF signalling pathway (Del Toro et al., 2003). Tissue hypoxia is one of the common features of cardiovascular disorders. Hence, elucidation of HIF-α signalling in VSMCs may contribute to the discovery of a therapeutic target in the managing cardiovascular remodelling.

1.8.2 HIF family and structure

HIFs is a family of transcription factors that are crucial regulators of oxygen homeostasis and many other processes (Semenza, 2000; Wenger, 2002). HIFs

are heterodimers consists of α and β subunits (Wang and Semenza, 1995). The HIF-α subunits are inducible and stable under hypoxia but rapidly degrade in normoxia (Semenza et al., 1994). There are three different HIF-α proteins: HIF-1α, HIF-2α and HIF-3α. HIF-1α and HIF-2α appear closely related to interacting with hypoxia response elements (HREs) to induce transcriptional activity (Pugh and Ratcliffe, 2003). In contrast, HIF-3α has been understood to be involved in the negative regulation of these responses (Makino et al., 2001). These proteins are members of the basic Helix-Loop-Helix–Per-Arnt-Sim (bHLH–PAS) family (Ke and Costa, 2006). Following the PAS region is an oxygen-dependent degradation domain (ODDD), required for the mediation of the oxygen-regulated stability, and a transactivation domain (TAD) is important in regulating gene transcription. HIF-1α and HIF-2α have two TADs which are located at the N and C-terminus (N-TAD and C-TAD); however, HIF-3α has only one TAD at the N-terminus (Hara et al., 2001). The HIF-β subunits are members of the aryl hydrocarbon receptor nuclear translocator (ARNT) family. They are also known as HIF-1β (ARNT1), HIF-2β (ARNT2) and HIF-3β (ARNT3) that associate with the HIF-α subunits. Similar to the HIF-α subunits, HIF-β contains bHLH, PAS and TAD domains, but they lack an ODDD, which leads to them being stable and constitutively expressed in all tissues under normoxic conditions (Mandl and Depping, 2014) (Figure 1.9).

The oxygen-dependent regulation of HIF-α subunits is critical for their role as responders to hypoxia. In the presence of oxygen, HIF-α subunits degrade rapidly, which is mediated by prolyl hydroxylase domain (PHD) proteins, members of the 2-oxoglutarate/iron-dependent dioxygenase superfamily. These proteins hydroxylate specific prolyl residues in the ODDD of HIF-α subunits.

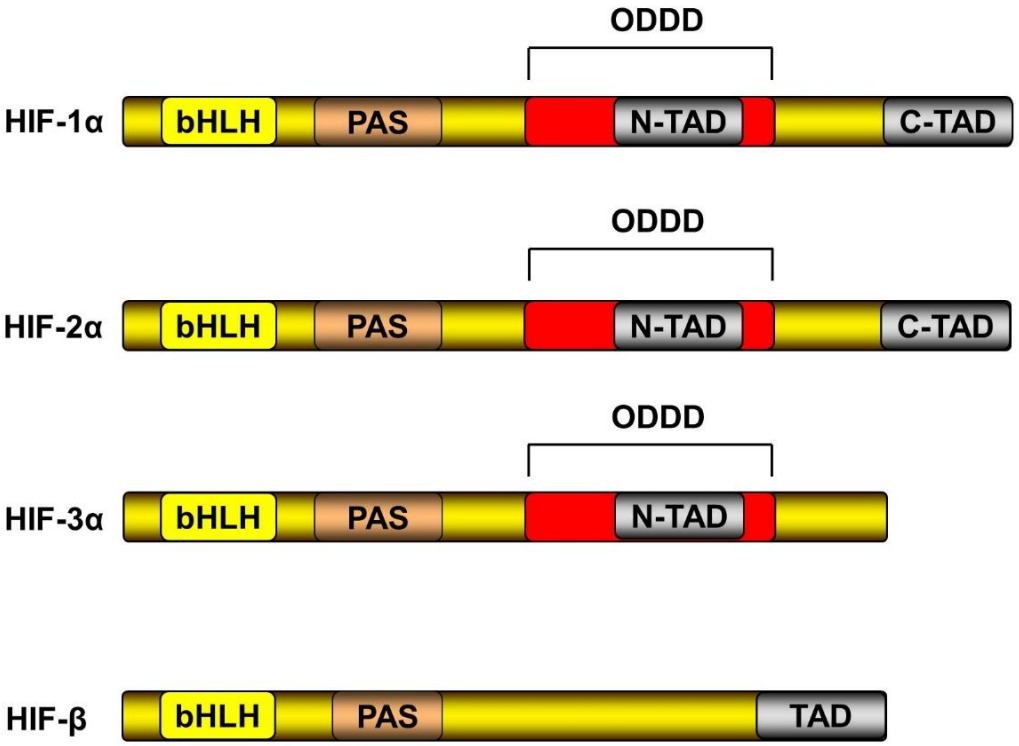

Figure 1.9 Hypoxia-inducible factor (HIF) subunit domain structures. The basic structure of HIF-α and HIF-β proteins showing the layout of functional domains. HIF-1α and HIF-2α both contain bHLH, PAS and TAD functional domains (C-TAD and N-TAD). HIF-3α contains only bHLH, PAS and N-TAD. Furthermore, the HIF-1α, HIF-2α, and HIF-3α structures include the ODDD domain, which is involved in protein stabilisation and mediation of the oxygen-regulated stability. HIF-β contains bHLH, PAS and TAD domains, which is not regulated by intracellular oxygen concentration.

HIF: hypoxia-inducible factor; bHLH: basic Helix-Loop-Helix; PAS: Per-Arnt-Sim; C-TAD: C-terminus transactivation domain; N-TAD: N-terminus transactivation domain; ODDD: oxygen-dependent degradation domain

Hydroxylation at these sites mediates interactions with the von Hippel-Lindau (VHL) E3 ubiquitin ligase complex, which targets the HIF-α proteins for proteasomal destruction (Pugh and Ratcliffe, 2003; Maxwell et al., 1999). Members of the PHD family (PHD1, PHD2, and PHD3) are widely expressed in tissues with different activity depending on the tissue oxygen tension (Jaakkola et al., 2001; Ivan et al., 2001).

In hypoxia, oxygen is limited for the hydroxylation of HIF-α proteins by PHDs. The stabilised HIF-α proteins translocate into the nucleus. After forming a heterodimer complex with HIF-β, HIF-α recognises and binds to the HREs of its target genes for engagement with the basal transcriptional machinery and gene transcription in the nucleus (Wenger, 2002) (Figure 1.10). In addition to the PHD-mediated hydroxylation in the ODDD, HIF-α activity is also regulated by asparagine hydroxylation in the C-TAD, and this process is catalysed by the factor-inhibiting hypoxia-inducible factor (FIH) protein (Wenger, 2002; Mahon et al., 2001). Hydroxylation of asparagine at these residues can block the interaction of the HIF-α C-terminal domain with the transcriptional coactivator p300 (Pugh and Ratcliffe, 2003).

1.8.3 Differential roles of HIF-1 and HIF-2

Recent evidence suggests that HIF-1α and HIF-2α are important to respond to hypoxia in different cell types (Sowter et al., 2003). Both HIF-1α and HIF-2α can drive the transcription of target genes; however, it has been reported that these two factors display some differences in their regulation for the genes. HIF-1α targets the expression of multiple genes encoding angiogenic growth factors and cytokines, such as *CXCR4*, *stromal cell-derived factor 1* (*SDF-1*), and

angiopoietin 2 (Semenza, 2009). HIF-2α appears to regulate the expression of genes, such as *Oct-4*, *erythropoietin*, and *CACNA1A* (Covello et al., 2006; Hu et al., 2003; Wang et al., 2005). In addition to the target gene transcription, HIF-1α and HIF-2α have been shown to play a critical role in pathological scenarios, such as cancer (Kim et al., 2009; Semenza, 2010) and systemic and pulmonary vascular responses to hypoxia (Semenza, 2009). Heterozygous *hif-2α*$^{+/-}$ mice did not develop pulmonary hypertension during prolonged hypoxia (Pugh and Ratcliffe, 2003; Labrousse-Arias et al., 2016). Microenvironment activation of HIFs in cancer and vascular remodelling occurs at a different level in oxygen tensions. It has been observed that HIF-1α and HIF-2α proteins accumulate at different oxygen concentrations in specific cell types. HIF-1α is stabilised at lower oxygen concentration (0-2%), whereas HIF-2α accumulates at more moderate concentrations (2-5%) in HeLa and neuroblastoma cells (Keith et al., 2011).

Studies of many cell types show that HIF-2α, like HIF-1α, is also primarily mediated by the oxygen-dependent proteasomal degradation by PHDs (Zhao et al., 2015). The activity of PHDs depends on the tissue oxygen tension to control the abundance of HIF proteins. Different PHD can differ in their activity to regulate HIF-1α or HIF-2α proteins. Compared to PHD1 and PHD3, HIF-1α is most strongly induced by the reduction of PHD2. Knockdown of PHD1 or PHD3 was effective in the upregulation of HIF-2α, however (Appelhoff et al., 2004). Such specific regulation may work to balance the activities of HIF-1α and HIF-2α to hypoxic response in different cellular contexts.

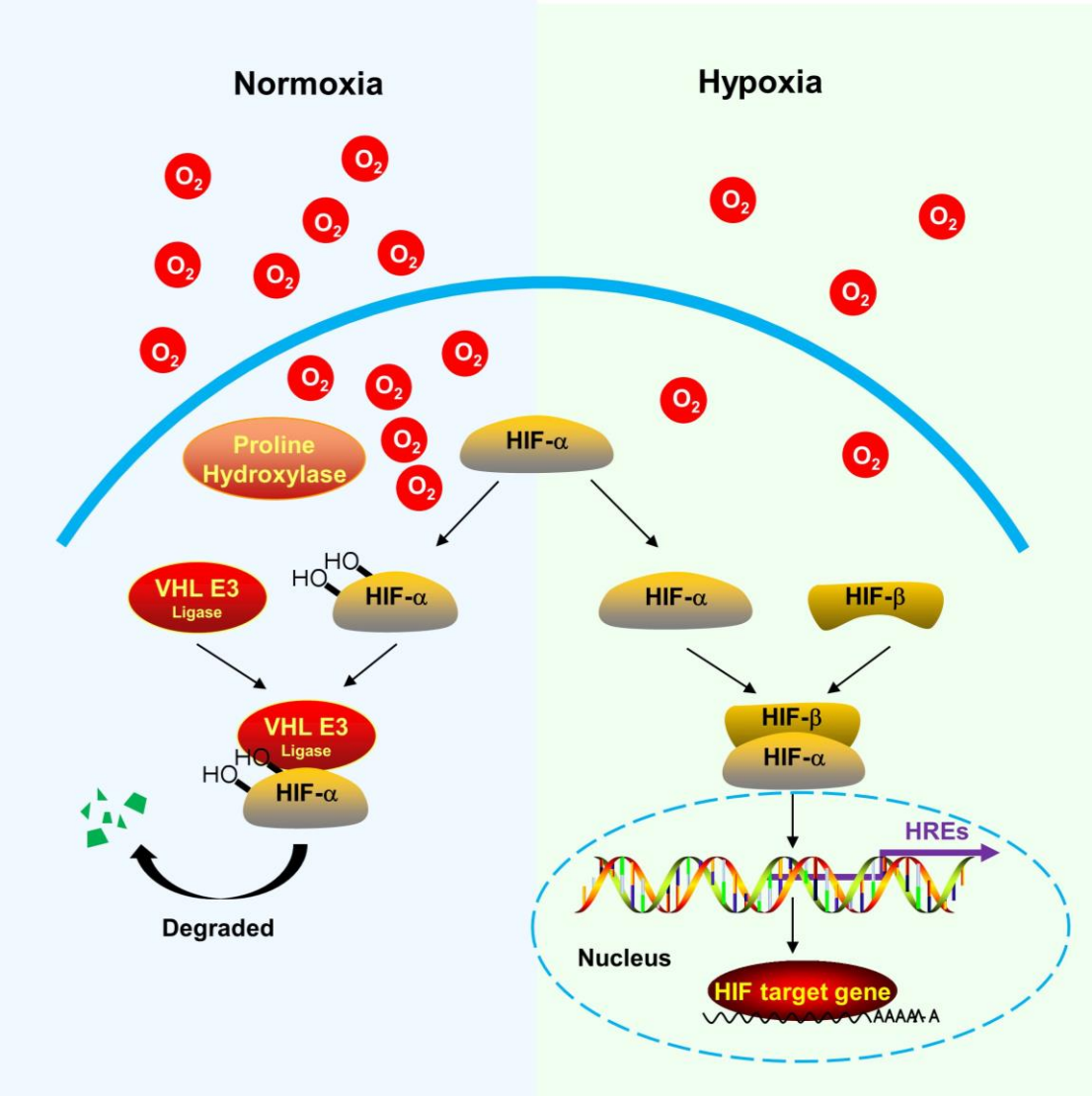

Figure 1.10 Schematic representation of the hypoxia-inducible factor (HIF) pathway. In normoxia, HIF-α binds to VHL E3 ligase leading to proteasomal degradation. During hypoxia, the activity of both PHD is reduced due to a lack of oxygen. HIF-α no longer binds to VHL E3 ligase and accumulates in the cytoplasm, which then dimerises with HIF-β to form the HIF molecule. The HIF complex is activated and then binds to HREs, leading to upregulating transcription of HIF downstream genes.

HIF: hypoxia-inducible factor; VHL E3: Von Hippel-Lindau E3; PHD: prolyl hydroxylase domain; HRE: hypoxia response element

1.8.4 Expression of HIF-1 and HIF-2 and their roles in disease

Cells and organs need to adapt to changes in oxygen supply. HIF pathway has been linked to the embryonic development and pathophysiology of numerous human diseases. Activation of HIF-1α is the most recognised mechanism to influence the expression of target genes in a tissue-specific manner. For example, HIF-1α influences erythropoiesis and glucose transporters, which is related to the capacity of oxygen transportation and glycolytic pathway, respectively (Semenza et al., 1991). For angiogenesis and VSMC proliferation, vascular endothelial growth factor (VEGF) is the most prominent HIF-1α target gene (Forsythe et al., 1996). Deletion of the HIF-1α resulted in abnormal vascular development and lethality in mice. Moreover, genes coding for iNOS (NO production) (Palmer et al., 1998), heme oxygenase 1 (HO-1) (carbon monoxide (CO) production) (Lee et al., 1997), and endothelin 1 (vascular tone) (Hu et al., 1998) are also targeted by HIF-1α to influence the vascular tone. Interestingly, the HIF-1α overexpression has been detected in various human cancers and thought to be involved in tumour size and metastases. The association between HIF-1α overexpression and overall patient survival, mortality, recurrence/ disease-free survival, or distant-metastasis-free survival has been observed in several studies (Semenza, 2003; Ke and Costa, 2006).

In contrast to HIF-1α, the roles of HIF-2α in the pathogenesis of disease have not been extensively studied. The HIF-2α expression is highly expressed in vascular structures (Jain et al., 1998), but also is tissue-specific in the endothelium, liver, lungs, kidneys, heart, brain, and intestine (Wiesener et al., 2003). HIF-2α, like HIF-1α, regulates the hypoxia-target genes to influence several biological processes, such as erythropoiesis, stemness/self-renewal, cell proliferation,

apoptosis, invasion, redox homeostasis, and angiogenesis (Zhao et al., 2015). Although HIF-1α and HIF-2α are the master regulators of oxygen homeostasis, they have different and nonredundant functions during cellular development. HIF-1α participates in cell proliferation and migration during early angiogenesis, whereas HIF-2α plays a role in the remodelling and maturation of the microvasculature to control vascular morphogenesis (Befani and Liakos, 2018).

1.9 Aims of the study

Ca^{2+} homeostasis is essential for the normal function of cells. Although there is an increasing number of studies focusing on the function of Kv7 channels in SMCs in health and diseases (Haick and Byron, 2016), the effects of Kv7 channel activity on Ca^{2+} signalling have not been evaluated completely. When Kv7 channels are inhibited, this leads to depolarisation which in turn, may result in the opening of VGCCs and an increase in $[Ca^{2+}]_i$ levels. In addition, hypoxia can alter $[Ca^{2+}]_i$ levels and may contribute to the disturbance of Ca^{2+} homeostasis in cardiovascular and pulmonary disease. The pathological changes of VSMCs involve in the unbalanced modulation of Ca^{2+} signalling. We hypothesise that Kv7 channels might regulate the depolarising mechanisms responsible for $[Ca^{2+}]_i$ regulation and control of excitability and contractility of VSMCs. We further hypothesise that vasoactive hormones and hypoxia may target the Kv7-VGCC axis to modulate VSMC function. Accordingly, this was achieved by means of the following objectives:

1. To investigate the effect of direct Kv7 inhibition or GPCR-mediated Kv7 inhibition on the $[Ca^{2+}]_i$ in VSMCs and test the relationships between Kv7 channels, and VGCCs, PLC, and ER Ca^{2+} channels in VSMCs.

2. To characterise the effects of hypoxia on $[Ca^{2+}]_i$ and how the Kv7-VGCC axis is affected by the hypoxia in VSMCs.
3. To further investigate the role of Kv7s, L- and T-type VGCCs expression on $[Ca^{2+}]_i$ response to hypoxia or chemical hypoxia by assessing gene expression changes in VSMCs.
4. To test the expression of Kv7 channel subunits and explore their role in $[Ca^{2+}]_i$ regulation in the primary human internal mammary artery (IMA) and saphenous vein (SV) SMCs.

Chapter 2

Materials and Methods

2.1 Cell cultures

2.1.1 Rat A7r5 cells

Rat A7r5 cells are SMCs derived from rat thoracic aorta. These cells are widely used as models of non-differentiated, neonatal and neointimal VSMCs in culture to determine the functionality of SMC in health and disease (Kimes and Brandt, 1976). The culture forms parallel arrays of spindle-shaped cells which display vascular smooth muscle differentiation features, including a unique repertoire of contractile proteins, such as smooth muscle α-actin and smooth muscle myosin heavy chain (Figure 2.1) (Duckles, 2013; Kennedy et al., 2014). A7r5 cells are prone to obtain different patterns of gene expression and protein regulation upon different conditions to provide a convenient model system to study Ca^{2+} channels and mechanisms of Ca^{2+} regulation (Gollasch et al., 1998).

They were obtained from the European Collection of Cell Cultures, and cultured in complete growth media, consisting of Dulbecco's Modified Eagle Medium (DMEM; Gibco Life Sciences, Paisley, Scotland, UK) supplemented with 10% Fetal Bovine Serum (FBS; Biosera, Ringmer, UK). Cells were cultured at 37°C in a humidified incubator with 95% air and 5% CO_2. Half of the media volume was changed every 3-4 days. A7r5 cells were passaged every 7 days from 75 cm^2 culture flasks as follows: the culture media was removed from the flasks using the aspirator and cells were washed with 10 ml Phosphate Buffered Saline (PBS).

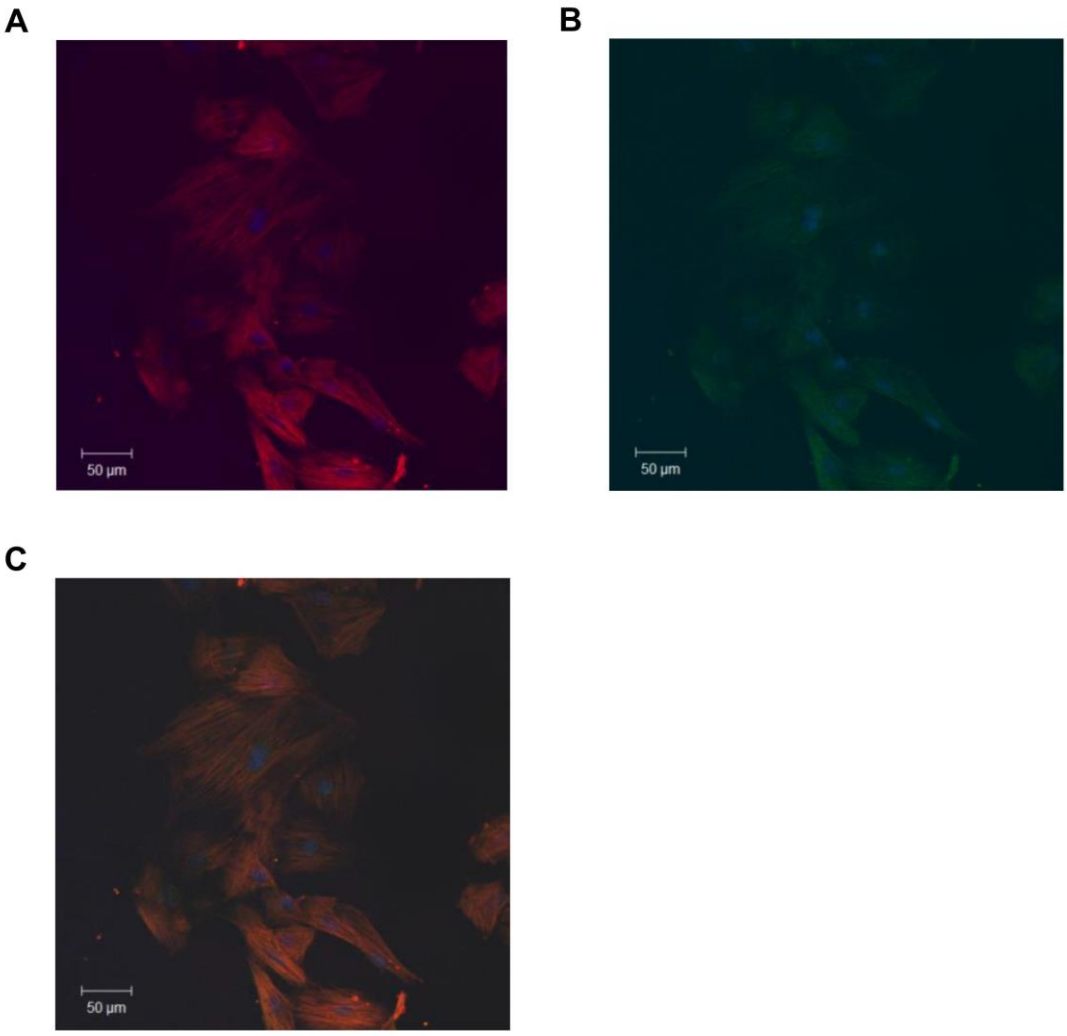

Figure 2.1 Immunocytochemistry of A7r5 cells. Simultaneous incubation with anti-smooth muscle α-actin (red; A) and anti-myosin heavy chain antibodies (green; B). Co-localisation of smooth muscle α-actin and myosin heavy chain (C). Adapted from (Duckles, 2013)

The PBS was replaced with 2 ml of 0.05% trypsin-EDTA (Gibco, Cambridge, UK) in the same flasks. After 4 minutes in a humidified incubator, cells were checked under a microscope to confirm the detachment from the surface. The cells were resuspended carefully with 10 ml of complete growth media to neutralise the trypsin in a 50 ml centrifuge tube and then centrifuged for 6 minutes at 600 g. After centrifugation, the supernatant was removed, and the cell pellet was resuspended in 5-10 ml of culture media (depending on the required density). Cells were used for up to 15 passages.

2.1.2 Human internal mammary artery and saphenous vein SMCs

Human VSMCs were isolated from the internal mammary artery (IMA) and saphenous vein (SV) of consented patients undergoing coronary artery bypass graft (CABG) surgical procedure; the cells were provided by Dr Karen E. Porter (Division of Cardiovascular and Diabetes Research, Faculty of Medicine and Health, University of Leeds, UK). All patients had coronary artery disease without other comorbidities. Specimens were transported to the laboratory under sterile conditions and immediately prepared for culture. Vessels were opened longitudinally after the removal of adventitia and endothelium. Segments of vessels were immersed in 2 ml of media (DMEM containing 10% FBS). Segments were then chopped into fragments around ~1 mm^2 in size. Fragments along with media were then transferred to a 25 cm^2 culture flask at 37°C in a humidified incubator with 95% air and 5% CO_2. Within 7-10 days, cells migrated out from the explants and, once confluent, the cells were passaged using 1 ml of 0.05% trypsin-EDTA into a 75 cm^2 flask. The culture media and process of passaging were the same as for rat A7r5 cells using the DMEM and 10% FBS. Half the

media was changed twice weekly. Human IMA and SV SMCs were used at passages between P3 and P6.

2.1.3 HEK293 cell culture and transfection

Human Embryonic Kidney 293 (HEK 293) cells were transfected with cDNA encoding human Cav3.2 (originally a gift from Prof. E. Perez-Reyes, University of Virginia, Charlottesville, VA, USA) and KCNQ5 (provided by Prof. Mark Shapiro, University of Texas Health Science Centre at San Antonio, Texas, USA) channel proteins for the control of western blotting. HEK293 cells were cultured to 80% confluency before passaging. Then, cells were plated in 24-well plate in growth medium consists of DMEM with penicillin (100 U/mL), streptomycin (100 µg/mL) and 10% FBS. On the day of transfection, FBS-containing media were pre-warmed to 37°C. FuGene HD transfection reagent (Promega, UK) and Molecular Biology Grade Water (ThermoFisher Scientific, UK) were used as the transfection solutions according to the manufacturer's instruction. In brief, 1.5 µl FuGene and 400 ng plasmid were added to transfection water with a final volume of 25 µl to mix. The mixture was left to stand at room temperature for 20 minutes. Media was removed from the selected wells, followed by replacement with 0.5 ml of fresh pre-warmed media, and transfection mixture was then added to the selected wells. The plate was incubated in a humidified incubator (37°C, 5% CO_2) for 24-48 hours before experiments.

2.2 Hypoxia

The cell suspension of rat A7r5 cells, human IMA or SV SMCs, was directly aliquoted into 25 cm^2 flasks for RT-PCR, onto glass coverslips in 24-well tissue

culture plates for microfluorimetry or plated on 6-well plates for western blotting. Once at 70-80% confluence, cells were either kept in the same way as the control cells, but 24 hours prior to experimentation, they were transferred to a humidified incubator equilibrated for the hypoxic condition (1.0% O_2 and 5.0% CO_2 balanced with N_2) or added 1 mM dimethyloxalylglycine (DMOG), prolyl hydroxylase inhibitor into the culture media (chemical hypoxia). Cells were re-exposed to room air for no longer than 1 hour before ribonucleic acid (RNA) purification, protein lysis or measurement of $[Ca^{2+}]_i$.

2.3 Western blotting

A7r5 cells used for western blotting were plated in 6-well plates. Post-treatment (hypoxia or DMOG incubation), then the culture media was removed, and cells were washed with PBS twice. Cells were then lysed with 200 µl lysis buffer containing EDTA-free Protease Inhibitor Cocktail (Sigma, UK; 1 tablet contains protease inhibitors sufficient for a volume of 10 ml extraction solution) per well. The cells were detached using mechanical trituration, and lysates were transferred into a clean 1.5 ml microcentrifuge tube and centrifuge at 16,000 g for 10 minutes at 4°C. Protein levels in the lysates were assessed using the Bradford method (Bradford, 1976). The cell lysate was incubated with Laemmli sample buffer (Bio-Rad) at 95°C for 5 minutes before the equal amount of protein (50 µg/well) was loaded into the wells of the SDS-PAGE gels (4-20% Mini-PROTEAN® TGX™ Precast Protein Gels). Electrophoresis was conducted at a voltage of 120V for 80 minutes. The proteins were transferred to a PVDF membrane using a semi-dry transfer method, and then PVDF was blocked in 5% non-fat dried milk powder (all Bio-Rad, UK) in buffer (52 mM Tris-HCl, 10 mM Tris

Base, 150 mM NaCl, 0.1 mM EDTA, 0.1% Tween-20) for 1 hour at room temperature. Membranes were then incubated overnight in a rocking incubator at 4°C with primary antibody followed by the corresponding anti-rabbit (or anti-mouse) secondary antibody at 1:1000 dilution incubation for 1 hour at room temperature. Protein targets were probed for using the antibodies listed in Table 2.1. Western blot development was carried out using the SuperSignal West Pico Chemiluminescent Substrate (ThermoFisher Scientific, UK) and the G-box camera system (Genesys, UK). The protocol for western blotting is summarised in Figure 2.2.

2.3.1 Quantification of western blots

The antibody specificity was confirmed using transfected (positive) or non-transfected (negative) HEK293 cells, as described in Section 2.1.3. The quantification of the western blots was analysed by densitometry with ImageJ to select and determine the background-subtracted density of the bands. The output was copied to Excel or GraphPad Prism version 7 (GraphPad Software, Inc.) for the band analysis. All densitometry values were normalised to β-actin (anti-Rabbit 1:1000; Cell Signaling).

2.4 Immunofluorescence

Immunofluorescence experiments were conducted by Frederick Jones (PhD student) and Zhongze Yuan (visiting medical student). The general protocol used for immunodetection in A7r5 cells was as follows, cells were plated onto 24-well culture plates containing circular glass coverslips (10 mm, thickness 0) and kept

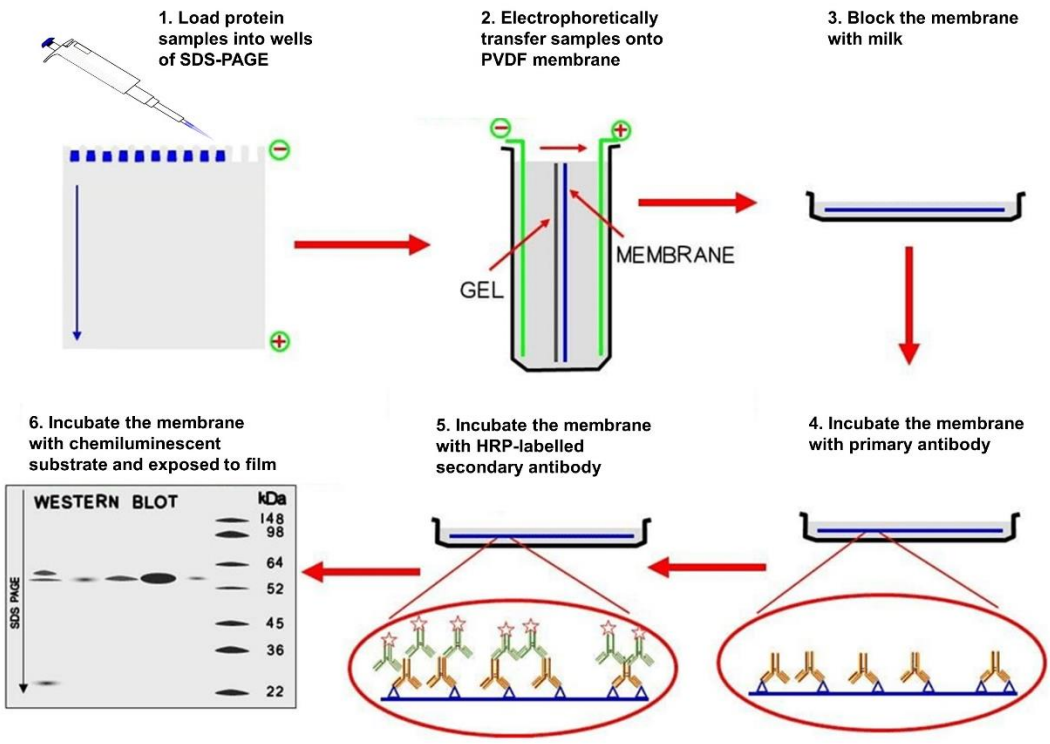

Figure 2.2 General protocol for western blotting. Western blotting is a method to detect and identify individual proteins. A mixture of proteins is separated based on molecular weight and then transferred to a membrane producing a band for each protein. The main steps in the whole process are sample preparation, electrophoretic transfer of samples, blocking, primary antibody incubation, secondary antibody incubation, and image detection. Modified from https://microbeonline.com/western-blot-technique-principle-procedures-advantages-and-disadvantages/

in a humidified incubator at 37°C in 95% air and 5% CO_2 until they reached about 50% confluency. Then some 24-well plates containing cells were kept under hypoxic conditions (1% O_2, 5% CO_2 and 94% N_2) or treated with a hypoxic mimic agent (DMOG) for 24 hours prior to the staining procedure. The cell layers were washed twice with PBS for 5 minutes at room temperature and then fixed by immersing in 4% paraformaldehyde (PFA, Sigma, UK) for 10 minutes. The fixed cells were washed three times with PBS and then blocked by immersing in 5% normal donkey serum in PBS containing 0.05% Tween 20 and 0.25% Triton X-100 for 30 minutes to permeabilise the cells. Blocking buffer was removed prior to the addition of primary antibody and slices were then treated with the primary antibodies against Kv7.1-5 and Cav3.2 (Table 2.1) for 1 hour 15 minutes. The cells were washed three times with PBS and incubated for 2 hours in the dark with the secondary antibody solution (1:1000 dilution) (Table 2.1). Cells were then washed three times with PBS and mounted onto glass microscope slides. DAPI (4′,6-diamidino-2-phenylindole) was used in the mounting medium (Vectashield) to stain the cell nuclei. Cells were imaged using inverted confocal microscope LSM880 (Zeiss) with a 40x objective at wavelength 405 (DAPI) and 555 (antibody). Zeiss Zen software and Fiji ImageJ software were used to produce and analyse images.

2.4.1 Quantification of immunofluorescence

Quantification of the immunofluorescence was analysed by the fluorescence intensity with Fiji ImageJ to outline cells and measure the background-subtracted fluorescence within the region of interest (ROI). An adjacent cell-free region was selected as the background. The output was copied to Excel for the intensity analysis.

Table 2.1 Primary and secondary antibodies used in western blotting and immunofluorescence experiments

	Anti-KCNQ1 (Santa Cruz, SC-365186)	Anti-KCNQ2 (Santa Cruz, SC-271852	Anti-KCNQ3 (Alomone, APC-051)	Anti-KCNQ4 (Neuromab, 75-082)	Anti-KCNQ5 (Abcam, ab19319	Anti-KCNQ5 (Millipore, AB5599)	Anti-Cav3.2 (Alomone, ACC-025)
Poly/ Monoclonal	Mouse Monoclonal	Mouse Monoclonal	Rabbit Polyclonal	Mouse Monoclonal	Rabbit Polyclonal	Rabbit Polyclonal	Rabbit Polyclonal
Western Blotting Dilution	N/A	N/A	N/A	N/A	N/A	1:500	1:500
Western blotting Secondary Antibody	N/A	N/A	N/A	N/A	N/A	Anti-Rabbit HRP-linked (Cell Signaling, UK)	Anti-Rabbit HRP-linked (Cell Signaling, UK)
Immunofluorescence Dilution	1:500	1:500	1:500	1:200	1:500	N/A	1:200
Immunofluorescence Secondary Antibody	Donkey anti-mouse 555 (Thermo Fisher Scientific, UK)	Donkey anti-mouse 555 (Thermo Fisher Scientific, UK)	Donkey anti-rabbit 555 (Thermo Fisher Scientific, UK)	Donkey anti-mouse 555 (Thermo Fisher Scientific, UK)	Donkey anti-rabbit 555 (Thermo Fisher Scientific, UK)	N/A	Donkey anti-rabbit 555 (Thermo Fisher Scientific, UK)

2.5 Fluorescence imaging

2.5.1 Fura 2-AM Ca^{2+} imaging

Fura 2-AM (ThermoFisher Scientific, UK) was used as the $[Ca^{2+}]_i$ indicator for the microfluorimetry experiments. This Ca^{2+} fluorescent probe is an acetoxymethyl (AM) ester which is a cell membrane-permeable derivative of the calcium chelator Fura2. Like other AM dyes, Fura 2-AM is sufficiently hydrophobic and, thus, membrane permeable to be passively loaded into cells. When inside the cells, the intracellular esterase cleaves the AM ester group and ensure the dye remains inside the cell. Fura2 is a ratiometric dye which can bind Ca^{2+} ion with the sensitivity ranging from ~100 nM to ~100 µM (Paredes et al., 2008). The UV light-excitable dye has two excitation wavelengths (340 nm and 380 nm) while maintaining a fixed emission wavelength at 510 nm. In the presence of higher $[Ca^{2+}]_i$, peak Fura2 fluorescence (at 510 nm emission) is observed at a wavelength of ~340 nm and in lower $[Ca^{2+}]_i$ conditions at ~380 nm. Therefore, changes in $[Ca^{2+}]_i$ can be expressed as changes in the ratio of the fluorescence at 340 and 380 nm (Grynkiewicz et al., 1985). Figure 2.3 shows the fluorescence excitation spectra for Fura2. When Fura2 is excited at 340 nm, an increase of Ca^{2+} concentration cause a rise in fluorescence emission at 510 nm, whereas when indicator dye is excited at 380 nm, a decrease of the Ca^{2+} concentration causes a rise in fluorescence emission at 510 nm. The wavelength shifts from 340 nm to 380 nm while Ca^{2+} bound state of the dye moves to a Ca^{2+} free state. The simultaneous changes in absorption spectra and ratiometric property of Fura2 result in a more reliable measurement of Ca^{2+} concentration. The use of ratiometric fluorescence (compared to absolute fluorescence intensity) is also key to avoid issues of different loading and illumination intensity. Greater uptake

of the dye also aids to reduce artefactual information by accounting for any differences in cell thickness, loading or loss of dye, and photobleaching (Becker and Fay, 1987). Therefore, the simplicity and sensitivity of using Fura2 allow data from different experiments to be compared and correlate directly to $[Ca^{2+}]_i$ (Paredes et al., 2008).

Given this, Ca^{2+} concentration can be measured by the Fura2 ratio using the equation presented by Grynkiewicz *et al.* (Grynkiewicz et al., 1985).

$$[Ca] = K_d (R - R_{min} / R_{max}-R) (S_{f2} / S_{b2})$$

Where:

[Ca] is the calcium concentration

K_d is the effective dissociation constant for Fura2, which is the $[Ca^{2+}]_i$ when the concentration of Ca^{2+} bound and free Fura2 are equal.

R is the Fura2 ratio defined as the fluorescence intensity induced by λ_1, (F_1, 340 nm) divided by the fluorescence intensity induced by λ_2 (F_2, 380 nm).

R_{min} = 340/380 ratio when the $[Ca^{2+}]$ is 0.

R_{max} = 340/380 ratio when $[Ca^{2+}]$ is a maximum or much higher than K_d.

S_{f2} is F_2 (380 nm) when Ca^{2+} is not bound to Fura2.

S_{b2} is F_2 (380 nm) when Ca^{2+} is fully bound to Fura2.

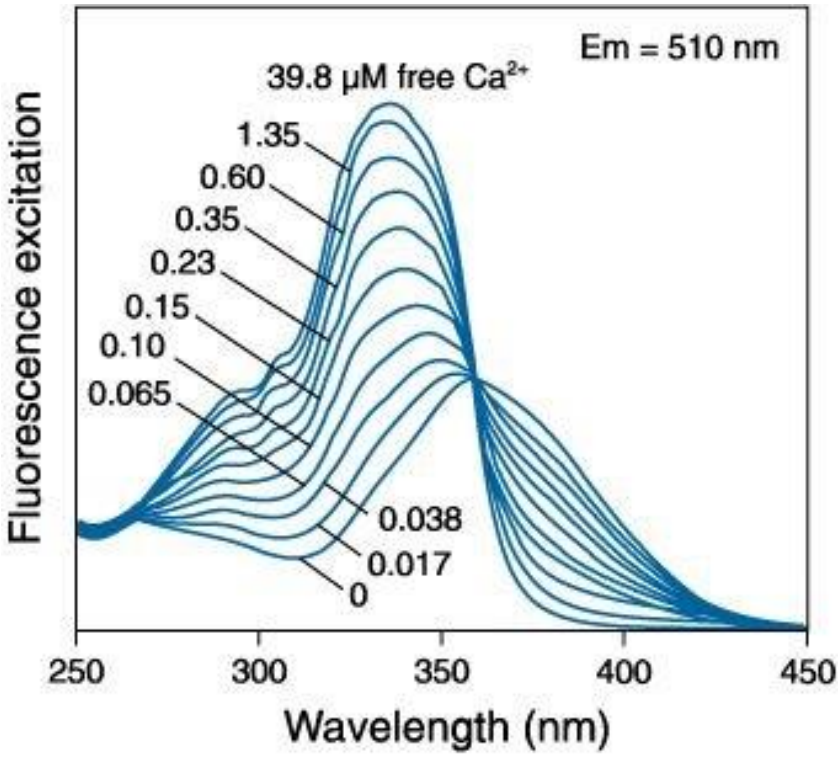

Figure 2.3 Fluorescence excitation spectra of Fura2 in solutions containing 0-39.8 µM free Ca^{2+}. Diagram taken from Fura 2-AM product information www.thermofisher.com

The technique is useful in combination with pharmacological agents to evaluate sources of intracellular or extracellular Ca^{2+} using Ca^{2+} mobilising drugs and receptors. The pattern of elevation in $[Ca^{2+}]_i$ and response to that elevation are associated with the agonist and cell types. However, there are some limitations to the accuracy $[Ca^{2+}]_i$ measurements with Fura2. For example, K_d is dependent on pH, temperature, the amount of Mg^{2+}, and other ions present (Paredes et al., 2008). Furthermore, issues associated with the indicator dye can also contribute to inaccuracies, such as the nonhomogeneous intracellular distribution of the indicator, and incomplete hydrolysis of Fura 2-AM can result in the inaccurate estimation of the $[Ca^{2+}]_i$. For these reasons, data obtained from experiments were expressed as ratio signals in this thesis.

2.5.2 Changes of $[Ca^{2+}]_i$ using the Cairn Photometry System

$[Ca^{2+}]_i$ of A7r5 cells, IMA and SV SMCs were measured microfluorimetrically. Cells were plated on circular glass coverslips (10 mm, thickness 0) in 24-well plates and kept in a humidified incubator (37°C; 95% air; 5% CO_2). Once the cell monolayer was confluent, the coverslips were transferred onto a 35 mm petri dish and washed with the Ca^{2+} containing buffer twice. Then, the cells were loaded with 4 μM Fura 2-AM (ThermoFisher Scientific, UK) dissolved in Ca^{2+} containing buffer without pluronic acid for 40 minutes in the dark at 37°C. The Ca^{2+} containing buffer was composed of (in mM) 135 NaCl, 5 KCl, 1.2 $MgSO_4$, 2.5 $CaCl_2$, 5 HEPES, and 10 glucose (pH7.4 with NaOH). The osmolality was adjusted to 300 mOsm with sucrose. After 40 minutes, the loading solution was pipetted out, and the cells were washed with 1 ml of Ca^{2+} containing buffer. Coverslips then incubated in Ca^{2+} containing buffer to allow for de-esterification of the Fura 2-AM for 10 minutes at 37°C in the dark.

After the incubation period, the coverslip was broken into fragments with a diamond pencil. Fragments of coverslips were then transferred to a perfusion chamber mounted on an inverted epi-fluorescence microscope with the appropriate buffer perfused at a rate of 2-3 ml/min. The perfusion system consisted of five 50 ml disposable syringes (Merck, UK), which acted as reservoirs connected to a 6-way manifold (Hamilton GB Ltd., UK) via lengths of Tygon tubing (2.5 mm outside diameter, 0.83 mm inside diameter; Merck, UK). Various compounds and drugs were applied to the perfusion chamber from the appropriate reservoir via the Hamilton manifold to investigate the changes of $[Ca^{2+}]_i$ modulated by Kv7 channels in VSMCs. The high K^+ solution needed for experiments were made with isotonic Na^+ substitution in the perfusate containing 50 mM K^+ (see specific results chapters for details). The perfusate was continuously removed from the chamber via a suction tube connected to a peristaltic pump (Gilson, Minipulse 3, Anachem, UK).

The cellular Ca^{2+} responses were recorded using a Cairn Research ME-SE Photometry system (Cairn Research, Faversham, UK). The fluorophore was excited by the energy produced from a Xeon Arc lamp. A monochromator was used to induce the alternating excitation at 340 to 380 nm fluorescence. Emitted fluorescence (510 nm) passed through the dichroic mirror onto the photomultiplier tube, which converted this light energy into electrical energy. The Cairn Optoscan was then used to analyse the data, and the Acquisition Engine 1.6.1 software was used to record the individual wavelength traces and the representing 340/380 nm ratio.

2.5.3 Analysis of microfluorimetry traces from VSMCs

After obtaining the traces via Cairn Photometry System, Graphing (in house program) and GraphPad Prism version 7 (GraphPad Software, Inc.) were used to plot and analyse the data. Changes in $[Ca^{2+}]_i$ (Δ ratio units F340/380) were calculated by subtracting the basal Fura2 ratio (A1) from the peak Fura2 ratio (A2) in each trace (Figure 2.4A). The number of spikes was counted and divided by the time period (in seconds) (T2-T1) to acquire the frequency of Ca^{2+} oscillations, which was expressed as spikes per second (spikes/s) (Figure 2.4B). Decay in spike frequency was in response to experimental drugs was measured, as shown in Figure 2.4C. Control spike frequency was measured from the onset of the first spike (F1; T2-T1). The drug effect on the spike frequency was calculated as frequency from the onset of the drug application and until the end of the drug's application (F2; T3-T2) (Figure 2.4C). The Graphing program was also used to calculate the integral (AUC: area under the curve) of the 50 mM K^+ buffer or agonist evoked transient Ca^{2+} responses in our experiments (Figure 2.4D). This method of quantification was chosen to account for variability in the kinetics of some responses. The results are shown as means ± stand error of the mean (S.E.M.) along with example traces in the following results chapters.

2.5.4 Imaging of membrane potential (E_m) using FluoVolt

Relative changes in plasma membrane potential (E_m) were measured using a FluoVolt voltage-sensitive dye kit (ThermoFisher Scientific, UK). FluoVolt can give a faster and brighter signal to measure relative changes in E_m (typically 25% per 100 mV) compared to commonly used optical dyes, such as Di-8-ANEPPS and RH237 (Park et al., 2013).

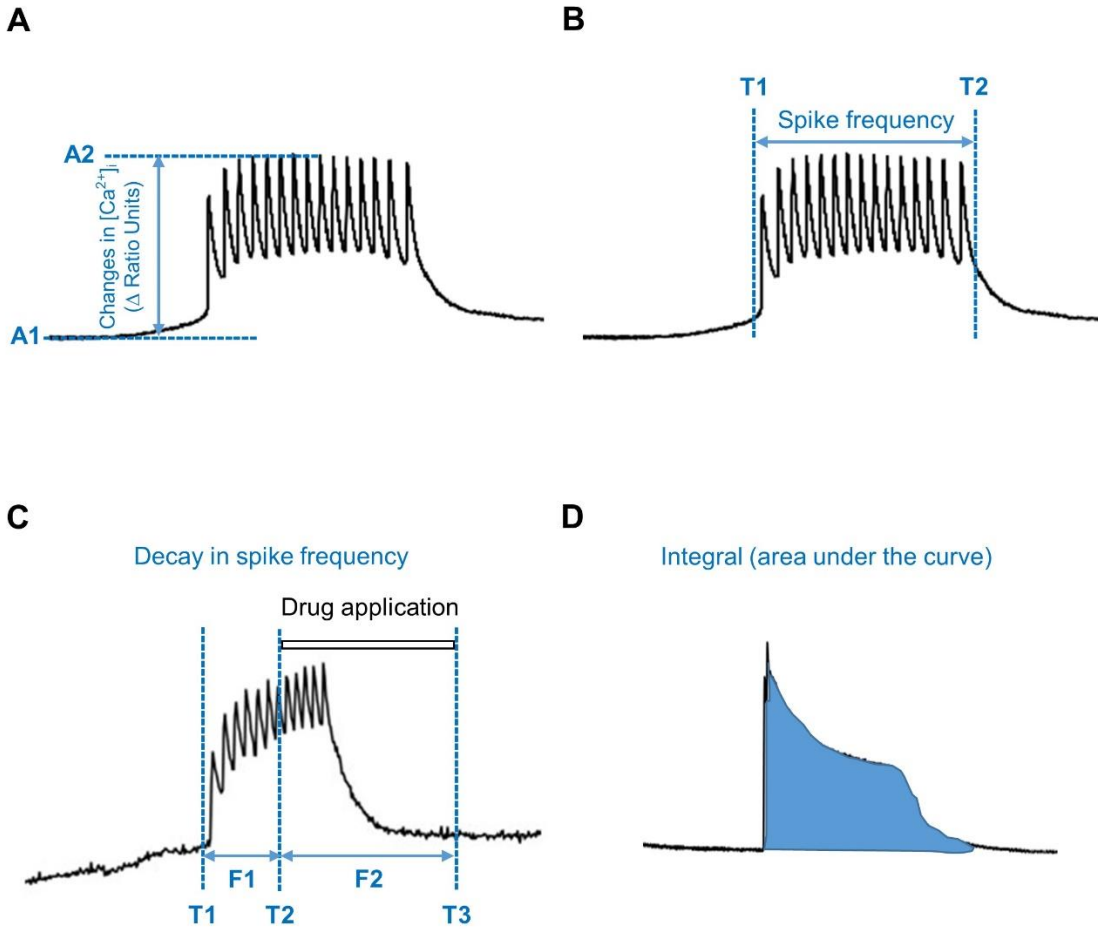

Figure 2.4 Analysis of Ca^{2+} microfluorimetry traces. Illustrating analysis parameters used for $[Ca^{2+}]_i$. (**A**) Demonstration of the change in $[Ca^{2+}]_i$ (Δ ratio units F340/380) (A2-A1). (**B**) Demonstration of how spikes per second were calculated (T2-T1). (**C**) Demonstration of decay effect (F2/F1). (**D**) Demonstration of how integrals were calculated the area under the curve.

Cells were plated in 24-well plates following the same procedure as described above for Ca^{2+} microfluorimetry (described in section 2.5.2). Cells were loaded with FluoVolt indicator dye in 2 ml of Ca^{2+} containing buffer supplemented with the dye (1:1000x), PowerLoad Concentrate (1:100x) and Background Suppressor (1:10x), for 30 minutes in the dark at 37°C. For simultaneous recordings of Ca^{2+} transients and action potentials, rat A7r5 cells were also loaded with the Fura 2-AM (Thermo Fisher Scientific, UK). Then, the loading solution was pipetted out, and the cells were washed with 1 ml of Ca^{2+} containing buffer. Fragments of coverslips were briefly placed in Cairn Photometry System (described in section 2.5.2) using a FITC filter cube, and cells were sequentially excited at 340, 380 and 488 nm (Fura 2-AM and FluoVolt loaded samples). Images were collected and quantified using the Cairn Optoscan and the Acquisition Engine 1.6.1. Data were analysed and plotted using Microsoft excel and Graph Pad Prism version 7 (GraphPad Software, Inc.). Changes of E_m were expressed as $\Delta F/F_0$ in cells. Analysis and correlation of dynamic fluorescence imaging data were performed with the help of Dr. Pierce Mullen with Python software.

2.6 Real-time polymerase chain reaction (RT-PCR)

The expression of genes coding for Kv7 and VGCC channels (Cav1 for L- and Cav3 for T-type) subunits in rat A7r5 cells was quantified via Real-Time Polymerase Chain Reaction (RT-PCR). This technique was then used to investigate the difference in mRNA expression of Kv7 and VGCC channel subunits between human IMA and SV SMCs. RT-PCR is the most sensitive technique for the detection and accurate quantification of gene expression.

This method is based on the detection of the fluorescence produced by fluorescently-labelled and gene-specific primers at particular thermal cyclers. The number of cycles required for the fluorescent signal to cross the threshold to detect a real signal (C_t) is used to calculate the initial template amount.

2.6.1 RNA generation

When cells grew to 70-80% confluence in 25 cm^2 culture flasks, they were washed with PBS and dissociated using 0.5 ml trypsin for 4 minutes (37°C; 95% air; 5% CO_2). Enzyme activity was stopped by adding 5 ml ice-cold PBS. The cell suspension was centrifuged at 600 g for 6 minutes, and RNA was generated from cell lysates using the Aurum Total RNA Isolation Protocol (Bio-Rad, Hemel Hempstead, UK). The supernatant was discarded, and lysis buffer (350 µl) was added to each cell pellet with pipetting up and down approximately 15 times. 70% ethanol (350 µl) (molecular biology grade, Sigma, UK) was then added, and the suspension mixed by pipetting up and down approximately 15 times. Each lysate was transferred to an RNA binding column and centrifuged (13,000 g for 30 seconds). Flow-through was discarded, and low-stringency wash solution (700 µl) was added before the centrifugation (13,000 g for 30 seconds). Again, flow-through was discarded, and RNAase-free DNAase I (80 µL) added to each column. The columns were further incubated at room temperature for 15 minutes and then centrifuged (13,000 g for 30 seconds). Flow-through was discarded, high-stringency wash solution (700 µl) was added, and the columns centrifuged (13,000 g for 30 seconds). Then, flow-through was again discarded, and low-stringency wash solution (700 µl) was added prior to the centrifugation (13,000 g for 1 minute). Again, flow-through was discard and the columns centrifuged again (13,000 g for a further 2 minutes). Then, each spin column was transferred to a

new elution tube, and elution buffer (80 µL, pre-warmed to 70°C) was added and columns were incubated at room temperature for 1 minute. The columns were then centrifuged (13,000 g for 2 minutes) to elute total RNA. If cDNA was not immediately generated, RNA samples were frozen at -80°C.

2.6.2 RNA quantification

The quantity and purity of RNA were measured using a NanoDrop 1000 spectrophotometer (ThermoFisher Scientific, UK), which measures the concentration of RNA in a sample using the light absorbance in the UV range. Sample (1-2 µL) was loaded to the measurement pedestal, and the purity was measured using the 260/280 nm absorbance ratio (Figure 2.5). The absorbance at 260 nm allows the calculation of the sample concentration (ng/uL). A 260/280nm ratio in the range of ~2.0 is generally accepted as “pure” RNA. A lower ratio indicates protein or phenol contamination; these samples were discarded.

2.6.3 cDNA generation

A cDNA template was generated from extracted RNA samples using the iScript cDNA Synthesis protocol (Bio-Rad, UK). Firstly, RNA samples and reagents were defrosted on ice. The amount of 20 µl reaction solution (Table 2.2) was transferred into a dome-capped PCR tube and placed in the 3Prime thermal cycler (Techne, UK). The program profile is 5 minutes at 25°C, 30 minutes at 42°C, 5 minutes at 85°C and holding at 4°C. Samples were then centrifuged and stored at -20°C.

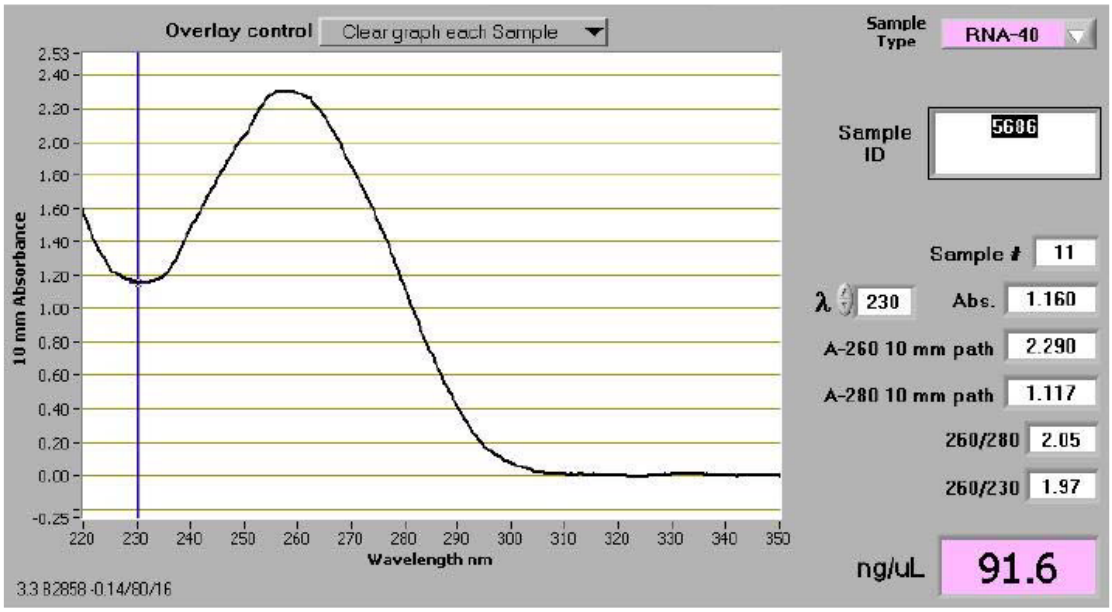

Figure 2.5 Example of a Nanodrop measurement. The quantity and purity of RNA were measured using a Nanodrop spectrophotometer. The graph shows a peak absorbance at 260 nm, which makes it the standard for quantitating nucleic acid samples.

Table 2.2 Composition of iScript reaction solution

Component	Volume per Reaction
5x iScript reaction mix	4 ul
Reverse Transcriptase	1 ul
RNA template (up to 1ug total RNA)	X ul
Nuclease-free water	X ul
Total Volume	20 ul

2.6.4 RT-PCR protocol

RT-PCR was conducted using TaqMan probes for Cav1.X, Cav3.X, KCNQ and the endogenous housekeeper gene hypoxanthine phosphoribosyltransferase 1 (HPRT1) (all from Applied Biosystems, UK). All samples consisted of 1 µl of cDNA and 19 µl of RT-PCR reaction mix (Table 2.3). Firstly, 19 µl of the RT-PCR reaction mix was added to a 96-well PCR plate, followed by 1 µl of sample cDNA in the same plate. The plate was then sealed with an optical adhesive cover and centrifuged briefly. Quantitative analysis of mRNA expression was carried out using a CFX Connect System (Bio-Rad, UK). The reaction profile was 2 minutes at 50°C, 10 minutes at 95°C, 15 seconds at 95°C and 1 minute at 60°C for 60 cycles. The probes used in the experiments are listed in Table 2.4. The rat and human gene sequences where aligned and tested for the similarity to confirm the use of human primers for the rat gene products.

Table 2.3 Composition of RT-PCR reaction mix

Component	Volume per Reaction
Taqman Universal PCR Master Mix (Applied Biosystems, UK)	10 µl
Taqman probes (Applied Biosystems, UK)	0.5 µl
DNase/RNase-free water (Qiagen, Germany)	8.5 µl
Total Volume	19 ul

Table 2.4 Primers used for RT-PCR analysis of mRNA expression

Rat Primer	Assay ID	Human Primer	Assay ID
Housekeeping gene			
Hprt1	Rn01527840_m1	*HPRT1*	Hs02800695_m1
L-type VGCCs			
Cacna1s	Rn01490941_m1	*CACNA1S*	Hs00163885_m1
Cacna1c	Rn00709287_m1	*CACNA1C*	Hs00167681_m1
Cacna1d	Rn01453395_m1	*CACNA1D*	Hs00167753_m1
Cacna1f	Rn00586734_m1	*CACNA1F*	Hs00913770_m1
T-type VGCCs			
Cacna1g	Rn01299126_m1	*CACNA1G*	Hs00367969_m1
Cacna1h	Rn01460348_m1	*CACNA1H*	Hs01103527_m1
Cacna1i	Rn01505208_m1	*CACNA1I*	Hs01096207_m1
Kv7 channels			
Kcnq1	Rn00583376_m1	*KCNQ1*	Hs00923522_m1
Kcnq2	Rn00591249_m1	*KCNQ2*	Hs01548339_m1
Kcnq3	Hs01120412_m1	*KCNQ3*	Hs01120412_m1
Kcnq4	Rn01518851_m1	*KCNQ4*	Hs00542548_m1
Kcnq5	Rn01512013_m1	*KCNQ5*	Hs01068536_m1

2.6.5 Analysis of RT-PCR data from VSMCs

All measurements were made in triplicate. Data were analysed using the CFX software (Bio-Rad, UK), and RNA abundance relative to the housekeeper gene HPRT1 was measured with ΔC_t and then calculated with $2^{-\Delta\Delta Ct}$ (Livak and Schmittgen, 2001). The amount of target, normalised to the endogenous control and relative to a calibrator is calculated as follows:

$RQ = 2^{-\Delta Ct}$

Where:

RQ is the relative quantification value of the target gene.

C_t is the number of cycles to cross the threshold for a target gene in samples.

ΔC_t is the difference of C_t values between target and reference gene (HPRT1).

The relative expression of mRNA levels to the housekeeper gene was expressed by multiplying $2^{-\Delta CT}$ by 100. Statistical analysis was conducted with GraphPad Prism version 7 (GraphPad Software, Inc.).

2.7 End-point PCR

End-point PCR was carried out to detect the expression of Kv7 channel and VGCC subtypes using 2.0% agarose gel electrophoresis with gels containing SYBR Safe DNA stain (Invitrogen, UK). Initially, the agarose was added in TAE (40 mM Tris, 20 mM Acetic acid, 1 mM EDTA) in a microwavable flask. The agarose was dissolved by pulsed microwave, and the agarose solution was cooled down to about 50°C. The SYBR Safe DNA stain (1:10,000x) was added in agarose solution. After mixing well, the agarose solution was poured into a gel tray with the well comb in place. Samples were prepared and mixed with loading buffer (Invitrogen, UK) and run along with a 100bp DNA molecular weight ladder (Invitrogen, UK). Gels were run using a horizontal electrophoresis unit (Bio-Rad, UK) with TAE buffer (1x), and the CCD camera system (Bio-Rad Gel Doc EQ System, UK) was used to capture images.

2.8 Compounds/chemicals

The chemical compounds used in experiments are listed in Table 2.5.

Table 2.5 Drugs used in experiments

Name	Concentration	Effect	IC_{50}/ EC_{50}/Reference
XE991	10 μM	Kv7 channel inhibitor	1-5 μM (Wang et al., 1998; Wang et al., 2000; Søgaard et al., 2001)
Bradykinin	250 nM	GPCR ligand (B2R); mobilises IP_3 Ca^{2+} stores; vasoactive agent	1 nM (Liu et al., 2010; Gamper and Shapiro, 2015; Kawaguchi et al., 2015)
Arginine vasopressin (AVP)	100 pM-300 nM	GPCR ligand (V1AR); mobilises IP_3 Ca^{2+} stores; vasoconstriction	0.24 nM (Brueggemann et al., 2007; Henderson and Byron, 2007; Gamper and Shapiro, 2015)
Retigabine	10 μM	Kv7 channels opener	7-14 μM (Iannotti et al., 2010; Jepps et al., 2013)
Nifedipine	2 μM	L-type Ca^{2+} channels blocker	55 nM (Scragg et al., 2007)
NNC 55-0396	3 μM	T-type Ca^{2+} channels blocker	7 μM (Huang et al., 2004).
Edelfosine	10 μM	PLC inhibitor	9.6 μM (Horowitz et al., 2005; Powis et al., 1992)
2-Aminoethyl diphenylborinate (2-APB)	100 μM	IP_3Rs inhibitor	42-50 μM (Maruyama et al., 1997; Mignen et al., 2005)
Tetracaine	100 μM	RyRs inhibitor	53.9 μM (Fauconnier et al., 2013)
Dimethyloxalyl-glycine (DMOG)	1 mM	Prolyl hydroxylase inhibitor (HIF-1α stabilisation and accumulation)	9.3 μM (Yuan et al., 2014; Sears et al., 2008; Epstein et al., 2001)
HIF-2α antagonist 2 (H2A)	20 μM	HIF-2α antagonist	0.3-10 μM (Dai et al., 2018; Scheuermann et al., 2013)

NNC 55-0396 and edelfosine were from Tocris Bioscience (UK), and all other chemicals were obtained from Sigma-Aldrich (UK). XE991, retigabine, nifedipine, and 2-Aminoethyl diphenylborinate were made up in dimethylsulphoxide (DMSO), and the final concentration of DMSO used did not exceed 0.1%. Figure legends in the results chapters provide more specific details.

2.9 Statistical analysis

Fura2 and RT-PCR results are expressed as means ± S.E.M. Data were tested for normality using the Shapiro-Wilk test for normality and the ROUT method (with Q set to 1%) to detect the outliers. Normally distributed data were analysed by the *t*-test or ANOVA with Sidak post hoc test, as appropriate. If the data did not satisfy the normality requirement, then Wilcoxon-Signed (paired comparison), Mann-Whitney (unpaired comparison) and Kruskal-Wallis ANOVA to compare more than 2 datasets (in conjunction with Mann-Whitney to compare individual datasets) were applied in the analysis. All data sets represent at least 3 independent preparation. *P* values less than 0.05 were considered to indicate a significant difference between the groups. Statistical analysis of biological repeats was performed using GraphPad Prism version 7 (GraphPad Software, Inc.).

Chapter 3

Role of Kv7 channels in control over intracellular Ca^{2+} dynamics in vascular smooth muscle cells

3.1 Introduction

Vascular tone is actively regulated by vasoactive stimuli which control the contractility of VSMCs. The main mechanisms of such control operate via the intracellular Ca^{2+} signals orchestrating the contraction. Thus, depolarisation of VSMCs membrane potential (E_m) results in the opening of L-type VGCCs (Moosmang et al., 2003), while activation of GPCRs can induce the release of Ca^{2+} from the SR/ER (Allbritton et al., 1992). Kv channels represent a primary effector system for adjusting the resting E_m in VSMCs and other cell types (Yuan, 1995; Evans et al., 1996). Some of these Kv channels are partially open in resting VSMCs and stabilise the resting E_m at negative voltages to prevent the opening of VGCCs. Inhibition of these Kv channels in VSMCs results in depolarisation which, in turn, may lead to VGCCs activation, and hence vasoconstriction (Tykocki et al., 2017). To date, the functional roles of some Kv channels in smooth muscle have been examined, especially the Kv1, Kv2 and Kv7 families (Stott et al., 2014; Lu et al., 2002; Mackie and Byron, 2008; Mani et al., 2013). Furthermore, several vascular diseases such as hypertension, diabetes and atherosclerosis were shown to be associated with the abnormal function or expression of Kv channels (Cox, 2005). Yet, the exact role of specific Kv channels in the intracellular Ca^{2+} dynamics and in the hormonal control of such dynamics has not been fully elucidated.

One Kv channel subfamily, Kv7/KCNQ channels, has attracted considerable attention for their role in the control of vascular tone (reviewed in (Greenwood and Ohya, 2009; Mackie and Byron, 2008)). Five members of the family (Kv7.1 to Kv7.5) are widely expressed in excitable and some non-excitable (e.g. epithelial) cells (Gamper and Shapiro, 2015). These channels have a very negative activation threshold (negative to -60 mV), slow kinetics and no inactivation, which allow them to exert a strong 'clamp' over the E_m of cells (Stott et al., 2014; Nelson and Quayle, 1995). Kv7.1 subunit is mostly expressed in cardiac and epithelial tissues while Kv7.2-Kv7.5 subunits were long considered to be mostly neuronal (Soldovieri et al., 2011), yet, recent evidence suggests that several Kv7 subunits express in VSMCs with Kv7.5 considered to be the major subunit (Brueggemann et al., 2007; Brueggemann et al., 2011). The activity of all Kv7 channels depends on the presence of PIP_2 in the plasma membrane, which is thought to stabilise the channel in the open state (Li et al., 2005; Suh and Hille, 2002; Zhang et al., 2003). Many GPCRs, including the receptors for vasoactive peptides vasopressin, angiotensin II and bradykinin, can inhibit Kv7 channels in a well-established signalling cascade which includes activation of PLC by $G\alpha_{q/11}$ G protein. PLC then hydrolyses PIP_2 to IP_3 and DAG, with the depletion of membrane PIP_2 being a major factor mediating the suppression of channel activity with other contributors being intracellular Ca^{2+} and PKC, reviewed in (Gamper and Shapiro, 2015; Hernandez et al., 2008). As a general rule, such receptor-mediated Kv7 channel inhibition depolarises the cell and can trigger action potential firing and contraction (Stott et al., 2014; Brueggemann et al., 2007; Chadha et al., 2014).

Arginine vasopressin (AVP) is a nonapeptide hormone synthesised in the hypothalamus, which is an essential regulator of the body's osmotic balance, blood pressure, sodium homeostasis, and kidney functioning (Barrett et al., 2007). In the vasculature, AVP acts the V1AR and induces vasoconstriction in VSMCs by increasing $[Ca^{2+}]_i$ via the influx of Ca^{2+} from L-type Ca^{2+} channels (Large, 2002). AVP is an effective therapy to treat patients with vasodilatory shock or intraoperative hypotension (Barrett et al., 2007) and elevated local AVP concentrations were shown to be involved with the maintenance of vasospasm (Mani et al., 2013). Kv7 channels have physiological roles in regulating vascular tone and vasoconstriction, including by being downstream targets of vasoactive hormones (Mackie and Byron, 2008; Greenwood and Ohya, 2009; Ng et al., 2011), which may result from the modulation of $[Ca^{2+}]_i$. Thus, a previous study demonstrated that a physiological concentration of AVP (100 pM) could suppress the Kv7.5 channel currents via PKC activation to depolarise E_m in A7r5 rat aortic SMCs (Brueggemann et al., 2007). On the other hand, retigabine, a Kv7 activator with anti-epileptic and analgesic properties (Stott et al., 2014; Rundfeldt, 1997), attenuated the basilar artery vasospasm in rats with subarachnoid haemorrhage (Mani et al., 2013).

Despite this growing evidence, a direct effect of Kv7 channel activity on $[Ca^{2+}]_i$ in VSMCs has not been systematically evaluated. Understanding the mechanisms controlling $[Ca^{2+}]_i$ in VSMCs could identify novel approaches for the treatment of cardiovascular disease, including pulmonary hypertension. In the present study, we examined the influence of Kv7 channel activity on $[Ca^{2+}]_i$ in A7r5 rat aortic SMCs.

3.2 Results

3.2.1 Contribution of L- and T-type VGCCs to depolarisation-induced Ca^{2+} transients in A7r5 cells

We reasoned that since Kv7 channels control the resting E_m of cells and because these channels are voltage-gated, they may exert a degree of control over the Ca^{2+} influx through the VGCCs. Thus, as a first step, we investigated the contribution of the most abundantly expressed VGCC isoforms to the depolarisation-induced Ca^{2+} influx in A7r5 rat VSMCs. Depolarisation was produced with perfusion with a 'High-K^+' solution, which was similar to the standard bath solution but 50 mM K^+ was added by the equimolar substitution of NaCl with KCl. Figure 3.1A shows an example of A7r5 cells response to 50 mM K^+ buffer: a rapid transient increase in $[Ca^{2+}]_i$ followed by a slow decline, presumably due to VGCCs inactivation and extrusion of Ca^{2+} from the cytosol by Ca^{2+} ATPases and/or Na^+/Ca^{2+} exchanger. A limited number of rapid oscillations was often observed during the transient. There was a slight but transient rise in $[Ca^{2+}]_i$ upon the removal of extracellular high K^+, suggesting the Ca^{2+} influx via Ca^{2+} channels within the cell membrane. SMCs mainly express L- and T-type VGCCs, while other isoforms are not significantly expressed (Catterall, 2011; Cribbs, 2006). Accordingly, nifedipine, L-type Ca^{2+} channel blocker (Striessnig et al., 2015) and NNC 55-0396, a structural analogue of mibefradil which selectively inhibits T-type Ca^{2+} channels (Li et al., 2005), suppressed the amplitude and the area under the curve (AUC) of high-K^+-induced $[Ca^{2+}]_i$ transients by 95.9 ± 2.3% (n=5) and by 85.0 ± 13.3% (n=5), respectively (Figure 3.1B, C). Co-application of both inhibitors completely abolished the high-K^+-induced Ca^{2+} transients, suggesting that L- and T-type channels account almost entirely for the Ca^{2+} influx (Figure 3.1D, E). Nifedipine-induced inhibition was somewhat stronger than that

produced by NNC 55-0396, but the effect did not reach statistical significance. Co-application of both inhibitors completely abolished the high-K^+-induced Ca^{2+} transients (Figure 3.1E).

These results suggest that both L- and T-type Ca^{2+} channels contribute to the depolarisation-induced Ca^{2+} influx in A7r5 cells. The additivity of the nifedipine and NNC 55-0396 effects perhaps arose from less than perfect selectivity. End-point PCR was carried out to detect and confirm the expression of channel subtypes, and RT-PCR was performed to evaluate the relative mRNA abundance of genes coding for L-type (*Cacna1s*, *Cacna1c*, *Cacna1d*, *Cacna1f;* coding for Cav1.1, Cav1.2, Cav1.3 and Cav1.4, respectively) and T-type (*Cacna1g*, *Cacna1h*, *Cacna1i*; coding for Cav3.1, Cav3.2 and Cav3.3, respectively) VGCC subunits. We found that *Cacna1c* (Cav1.2) L-type and *Cacna1g* (Cav3.1) T-type Ca^{2+} channel genes were the predominant subtypes in A7r5 cells (Figure 3.2A, B).

3.2.2 Kv7 channel inhibition induces Ca^{2+} oscillations linked to L- and T-type VGCCs activity

We next tested if Kv7 inhibition would depolarise VSMCs and trigger Ca^{2+} influx. Exposure of A7r5 cells to a specific Kv7 channel inhibitor, XE991 (10 µM), induced a sustained $[Ca^{2+}]_i$ elevation and evoked Ca^{2+} oscillations while the drug was present in the perfusate; both effects recovered upon XE991 washout (albeit with a delay of ~50 s; Figure 3.3A).

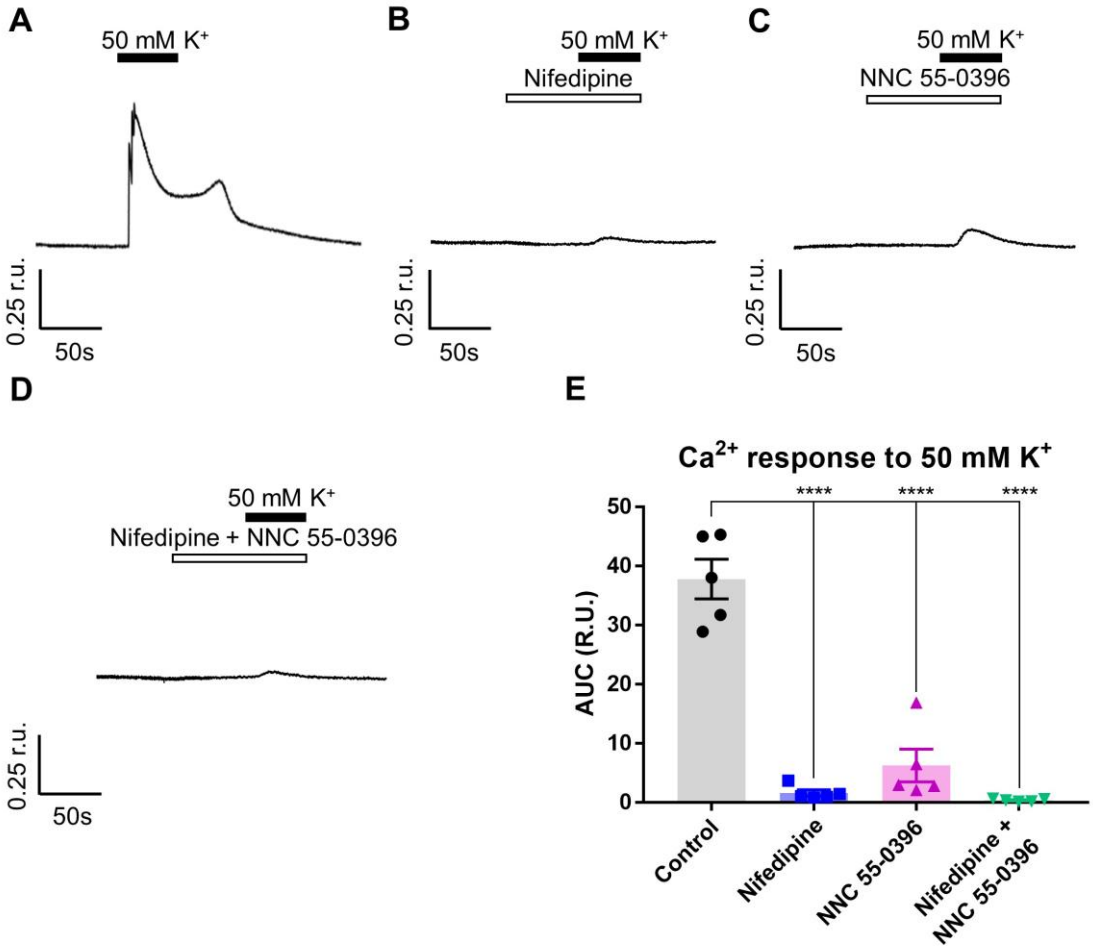

Figure 3.1 Contribution of L- and T-type VGCCs to depolarisation-induced Ca^{2+} transients in A7r5 cells. (**A**) Representative example trace showing rises in $[Ca^{2+}]_i$ evoked by depolarising cells with 50 mM K^+-containing buffer (the period indicated by the solid bar). (**B-C**) Example traces of high-K^+-induced Ca^{2+} transients recorded in the presence of L-type (nifedipine; 2 µM; B) or T-type (NNC 55-0396; 3 µM; C) Ca^{2+} channel blockers (as indicated). (**D**) Example trace of high-K^+-induced Ca^{2+} transients recorded in the presence of both nifedipine (2 µM) and NNC 55-0396 (3 µM) (as indicated). (**E**) Bar graph showing the mean AUC of the response to 50 mM K^+ buffer (control group represented in panel A) and cell groups in the presence of nifedipine or NNC 55-0396 (represented in panel B-D). In panel E data are presented as mean ± S.E.M.; Statistics performed using ANOVA with Sidak test, ****P<0.0001 (n=5).

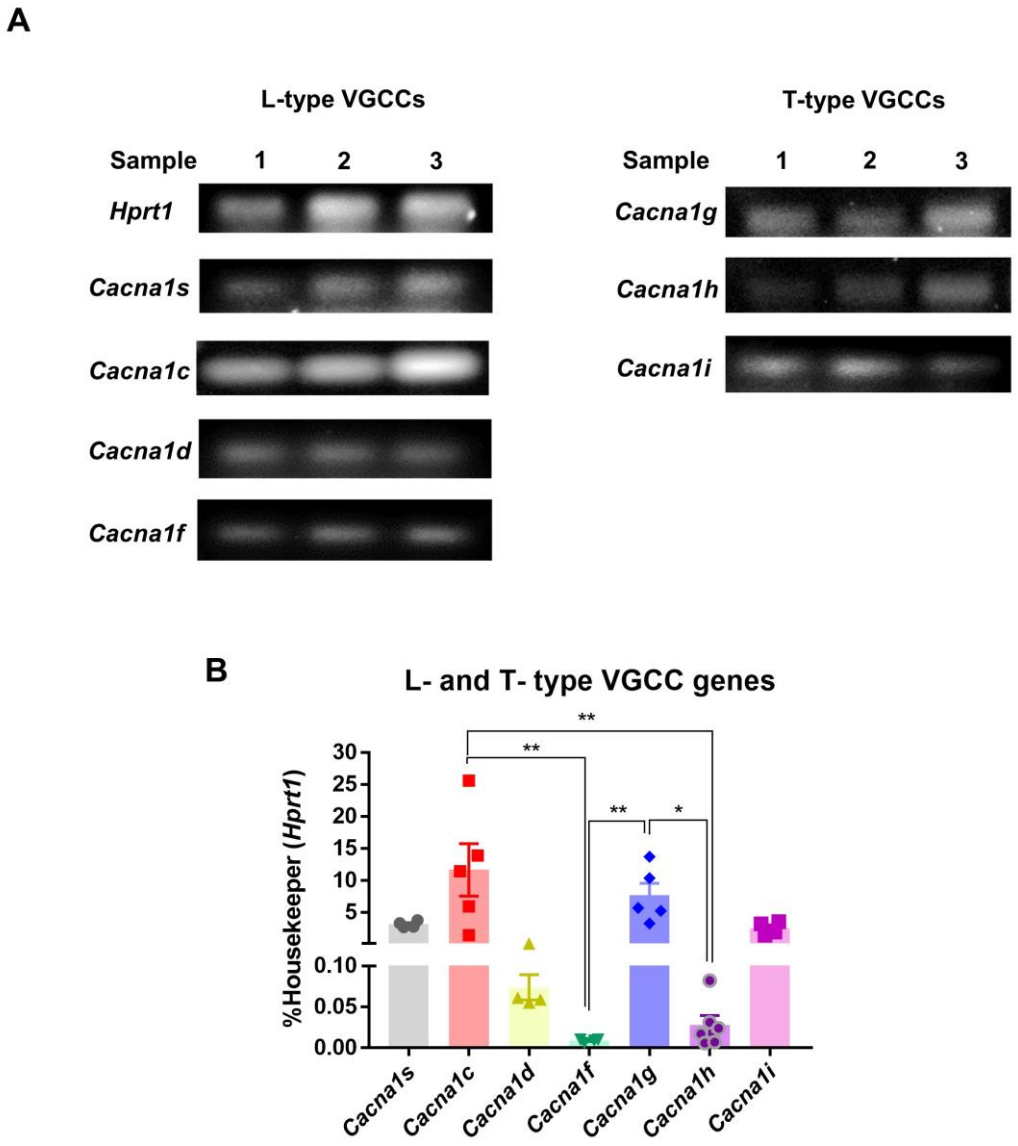

Figure 3.2 Cav1.2 L-type and Cav3.1 T-type Ca^{2+} channel genes are the predominant VGCC subtypes in A7r5 cells. (**A**) Agarose gels stained with SYBR safe to visualise the RT-PCR products corresponding to L-type (*Cacna1s*, *Cacna1c*, *Cacna1d*, *Cacna1f*) and T-type (*Cacna1g*, *Cacna1h*, *Cacna1i*) VGCCs genes. (**B**) Quantification of RT-PCR results exemplified in panel A, the expression is normalised to that of a housekeeping gene, *Hprt1*. In panel B data are presented as mean ± S.E.M.; Statistics performed using ANOVA with Sidak test, *P<0.05, **P<0.01 (n≥4).

Depolarisation with high-K^+ caused larger $[Ca^{2+}]_i$ elevation than these produced by XE991 (Figure 3.3B); the difference is likely to reflect the fact that high-K^+ application engages the entire repertoire of K^+ channels expressed, while XE991 only accounts for the contribution of Kv7 channels. We then tested if the Kv7 channel activator, retigabine, can offset XE991-induced Ca^{2+} signals by potentiating Kv7 channel currents and hyperpolarising the E_m away from the activation threshold of VGCCs (Main et al., 2000; Apostolova et al., 2017). Retigabine (10 µM) applied along with the XE991 promptly abolished the oscillations and lowered $[Ca^{2+}]_i$ back to the baseline (Figure 3.3C, 3.4A).

To test if the $[Ca^{2+}]_i$ increase and oscillations induced by XE991 required Ca^{2+} influx from the extracellular space via VGCCs, we used nifedipine and NNC 55-0396. In the first experiment, XE991 (10 µM) was applied first to induce oscillations, then nifedipine (2 µM) was applied in the continued presence of XE991. Nifedipine virtually abolished the oscillations and reverted $[Ca^{2+}]_i$ elevation induced by XE991 (Figure 3.3D, 3.4B). NNC 55-0396 produced qualitatively similar effects, but it took longer to block oscillations (Figure 3.3E, 3.4C). Retigabine, nifedipine and NNC 55-0396 effectively abolished Ca^{2+} oscillations (Figure 3.4). These data demonstrated that the XE991-induced $[Ca^{2+}]_i$ increase required Ca^{2+} entry via both L- and T-type Ca^{2+} channels.

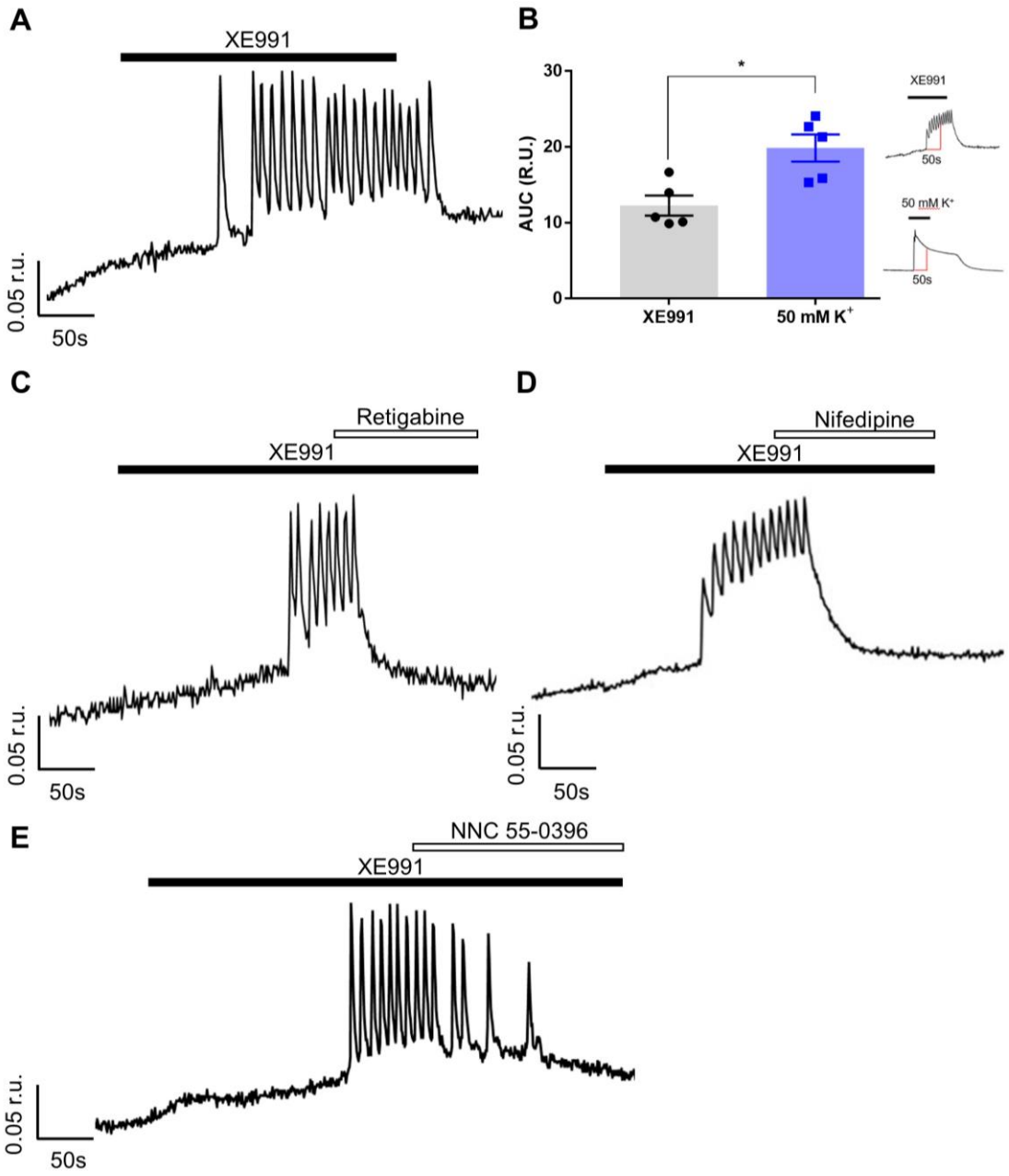

Figure 3.3 Kv7 channel inhibition induces Ca^{2+} oscillations linked to L- and T-type VGCCs activity. (**A**) Representative example trace showing Ca^{2+} oscillations evoked by Kv7 channel inhibitor, XE991 (10 µM). (**B**) Comparison of amplitude of Ca^{2+} signals induced by XE991 and 50 mM K^+, estimated as AUC during first 50s of stimulus application (corresponding to the duration of high-K^+ stimulation; exemplified in the inset on the right). (**C-E**) Example traces of XE991-induced Ca^{2+} transients recorded in the presence of Kv7 channel opener, retigabine (10 µM; C), nifedipine (2 µM; D) or NNC 55-0396 (3 µM; E) (as indicated). In panel B data are presented as mean ± S.E.M.; Statistics performed using paired student's t-test, *P<0.05 (n=5).

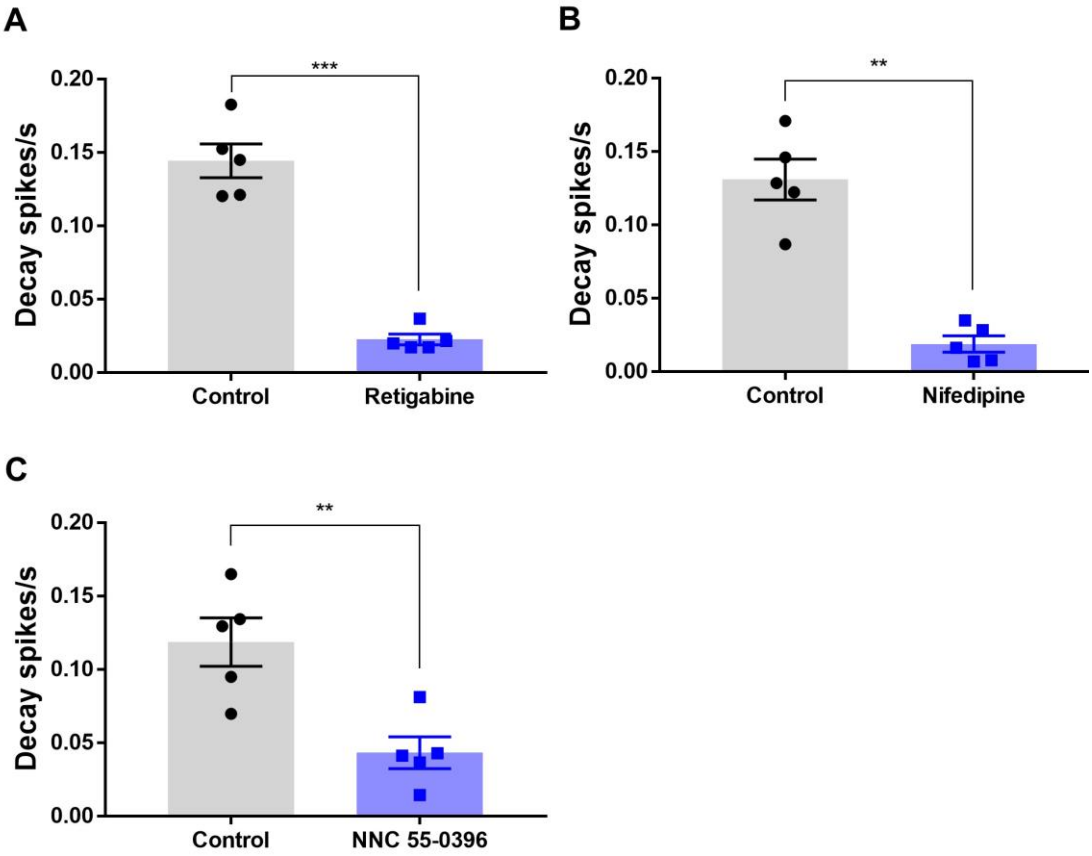

Figure 3.4 Retigabine and nifedipine abolish Ca^{2+} oscillations induced by XE991. (**A-C**) Bar graphs summarising the effects of retigabine (A), nifedipine (B) or NNC 55-0396 (C) on the XE991-induced Ca^{2+} spike frequency (spikes/s). Control is the spike frequency in the presence of XE991 measured from the onset of the first spike. For quantification of drug effect, spike frequency was calculated from the onset of the drug application and until the end of the application of XE991. In panels A-C data are presented as mean ± S.E.M.; Statistics performed using paired student's t-test, **P<0.01, ***P<0.001 (n=5).

We next asked what is the nature of $[Ca^{2+}]_i$ oscillations induced by XE991 - might these be induced by the depolarisation-induced action potentials? We loaded A7r5 cells with two fluorescent dyes: Fura2 for measuring Ca^{2+} levels and a voltage-sensitive dye FluoVolt (Miller et al., 2012) for measuring changes in membrane potential (E_m). We then performed a triple-wavelength (340, 380 and 488 nm) simultaneous recordings of $[Ca^{2+}]_i$ and E_m changes in response to XE991. Figure 3.5 displays temporally-aligned ratiometric Ca^{2+} trace (black) and FluoVolt E_m trace (red); XE991 induced slow E_m depolarisation followed by a burst of sharp spikes which were temporally well-correlated with $[Ca^{2+}]_i$ (Figure 3.5A). Peak cross correlation between the FluoVolt E_m and the ratiometric Ca^{2+} signal was 0.6 ± 0.18, occurring at a time lag of 3 ± 0.5 seconds (n=5) (Figure 3.5B). Both $[Ca^{2+}]_i$ oscillations and E_m spikes were abolished by retigabine.

We next investigated the expression of *Kcnq* genes in A7r5 cells with RT-PCR using selective primers for *Kcnq1-5* isoforms. We detected transcripts for *Kcnq1*, *Kcnq4* and *Kcnq5,* with *Kcnq5* being the most and *Kcnq1* the least abundant (Figure 3.6A, B). *Kcnq2* and *Kcnq3* transcripts were undetectable. Consistent with the RT-PCR results, we detected the expression of Kv7.5 and Kv7.4, but not Kv7.1-Kv7.3 in A7r5 cells using immunohistochemistry (Figure 3.6C); Kv7.5 was again found to be most abundantly expressed. However, these data were not statistically compared because the primary antibody affinities to their respective epitopes are not uniform and cannot be meaningfully normalised. This means that fluorescence intensities of labelling produced by antibodies against different proteins cannot be directly statistically analysed to deduce the relative abundance of corresponding proteins.

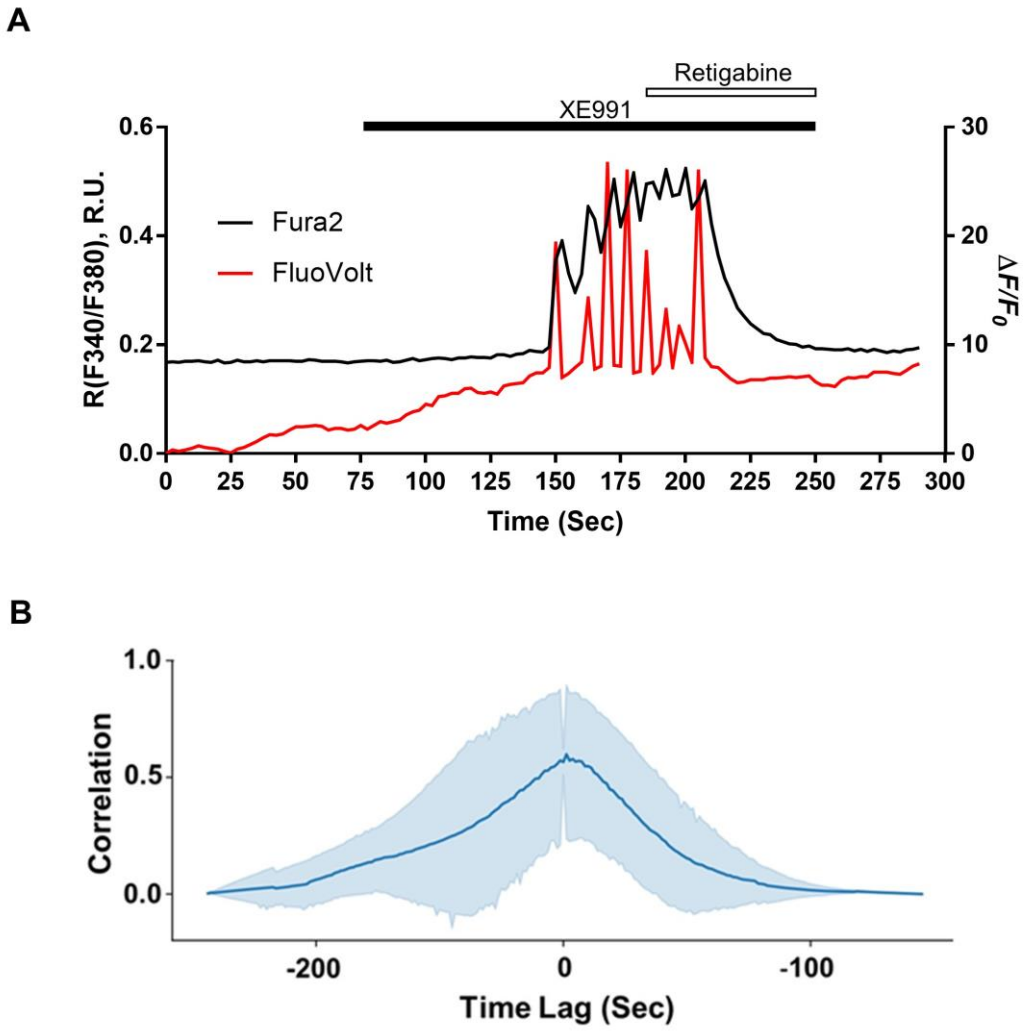

Figure 3.5 Retigabine attenuates XE991-induced Ca^{2+} oscillations and voltage spikes in A7r5 cells. (**A**) Representative example traces showing the superimposed Fura2 ratiometric Ca^{2+} recording (black) and FuoVolt membrane potential recording (measured as $\Delta F/F_0$; red) during application of XE991 (10 µM) and retigabine (10 µM) during periods indicated by horizontal bars. (**B**) Cross correlation of the normalised ratiometric Ca^{2+} signal with the normalised FluoVolt signal indicated the time lag between the signals at which the peak correlation occurred (n=5).

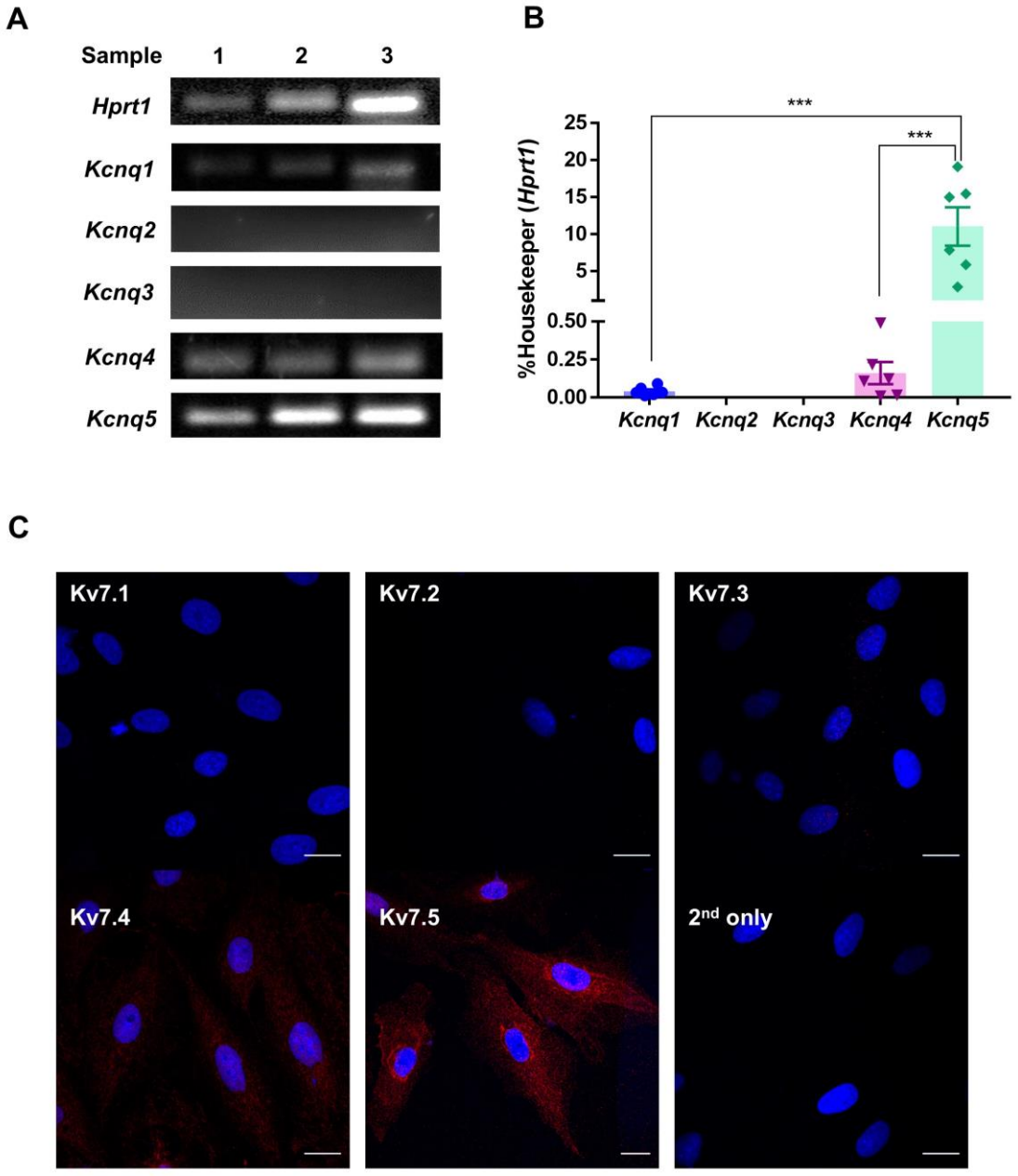

Figure 3.6 Expression of *Kcnq* genes and Kv7 proteins in A7r5 cells. (**A**) Agarose gels stained with SYBR safe to visualise the RT-PCR products of *Kcnq1*, *Kcnq2*, *Kcnq3*, *Kcnq4* and *Kcnq5*. (**B**) Quantification of RT-PCR results exemplified in panel A, the expression is normalised to that of a housekeeping gene, *Hprt1*. (**C**) Immunofluorescence labelling of Kv7.1-Kv7.5 channel subunits in A7r5 cells, scale bars are 20 µm. In panel B data are presented as mean ± S.E.M.; Statistics performed using ANOVA with Sidak test, ***P<0.001 (n=6).

The fact that *Kcnq5* was found to be the main *Kcnq* gene expressed in A7r5 cells is consistent with previous findings (Brueggemann et al., 2007) and explains good reversibility of the excitatory action of 10 µM XE991 with retigabine. Indeed, while Kv7.1-Kv7.4 channels are highly sensitive to XE991 with IC_{50}s in the range of 1-5 µM (Wang et al., 1998; Wang et al., 2000; Søgaard et al., 2001) and the Kv7.5 is much less sensitive with IC_{50} in the range of 60 µM (Schroeder et al., 2000). Thus, while currents conducted by Kv7.2/Kv7.3 channels are completely abolished by 10 µM XE991 (Wang et al., 1998), Kv7.5 is inhibited by just 40% at this concentration (Jensen et al., 2005).

3.2.3 AVP-induced Ca^{2+} oscillations can be abolished by Kv7 channels activator or L- and T-type VGCCs blockers

To investigate if the control over the E_m and $[Ca^{2+}]_i$ exerted by the Kv7 channels in VSMCs is relevant for the hormonal regulation of vascular tone, we used AVP (100 pM), which has been reported to inhibit KCNQ currents (Brueggemann et al., 2007). AVP is a hormone with a prominent vasoconstrictor effect, which acts in the vasculature via the primary receptor, V1AR. This receptor belongs to the $G_{q/11}$ type of GPCRs which act via the PLC pathway (Large, 2002). Exposure to AVP induced slow $[Ca^{2+}]_i$ elevation followed by a period of repetitive Ca^{2+} oscillations lasting throughout the AVP application; washout of the AVP was followed by a gradual return to the baseline (Figure 3.7A). Retigabine promptly abolished AVP-induced Ca^{2+} oscillations and reverted the elevated $[Ca^{2+}]_i$ to the baseline (Figure 3.7B, 3.8A).

To test the contribution of L- and T-type Ca^{2+} channels to the AVP-induced Ca^{2+} oscillations, we used nifedipine and NNC 55-0396. In the presence of nifedipine, AVP-induced Ca^{2+} oscillations were rapidly stopped, and the $[Ca^{2+}]_i$ returned to the basal level (Figure 3.7C, 3.8B). In the presence of NNC 55-0396, AVP-induced Ca^{2+} oscillations were often gradually stopped in a time-dependent manner, but the oscillation frequency in the presence of NNC 55-0396 did not reach the significance, as compared to AVP applied alone and delayed oscillations are observed in some cases (Figure 3.7D, 3.8C). Of note was also a considerable range of response times to AVP – i.e. the time it took for oscillations to occur varied within 250 s to 550 s (Figure 3.7A vs. D). Although the effect of three compounds was effective to inhibit AVP-stimulated Ca^{2+} oscillations, retigabine and nifedipine were the strongest to abolished Ca^{2+} oscillations (Figure 3.8).

We also performed triple-wavelength simultaneous recordings of $[Ca^{2+}]_i$ and E_m changes in response to AVP (Figure 3.9). Similar to XE991, AVP induced slow E_m depolarisation followed by a burst of sharp spikes which were temporally well-correlated with $[Ca^{2+}]_i$ (Figure 3.9A); peak cross correlation between the FluoVolt E_m and the ratiometric Ca^{2+} signal was 0.84 ± 0.01, occurring at a time lag of 2.5 ± 1.4 seconds (n=4) (Figure 3.9B). These $[Ca^{2+}]_i$ oscillations and E_m spikes were abolished by retigabine. Collectively, these data indicate that Kv7/KCNQ channels are present and functional in A7r5 cells and that treatment with a physiological concentration of AVP (100 pM) leads to depolarisation and Ca^{2+} influx through both L- and T-type Ca^{2+} channels; these effects were abolished by retigabine and were qualitatively very similar to these produced by the XE991.

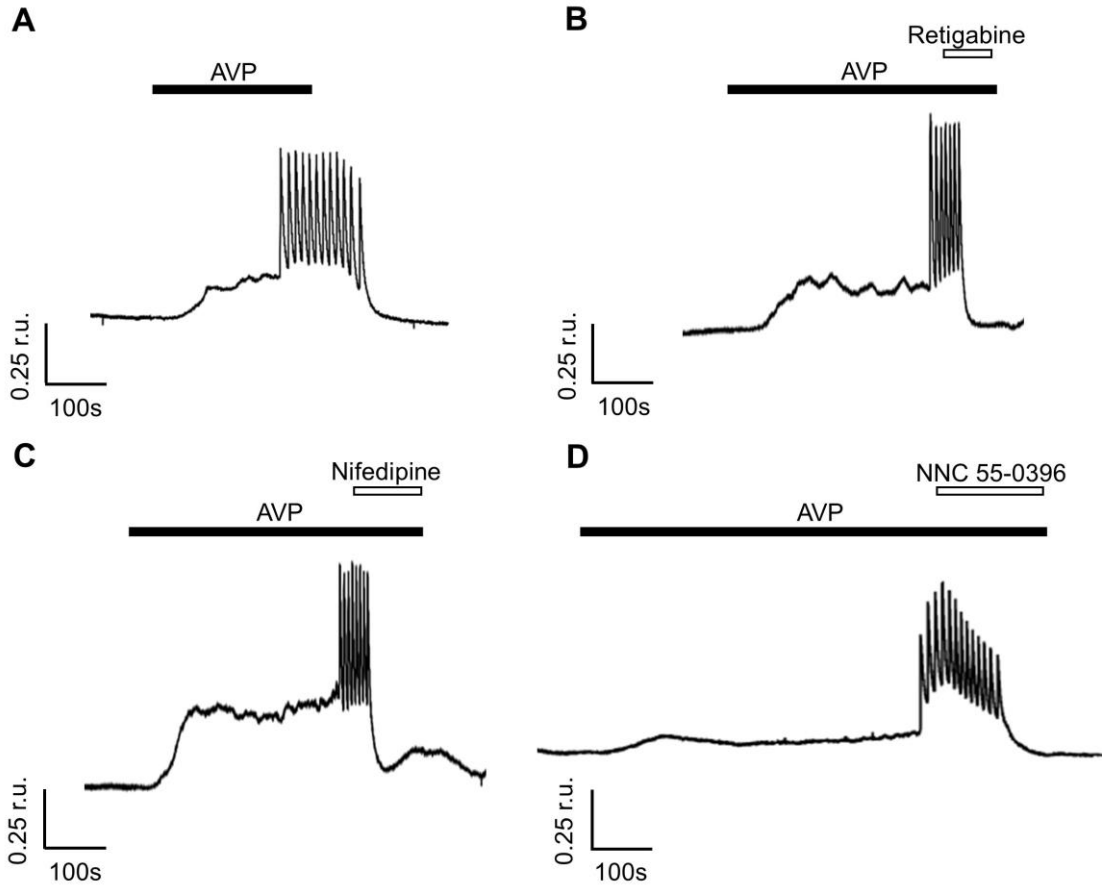

Figure 3.7 AVP-induced Ca^{2+} oscillations can be abolished by Kv7 activator, L- and T-type VGCCs blockers. (**A**) Representative example trace showing Ca^{2+} oscillations evoked by the physiological concentration of the vasoactive hormone, vasopressin (AVP; 100 pM) in A7r5 cells. (**B-D**) Example traces of AVP-induced Ca^{2+} transients recorded in the presence of retigabine (10 μM; B), nifedipine (2 μM; C) or NNC 55-0396 (3 μM; D) (as indicated).

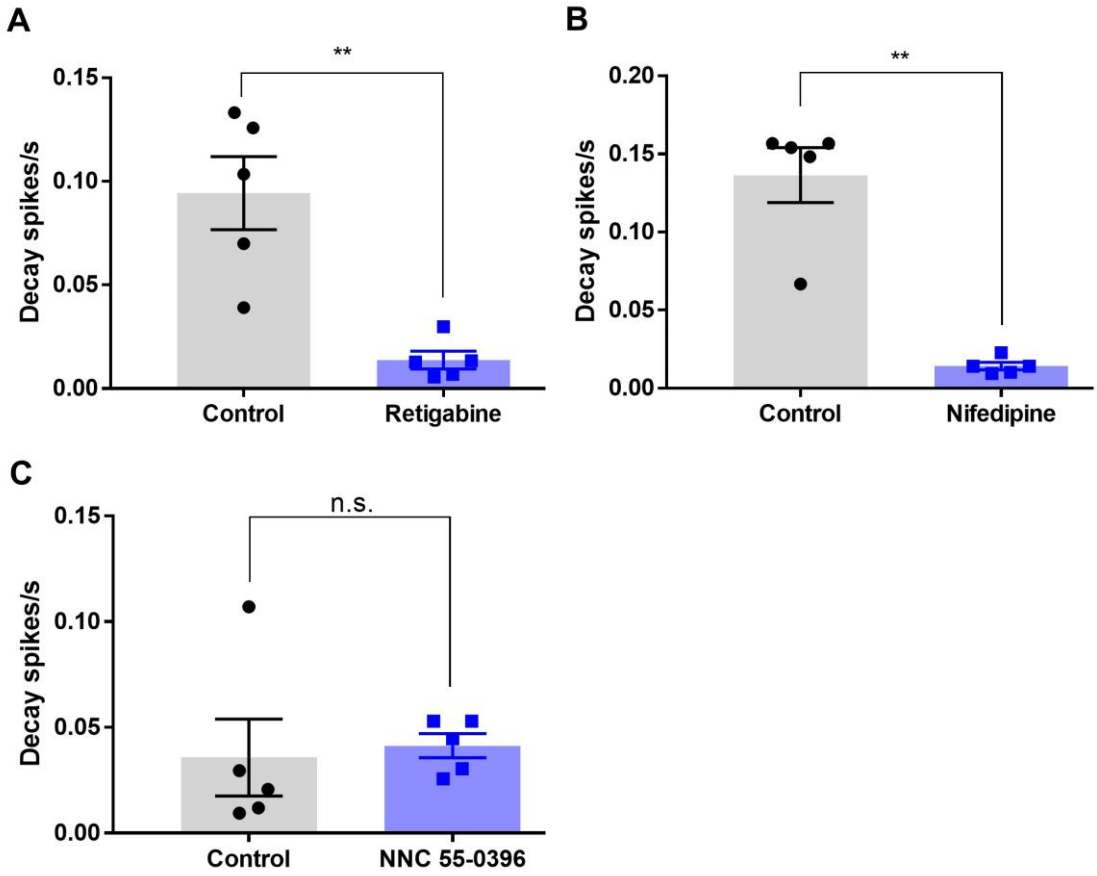

Figure 3.8 AVP-induced Ca^{2+} oscillations can be abolished by Kv7 activator, L- and T-type VGCCs blockers (continuing). (**A-C**) Bar graphs summarising the effects of retigabine (A), nifedipine (B) or NNC 55-0396 (C) on the AVP-induced Ca^{2+} spike frequency (spikes/s). Control is the spike frequency in the presence of AVP measured from the onset of the first spike. For quantification of drug effect, spike frequency was calculated from the onset of the drug application and until the end of the application of AVP. In panels A-C data are presented as mean ± S.E.M.; Statistics performed using paired student's t-test, n.s., not significant, **P<0.01 (n=5).

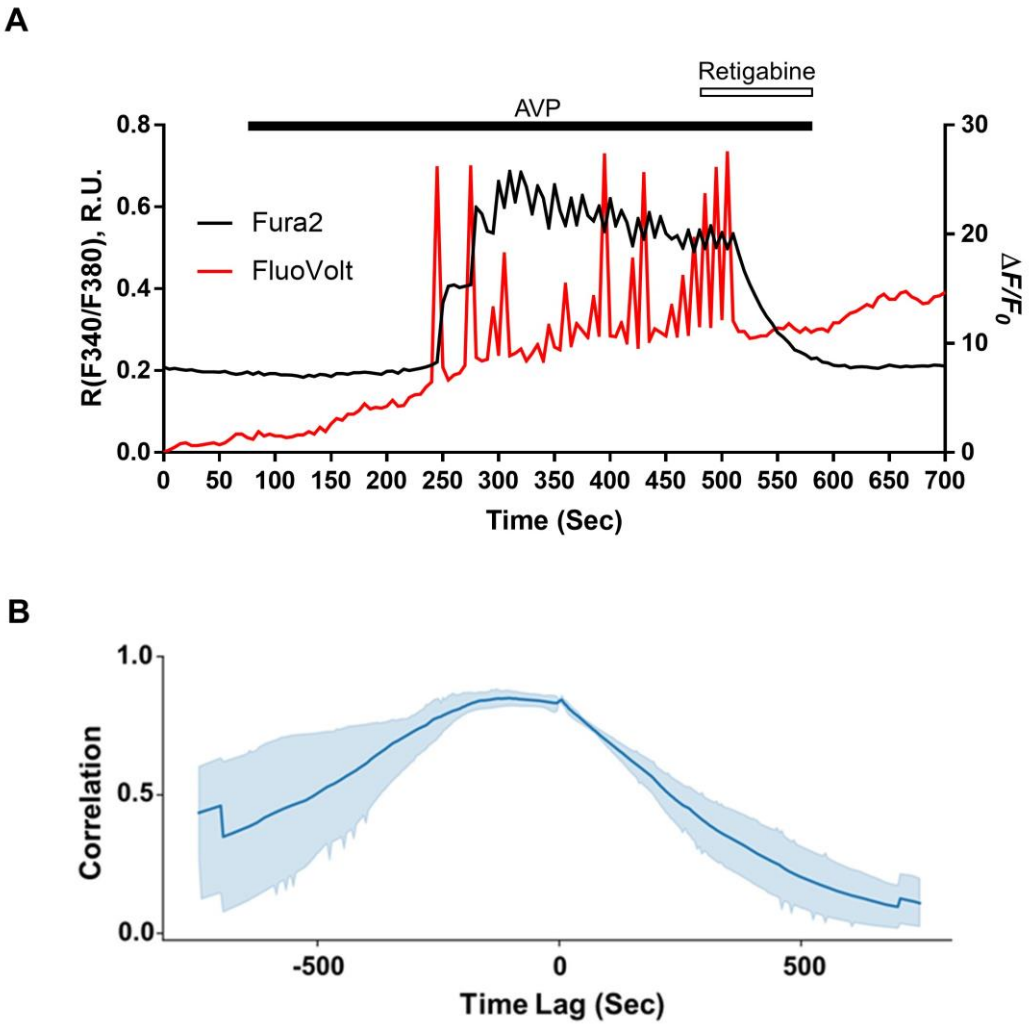

Figure 3.9 Retigabine attenuates AVP-induced Ca^{2+} oscillations and depolarisation in A7r5 cells. (**A**) Representative example traces showing the superimposed Fura2 ratiometric Ca^{2+} recording (black) and FluoVolt membrane potential recording (measured as $\Delta F/F_0$; red) during application of AVP (100 pM) and retigabine (10 µM) during periods indicated by horizontal bars. (**B**) Cross correlation of the normalised ratiometric Ca^{2+} signal with the normalised FluoVolt signal indicated the time lag between the signals at which the peak correlation occurred (n=4).

3.2.4 AVP-induced Ca^{2+} oscillations are reduced by inhibition of PLC and ER Ca^{2+} release channels

Even though both XE991 and AVP produced very similar effects on $[Ca^{2+}]_i$ and E_m, suggesting a common mechanism, a Kv7 channel inhibition, the action of these two agents on the Kv7 channels is different. While XE991 is a direct ion channel blocker, the action of AVP on the Kv7 channels depends on the PLC-mediated signalling cascade, which inhibits Kv7s by a combination of PIP_2 hydrolysis, PKC activation and ER Ca^{2+} release (Gamper and Shapiro, 2015). Edelfosine is a PLC inhibitor that is used as a test for the involvement of PLC in a signalling pathway (Horowitz et al., 2005). Ten minutes of pretreatment of A7r5 cells with edelfosine (10 µM) attenuated the $[Ca^{2+}]_i$ response to AVP (100 pM) in A7r5 cells (Figure 3.10A). There was a marginally significant difference (p=0.051) in peak Ca^{2+} levels between the control (untreated) and edelfosine-treated groups (Figure 3.10B). There were some occasional Ca^{2+} spikes, but the Ca^{2+} response and spike frequency were significantly reduced (Figure 3.10C, D).

Since PLC activation produces IP_3 and triggers ER store release, we next analysed the contribution of IP_3Rs and RyRs to the AVP-induced Ca^{2+} signals in A7r5 cells using 2-APB or tetracaine, respectively. 2-APB is a membrane-permeable IP_3Rs inhibitor that does not affect RyRs (Maruyama et al., 1997). Two minutes pretreatment with 2-APB (100 µM) significantly attenuated the amplitude of the sustained $[Ca^{2+}]_i$ elevation induced by AVP (100 pM); it did not completely abolished oscillations but reduced their amplitude (Figure 3.11A, D, E). RyRs inhibitor, tetracaine (100 µM), effectively inhibited the amplitude and frequency of Ca^{2+} oscillation caused by AVP, and when applied together, 2-APB and tetracaine significantly attenuated $[Ca^{2+}]_i$ response to AVP (Figure 3.11B-E).

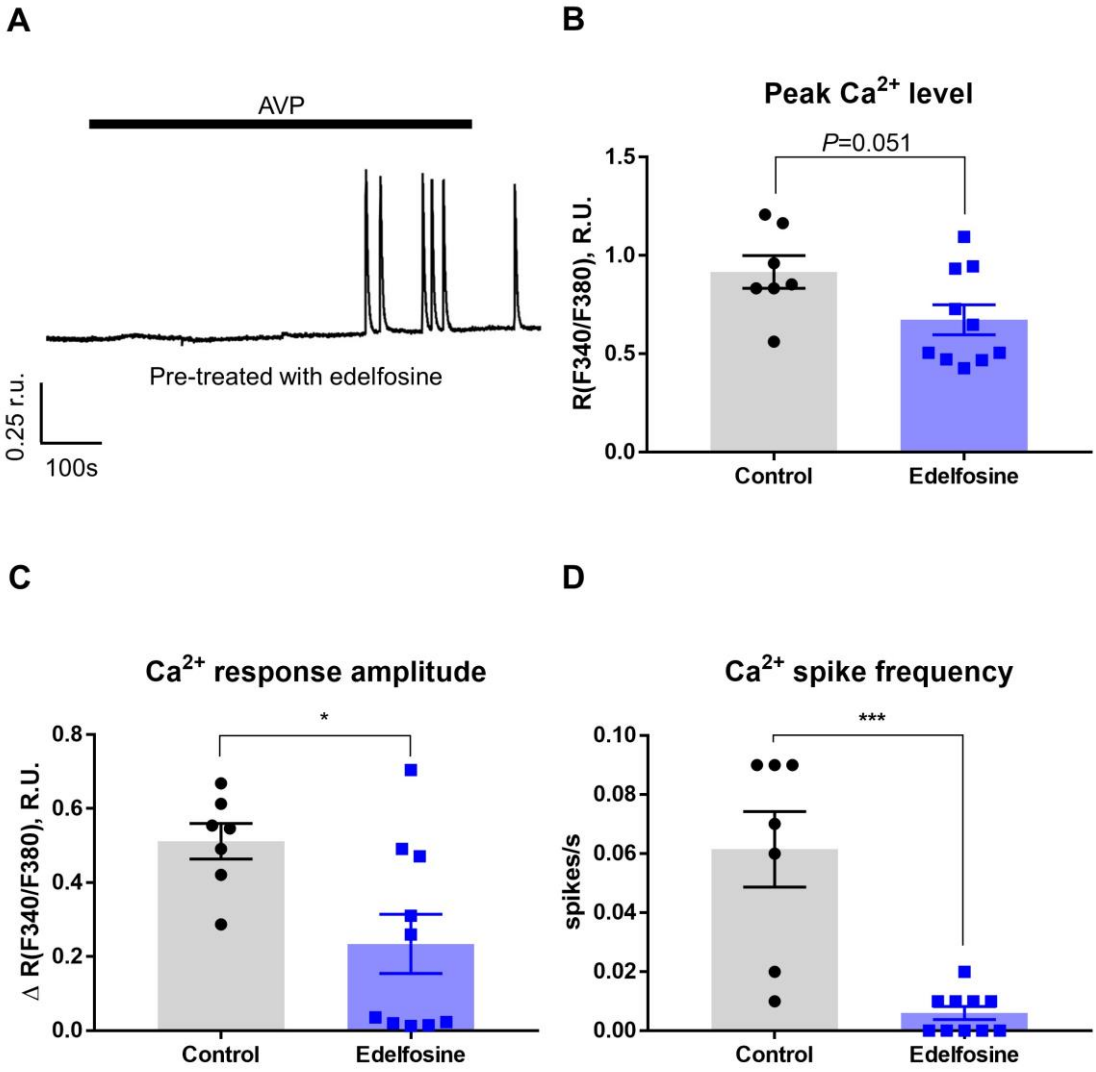

Figure 3.10 AVP-induced Ca^{2+} oscillations are reduced by inhibition of PLC. (**A**) Representative example trace showing Ca^{2+} oscillations evoked by AVP (100 pM) in A7r5 cells pretreated with the phospholipase C (PLC) inhibitor, edelfosine (10 µM). (**B-D**) Bar graphs summarising the effects of edelfosine on the peak Ca^{2+} level (B), Ca^{2+} response amplitude (ΔR; C) and Ca^{2+} spike frequency (spikes/s) (D) induced by AVP. In panels B-D data are presented as mean ± S.E.M.; Statistics performed using unpaired student's t-test, *P<0.05, ***P<0.001 (Control, n=7; Edelfosine, n=10).

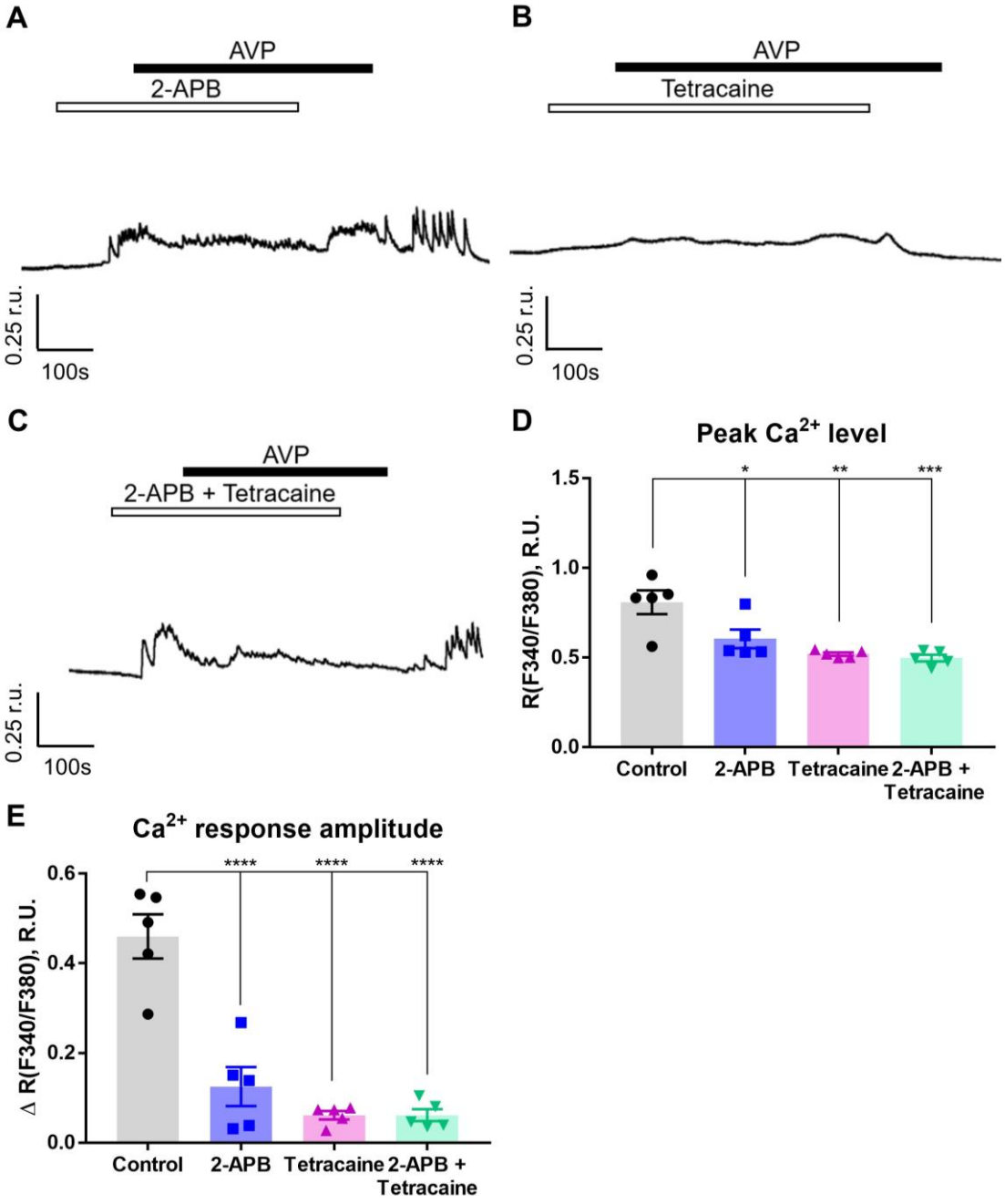

Figure 3.11 AVP-induced Ca^{2+} oscillations are reduced by inhibition of ER Ca^{2+} release channels. (**A-C**) Representative example traces of AVP-induced Ca^{2+} transients recorded in the presence of 2-APB (IP_3R_s inhibitor; 100 μM; A), tetracaine (RyRs inhibitor; 100 μM; B) or both 2-APB and tetracaine (C), as indicated. (**D-E**) Bar graphs summarising the effects of 2-APB or tetracaine on the peak Ca^{2+} level (D) and Ca^{2+} response amplitude (ΔR; E) induced by AVP. In panels D-E data are presented as mean ± S.E.M.; Statistics performed using ANOVA with Sidak test, *P<0.05, **P<0.01, ***P<0.001, ****P<0.0001 (n=5).

We next tested if PLC is required for the Ca^{2+} oscillations evoked by the Kv7 channel inhibitor. A7r5 cells were pre-treated (10 minutes) with edelfosine, and the effect of XE991 (10 μM) was explored with Ca^{2+} imaging. Edelfosine (10 μM) did not inhibit Ca^{2+} oscillations (Figure 3.12A): neither the amplitude of sustained $[Ca^{2+}]_i$ elevation nor spike frequency were different from control (Figure 3.12B-D). These data indicate that PLC activation and ER Ca^{2+} release are the necessary factors linking AVP to Kv7 channel inhibition in A7r5 cells. At the same time, Ca^{2+} response triggered by direct inhibition of Kv7 channels with XE991 did not require PLC activation.

3.3 Discussion

Our study establishes the role for Kv7 channels in control over intracellular Ca^{2+} signalling in VSMCs. First, we show that in A7r5 cells, inhibition of endogenous Kv7 channels is sufficient to depolarise the membrane potential to trigger E_m spikes, mirrored by $[Ca^{2+}]_i$ oscillations. Kv7.5 and Kv7.4 were found to be the main Kv7 subunits expressed in A7r5 VSMCs, with Kv7.5 expressed at highest levels. A low level of *Kcnq1* transcript was found in A7r5 cells by RT-PCR, but Kv7.1 expression was undetectable by immunohistochemistry. These findings are consistent with previous studies, which demonstrated that *Kcnq1*, *Kcnq4* and *Kcnq5* were expressed in SMCs of different origins (Greenwood and Ohya, 2009); *Kcnq1* was the most abundant in a mouse portal vein (Ohya et al., 2003). Some studies showed higher levels of *Kcnq4*, followed by *Kcnq1* and *Kcnq5* in rodent aorta, mesenteric artery, and pulmonary artery SMCs (Yeung et al., 2007; Joshi et al., 2009).

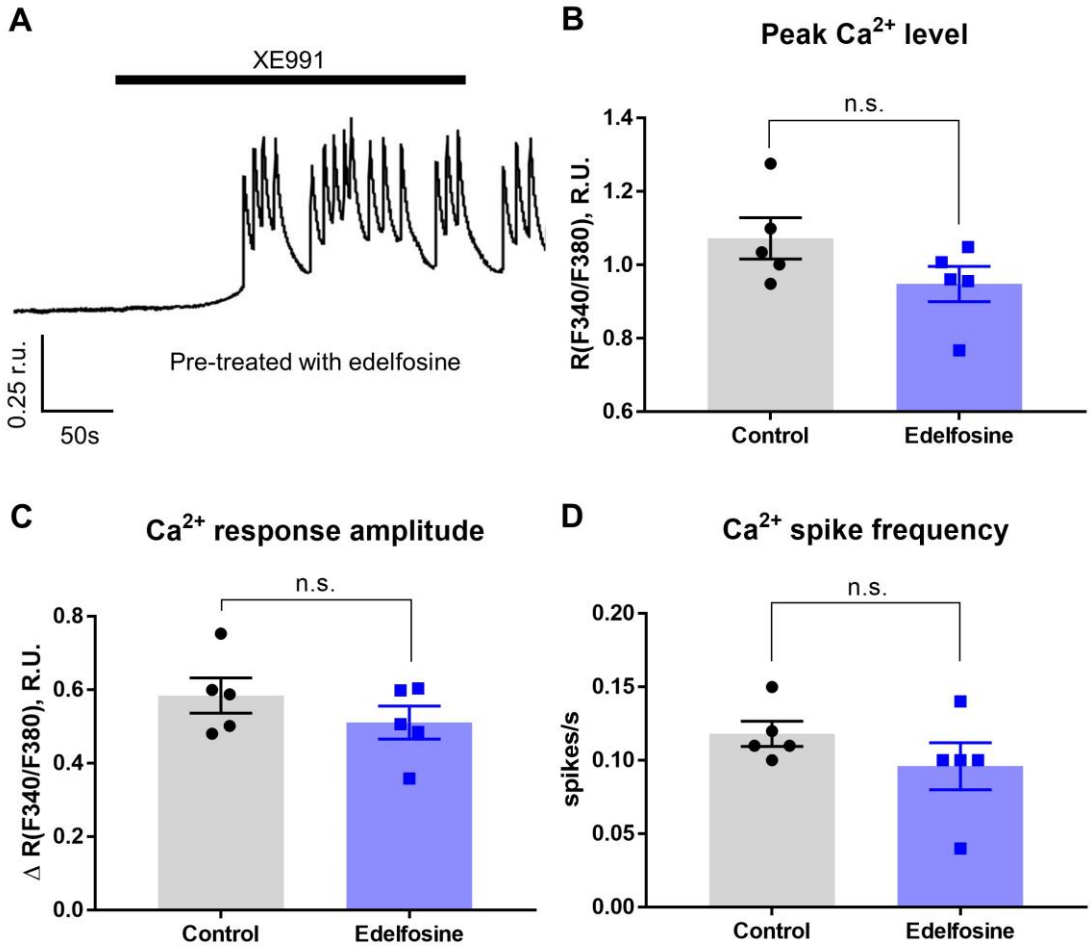

Figure 3.12 Ca^{2+} oscillations induced by Kv7 channel inhibition are insensitive to PLC inhibition. (**A**) Representative example trace showing Ca^{2+} oscillations evoked by XE991 (10 µM) in A7r5 cells pretreated with edelfosine (10 µM). The oscillations continued even after the XE991 was removed as compared to Figure 3.3A. (**B-D**) Bar graphs summarising the effects of edelfosine on the peak Ca^{2+} level (B), Ca^{2+} response amplitude (∆R; C), and Ca^{2+} spike frequency (spikes/s) during application of XE991 (D). In panels B-D data are presented as mean ± S.E.M.; Statistics performed using paired student's t-test, n.s., not significant (n=5).

However, another two studies found that in A7r5 cells only *Kcnq5* detectable (Brueggemann et al., 2007; Brueggemann et al., 2011). Interestingly, $[Ca^{2+}]_i$ elevations induced by bulk depolarisation with high-K^+ were larger than these produced by XE991 and contained much less oscillations; we hypothesise that this lack of continuous spiking is due to Ca^{2+} overload during sustained strong depolarisation produced by the high-K^+ solution, an effect which is not recapitulated by Kv7 channel inhibition. Indeed, according to the Nernst formalism, the elevation of extracellular K^+ to 50 mM would shift E_K to near -25 mV and reset the E_m accordingly. Inhibition of Kv7 channels with XE991 is expected to produce milder depolarisation, e.g. depolarisation by ~8 mV in response to 3 µM XE991 was reported in sensory neurons (Du et al., 2014). Since in A7r5 cells, the main Kv7 subunit is Kv7.5, which is by far the least sensitive to XE991 Kv7 subunit (Schroeder et al., 2000; Wang et al., 1998), even at 10 µM XE991 used in the present study, and even with contribution of Kv7.4, only partial inhibition of compound Kv7 current in A7r5 is expected. This would result in much less pronounced depolarisation, as compared to that produced by 50 mM extracellular K^+.

Second, we show that the depolarisation-induced $[Ca^{2+}]_i$ raises and the XE991-induced Ca^{2+} oscillations were dependent on Ca^{2+} influx via the L- and T-type VGCCs. There are two important classes of VGCCs in VSMCs: the high-voltage-activated (HVA) L-type Ca^{2+} channels and low voltage-activated (LVA) T-type Ca^{2+} channels (Bean et al., 1986; Benham and Tsien, 1987). Smooth muscle contractility is mainly dependent on an increase of $[Ca^{2+}]_i$ through the L-type Ca^{2+} channels (Amberg and Navedo, 2013). We found that *Cacna1c*, coding for Cav1.2 L-type subunit and *Cacna1g*, coding for Cav3.1 T-type subunit were the

predominant L- and T-type channel α-subunit transcripts expressed in A7r5 cells. A decrease of Kv channel activity either by the direct inhibition of the channel activity or by reduced expression can trigger an influx of Ca^{2+} via L-type Ca^{2+} channels (Nelson et al., 1990; Fleischmann et al., 1994). Therefore, blockade of Kv7 channels with XE991 in VSMCs may induce E_m depolarisation to induce action potentials and Ca^{2+} influx via the L-type Ca^{2+} channels ((Stott et al., 2014); present study). We also report that the Ca^{2+} rises induced by XE991 were reversed by T-type Ca^{2+} blocker, NNC 55-0396, which abolished the Ca^{2+} oscillations gradually but completely. This could be explained by the contribution of low-threshold T-type Ca^{2+} channels to the spike initiation (Kim et al., 2001; Huguenard and Prince, 1994), such that T-type channel inhibition could reduce or block spike generation. However, cross-inhibition of L-type Ca^{2+} channels by NNC 55-0396 (and also a degree of inhibition of T-type channels by nifedipine) cannot be presently excluded. Importantly, XE991-induced oscillations of both, E_m and $[Ca^{2+}]_i$ were completely blocked by the Kv7 opener, retigabine, indicating strong control over the excitability and Ca^{2+} signalling in VSMCs exerted by the Kv7 channels. The inhibitory effect of retigabine was even stronger than that of the L-type VGCC blocker nifedipine, which is widely prescribed to treat cardiovascular disease (Brown et al., 2000). Thus, Kv7 openers may have potential clinical use, i.e. to promote vasodilatation.

Third, we show that the vasoconstrictor hormone AVP exerts effects on E_m and $[Ca^{2+}]_i$ that are very similar to these of XE991. Indeed, the main mechanism of action of such hormones to stimulate rhythmic constrictions of arteries has been recognized as depolarisation of the E_m to open VGCCs (Large, 2002). It has been shown that in A7r5 cells, the physiological concentration of AVP (100 pM) leads

to activation of PLC and PKC followed by inhibition of an outward voltage-sensitive K^+ current (I_{Kv}), which in turn, depolarised E_m to activate L-type Ca^{2+} channels and produce repetitive Ca^{2+} spiking, an effect which appeared to be mediated by Kv7.5 (Brueggemann et al., 2007). It has to be acknowledged that the AVP-induced Ca^{2+} signalling in SMCs is complex and may differ mechanistically between the SMC types. Thus, Ca^{2+}-induced Ca^{2+} release via RyRs (Yip and Sham, 2011) and DAG-sensitive TRPC6 channels were also reported to contribute to AVP-induced membrane depolarisation and Ca^{2+} oscillations at physiological concentrations of AVP (10–100 pM) in A7r5 cells (Mani et al., 2009; Soboloff et al., 2005). Moreover, activation of the RhoA/ROCK pathway by AVP was reported to stimulate nonselective cation influx (TRPC channels) via DAG-PKC signalling in VSMCs (Martinsen et al., 2012). RhoA/ROCK pathway can also interfere with Ca^{2+} signalling through VGCCs, contributing to the control of SMCs contraction and relaxation. Thus, inhibition of VGCC-mediated Ca^{2+} influx in VSMCs by Rho-kinase inhibitors has been reported (Guan et al., 2019), however, the mechanisms linking RhoA/ROCK requires further investigation.

While the complexity of the receptor-mediated Ca^{2+} signalling in VSMCs should not be underestimated, our data suggest that AVP-mediated Kv7 inhibition, subsequent depolarisation and activation of L- and T-type Ca^{2+} channels strongly contribute to AVP signalling in A7r5 cells. Specifically, we found that AVP mimics XE991 to generate Ca^{2+} spiking in A7r5 cells: both compounds depolarised E_m (as measured with FluoVolt) and induced $[Ca^{2+}]_i$ oscillations. The effect of AVP took longer to develop but resulted in a similar spike frequency to that of XE991

(Figure 3.7). The effects of both compounds were blocked by VGCC inhibitors and retigabine.

Yet, there is an important difference between the way AVP and XE991 act upon Kv7 channels, with the former being a GPCR ligand acting via intricate intracellular signalling cascade while the latter being a direct ion channel inhibitor. G protein-coupled vasoconstrictor agonist can induce early (transient) and late (sustained) phases of constriction via IP_3-mediated Ca^{2+} release and Ca^{2+} entry from L-type Ca^{2+} channels, respectively (Henderson and Byron, 2007). Higher AVP concentrations (>1 nM) can stimulate the activation of PLC, which results in the production of IP_3 and the release of intracellular Ca^{2+} in A7r5 cells (Henderson and Byron, 2007). PLC-mediated inhibition of Kv7 channels is one of the signature effects of $G_{q/11}$-coupled GPCR (Delmas and Brown, 2005). Within the multiple branches of this well-studied signalling cascade, PIP_2 depletion (Suh and Hille, 2002; Zhang et al., 2003), IP_3-mediated ER Ca^{2+} release (in concert with calmodulin) (Gamper and Shapiro, 2003; Gamper et al., 2005; Chang et al., 2018) and activation of PKC (following release of DAG, a product of PIP_2 hydrolysis) (Hoshi et al., 2003; Bal et al., 2010; Zhang et al., 2011) are the major events that can independently produce Kv7 channel inhibition. In reality though all three mechanisms usually act in concert, although contribution of each individual mechanism to the total Kv7 inhibition varies between cell and tissue types dramatically (Gamper and Shapiro, 2015). Our findings suggest that even at a fairly low concentration of 100 pM, AVP mediates the recruitment of the PLC-IP_3 signal transduction mechanism to induce Ca^{2+} spiking in A7r5 cells, presumably via the Kv7 channel inhibition. Thus, PLC inhibitor attenuated the amplitude of $[Ca^{2+}]_i$ elevation and mean spike frequency induced by AVP.

Moreover, inhibition of IP_3Rs and RyRs with 2-APB and tetracaine, respectively, also attenuated the AVP-induced Ca^{2+} oscillations (Figure 3.11), suggesting that ER-released Ca^{2+} contributes specifically to Kv7 channel inhibition in A7r5 cells, as was suggested earlier for neurons (Gamper and Shapiro, 2003; Hernandez et al., 2008).

It must be noted that edelfosine, 2-APB and tetracaine are not entirely selective for their targets. Thus, edelfosine, in addition to inhibiting PLC, also activates platelet-activating factor (PAF) receptors (Alonso et al., 1997). While 2-APB inhibits the IP_3Rs without an effect on the RyRs (Maruyama et al., 1997), it also inhibits TRPC3/6/7 channels and TRPM8 channel in VSMCs (Bencze et al., 2015; Zholos, 2010). Tetracaine, a RyRs antagonist which is used to eliminate RyR-dependent Ca^{2+} sparks (Csernoch et al., 1999; Curtis et al., 2008), is also reported to influence Kv channels (Komai and McDowell, 2001). Thus, caution is needed in interpreting the results presented in Figure 3.10 and 3.11. Importantly, AVP does not directly affect either L- and T-type Ca^{2+} channels currents in A7r5 cells (Byron, 1996), suggesting both these VGCCs are engaged indirectly, e.g. via the depolarisation produced by the Kv7 channel inhibition. While the fact that retigabine inhibits AVP responses does not explicitly proves that AVP-induced depolarisation and Ca^{2+} oscillations are mediated by Kv7 channel inhibition, the combination of the effects of XE991, the dependence of the AVP action on PLC activity, and the wealth of data on strong inhibition of Kv7 channels by PLC-coupled GPCR do suggest that AVP-mediated Kv7 inhibition is a strong contributor the observed effects of AVP on E_m and $[Ca^{2+}]_i$ in A7r5 VSMCs.

To our knowledge, no previous studies have demonstrated the clear relationship between the Kv7 channels, vasoconstrictor hormones and the regulation of $[Ca^{2+}]_i$. While a 10-100 pM concentration of AVP produced Ca^{2+} spiking, these concentrations did not stimulate an appreciable release of intracellular Ca^{2+} stores (Byron, 1996). We propose that direct (XE991) and GPCR-mediated (AVP) Kv7 channel inhibition results in Ca^{2+} oscillations in A7r5 cells through activation of L- and T-type VGCCs and the local release of Ca^{2+} from the ER. This signal transduction is of great importance for both, a basic understanding of vascular physiology and the identification of novel therapeutic strategies to control vascular tone with retigabine or its successors (e.g. drugs tailored to selectively activate Kv7.5).

3.4 Summary

- Inhibition of Kv7 channels induces Ca^{2+} signals through L- and T-type VGCCs in A7r5 cells.
- PLC mediated Kv7 inhibition is likely to contribute to Ca^{2+} oscillations induced in A7r5 cells by AVP.
- Kv7 activator, retigabine, strongly suppresses $[Ca^{2+}]_i$ oscillations induced by AVP or direct Kv7 channel inhibition.

Chapter 4

Hypoxic remodelling of Ca^{2+} signalling in vascular smooth muscle cells

4.1 Introduction

Hypoxia is one of the main components of ischaemia, which presents as insufficient blood flow to provide adequate oxygenation, this, in turn, leads to adverse effects within the cardiovascular system and causes disease including atherosclerosis, hypertension and PAH (see section 1.7). The hypoxia exerts complex effects on vascular contractility and causes structural remodelling of the vasculature. An increase in $[Ca^{2+}]_i$ is central to various pathological processes to hypoxic response, and an important source of this $[Ca^{2+}]_i$ elevation is Ca^{2+} influx from the extracellular space. As discussed in Chapter 3, VSMCs mainly express Cav1.2 L- and Cav3.1 T-type Ca^{2+} channels, which are responsible for Ca^{2+} influx during the action potential (Hughes, 1995). We have shown that Kv7 channels are essential in regulating the E_m to influence $[Ca^{2+}]_i$ in VSMCs. A hypoxic exposure may result in VSMC contraction via the inhibition or downregulation of Kv channels or the alternations of other ion channels such as VGCC, TRPC, SOCC and ER Ca^{2+} stores (Yuan, 2001; Toescu, 2004; Lai et al., 2015).

Inhibition of Kv7 channels increases the vascular tone in the portal vein, aorta, mesenteric and pulmonary arteries (Yeung and Greenwood, 2005; Joshi et al., 2006; Yeung et al., 2007; Mackie et al., 2008). On the contrary, activation of Kv7 channels with retigabine can cause vascular relaxation (Yeung et al., 2007). Therefore, Kv7 channels may be able to counteract the depolarisation caused by

hypoxia, which promotes Ca^{2+} influx via VGCCs and vasoconstriction (Sedivy et al., 2015). During hypoxia, an increase of $[Ca^{2+}]_i$ is mediated, at least partially, by the activation of VGCCs, with the T-type VGCCs being the main contributor in the hypoxia-associated pathological processes of myocardial infarction and PAH. (Aley et al., 2008; Wan et al., 2013; Gonzalez-Rodriguez et al., 2015). Kv7 channel openers have been suggested to counteract the changes in vascular tone induced by chronic hypoxia (Morecroft et al., 2009). Yet, a more precise understanding of relationships between hypoxia, Kv7 channels and $[Ca^{2+}]_i$ is needed to gain mechanistic insight into the effect of hypoxia on vascular function. We thus propose that Kv7 channels might be partially downregulated or inhibited by hypoxia in VSMCs, however, there is still residual Kv7 activity which can still influence E_m and $[Ca^{2+}]_i$ in hypoxic condition.

The family of HIF proteins encompasses transcription factors responsible for hypoxic changes in gene expression pattern, including ion channels (Del Toro et al., 2003; Semenza, 2001). Under normoxia, HIF-1α and HIF-2α are hydroxylated by PHD proteins, members of the 2-oxoglutarate/iron dependent dioxygenase superfamily. PHD proteins hydroxylate proline residues in the ODDD of HIF-α subunits. The hydroxylated residues are subsequently bound to the VHL E3 ubiquitin ligase complex, leading to rapid degradation of HIF-α. Under hypoxia, these oxygen-dependent hydroxylation reactions are not performed, and HIF-1α/2α are ubiquitously expressed, which promotes genes transcription (see Figure 1.10). Thus, it seems logical to suppose that hypoxia influences $[Ca^{2+}]_i$ by affecting the function/expression of Kv7 channels and VGCCs, and HIFs could play a critical role in this process.

Dimethyloxalylglycine (DMOG) is a cell-permeable competitive inhibitor of PHDs, which mimics some hypoxic effects via the stabilisation of HIF-1α expression (Yuan, et al., 2014). Application of DMOG is used experimentally to investigate if the hypoxic effect of interest is mediated by the HIF-1α transcription factor. Selective HIF-2α inhibitor (H2A) is another tool for testing cellular effects of this HIF isoform (Scheuermann et al., 2013). The role of HIF-2α in VSMCs is less understood, but it was shown that inhibition of HIF-2α reversed PAH-induced vascular remodelling and right heart failure (Dai et al., 2018). Here we used hypoxic treatment, DMOG and H2A to investigate the effects of hypoxia on Ca^{2+} signalling in VSMCs (with the particular focus on the Kv7-VGCC axis) and to probe the contribution of HIF1α/2α to these effects.

4.2 Results

4.2.1 Effects of hypoxia on basal $[Ca^{2+}]_i$ and depolarisation-induced Ca^{2+} entry in A7r5 cells

To investigate the effects of hypoxia on Ca^{2+} homeostasis in VSMCs, we cultured rat A7r5 cells under hypoxia (1% O_2) or in the presence of DMOG (1 mM) or hypoxia (1% O_2) along with H2A (20 µM) (Hypoxia/H2A) for 24 hours (24h) prior to carrying out the experiments. Cells were loaded with Fura2, as in previous experiments, and thereafter superfused with 50 mM K^+ solution (isotonic substitution of Na^+) to investigate Ca^{2+} entry via VGCCs. Depolarisation with 50 mM K^+ solution led to sharp but reversible Ca^{2+} transients in normoxic A7r5 cells (Figure 4.1A). In contrast, after hypoxic incubation, depolarisation with high-K^+ produced a biphasic effect: a sharp initial rise, then followed by prolonged Ca^{2+} oscillations after the washout of high K^+ (Figure 4.1B). There were no oscillations

in DMOG or Hypoxia/H2A cells during the high K^+ washout period (Figure 4.1C, D).

Basal and peak Ca^{2+} levels were not significantly different between normoxic and hypoxic cells (Figure 4.2A-C). However, the peak amplitude and AUC of high-K^+-induced Ca^{2+} transients in cells treated with DMOG or Hypoxia/H2A were significantly reduced (AUC: 37.79 ± 7.51, n=5 in normoxia vs. 24.34 ± 4.10, n=4 in DMOG vs. 11.74 ± 6.65, n=5 in Hypoxia/H2A; Figure 4.2C). The time course of the recovery of $[Ca^{2+}]_i$ after the washout of high-K^+ solution was the fastest in Hypoxia/H2A with 50.23 ± 10.71 seconds (n=5); measured during the period from peak Ca^{2+} level to return to the basal Ca^{2+} level (Figure 4.2D). The prolonged oscillations were observed with a frequency of 0.17 ± 0.05 spikes/s (n=5) in hypoxic cells but not in other experimental conditions (Figure 4.2E). These data indicate that hypoxia induces a hyperexcitable phenotype in A7r5 cells; this effect is prevented by H2A, but it is not mimicked by DMOG, implicating HIF-2α as a necessary mediator of this hypoxic effect.

4.2.2 Effects of hypoxia on the contribution of Ca^{2+} entry via L- and T-type Ca^{2+} channels in A7r5 cells

The focus of the study was then directed to test the separate contributions of two VGCC types to the rise of $[Ca^{2+}]_i$ in cells under hypoxic and DMOG conditions. Cells were perfused with a buffer solution containing 2.5 mM Ca^{2+} along with nifedipine (2 μM) or NNC 55-0396 (3 μM) to block L- or T-type Ca^{2+} channels before depolarisation with 50 mM extracellular K^+ solution.

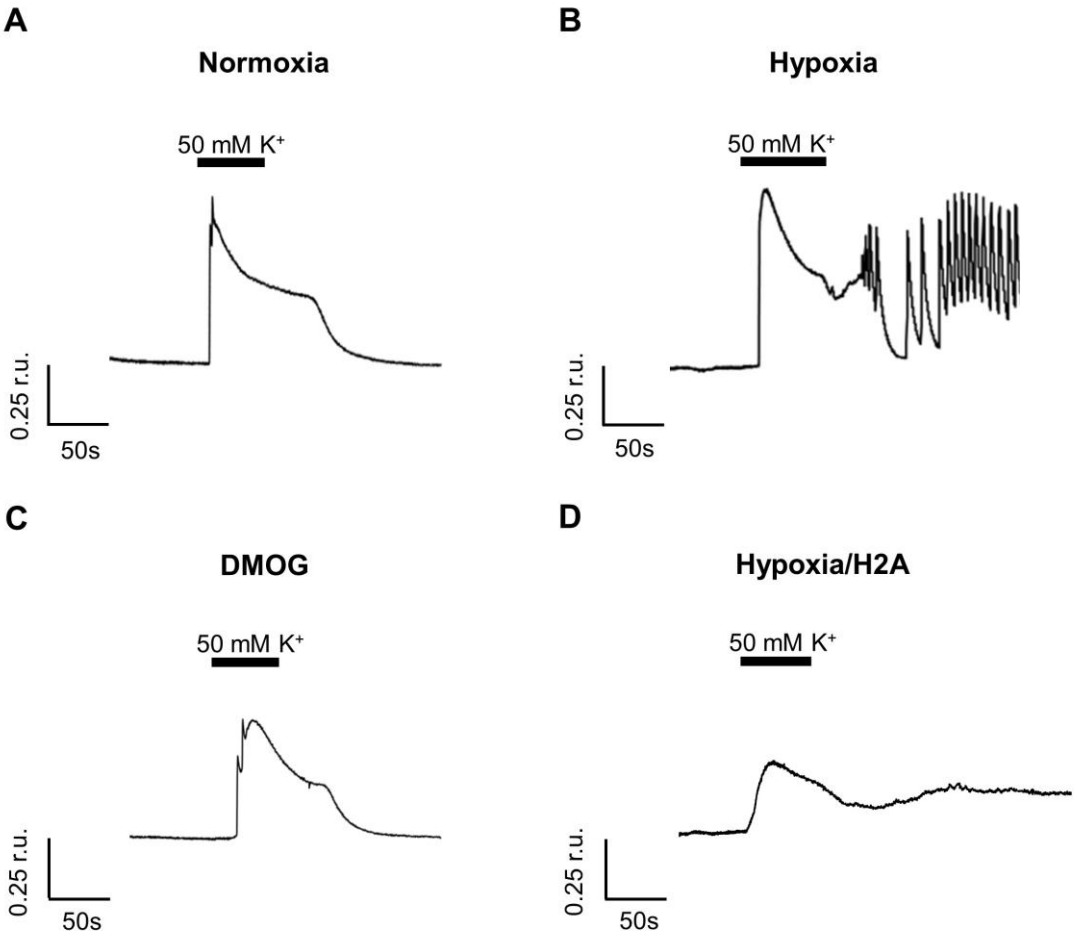

Figure 4.1 Representative example traces of the effects of hypoxia on depolarisation-induced Ca^{2+} transients in A7r5 cells. Rises in $[Ca^{2+}]_i$ evoked by depolarising cells with 50 mM K^+-containing buffer (the period indicated by the solid bar) in normoxic (A), hypoxic (1% O_2, 24h; B), DMOG (1 mM, 24h; C), and hypoxia/H2A (1% O_2 along with H2A 20 µM, 24h; D) conditions.

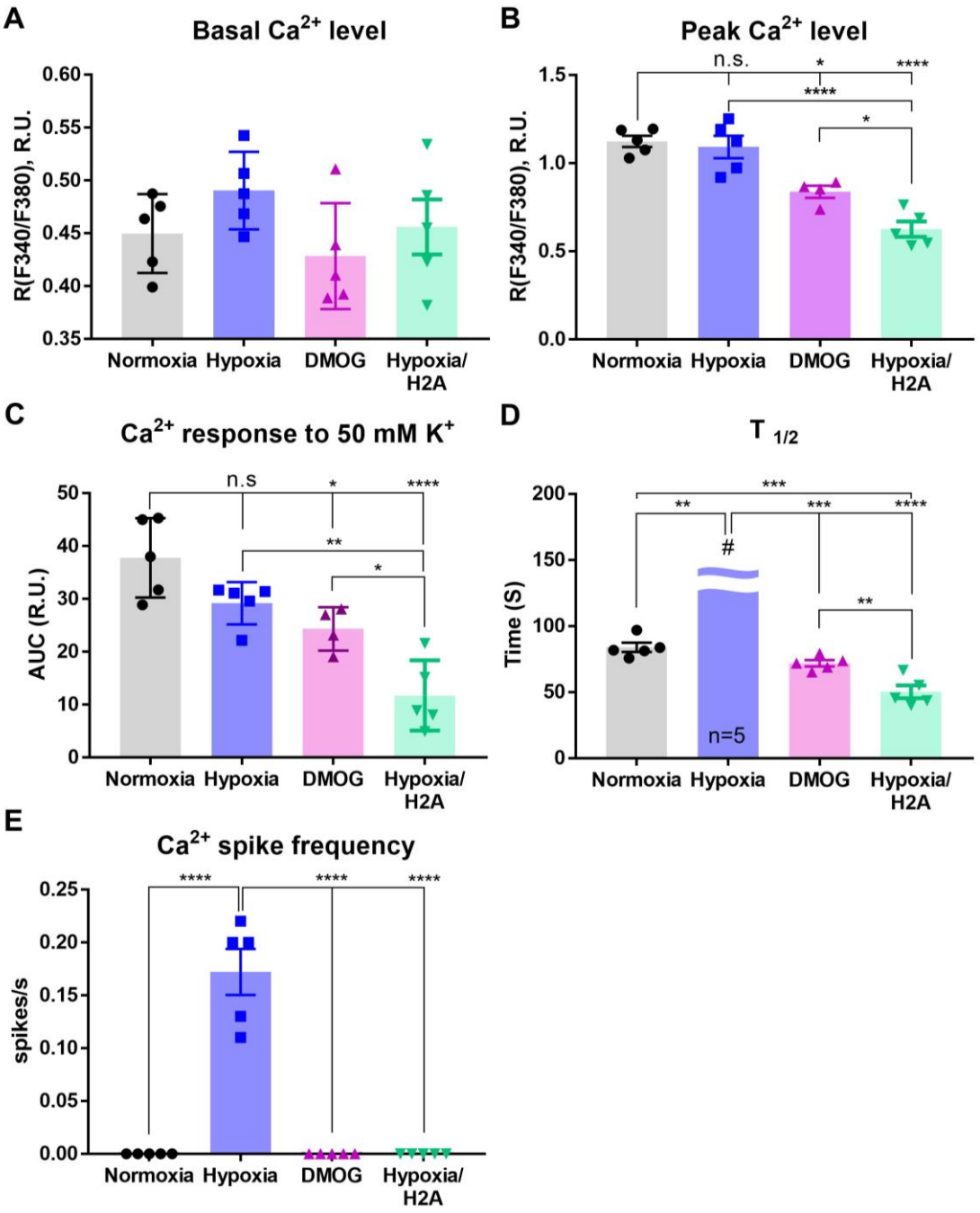

Figure 4.2 Effects of hypoxia on depolarisation-induced Ca^{2+} entry in A7r5 cells. (**A-E**) Bar graphs summarising the effects of hypoxia on basal Ca^{2+} level (A), peak Ca^{2+} level (B), Ca^{2+} response amplitude (AUC; C), the time course ($T_{1/2}$) of the recovery of $[Ca^{2+}]_i$ from peak to the basal Ca^{2+} level (D) and Ca^{2+} spike frequency (spikes/s) (E) in response to 50 mM K^+ buffer. In panel D, the hash mark (#) showed continuous oscillations under hypoxia; hence decay time was longer than the observation time in this experiment. Data are presented as mean ± S.E.M.; Statistics performed using ANOVA with Sidak test, *P<0.05, **P<0.01, ***P<0.001, ****P<0.0001 (n≥4).

Representative example traces of responses to high-K^+ depolarisation in the presence of nifedipine are shown in Figure 4.3A-C. In hypoxic cells, nifedipine produced a similar inhibiting effect in $[Ca^{2+}]_i$ response to high-K^+, as compared to normoxic cells (AUC: 1.61 ± 1.19, n=5 in normoxic cells vs. 1.07 ± 0.73, n=5, in hypoxic cells, not significant; Figure 4.3D, E), however, the inhibition was much less pronounced in the case of the DMOG treatment (AUC: 12.88 ± 2.41, n=5, $p<0.0001$), as compared to control or hypoxic treatment. Thus, nifedipine inhibited high-K^+-induced $[Ca^{2+}]_i$ transients in normoxic, hypoxic and DMOG-treated cells by 95.9 ± 2.3%, 96.3 ± 2.4%, and 56.5 ± 11.3%, respectively.

The decrease in rises of $[Ca^{2+}]_i$ due to inhibition of T-type Ca^{2+} channels was much less pronounced in hypoxic and DMOG-treated cells compared to normoxic cells as represented by the example traces (Figure 4.4A-C), peak Ca^{2+} level (Figure 4.4D) and Ca^{2+} response (AUC: 3.60 ± 1.94, n=4 in normoxic cells vs. 7.40 ± 1.44, n=5, $p<0.01$ in hypoxic cells and 8.92 ± 1.62, n=5, $p<0.001$ in DMOG-treated cells; Figure 4.4E). Thus, NNC 55-0396 inhibited high-K^+-induced $[Ca^{2+}]_i$ transients in normoxic, hypoxic and DMOG cells by 85.0 ± 13.3%, 74.2 ± 6.5% and 65.4 ± 11.3%, respectively. These observations reinforced the major role of L-type Ca^{2+} channels in response to depolarisation under the hypoxic environment but also revealed a decrease of T-type channel contribution in both, the hypoxia and DMOG treatment and also a reduction in nifedipine efficacy specific to DMOG treatment.

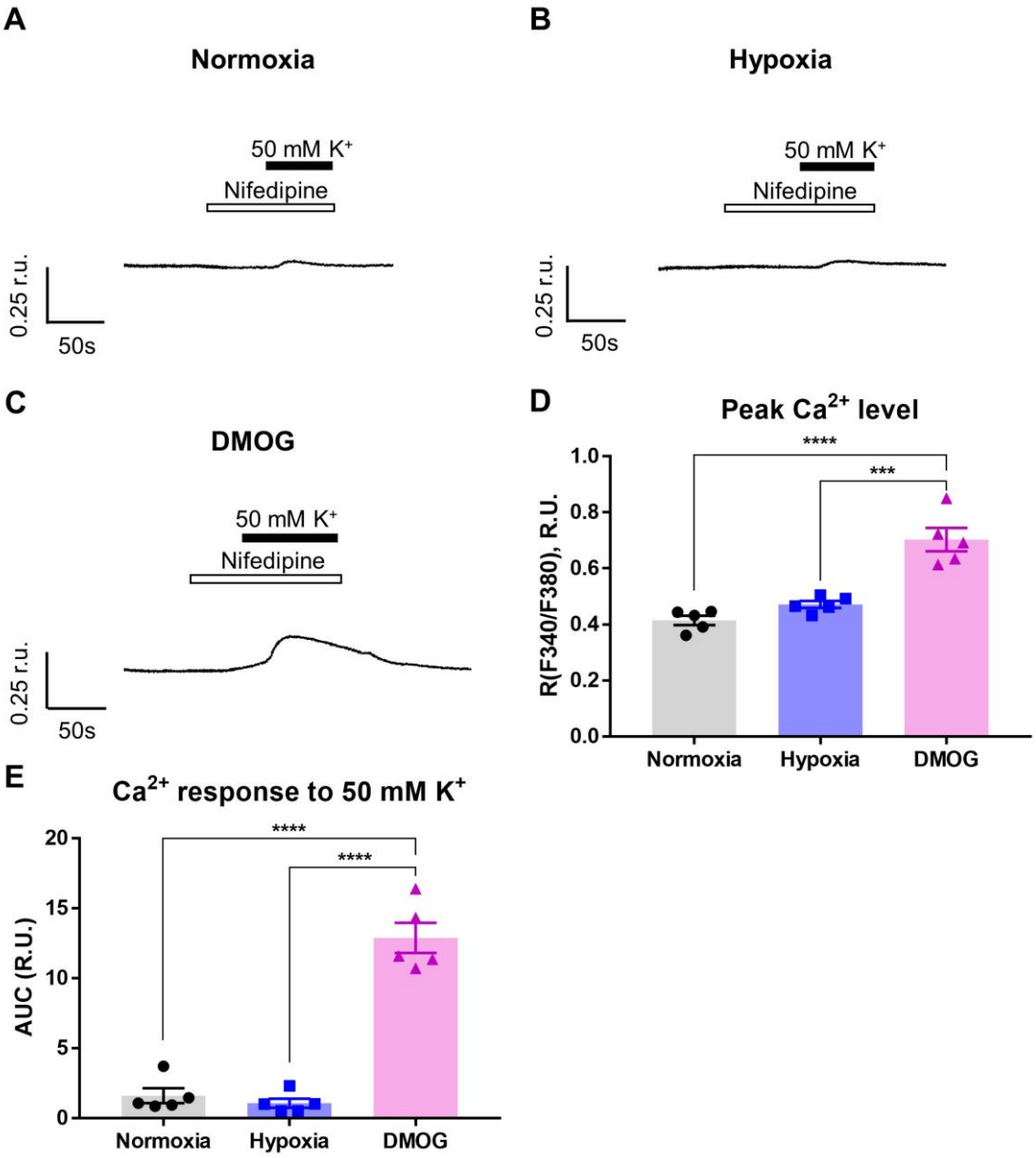

Figure 4.3 Nifedipine effectively inhibits depolarisation-induced Ca^{2+} entry in hypoxic A7r5 cells. (**A-C**) Representative example traces of high-K^+-induced Ca^{2+} transients recorded in the presence of L-type (nifedipine; 2 µM) Ca^{2+} channel blocker (as indicated) in normoxic (A), hypoxic (B), and DMOG-treated (C) cells. (**D-E**) Bar graphs summarising the inhibiting effect of nifedipine on the peak Ca^{2+} level (D) and the mean AUC of the response (E) to 50 mM K^+ buffer. In panels D-E data are presented as mean ± S.E.M.; Statistics performed using ANOVA with Sidak test, ***P<0.001, ****P<0.0001 (n=5).

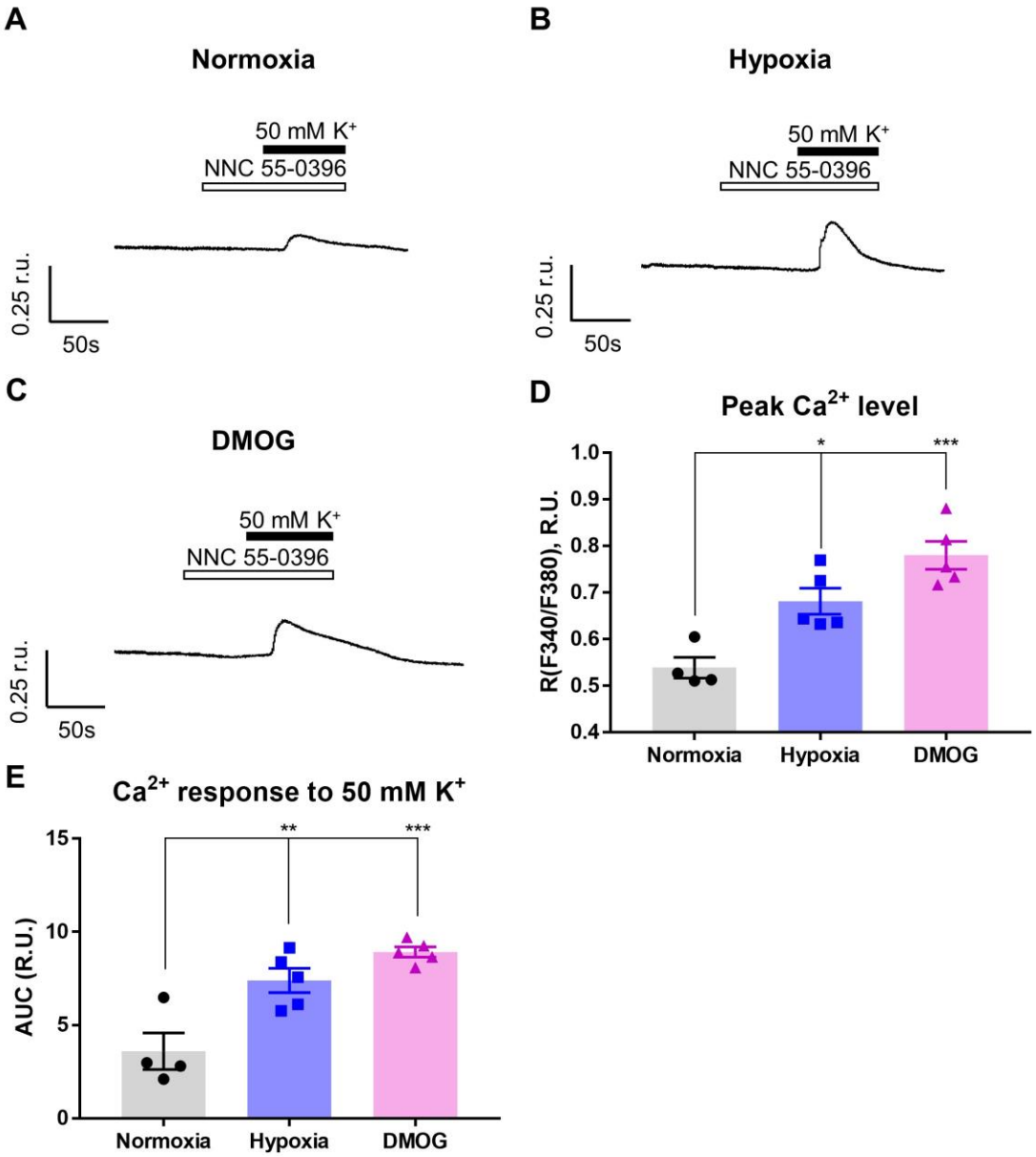

Figure 4.4 NNC 55-0396 is less efficacious to inhibit depolarisation-induced Ca^{2+} entry in hypoxic A7r5 cells. (**A-C**) Representative example traces of high-K^+-induced Ca^{2+} transients recorded in the presence of T-type (NNC 55-0396; 3 µM) Ca^{2+} channel blocker (as indicated) in normoxic (A), hypoxic (B), and DMOG-treated (C) cells. (**D-E**) Bar graphs summarising the inhibiting effect of NNC 55-0396 on the peak Ca^{2+} level (D) and the mean AUC of the response (E) to 50 mM K^+ buffer. In panels D-E data are presented as mean ± S.E.M.; Statistics performed using ANOVA with Sidak test, *P<0.05, **P<0.01, ***P<0.001 (n≥4).

4.2.3 Hypoxia and DMOG reshape Ca^{2+} signalling induced by Kv7 channel inhibition

To confirm the actions of Kv7/KCNQ channels under the hypoxic condition, we investigated the change of $[Ca^{2+}]_i$ induced by XE991 in hypoxic condition. We found that both hypoxia and DMOG changed Ca^{2+} response to Kv7 inhibitor XE991 (10 μM) in A7r5 cells in three important ways: 1) the Ca^{2+} response amplitude was reduced; 2) the oscillation frequency was increased and 3) $[Ca^{2+}]_i$ oscillations persisted without attenuation for several minutes of the XE991 washout (Figure 4.5, 4.6). This was in stark contrast with the normoxic cells, in which washout of XE991 resulted in fairly rapid termination of oscillation and recovery of $[Ca^{2+}]_i$ back to the baseline (Figure 4.5A). Following the washout of XE991, Ca^{2+} oscillations were persistent at a stable frequency for 2 minutes or longer in hypoxic or DMOG-treated cells (Figure 4.5B, C).

The basal Ca^{2+} levels were not significantly different among groups (Figure 4.6A). Peak Ca^{2+} level and amplitude response to XE991 were reduced by hypoxia and DMOG (ratio difference (ΔR): 0.58 ± 0.11, n=5 in normoxic cells vs. 0.38 ± 0.08, n=5 in hypoxic cells vs. 0.35 ± 0.15, n=5 in DMOG-treated cells; Figure 4.6B, C). The oscillations were observed with a higher frequency of 0.18 ± 0.02 and 0.17 ± 0.01 spikes/s in hypoxia and DMOG-treated cells, as compared to normoxic cells (0.12 ± 0.02 spikes/s; Figure 4.6D). Surprisingly, H2A treatment partially inhibited exaggerated $[Ca^{2+}]_i$ response to XE991 induced by hypoxia: the repetitive Ca^{2+} oscillations were ceased during the washout of XE991, and the transients declined toward the baseline (Figure 4.5D); however, oscillation frequency after drug removal remained higher in Hypoxia/H2A group than normoxic group (Figure 4.6E).

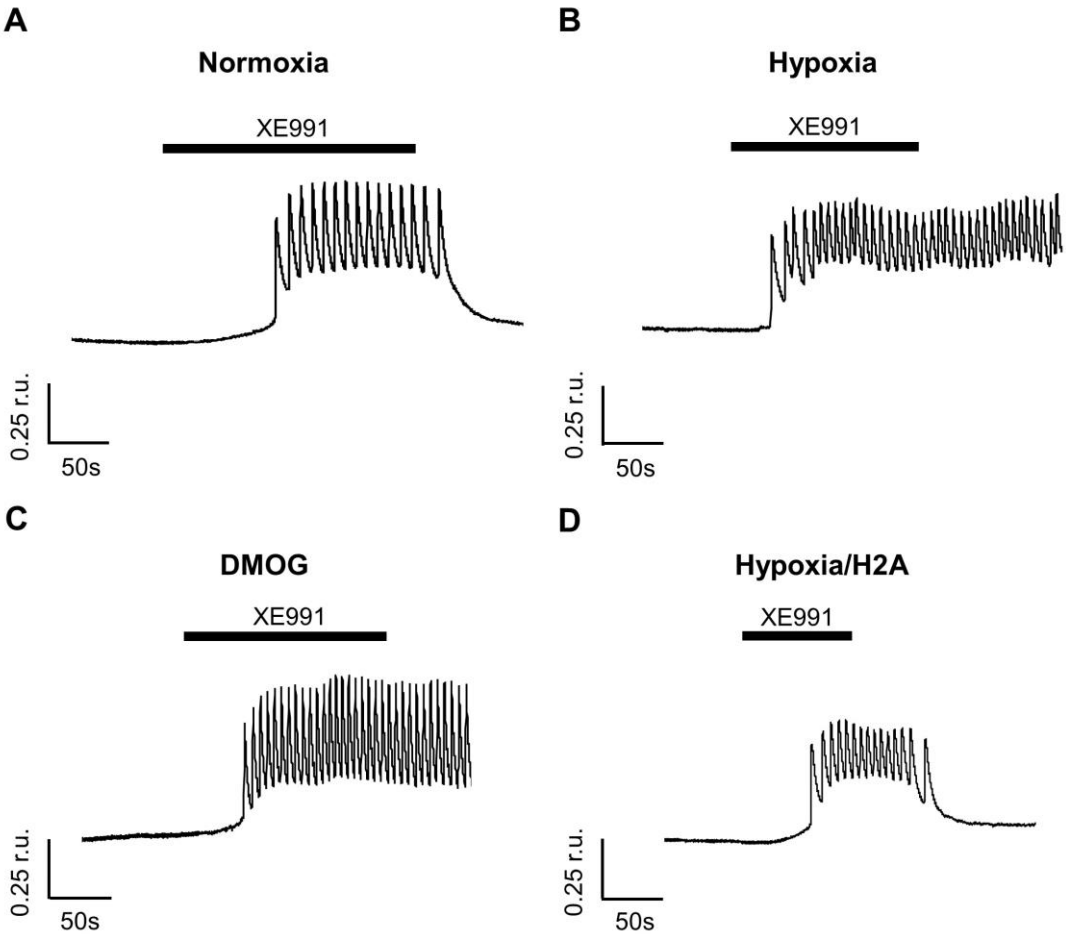

Figure 4.5 Hypoxia and DMOG enhance Ca^{2+} oscillations evoked by Kv7 channel inhibition in A7r5 cells. Rises in $[Ca^{2+}]_i$ evoked by Kv7 channel inhibitor (XE991; 10 µM). (**A-D**) Representative example traces of XE991-induced Ca^{2+} transients recorded (the period indicated by the solid bar) in normoxic (A), hypoxic (1% O_2, 24h; B), DMOG (1 mM, 24h; C), and hypoxia/H2A (1% O_2 along with H2A 20 µM, 24h; D) conditions.

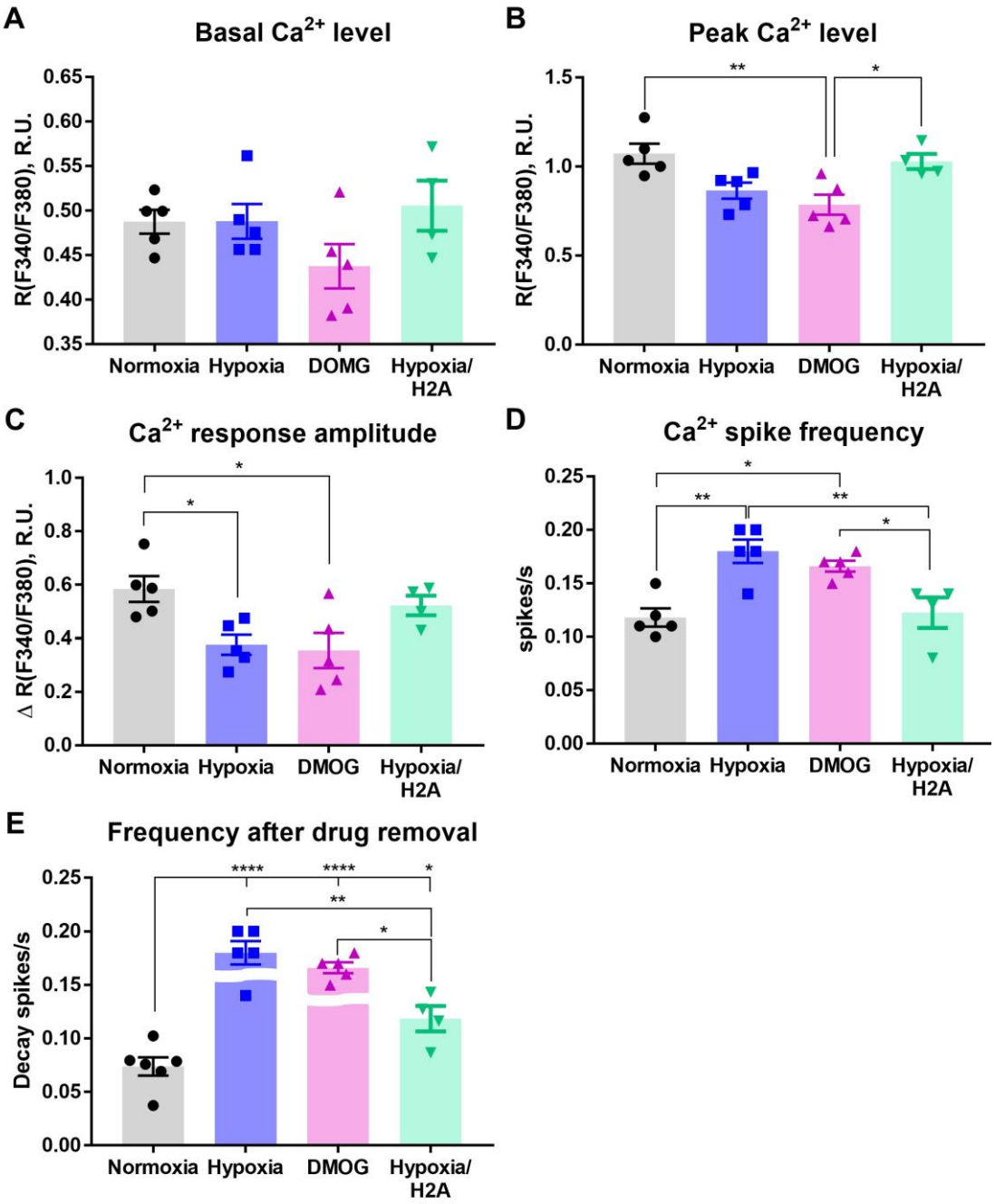

Figure 4.6 Effects of hypoxia on $[Ca^{2+}]_i$ evoked by the inhibition of Kv7 channels in A7r5 cells. (**A-E**) Bar graphs summarising the effects of hypoxia on basal Ca^{2+} level (A), peak Ca^{2+} level (B), Ca^{2+} response amplitude (ΔR; C), Ca^{2+} spike frequency (spikes/s) (D), and decay frequency after drug removal (E) induced by XE991 (10 µM). Data are presented as mean ± S.E.M.; Statistics performed using ANOVA with Sidak test, *P<0.05, **P<0.01, ****P<0.0001 (n≥4).

We then tested if the Kv7 channel activator, retigabine, can offset XE991-induced repetitive Ca^{2+} signals. XE991 was applied first to induce oscillations, then retigabine (10 µM) was applied in the continued presence of XE991. Importantly, even despite the enhancement of $[Ca^{2+}]_i$ after hypoxic or DMOG treatment, retigabine still efficiently stopped the XE991-induced Ca^{2+} oscillations and returned $[Ca^{2+}]_i$ to basal levels (Figure 4.7A, B), with transient oscillations at frequencies in hypoxic cells (0.07 ± 0.02 in control vs. 0.02 ± 0.01 spikes/s in retigabine, n=5, p<0.01; Figure 4.7C) and in DMOG-treated cells (0.08 ± 0.03 in control vs. 0.01 ± 0.003 spikes/s in retigabine, n=5, p<0.01; Figure 4.7D). This suggests that under hypoxic conditions, Kv7 channels are still available in VSMCs and can be recruited for quenching enhanced $[Ca^{2+}]_i$.

Nifedipine virtually abolished the persistent oscillations and reverted $[Ca^{2+}]_i$ elevation induced by XE991 in hypoxic or DMOG-treated cells (Figure 4.8A, B), with transient oscillations at frequencies in hypoxic cells (0.12 ± 0.02 in control vs. 0.02 ± 0.01 spikes/s in nifedipine, n=5, p<0.001; Figure 4.8C) and in DMOG-treated cells (0.10 ± 0.06 in control vs. 0.02 ± 0.01 spikes/s in nifedipine, n=5, p<0.05; Figure 4.8D). NNC 55-0396 (3 µM) produced similar effects but took longer to block oscillations in hypoxic condition (Figure 4.9A) and after DMOG treatment (Figure 4.9B), with transient oscillations at frequencies in hypoxic cells (0.28 ± 0.07 in control vs. 0.07 ± 0.01 spikes/s in NNC 55-0396, n=5, p<0.001; Figure 4.9C) and in DMOG-treated cells (0.15 ± 0.07 in control vs. 0.06 ± 0.03 spikes/s in NNC 55-0396, n=5, p<0.01; Figure 4.9D). Overall, the inhibition of XE991-induced Ca^{2+} signals was almost complete in the cells treated with Kv7 activator, L- or T-type Ca^{2+} channels blockers in normoxic, hypoxic and DMOG conditions.

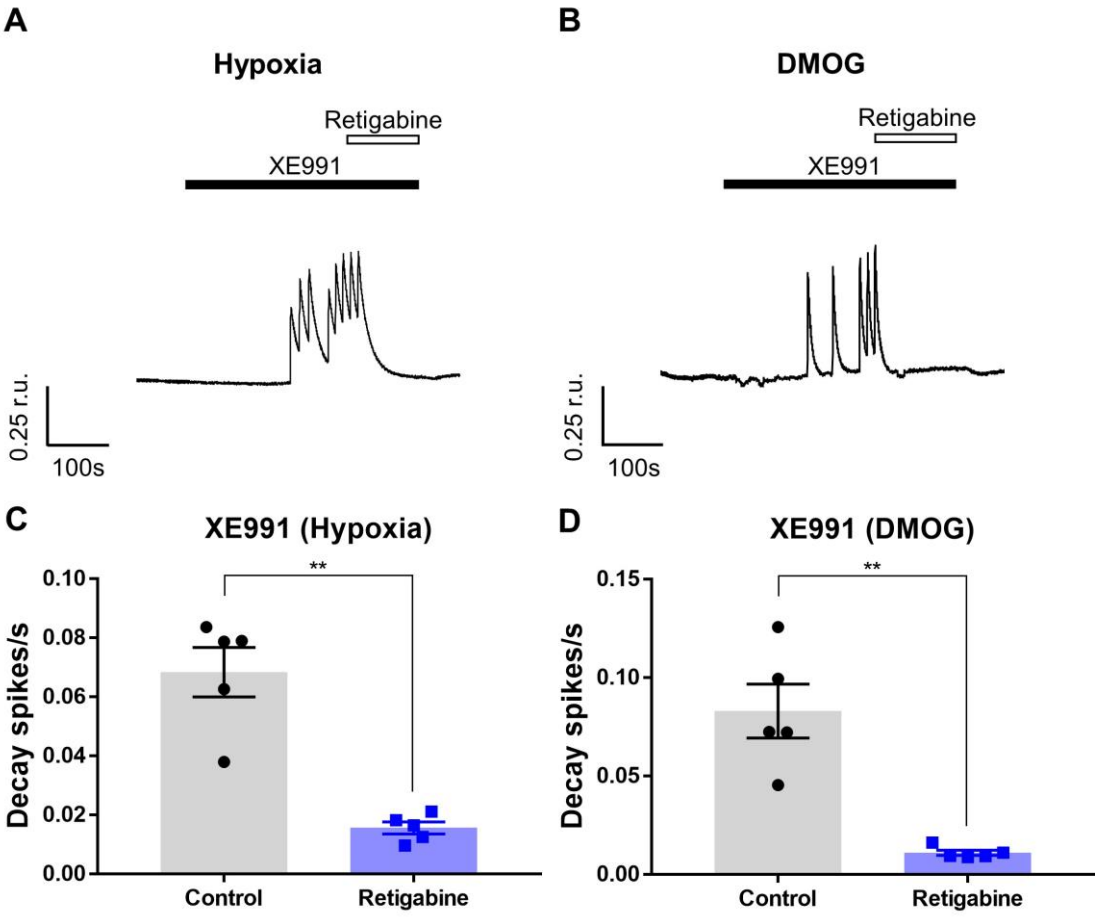

Figure 4.7 Retigabine inhibits XE991-induced repetitive Ca^{2+} oscillations in hypoxic or DMOG-treated cells. (**A-B**) Representative example traces showing Ca^{2+} oscillations evoked by XE991 (10 µM) in the presence of Kv7 channel opener, retigabine (10 µM) in hypoxic (1% O_2, 24h; A) or DMOG (1 mM, 24h; B) condition. (**C-D**) Bar graphs summarising the effects of retigabine on the XE991-induced Ca^{2+} spike frequency (spikes/s) in hypoxic (C) or DMOG (D) condition. Control is the spike frequency in the presence of XE991 measured from the onset of the first spike. For quantification of drug effect, spike frequency was calculated from the onset of the drug application and until the end of the application of XE991. In panels C-D data are presented as mean ± S.E.M.; Statistics performed using paired student's t-test, **P<0.01 (n=5).

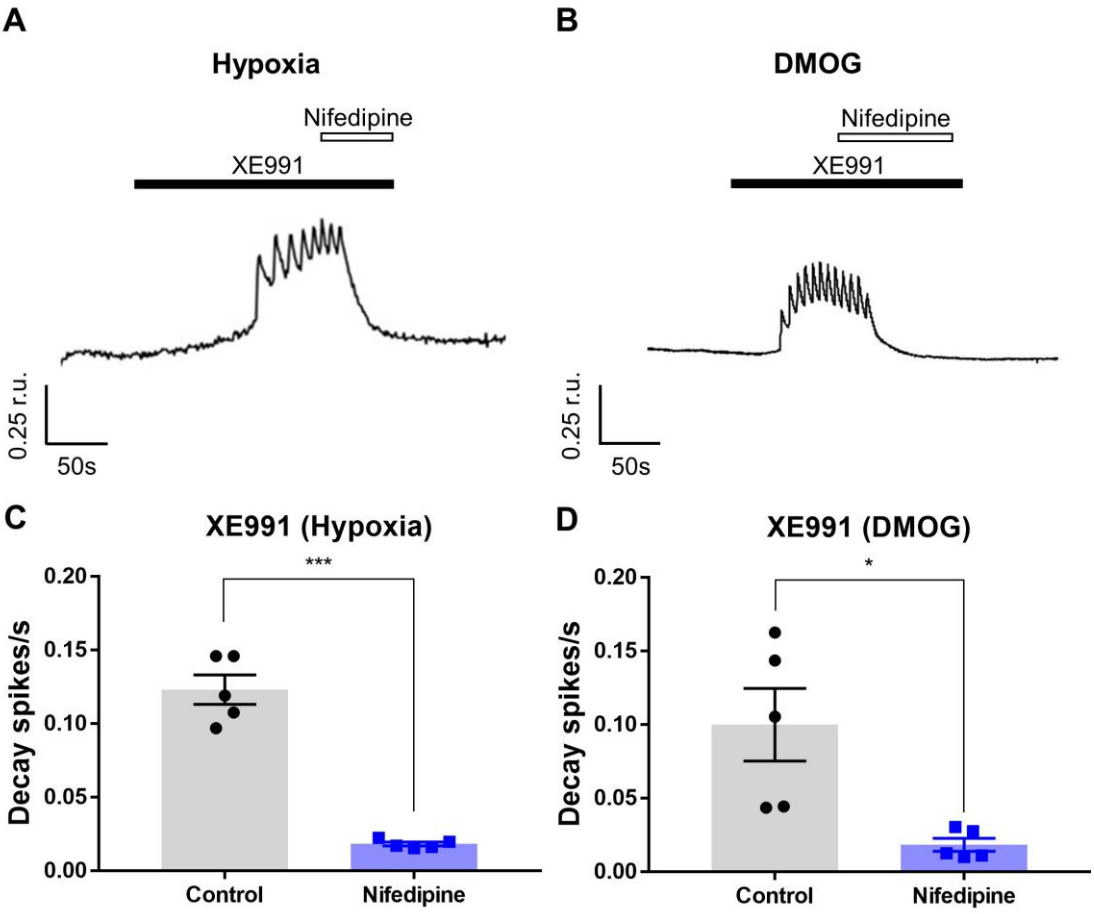

Figure 4.8 Nifedipine inhibits XE991-induced repetitive Ca^{2+} oscillations in hypoxic or DMOG-treated cells. (**A-B**) Representative example traces showing Ca^{2+} oscillations evoked by XE991 (10 µM) in the presence of nifedipine (2 µM) in hypoxic (1% O_2, 24h; A) or DMOG (1mM, 24h; B) condition. (**C-D**) Bar graphs summarising the effects of nifedipine on the XE991-induced Ca^{2+} spike frequency (spikes/s) in hypoxic (C) or DMOG (D) condition. Control is the spike frequency in the presence of XE991 measured from the onset of the first spike. For quantification of drug effect, spike frequency was calculated from the onset of the drug application and until the end of the application of XE991. In panels C-D data are presented as mean ± S.E.M.; Statistics performed using paired student's t-test, *P<0.05, ***P<0.001 (n=5).

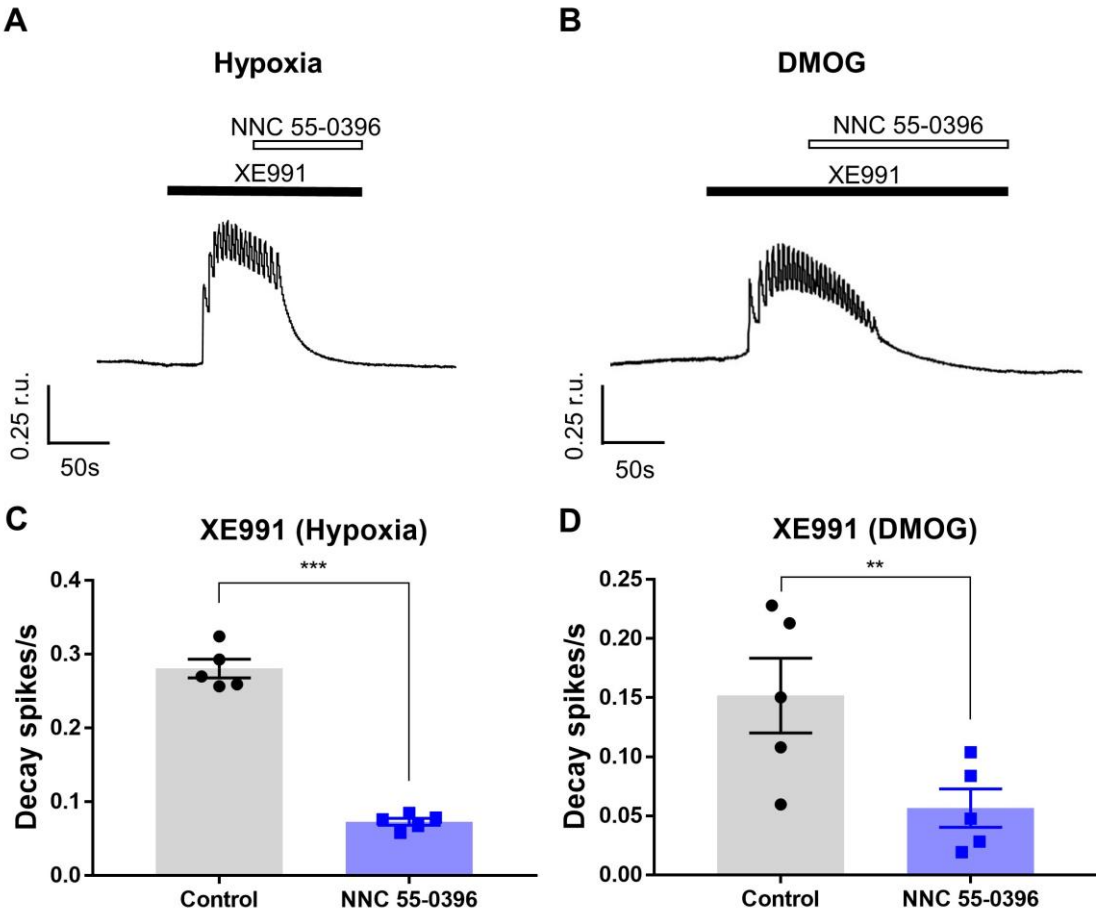

Figure 4.9 NNC 55-0396 inhibits XE991-induced repetitive Ca^{2+} oscillations in hypoxic or DMOG-treated cells. (**A-B**) Representative example traces showing Ca^{2+} oscillations evoked by XE991 (10 µM) in the presence of NNC 55-0396 (3 µM) in hypoxic (1% O_2, 24h; A) or DMOG (1mM, 24h; B) condition. (**C-D**) Bar graphs summarising the effects of NNC 55-0396 on the XE991-induced Ca^{2+} spike frequency (spikes/s) in hypoxic (C) or DMOG (D) condition. Control is the spike frequency in the presence of XE991 measured from the onset of the first spike. For quantification of drug effect, spike frequency was calculated from the onset of the drug application and until the end of the application of XE991. In panels C-D data are presented as mean ± S.E.M.; Statistics performed using paired student's t-test, **P<0.01, ***P<0.001 (n=5).

4.2.4 Hypoxia and DMOG enhance AVP-induced Ca^{2+} signalling

We then investigated the effect of hypoxic condition on the Ca^{2+} signals evoked by AVP in A7r5 cells. We found that both hypoxia and DMOG resulted in a similar pattern of responses to AVP: more frequent Ca^{2+} oscillations that were not reduced upon washout (Figure 4.10A-C). Interestingly, compared to XE991, H2A treatment did not attenuate $[Ca^{2+}]_i$ response to AVP: Ca^{2+} oscillations were still persistent during the washout of AVP (Figure 4.10D).

In hypoxia and DMOG-treated cells, exposure to AVP (100 pM) produced Ca^{2+} response, which did not differ from that of the normoxic cells in its basal, peak Ca^{2+} level and amplitude of Ca^{2+} response (Figure 4.11A-C); in hypoxia/H2A-treated cells, the amplitude of Ca^{2+} response to AVP was significantly reduced though (Figure 4.11C). Ca^{2+} oscillations during AVP expose were more frequent and persisted during the washout of AVP perfusate solution for much longer in hypoxia (0.11 ± 0.03 spikes/s, n=7, $p<0.05$), DMOG (0.12 ± 0.05 spikes/s, n=5, $p<0.05$) and hypoxia/H2A (0.12 ± 0.03, spikes/s n=5, $p<0.05$) than in normoxic conditions (0.06 ± 0.03 spikes/s, n=7; Figure 4.11D). These repetitive Ca^{2+} oscillations mainly originated from VGCCs; however, as was shown in Chapter 3, the liberation of Ca^{2+} from the ER Ca^{2+} channels (IP_3Rs or RyRs) may also contribute, especially in the case of AVP, which does stimulate the IP_3 release. This latter notion could potentially explain the fact that the amplitude of AVP-induced Ca^{2+} signals was not reduced by hypoxia/DMOG and will be discussed later (see section 4.2.7).

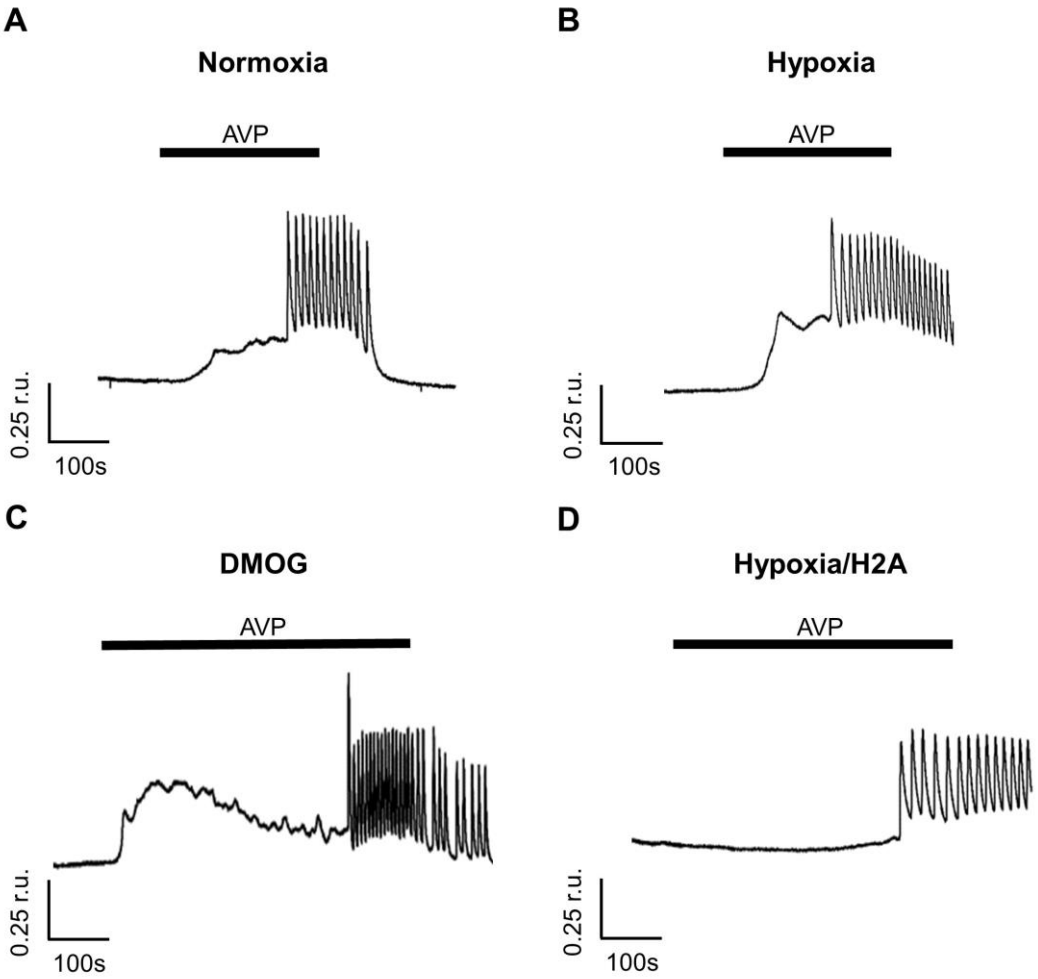

Figure 4.10 Hypoxia and DMOG enhance Ca^{2+} oscillations evoked by AVP stimulation in A7r5 cells. Rises in $[Ca^{2+}]_i$ evoked by the physiological concentration of the vasoactive hormone, vasopressin (AVP; 100 pM). (**A-D**) Representative example traces of AVP-induced Ca^{2+} transients recorded (the period indicated by the solid bar) in normoxic (A), hypoxic (1% O_2, 24h; B), DMOG (1 mM, 24h; C), and hypoxia/H2A (1% O_2 along with H2A 20 µM, 24h; D) conditions.

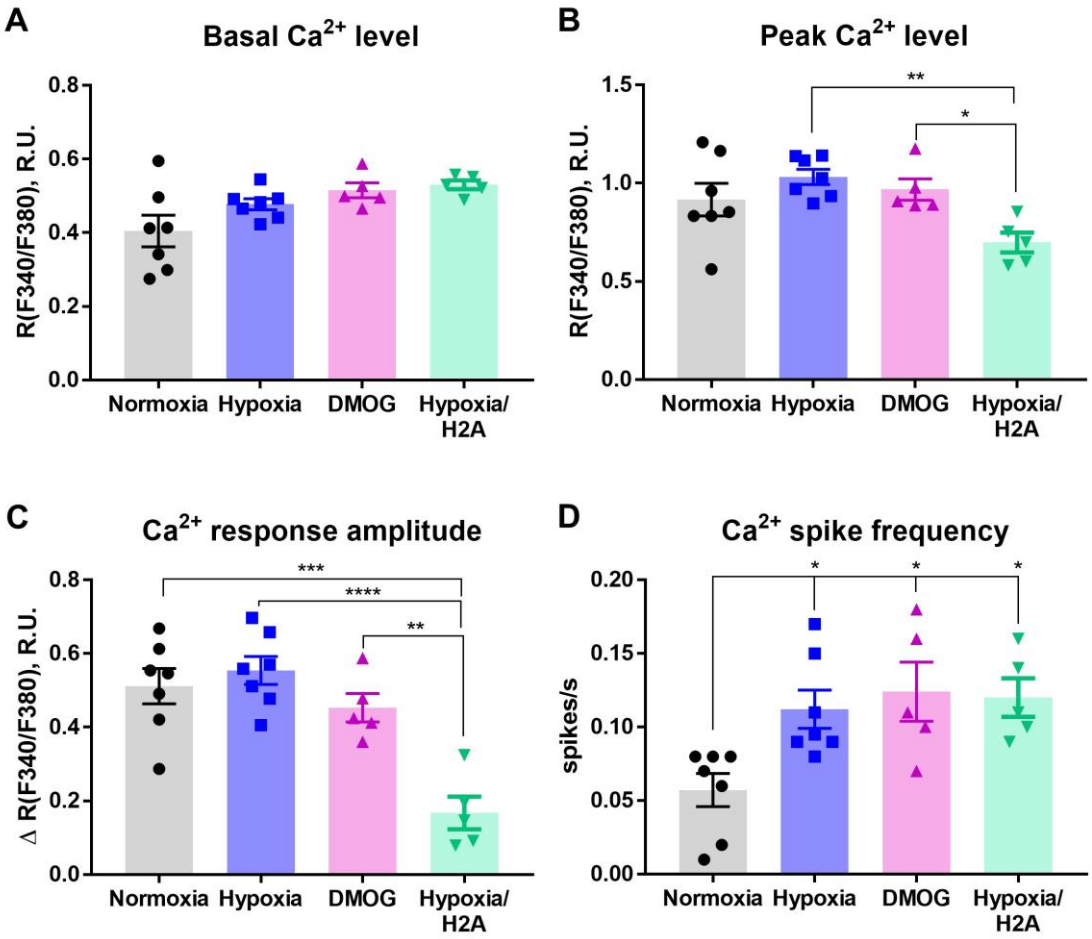

Figure 4.11 Effects of hypoxia on $[Ca^{2+}]_i$ induced by indirect Kv7 channels inhibition (AVP). (**A-D**) Bar graphs summarising the effects of hypoxia on basal Ca^{2+} level (A), peak Ca^{2+} level (B), Ca^{2+} response amplitude (ΔR; C), and Ca^{2+} spike frequency (spikes/s) (D) induced by AVP (100 pM). Data are presented as mean ± S.E.M.; Statistics performed using ANOVA with Sidak test, *P<0.05, **P<0.01, ***P<0.001, ****P<0.0001 (n≥4).

Next, we investigated the effects of retigabine and the contribution of the two VGCC subtypes to AVP-induced Ca^{2+} influx in cells under hypoxic or DMOG-treated condition. AVP responses were variable (especially after DMOG treatment), and in some cases, bursts of spikes were observed instead of continuous spiking. This made the quantification difficult, to circumvent that, retigabine or blockers were applied to the repetitive bursts with continued AVP perfusate, where possible. Application of retigabine (10 µM) abolished repetitive Ca^{2+} oscillations and returned $[Ca^{2+}]_i$ levels to the baseline (Figure 4.12A, B), with transient oscillations at frequencies in hypoxic cells (0.08 ± 0.03 in control vs. 0.01 ± 0.004 spikes/s after retigabine, n=5, $p<0.01$; Figure 4.12C) and in DMOG-treated cells (0.05 ± 0.03 in control vs. 0.02 ± 0.01 spikes/s after retigabine, n=5, $p<0.05$; Figure 4.12D).

Nifedipine (2 µM) or NNC 55-0396 (3 µM) also abolished the Ca^{2+} oscillations and lowered $[Ca^{2+}]_i$ back to the basal level. Figure 4.13A, B show the example traces of responses to AVP in the presence of nifedipine with decreased frequencies of oscillations in hypoxic cells (0.07 ± 0.05 in control vs. 0.009 ± 0.004 spikes/s after nifedipine, n=5, $p<0.05$; Figure 4.13C) and in DMOG-treated cells (0.09 ± 0.06 in control vs. 0.02 ± 0.01 spikes/s after nifedipine, n=5, $p<0.05$; Figure 4.13D). AVP-induced Ca^{2+} oscillations were also stopped by NNC 55-0396, example traces of responses to AVP shown in Figure 4.14A, B. Frequencies of decay oscillations were decreased from 0.09 ± 0.03 (control) to 0.03 ± 0.01 spikes/s (NNC 55-0396) in hypoxic cells (n=5, $p<0.01$; Figure 4.14C) and from 0.02 ± 0.01 (control) to 0.01 ± 0.003 spikes/s (NNC 55-0396; n=5, $p<0.05$; Figure 4.14D) in DMOG-treated cells. Again, these results indicated that vascular Kv7 channels retain tight control over Ca^{2+} entry in response to AVP in hypoxic or DMOG condition.

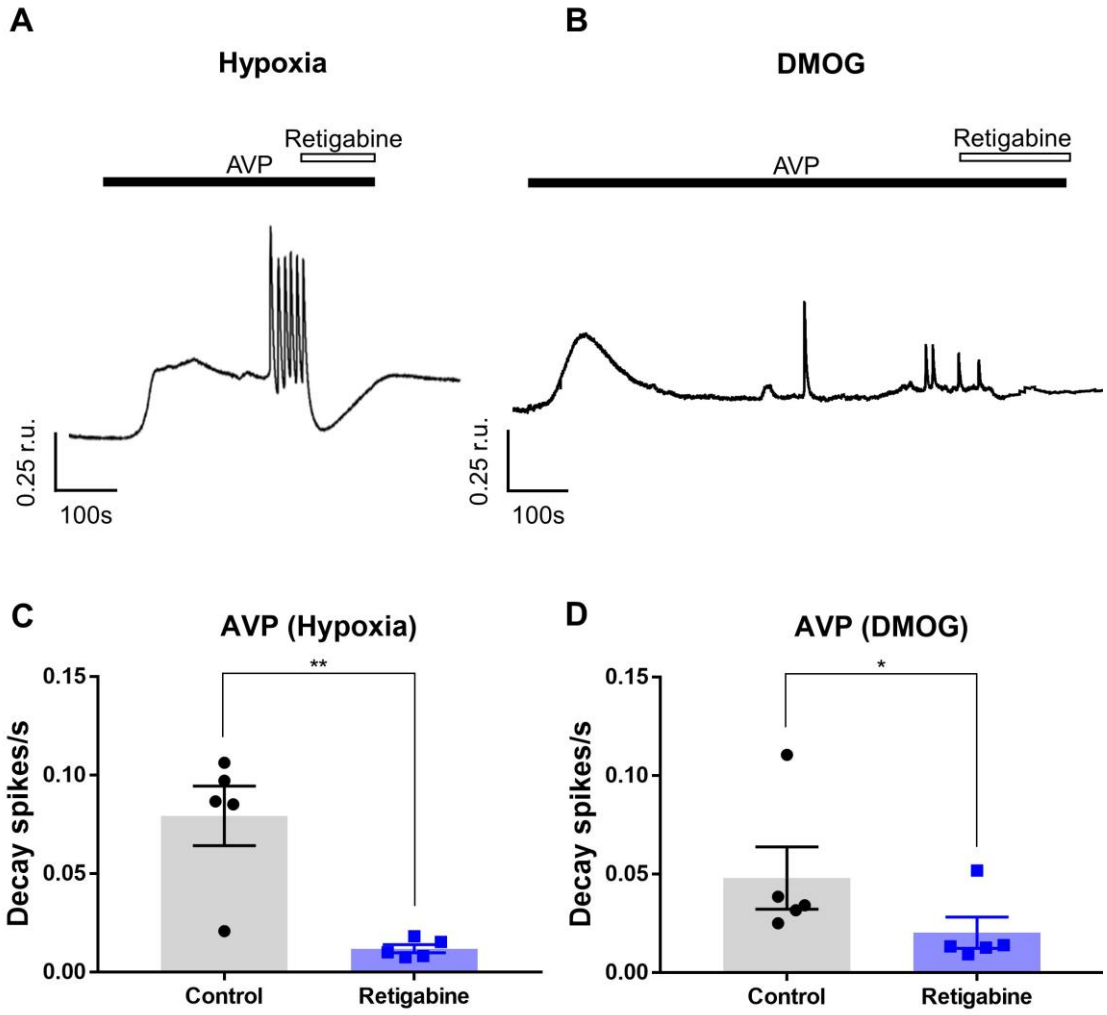

Figure 4.12 Retigabine inhibits AVP-induced repetitive Ca^{2+} oscillations in hypoxic or DMOG-treated cells. (**A-B**) Representative example traces showing Ca^{2+} oscillations evoked by AVP (100 pM) in the presence of retigabine (10 µM) in hypoxic (1% O_2, 24h; A) or DMOG (1 mM, 24h; B) condition. (**C-D**) Bar graphs summarising the effects of retigabine on the AVP-induced Ca^{2+} spike frequency (spikes/s) in hypoxic (C) or DMOG (D) condition. Control is the spike frequency in the presence of AVP measured from the onset of the first spike. For quantification of drug effect, spike frequency was calculated from the onset of the drug application and until the end of the application of AVP. In panels C-D data are presented as mean ± S.E.M.; Statistics performed using paired student's t-test, *P<0.05, **P<0.01 (n=5).

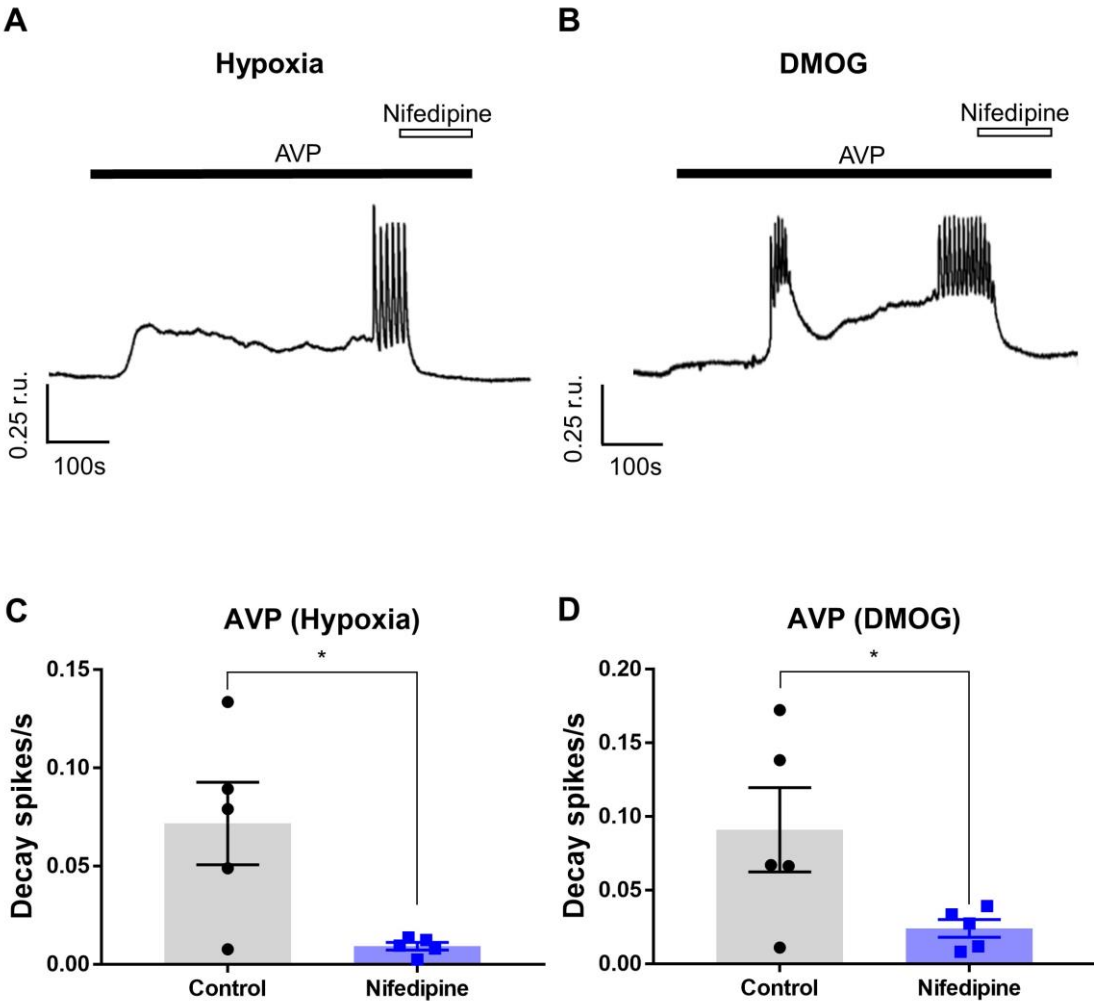

Figure 4.13 Nifedipine inhibits AVP-induced repetitive Ca^{2+} oscillations in hypoxic or DMOG-treated cells. (**A-B**) Representative example traces showing Ca^{2+} oscillations evoked by AVP (100 pM) in the presence of nifedipine (2 μM) in hypoxic (1% O_2, 24h; A) or DMOG (1 mM, 24h; B) condition. (**C-D**) Bar graphs summarising the effects of nifedipine on the AVP-induced Ca^{2+} spike frequency (spikes/s) in hypoxic (C) or DMOG (D) condition. Control is the spike frequency in the presence of AVP measured from the onset of the first spike. For quantification of drug effect, spike frequency was calculated from the onset of the drug application and until the end of the application of AVP. In panels C-D data are presented as mean ± S.E.M.; Statistics performed using paired student's t-test, *P<0.05 (n=5).

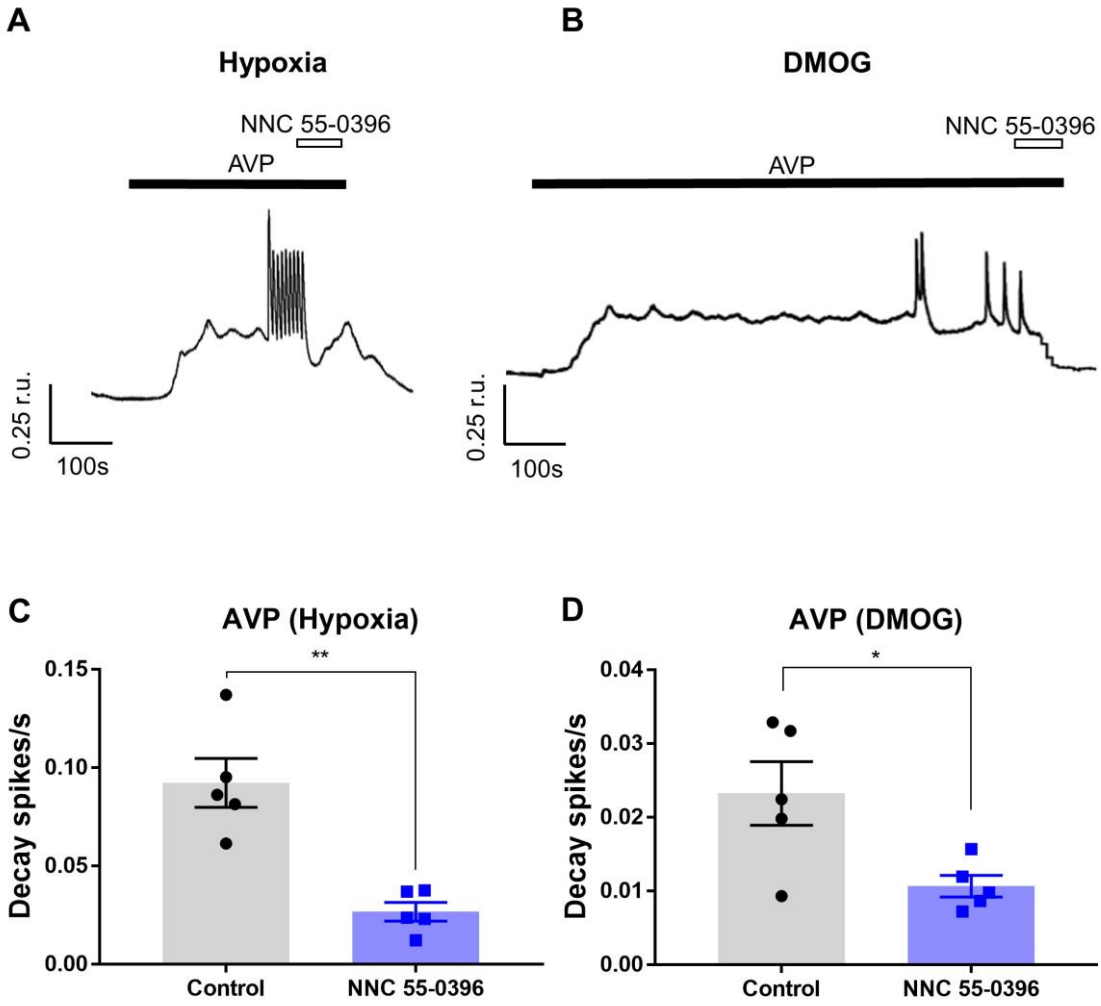

Figure 4.14 NNC 55-0396 inhibits AVP-induced repetitive Ca^{2+} oscillations in hypoxic or DMOG-treated cells. (**A-B**) Representative example traces showing Ca^{2+} oscillations evoked by AVP (100 pM) in the presence of NNC 55-0396 (3 μM) in hypoxic (1% O_2, 24h; A) or DMOG (1 mM, 24h; B) condition. (**C-D**) Bar graphs summarising the effects of NNC 55-0396 on the AVP-induced Ca^{2+} spike frequency (spikes/s) in hypoxic (C) or DMOG (D) condition. Control is the spike frequency in the presence of AVP measured from the onset of the first spike. For quantification of drug effect, spike frequency was calculated from the onset of the drug application and until the end of the application of AVP. In panels C-D data are presented as mean ± S.E.M.; Statistics performed using paired student's t-test, *P<0.05, **P<0.01 (n=5).

4.2.5 Hypoxia, but not DMOG upregulates the Cav3.2 T-type Ca^{2+} channels in A7r5 cells

VSMCs are known to express both Cav1 L- and Cav3 T-type VGCCs, and we have demonstrated the mRNA expression in normoxic A7r5 cells. As discussed in Chapter 3, we already confirmed that *Cacna1c* (Cav1.2) L- and *Cacna1g* (Cav3.1) T-type Ca^{2+} channel genes were the predominant VGCC subtypes in normoxic A7r5 cells (see Figure 3.2). As a next step, we investigated the effects of hypoxia on the mRNA expression of *Cacna1c* (L-type), *Cacna1g*, and *Cacna1h* (T-type) in A7r5 cells.

Exposure of cells to 1% O_2 or 1 mM DMOG for 24h did not significantly change levels of *Cacna1c* (Cav1.2) L-type and *Cacna1g* (Cav3.1) T-type Ca^{2+} channel transcript levels (Figure 4.15A, B). Surprisingly, hypoxia produced a selective and significant increase in *Cacna1h* transcript (Figure 4.15C), Cav3.2 (Figure 4.15D) and HIF-2α protein levels (data not shown). This effect was completely abolished by H2A. On the other hands, DMOG did not mimic the effect of hypoxia as neither *Cacna1h* transcript nor its protein levels were affected by the DMOG treatment (Figure 4.15C, D). Thus, it seems that HIF-2α may be responsible for this hypoxic effect. These results uncover specific upregulation of *Cacna1h* mRNA and Cav3.2 protein levels in A7r5 cells under hypoxic conditions. The hypoxia-induced upregulation of Cav3.2 T-type Ca^{2+} channel was also demonstrated by immunocytochemistry. Cav3.2 showed stronger immunoreactivity in hypoxic compared to normoxic cells by 80.7% (ROI: 2.10 ± 0.35 in hypoxic cells vs. 1.16 ± 0.66 in normoxic cells, at least n≥3 cells quantified, N=3 individual preparations, $p<0.05$; Figure 4.16). It has to be noted that hypoxia/H2A treatment resulted in the significant downregulation of *Cacna1c* and *Cacna1g* (Figure 4.15A, B).

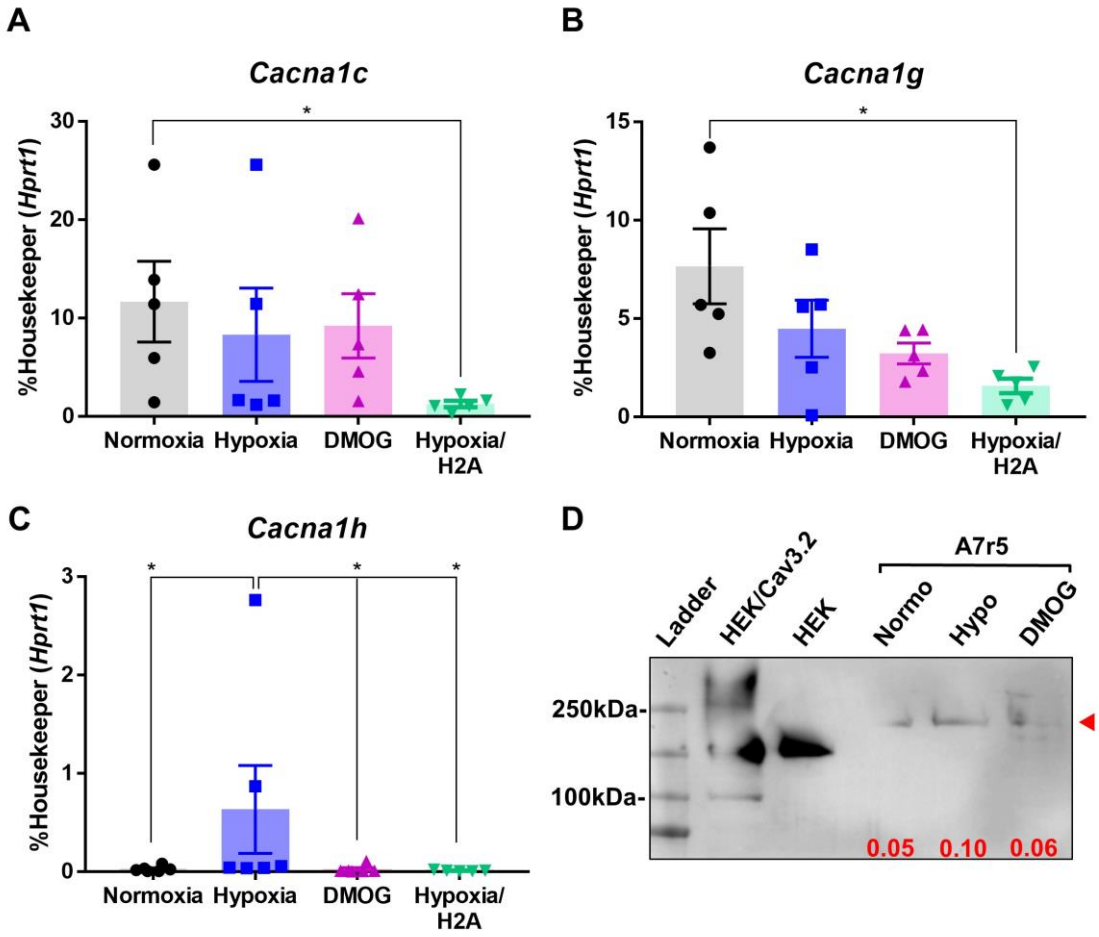

Figure 4.15 Hypoxia upregulates mRNA and protein expression of Cav3.2 T-type Ca^{2+} channel. A7r5 cells were subjected to hypoxia (1% O_2), DMOG (1 mM), hypoxia with H2A (20 µM) for 24h or maintained under normoxia. (**A-C**) Bar graphs showing the quantification of RT-PCR results for *Cacna1c* (A), *Cacna1g* (B) or *Cacna1h* (C); the expression is normalised to that of a housekeeping gene, *Hprt1*. (**D**) Western blot detection of Cav3.2 channel protein expression. The average normalised Cav3.2/β-action ratio for each condition is shown in red (normoxia and hypoxia, n=2; DMOG, n=1). In panels A-C data are presented as mean ± S.E.M.; Statistics performed using ANOVA with Sidak test (A, B) and Wilcoxon-Signed, Mann-Whitney and Kruskal-Wallis ANOVA test (C), *P<0.05 (n≥5).

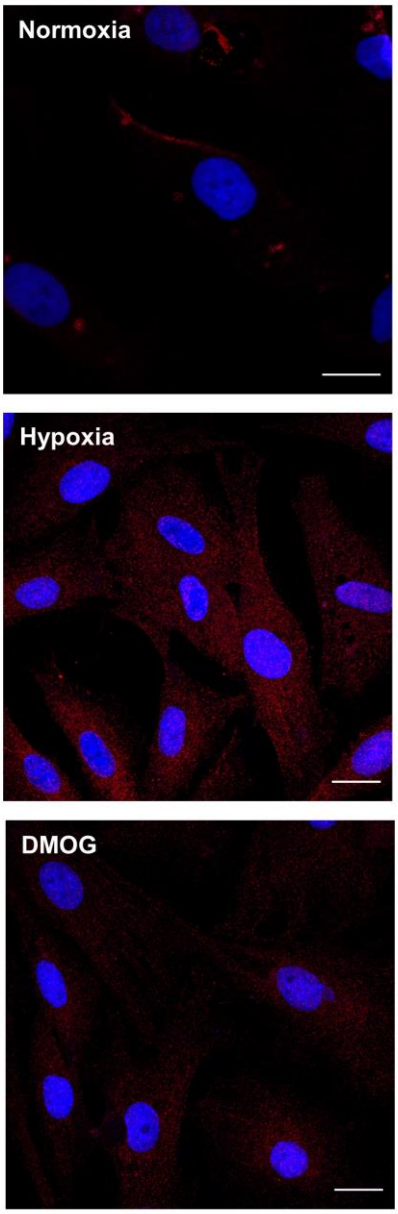

Figure 4.16 Cav3.2 immunoreactivity in A7r5 cells in normoxic and hypoxic conditions. Immunofluorescence labelling of Cav3.2 (red) in normoxia (upper), hypoxia (middle) or DMOG (lower) in A7r5 cells. Cell nuclei (blue) were stained with DAPI; scale bars are 20 µm.

It has to be pointed out that while *Cacna1h* (Cav3.2) transcript level was upregulated by hypoxia, it's level (relative to the housekeeping gene, *Hprt1*, was still an order of magnitude lower, as compared to that of *Cacna1c* (Cav1.2).

4.2.6 Hypoxia and DMOG downregulate Kv7.5 channel in A7r5 cells

We hypothesised that reduced expression and/or activity of Kv7 channels in hypoxic cells could have underlined the increased excitability (increased and prolonged oscillatory activity) of A7r5 cells in response to various depolarising treatment. Indeed, reduced functional activity of Kv7 channels would likely to result in i) more excitable cells and ii) reduced response to XE991; data presented in Figure 4.5 and 4.6 may have presented just such a combination (reduced amplitude of XE991-induced Ca^{2+} transient, but increased oscillation frequency and prolonged oscillations upon XE991 washout). In order to test this hypothesis, we next examined the mRNA expression level of *Kcnq* genes under hypoxia using the RT-PCR method. Hypoxia or DMOG treatment caused a general trend for downregulation of all *Kcnq* genes tested in A7r5 cells, but only for *Kcnq5*, the effect has reached significance (Figure 4.17A-C). The mRNA levels of *Kcnq5* was significantly decreased in the hypoxic cells compared to the normoxic cells (Figure 4.17C). The effect was mimicked by DMOG but not prevented by H2A, indicating that in contrast to the *Cacna1h,* hypoxic downregulation of *Kcnq5* is mediated by HIF-1α. Accordingly, the Kv7.5 immunoreactivity was also reduced after both, hypoxic and DMOG treatment, as tested by western blot (Figure 4.17D) and immunostaining by 38.7% (ROI: 3.37 ± 0.63 in normoxic cells vs. 2.07 ± 0.47 in hypoxic cells, at least n≥3 cells quantified, N=3 individual preparations p=0.18; Figure 4.18).

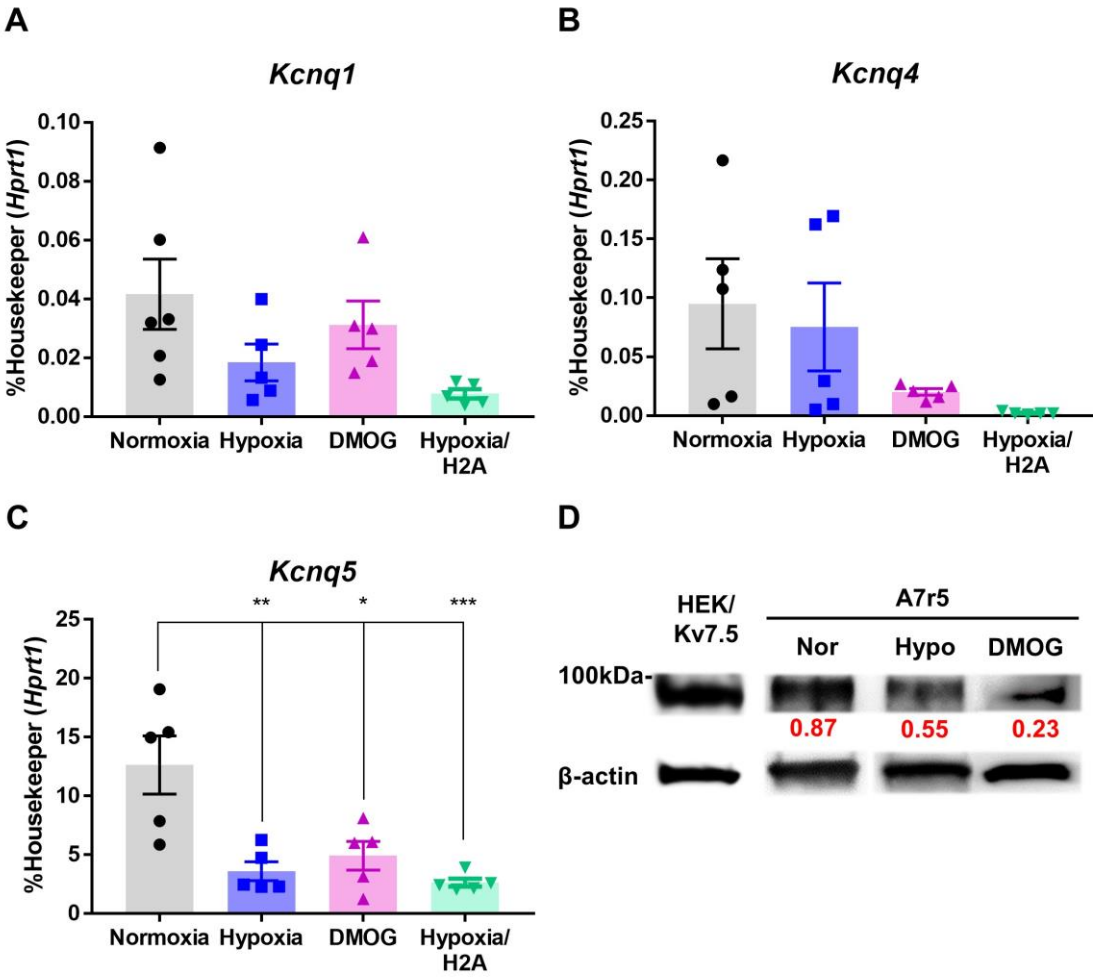

Figure 4.17 Hypoxia and DMOG downregulate mRNA and protein expression of Kv7 channels with significance in Kv7.5 subunit. A7r5 cells were subjected to hypoxia (1% O_2), DMOG (1 mM) or hypoxia with H2A (20 µM) for 24h or maintained under normoxia. (**A-C**) Bar graphs showing the quantification of RT-PCR results for *Kcnq1* (A), *Kcnq4* (B) or *Kcnq5* (C), the expression is normalised to that of a housekeeping gene, *Hprt1*. (**D**) Western blot detection of Kv7.5 channel protein expression. The average normalised Kv7.5/β-action ratio for each condition is shown in red. In panels A-C data are presented as mean ± S.E.M.; Statistics performed using ANOVA with Sidak test, *P<0.05, **P<0.01, ***P<0.001 (n=5).

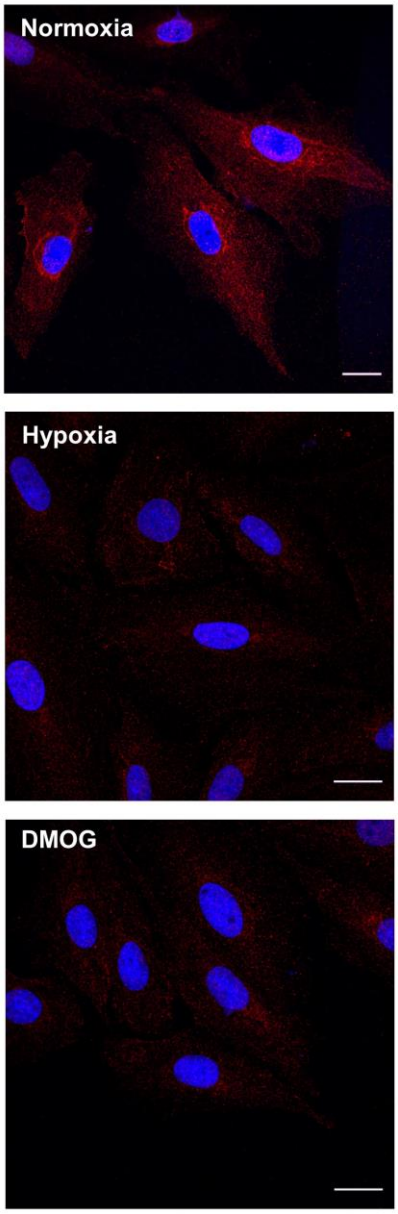

Figure 4.18 Kv7.5 immunoreactivity in A7r5 cells in normoxic and hypoxic conditions. Immunofluorescence labelling of Kv7.5 (red) in normoxia (upper), hypoxia (middle) or DMOG (lower) in A7r5 cells. Cell nuclei (blue) were stained with DAPI; scale bars are 20 μm.

In sum, the results described above suggested that 1) both hypoxia and DMOG induce downregulation of Kv7 channel expression, especially the main subunit, Kv7.5. 2) The amplitude of the depolarising effect of XE991 is reduced after hypoxia/DMOG treatment, but the cells are more excitable (consistent with the reduced functional activity of Kv7 channels). 3) Retigabine is still effective to reverse the depolarisation-induced Ca^{2+} signals in hypoxia/DMOG-treated cells. 4) Hypoxia but not DMOG induced upregulation of Cav3.2 expression. 5) L-type Ca^{2+} channels are the major contributor to the depolarisation-induced Ca^{2+} response in hypoxic A7r5 cells.

4.2.7 Effects of PLC inhibition and ER Ca^{2+} channel blockers on AVP-induced Ca^{2+} oscillations in hypoxic and DMOG conditions

Our previous work has shown that the ER-released Ca^{2+} in A7r5 cells does contribute to AVP-induced Ca^{2+} signalling (Chapter 3). In addition, a recent report showed that hypoxia enhanced PLC activation, IP_3 production, IP_3R opening, Ca^{2+} release, and contraction in mouse PASMCs (Yadav et al., 2018). Hence, in the next step, we investigated the effects of hypoxia and DMOG on PLC-IP_3 signalling and ER Ca^{2+} channels using 10 μM edelfosine (PLC inhibitor), 100 μM 2-APB (IP_3Rs inhibitor) and 100 μM tetracaine (RyRs inhibitor).

Under the hypoxic or DMOG-treated condition, edelfosine produced a similar inhibiting effect on AVP-induced Ca^{2+} signals compared to the normoxic condition (Figure 4.19A-C). Ten minutes pretreatment of A7r5 cells with edelfosine (10 μM) attenuated the $[Ca^{2+}]_i$ response to AVP (100 pM) in A7r5 cells, but there was no significant difference in peak Ca^{2+} and response amplitude among groups (Figure 4.19D, E). Although there were some occasional Ca^{2+} spikes, the frequency of

spikes was reduced in hypoxic or in DMOG-treated cells (number: 0.01 spikes/s, n=5 in hypoxia; 0.02 spikes/s, n=5 in DMOG; Figure 4.19F).

We next analysed the contribution of IP_3Rs and RyRs to the AVP-induced Ca^{2+} mobilisation in hypoxic condition. Cells were pretreated with either 2-APB (100 µM) or tetracaine (100 µM) for 2 minutes, then perfused continuously with AVP-containing buffer. 2-APB did not completely abolished oscillations (Figure 4.20A-C), moreover, in some cells it induced some Ca^{2+} response even before the application of AVP (Figure 4.20A-C), suggesting it may have a non-specific effect to activate some Ca^{2+} channels, such as TRPV or CRAC (Colton and Zhu, 2007; Xu et al., 2016). Thus, the effects of 2-APB are hard to interpret at present. Nevertheless, 2-APB attenuated the peak Ca^{2+} and amplitude of the sustained $[Ca^{2+}]_i$ elevation induced by AVP in both normoxic and DMOG conditions (Figure 4.20D, E). 2-APB was significantly less efficacious in reducing AVP-induced Ca^{2+} signals in hypoxic condition, as compared to normoxic and DMOG-treated cells (in the presence of 2-APB, AVP-induced ΔR: 0.41 ± 0.11, n=5 in hypoxic cells vs. 0.13 ± 0.09, n=5 in normoxic cells vs. 0.14 ± 0.04, n=4 in DMOG-treated cells; Figure 4.20E, cf. Figure 4.11).

When cells were treated with tetracaine, however, AVP still caused continuous Ca^{2+} oscillations in hypoxic cells and a mild increase of $[Ca^{2+}]_i$ in DMOG-treated cells (Figure 4.21A-D and F). The amplitude of $[Ca^{2+}]_i$ response to AVP in the presence of tetracaine was significantly higher in hypoxic condition (in the presence of tetracaine, AVP-induced ΔR: 0.20 ± 0.10, n=5 in hypoxic cells vs. 0.06 ± 0.02, n=5 in normoxic cells, $p<0.05$; Figure 4.21E, cf. Figure 4.11),

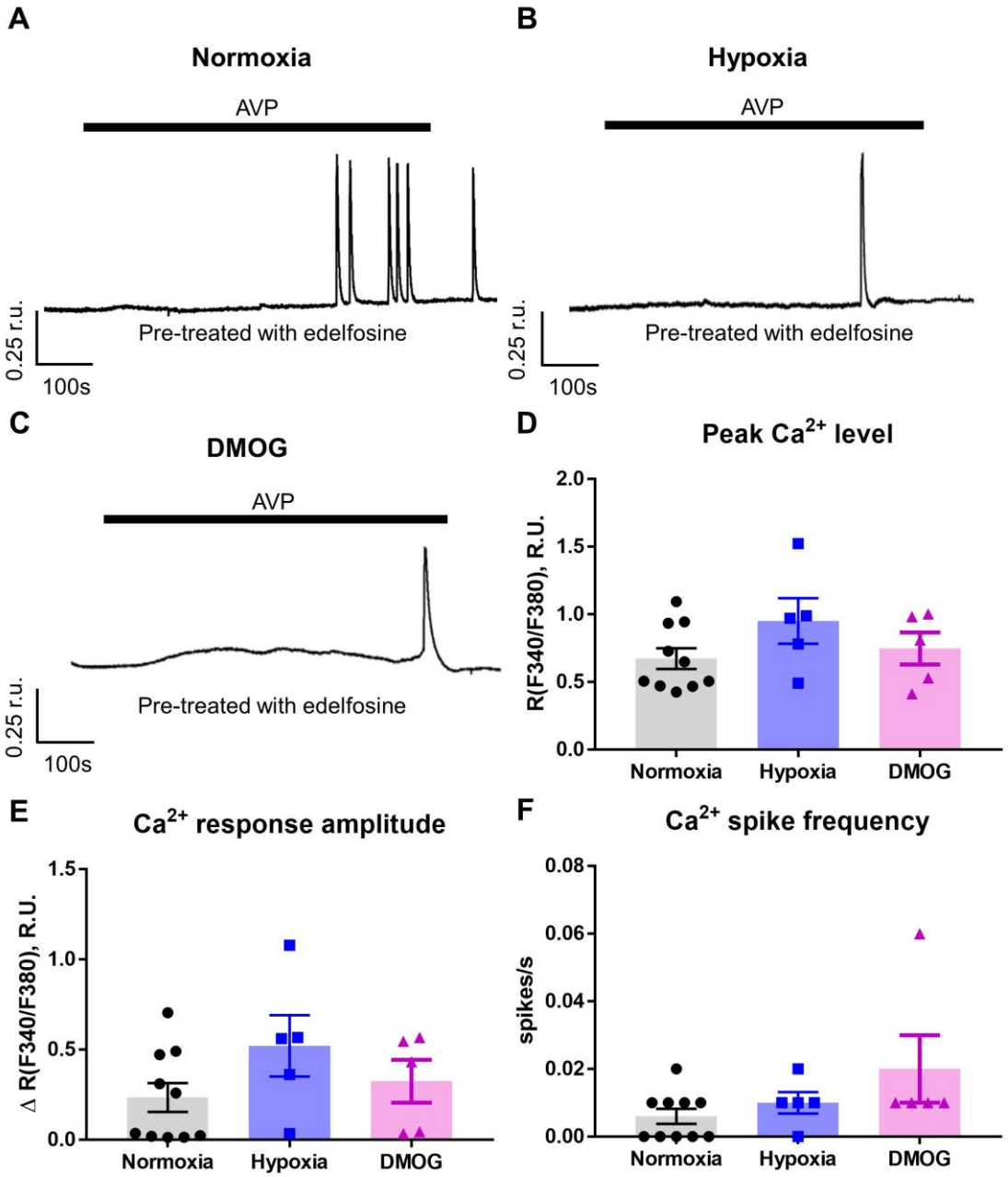

Figure 4.19 AVP-induced Ca^{2+} oscillations are sensitive to PLC inhibition in hypoxic condition. (**A-C**) Representative example traces showing Ca^{2+} transients evoked by AVP (100 pM) in A7r5 cells pretreated with PLC inhibitor, edelfosine (10 μM) in normoxic (A), hypoxic (B) or DMOG (C) condition. (**D-F**) Bar graphs summarising the effects of edelfosine on the peak Ca^{2+} level (D), Ca^{2+} response amplitude (ΔR; E) and Ca^{2+} spike frequency (spikes/s) (F) induced by AVP. In panels D-F data are presented as mean ± S.E.M.; Statistics performed using ANOVA with Sidak test (n≥5).

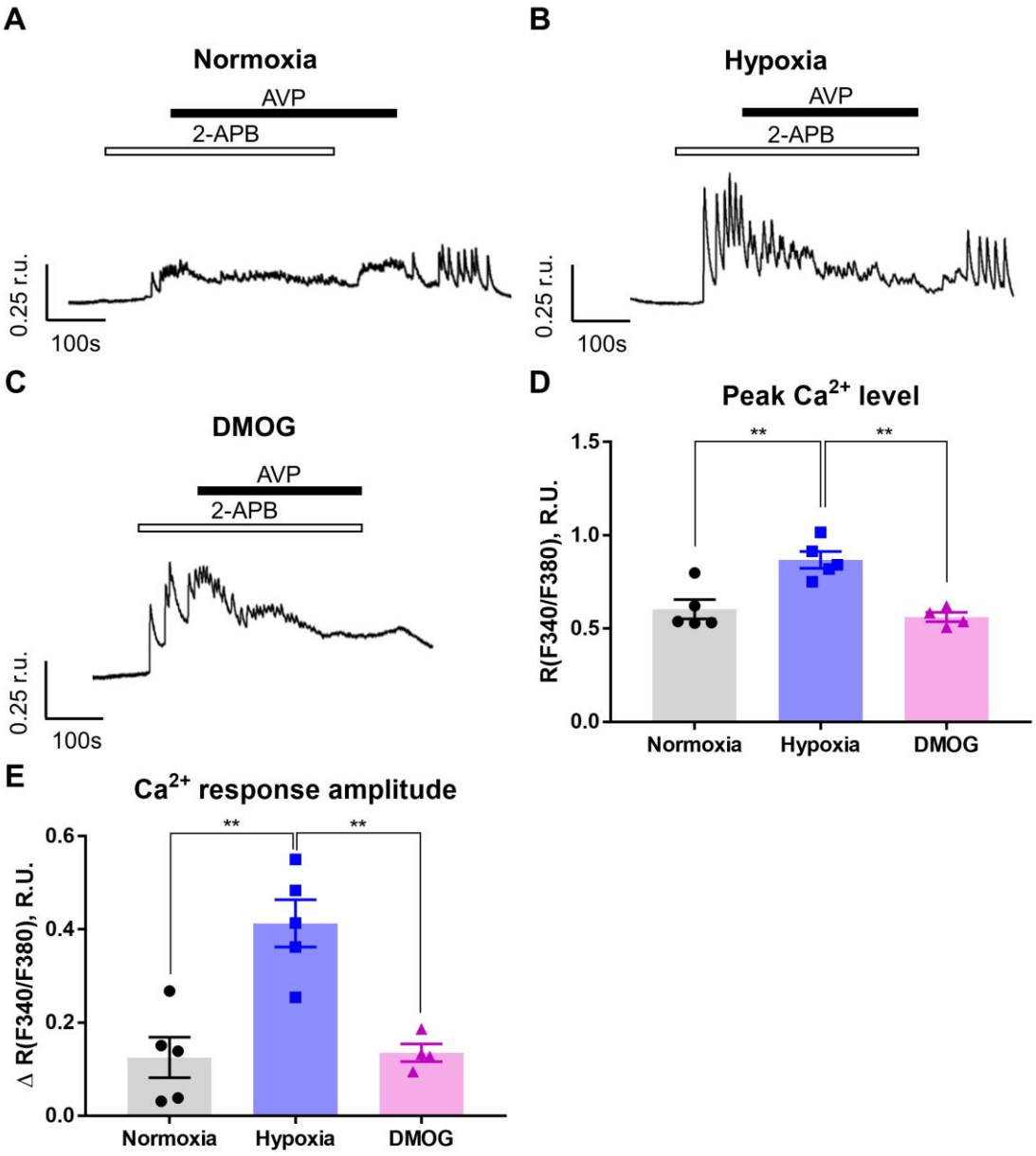

Figure 4.20 AVP-induced Ca^{2+} oscillations reduced by the IP_3Rs blocker in hypoxic condition. (**A-C**) Representative example traces showing Ca^{2+} transients evoked by AVP (100 pM) in A7r5 cells pretreated with 2-APB (IP_3Rs inhibitor; 100 µM) in normoxic (A), hypoxic (B) or DMOG (C) condition. (**D-E**) Bar graphs summarising the effects of 2-APB on the peak Ca^{2+} level (D) and Ca^{2+} response amplitude (ΔR; E) induced by AVP. In panels D-E data are presented as mean ± S.E.M.; Statistics performed using ANOVA with Sidak test, **P<0.01 (n≥4).

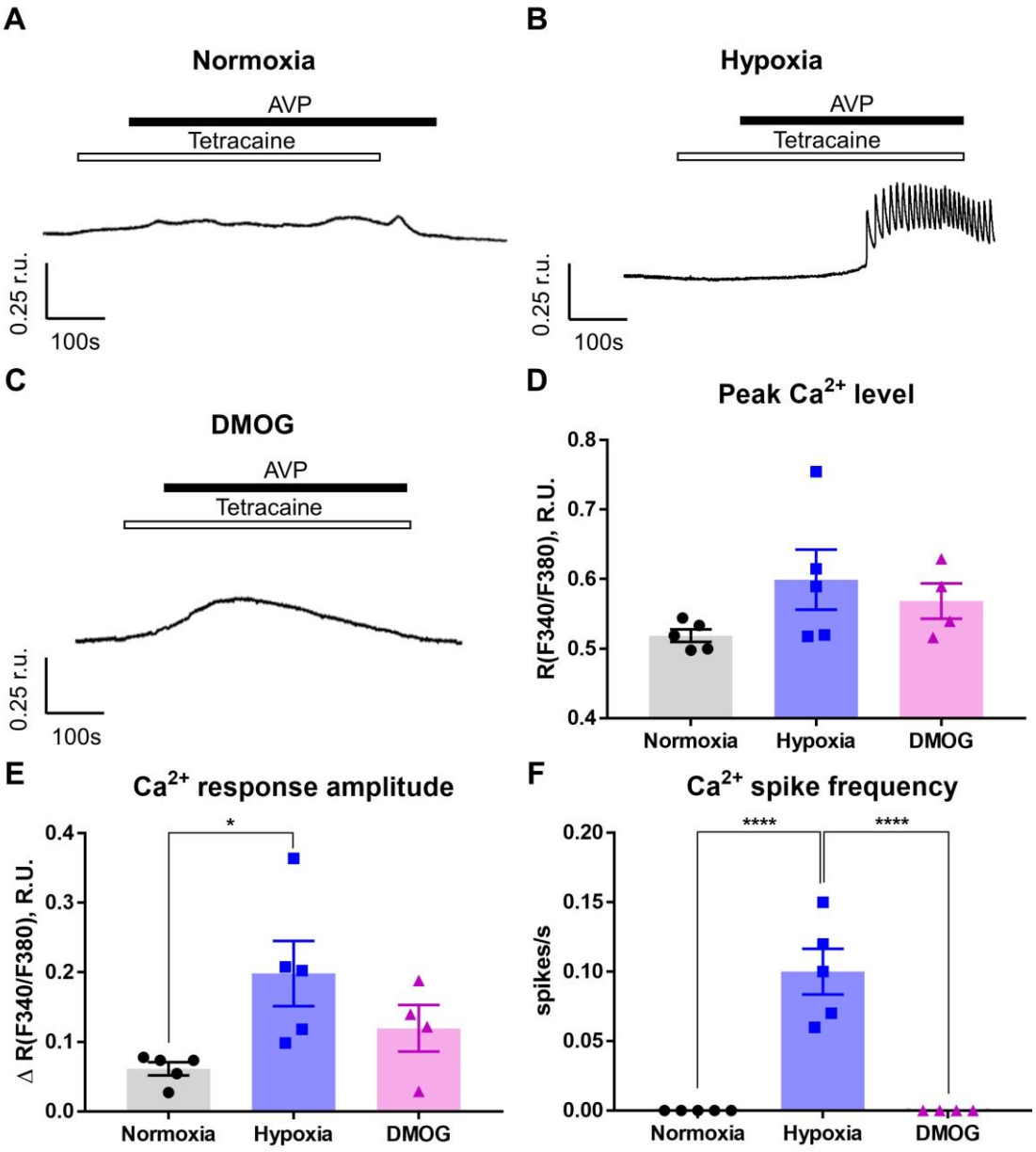

Figure 4.21 RyRs blocker does not inhibit AVP-induced Ca^{2+} oscillations in hypoxic condition. (**A-C**) Representative example traces showing Ca^{2+} transients evoked by AVP (100 pM) in A7r5 cells pretreated with tetracaine (RyRs inhibitor; 100 µM) in normoxic (A), hypoxic (B) or DMOG (C) condition. (**D-F**) Bar graphs summarising the effects of tetracaine on the peak Ca^{2+} level (D), Ca^{2+} response amplitude (ΔR; E) and Ca^{2+} spike frequency (spikes/s) (F) induced by AVP. In panels D-F data are presented as mean ± S.E.M.; Statistics performed using ANOVA with Sidak test, *P<0.05, ****P<0.0001 (n≥4).

suggesting lower efficacy of this agent to inhibit AVP-induced Ca^{2+} transients under hypoxic conditions. This may indicate the inhibition of either IP_3Rs or RyRs may alter the relative contribution of Ca^{2+} release via ER Ca^{2+} store to remodel $[Ca^{2+}]_i$ or the hyperactivity of IP_3Rs in the absence of ER Ca^{2+} overload, which has been reported in Alzheimer's disease (Cheung et al., 2008), although further experiments are needed to obtain better clarity.

Both application of 2-APB and tetracaine attenuated AVP-induced $[Ca^{2+}]_i$ oscillations in hypoxic or DMOG-treated cells (Figure 4.22A-C). As compared to normoxic cells, a similar reduction on AVP-induced $[Ca^{2+}]_i$ was found among groups in the peak Ca^{2+} level (Figure 4.22D) and the response amplitude of $[Ca^{2+}]_i$ in hypoxic or DMOG-treated cells (ΔR: 0.06 ± 0.03, n=5 in normoxic cells vs. 0.05 ± 0.01, n=5 in hypoxic cells vs. 0.11 ± 0.04, n=4 in DMOG-treated cells; Figure 4.22E). The results shown above suggest that ER Ca^{2+} channels are crucial factors in the AVP-stimulation in normoxic and hypoxic A7r5 cells.

4.3 Discussion

This chapter reports several findings revealing possible novel mechanisms behind the effects of hypoxia on Ca^{2+} homeostasis. First, we show that in hypoxia and DMOG condition, both direct (XE991) and GPCR mediated (AVP) Kv7 channel inhibition resulted in the increased frequency and duration of Ca^{2+} oscillations. Consistent with the above effects, our results show that hypoxia and DMOG treatment caused a significant downregulation of the Kv7.5 channel in A7r5 VSMCs. H2A did not abolish this effect, pointing to HIF-1α as a possible mediator.

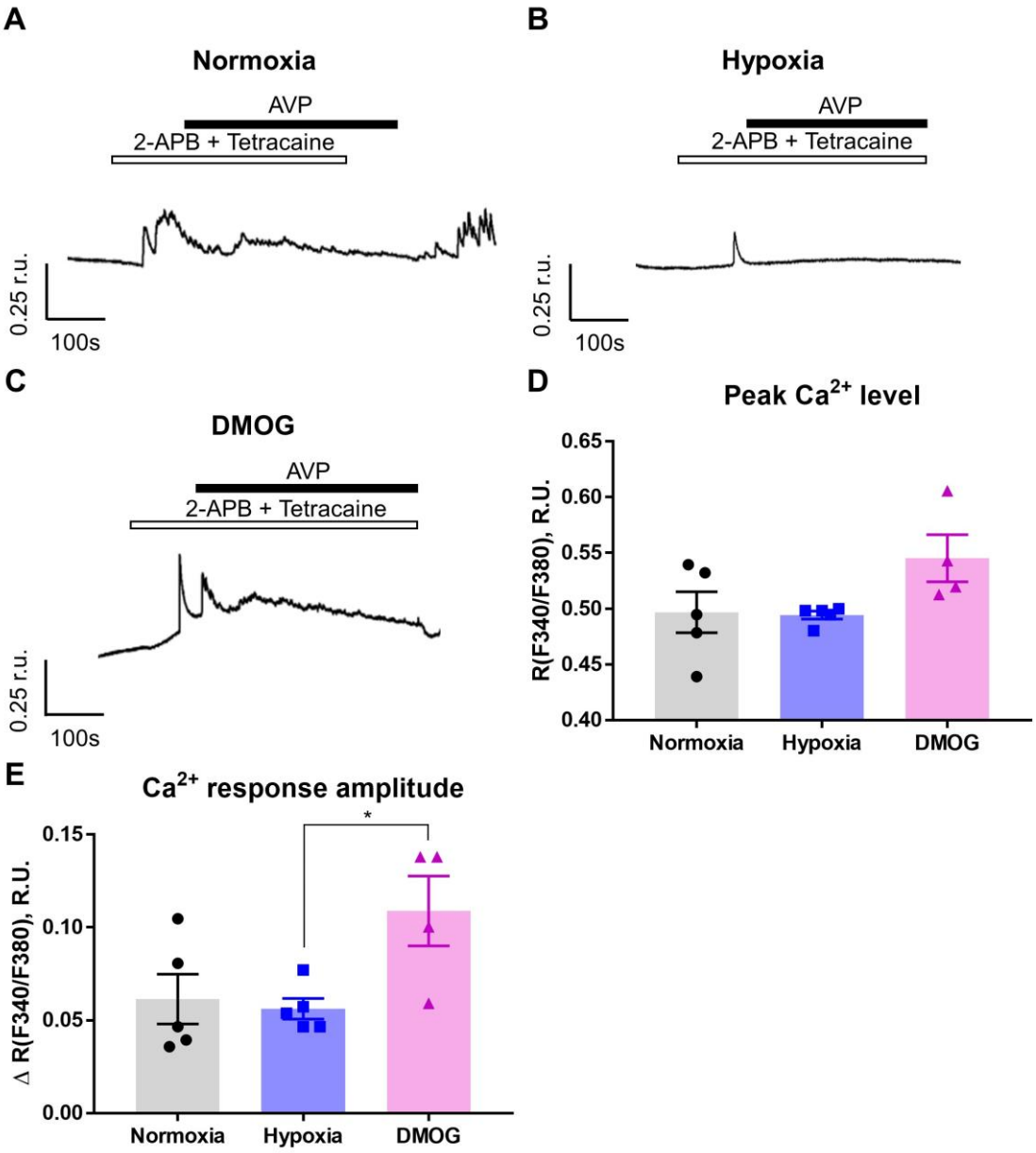

Figure 4.22 AVP-induced Ca^{2+} oscillations are reduced by inhibition of ER Ca^{2+} release channels. (**A-C**) Representative example traces of AVP-induced Ca^{2+} transients recorded in the presence of both 2-APB (100 μM) and tetracaine (100 μM) in normoxic (A), hypoxic (B) or DMOG (C) condition. (**D-E**) Bar graphs summarising the effects of both 2-APB and tetracaine on the peak Ca^{2+} level (D) and Ca^{2+} response amplitude (ΔR; E) induced by AVP. In panels D-E data are presented as mean ± S.E.M.; Statistics performed using ANOVA with Sidak test, *P<0.05 (n≥4).

It was shown previously that chronic hypoxia resulted in the downregulation of the mRNA expression in Kv1.2, Kv1.5, and Kv2.1 channels in PASMCs (Hong et al., 2004). While the effects of hypoxia on Kv7 channels and their roles on $[Ca^{2+}]_i$ were not fully known in VSMCs, it was shown that *Kcnq4* mRNA expression was downregulated in a hypoxic environment, but there was only a little change in the level of Kv7.4 protein expression. There were no significant differences in rat PASMCs *Kcnq1* and *Kcnq5* expression (Sedivy et al., 2015). Importantly, despite the decrease of the Kv7.5 channel abundance in hypoxia, retigabine was able to promptly stop the oscillations and return $[Ca^{2+}]_i$ to basal levels, indicating that Kv7 channels remain an essential player in the regulation of Ca^{2+} signalling under hypoxic/DMOG condition. Oscillations in $[Ca^{2+}]_i$ is associated with the vasoconstriction and vasomotion. The attenuation of repetitive $[Ca^{2+}]_i$ oscillations in hypoxic VSMCs by retigabine suggests that despite downregulation, there is still sufficient Kv7 activity in the hypoxic VSMCs to be pharmacologically targeted to offset hypoxic/ischaemic response in the vasculature. This potentially opens a new therapeutic window for novel treatments.

Second, we show a possible increase in T-type Ca^{2+} channel contribution to hypoxic Ca^{2+} cycling during the resting stage. Studies in VSMCs demonstrated that hypoxia might exert a contrasting effect on VGCCs in SMCs of different origin (Ureña et al., 1996) with the inhibition of L-type VGCCs (Smani et al., 2002) or the upregulation of T-type VGCCs (Lopez-Barneo et al., 2004) both being reported. In our study, analysis of the relative VGCC expression showed the declining trend in the mRNA expression of *Cacna1c* (Cav1.2) and *Cacna1g* (Cav3.1) VGCCs. Surprisingly, *Cacan1h* (Cav3.2) was significantly upregulated in hypoxic cells, an effect that was abolished by H2A but not mimicked under the

DMOG treatment of A7r5 cells. In high-K^+-induced Ca^{2+} transients, hypoxia caused prolonged Ca^{2+} oscillations during the high-K^+ washout, this effect was also abolished by H2A but not mimicked under the DMOG (Figure 4.1 and 4.2). Thus, it appears that increased excitability in response to bulk depolarisation and Cav3.2 upregulation is associated with HIF-2α. However, there may also be additional effects, for instance, post-translational modulations or other signalling events could alter the gating properties of T-type channels. For example, calmodulin-dependent kinase II was shown to stimulate T-type Ca^{2+} channel currents (Barrett et al., 2000).

Hypoxia upregulated the Cav3.2 channel in several cell lines, such as PC12, chromaffin, PASMCs and cardiac myocytes (Gonzalez-Rodriguez et al., 2015; Sellak et al., 2014; Del Toro et al., 2003; Wan et al., 2013), but remained unchanged in A7r5 cells under hypoxia (3% O_2; 12h) in one study (Sellak et al., 2014). Our experiments were performed at 1% O_2 for 24h, which are widely used conditions in the in vitro gene regulation studies (Hammond et al., 2014; Gonzalez-Rodriguez et al., 2015). This extended hypoxic incubation time may account for the difference between our study and that of Sellak and colleagues.

Although the molecular mechanisms underlying this upregulation are not entirely known, our data support the concept that the increased expression of Cav3.2 T-type VGCC may be intimately involved in the cellular Ca^{2+} loading in hypoxic VSMCs due to the increase in the Cav3.2 ‘‘window current’’ at resting E_m (Pluteanu and Cribbs, 2009). It has to be noted that even after upregulation in hypoxic condition, the *Cacna1h* transcript levels were still an order of magnitude lower as compared to that of *Cacna1c* (Cav1.2). Nifedipine remains to produce

more substantial inhibition in high-K^+ $[Ca^{2+}]_i$ transients, indicating a significant contribution of L-type VGCCs in hypoxic cells.

Other factors complicating the system are gaseous mediators (gasotransmitters), as their cellular metabolism is affected in hypoxic conditions. These include hydrogen sulfide (H_2S) and carbon monoxide (CO) (Prabhakar, 2012). CO has been reported to inhibit L- (Dallas et al., 2009) and T-type Ca^{2+} channels (Boycott et al., 2013); similar effects on T-type channels were reported for H_2S (Elies et al., 2014). However, the exact relationships between the HIF-α-induced transcriptional upregulation of Cav3.2 (present study) and their acute modulation by H_2S (Peers et al., 2012; Elies et al., 2016) and CO (Duckles et al., 2015; Dulak et al., 2008) remains to be elucidated.

Third, we show that there is a lesser contribution of ER Ca^{2+} release to AVP in hypoxic condition. Hypoxia alternatively reflects changes in Ca^{2+} homeostasis, which is regulated by complex coupling between ion channels, ER/SR, and mitochondria (Shimoda and Polak, 2011). We have shown that edelfosine (PLC inhibitor) attenuated the AVP-induced amplitude of $[Ca^{2+}]_i$ elevation and mean spike frequency in normoxic A7r5 cells (Chapter 3). Indeed, inhibition of PLC produced an inhibiting effect in hypoxic or DMOG-treated cells, as well as normoxic cells. Compared to normoxic cells, the inhibition of either IP_3Rs or RyRs to AVP-induced $[Ca^{2+}]_i$ produced a higher amplitude of Ca^{2+} elevation in hypoxic cells. Interestingly, instead of the mild elevation of $[Ca^{2+}]_i$, AVP still induced Ca^{2+} oscillations under the inhibition of RyRs in hypoxic cells, indicating the cross-talk between IP_3Rs and RyRs or another complex AVP-induced Ca^{2+} signalling in

SMCs, such as the participation of the RhoA/ROCK pathway in hypoxic VSMCs (Martinsen et al., 2012; Lu et al., 2017).

Release of Ca^{2+} from intracellular Ca^{2+} store plays a vital role in AVP-induced $[Ca^{2+}]_i$ increase (Henderson and Byron, 2007). Our study found that after 2-APB administration, sustained $[Ca^{2+}]_i$ oscillations were attenuated in hypoxic cells, but the inhibiting effect of 2-APB on IP_3Rs was less pronounced in hypoxic condition. Although we have shown that tetracaine could significantly attenuate AVP-induced $[Ca^{2+}]_i$ increase in normoxic A7r5 cells (see Figure 3.11B), our study did not show this inhibiting effect but instead the persistent Ca^{2+} oscillations in hypoxic condition. One reason for this discrepancy could be that the binding of IP_3 to IP_3Rs is enhanced by hypoxia (Yadav et al., 2018) or the activation of RyRs is unaffected by hypoxia (Smani et al., 2002). Alternatively, the ER Ca^{2+} load could be reduced under hypoxia, although further investigation is needed to establish the exact mechanism of this effect.

Nevertheless, the application of 2-APB and tetracaine did suppress the Ca^{2+} spikes and enhancement of $[Ca^{2+}]_i$ in hypoxic cells. These results suggest that in hypoxic VSMCs, the increase in $[Ca^{2+}]_i$ induced by AVP still required the release of Ca^{2+} from ER. It has to be pointed out that VGCCs inhibition with either nifedipine or NCC 55-0396 also abolished the AVP-induced oscillations. It is likely that AVP-induced Ca^{2+} release from the ER is an important first step in the AVP-mediated signalling cascade, which may trigger further depolarisation via inhibiting Kv7 channels, activating CaCC (and some other effects) with subsequent depolarisation, VGCC activation, engagement of Ca^{2+}-induced Ca^{2+}

release via RyRs and IP_3Rs. Yet, the exact contribution of ER Ca^{2+} release to AVP-induced Ca^{2+} signals is yet to be elucidated as the poor selectivity of IP_3R/RyR inhibitors compromises the interpretation of the results presented in Figures 4.20-23.

Finally, we present evidence that HIF-α signalling may play an essential role in regulating the expression of genes coding for ion channels under the low oxygen tension. Cellular responses to hypoxia can be chronic or acute response with the increased $[Ca^{2+}]_i$, and the underlying signalling mechanisms are still being energetically explored (Shimoda and Polak, 2011). Signalling cascades regulated by HIF-α are essential for the processes of cardiovascular remodelling during hypoxia. The involvement of HIF-1α was related to diabetes-induced retinopathy, neuropathy and vasculopathy under hypoxic condition (Duscher et al., 2017). The available information on the participation of HIF-α in the regulation of ion channel coding genes is very scant, however.

Hypoxia-induced vasoconstriction and associated pulmonary hypertension are mainly associated with the increased $[Ca^{2+}]_i$ in PASMCs. Although hypoxia decreased the mRNA and protein expressions of Kv1.1, Kv1.5, Kv2.1, Kv4.3, and Kv9.3 in PASMCs, the role of HIF in the regulation of these Kv channels was not fully documented (Del Toro et al., 2003). In our present study, DMOG treatment, that is reported to induce HIF-1α accumulation (Yuan et al., 2014) downregulated the Kv7.5 channel in A7r5 VSMCs. Similar downregulation was seen in cells that underwent a hypoxic treatment. This downregulation was not prevented by the HIF-2α inhibitor, H2A, indicating that *Kcnq* gene downregulation may indeed

depend on HIF-1α. However, *Cacna1h* (Cav3.2) was not increased under the H2A treatment in hypoxic A7r5 cells. This, in combination with the lack of effect of DMOG (upregulates HIF-1α) on *Cacna1h* levels (Figure 4.15) suggests that, in contrast to *Kcnq* genes, *Cacna1h* is regulated by HIF-2α. Interestingly, HIF-2α was reported to mediate the Cav3.2 channel upregulation in PC12 cells (Del Toro et al., 2003).

HIF is a pivotal regulator mediating a broad range of cellular and systemic responses to hypoxia (Semenza, 2000; Wenger, 2002). Administration of H2A diminished the prolonged Ca^{2+} oscillations in the presence of high extracellular K^+ or XE991 during the hypoxic period. In GPCR-mediated Ca^{2+} signalling, H2A did not reverse AVP-induced repetitive Ca^{2+} oscillations. This may indicate that increased Cav3.2 expression/activity may have a larger contribution to Ca^{2+} signalling produced by depolarisation induced by manipulations with K^+ channel activity but less so the GPCR-induced Ca^{2+} signalling. Our results demonstrate that Cav3.1 and Cav3.2 T-type Ca^{2+} channels may be differentially regulated by hypoxia, and, therefore, they may serve different functions in the myocyte in response to hypoxic $[Ca^{2+}]_i$. It has to be noted that, there are some distinct differences between the Ca^{2+} responses measured in hypoxia and the application of DMOG, including the decreased contribution of IP_3Rs or RyRs to AVP-induced $[Ca^{2+}]_i$ in A7r5 cells observed in hypoxia but not after DMOG treatment. The differences are likely to reflect the fact that DMOG only targets one component of the cellular response to hypoxia (HIF-1α). While DMOG treatment cannot recapitulate the hypoxia in its entirety, it is a useful experimental tool to investigate HIF-1α-mediated effects.

In summary, hypoxia augments the $[Ca^{2+}]_i$ response to XE991 or AVP in VSMCs, and this effect is mediated by HIF-α transcriptional regulation, especially the downregulation of the Kv7.5 subtype. On the other hand, the ability of the Kv7 activator, retigabine, to attenuate repetitive Ca^{2+} oscillations could support a role for the Kv7 channels as a crucial regulator of cellular Ca^{2+} influx under hypoxic condition. Such effects are likely to be of importance in pathophysiological states induced by hypoxia.

4.4 Summary

- Hypoxia enhanced $[Ca^{2+}]_i$ response to XE991 or AVP and downregulated *Kcnq5* (Kv7.5) subunit expression in A7r5 cells; an effect most likely mediated by HIF-1α transcriptional regulation.
- Hypoxia resulted in the upregulation of *Cacna1h* (Cav3.2) in VSMCs, an effect likely regulated by HIF-2α.
- Hypoxia enhanced Ca^{2+} oscillations induced by AVP, an effect which was abolished by PLC inhibition.
- The Kv7 activator, retigabine attenuated repetitive Ca^{2+} oscillations in A7r5 cells under hypoxic condition.

Chapter 5

Role of Kv7 channels in the control over Ca^{2+} signalling in human vascular smooth muscle cells

5.1 Introduction

VSMCs serve as primary effectors in the control of local blood flow by their contractile ability. The contraction is stimulated by an increase of $[Ca^{2+}]_i$. One of the primary sources of Ca^{2+} for VSMCs is influx through VGCCs, especially L-type VGCCs. Ca^{2+} homeostasis in VSMCs not only controls the contractility, but also influences neointima formation, which can lead to failure of coronary artery bypass surgery. IMA has been proved to have a higher patency rate than the SV for coronary artery bypass grafting (CABG) (Nwasokwa, 1995). However, vasospasm could happen if AVP is perioperatively used to treat refractory vasodilatory shock in CABG (Wei et al., 2002). Vasoconstriction may be caused by multiple mechanisms, such as sustained periods of hypoxia in VSMCs. Hypoxia can regulate cellular remodelling processes, which lead to the proliferation of VSMCs (Moudgil et al., 2006). Several vasodilators have been suggested to treat vascular spasm through specific mechanisms, such as nifedipine and verapamil (Ca^{2+} channel blockers).

In addition to AVP, bradykinin (BK) is another vaso- and neuroactive peptide which can be released upon tissue injury (Oza et al., 1990; Raidoo and Bhoola, 1998). BK and related kinins are released when kallikrein hydrolyses the substrate kininogen (Regoli and Barabe, 1980) to cause endothelium-dependent vasodilation by nitric oxide (NO) (Busse et al., 1993) or contribute to the inflammatory pain by inhibition of Kv7 channels in nociceptive afferent fibres

(Dray and Perkins, 1993; Liu et al., 2010). However, there is no ideal vasodilator which is effective for every situation. When the endothelium is disrupted, BK can directly bind B_2 receptor to induce Ca^{2+} signals via PLC cascade and lead to vasoconstriction (Yang et al., 1999). Recently, Zhang and colleagues showed that high doses of BK (10^{-10} to 10^{-5} mol/L) induced vascular contraction in haemorrhagic shock rats, which depends on the endothelium and myoendothelial gap junction (Zhang et al., 2015).

As discussed and evidenced in Chapter 3 and 4, Kv7 channels are expressed in the vasculature with Kv7.4 and Kv7.5 being the dominant Kv7 subunits in rat cultured VSMCs. Inhibition of Kv7 channels is expected to depolarise the E_m and induce the increase of $[Ca^{2+}]_i$ in VSMCs, indicating Kv7 subunits play an essential role in microvascular physiology (Byron and Brueggemann, 2018). Functional Kv7 channels are present in human arteries, providing a potential target for both, the therapeutic action and unwanted side effects of pharmacological agents which affect Kv7 channel activity (Ng et al., 2011). Indeed, while targeting vascular Kv7 channels may be beneficial for control over vascular tone and heart rate, the presence of vascular Kv7 channels represents a problem for the treatment of other diseases, such as epilepsy and pain using activator drugs (e.g. retigabine and its successors). Even though the presence of the Kv7 channels in some human vasculature was reported, there is a lack of information concerning their role in Ca^{2+} homeostasis in IMA and SV SMCs.

Differences in compressive forces and oxygen demand between the two cell types make it conceivable that the mechanisms regulating vascular tone within different blood vessel types may differ. The clinical use of AVP has increased

significantly in recent years (Yimin et al., 2013), but its use could cause vasospasm, which becomes a danger, for instance, when treating refractory vasodilatory shock during bypass surgery (Wei et al., 2002). On the other hand, retigabine, a Kv7 activator with anti-epileptic and analgesic properties (Stott et al., 2014; Rundfeldt, 1997), attenuated the basilar artery vasospasm in rats with subarachnoid haemorrhage (Mani et al., 2013). In this chapter, we identify the presence of Kv7 channels in human primary IMA and SV SMCs and demonstrate their role in the control of Ca^{2+} signalling therein. This work represents a vital step in translating the results from animal models into the possibility of targeting these channels for anti-vasospasm therapy in humans.

5.2 Results

5.2.1 Depolarisation-induced Ca^{2+} influx is mediated by VGCCs in human IMA and SV SMCs

As demonstrated earlier, VSMCs expressed both L- and T-type VGCCs. We used L-type Ca^{2+} channel blocker, nifedipine and T-type Ca^{2+} channel blocker, NNC 55-0396 to distinguish the separate contributions of both channel types to rises of $[Ca^{2+}]_i$ evoked by depolarisation with high K^+ buffer in cultured primary IMA and SV SMCs from human donors with coronary artery disease undergoing CABG (see Methods). In Fura2 Ca^{2+} imaging experiments shown in Figure 5.1A and B, black traces show example responses of IMA and SV SMCs to 50 mM extracellular K^+ buffer (produced by the equimolar substitution of NaCl with KCl), respectively. Depolarisation evoked transient rises of $[Ca^{2+}]_i$ in both cell types. Interestingly, depolarisation with high-K^+ caused significantly larger $[Ca^{2+}]_i$

elevation in SV SMCs, as compared to IMA SMCs (AUC: 16.84 ± 4.65, n=5 vs. 27.26 ± 4.1, n=5, $p<0.05$; Figure 5.1C).

Pre-treatment with nifedipine (2 μM) effectively suppressed the rises of $[Ca^{2+}]_i$ in both IMA and SV SMCs (Figure 5.1D, E), indicating a significant role of L-type Ca^{2+} channels in both cell types. Nifedipine suppressed the AUC of high-K^+-induced $[Ca^{2+}]_i$ transients in IMA and SV SMCs by 86.4 ± 13.1% (n=5) and 95.5 ± 2.0% (n=5), respectively. Pre-treatment with NNC 55-0396 (3 μM) also suppressed K^+-induced rises of $[Ca^{2+}]_i$ in both groups. Application of NNC 55-0396 decreased the AUC of the high-K^+-induced $[Ca^{2+}]_i$ transients in IMA and SV SMCs by 82.1 ± 12.2% (n=5) and 88.2 ± 3.6% (n=5), respectively (Figure 5.1D, E). There was no significant difference in the degree of inhibition exerted by nifedipine and NNC 55-0396 in IMA cells; however, nifedipine was more efficacious than NNC 55-0396 in SV SMCs, as compared to IMA SMCs (AUC of high-K^+ induced Ca^{2+} transients in the presence of nifedipine: 1.22 ± 0.51, n=5 vs. 3.32 ± 1.53, n=5, in the presence of NNC 55-0396; $p<0.05$; Figure 5.1E).

Cav1.2 L- and Cav3 T-type Ca^{2+} channels play essential roles in vasoconstriction in human VSMCs (Cribbs, 2006). To confirm the molecular identity of these channels in primary human SMCs, we performed endpoint and RT-PCR analyses in IMA and SV SMCs. We found that L-type (*CACNA1C*, *CACNA1D*) and T-type (*CACNA1G*, *CACNA1H*) VGCC subunits in both cell types (Figure 5.2A-D). The mRNA of *CACNA1I* only expressed in IMA SMCs (Figure 5.2A, B). *CACNA1S* and *CACNA1F* transcripts were not detectable (Figure 5.2B, D). *CACNA1C* (Cav1.2) L-type and *CACNA1G* (Cav3.1) T-type Ca^{2+} channel genes were the predominant subtypes in human IMA and SV SMCs (Figure 5.2A-D).

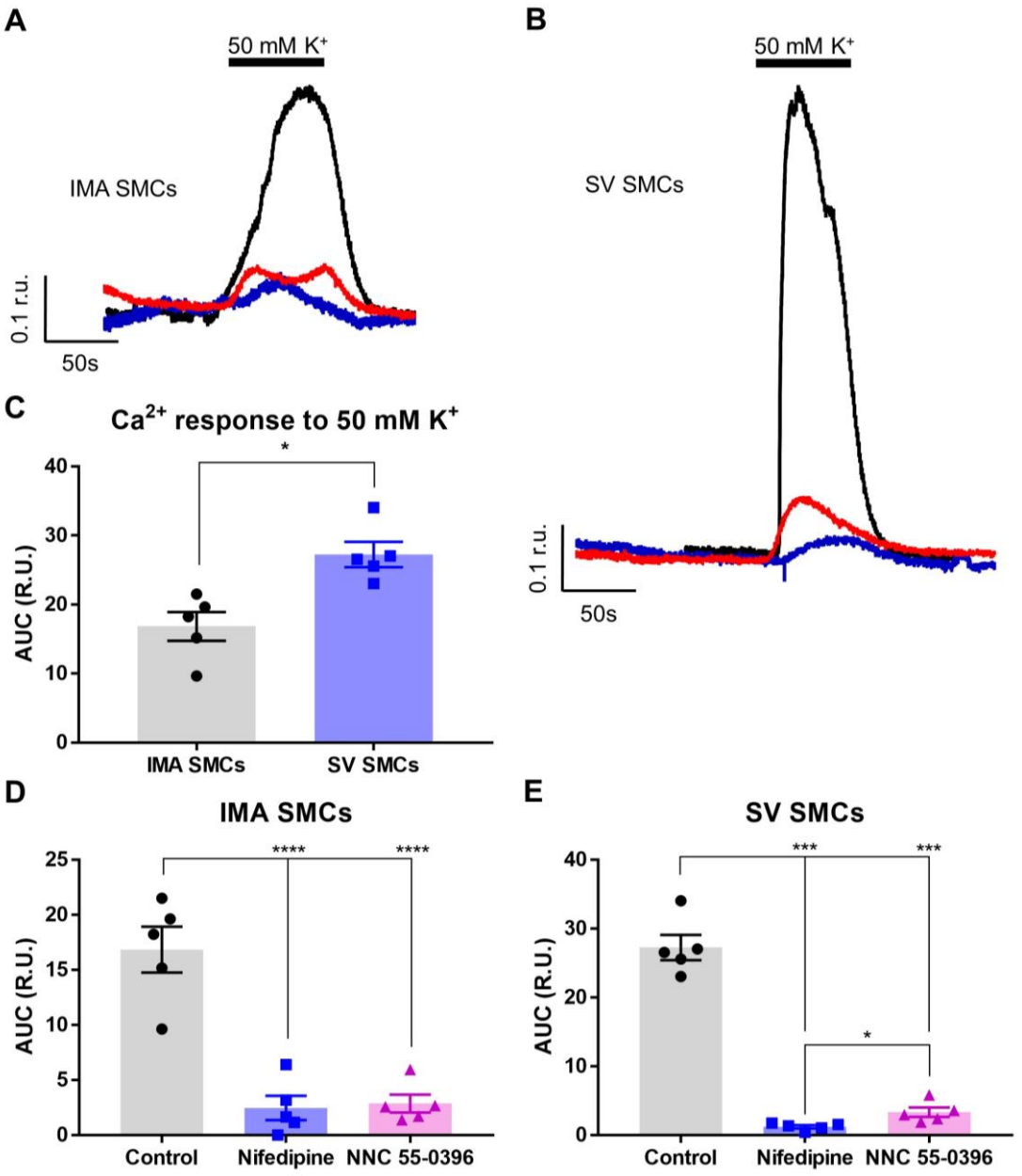

Figure 5.1 Contribution of L- and T-type Ca^{2+} channels to depolarisation-induced Ca^{2+} transients in IMA and SV SMCs. (**A-B**) Representative example traces showing rises in $[Ca^{2+}]_i$ evoked by depolarising cells with 50 mM K^+-containing buffer (the period indicated by the solid bar) in control conditions (black) or in the presence of L-type (nifedipine; 2 µM; blue) or T-type (NNC 55-0396; 3 µM; red) Ca^{2+} channel blockers (as indicated) in IMA (A) or SV (B) SMCs. (**C-E**) Bar graphs showing the mean AUC of the response to 50 mM K^+ buffer. Control group represented in panel C, and the presence of nifedipine or NNC 55-0396 in IMA (D) or SV (E) SMCs. In panels C-E data are presented as mean ± S.E.M.; Statistics performed using student's t-test (C) and ANOVA with Sidak test (D, E), *P<0.05, ***P<0.001, ****P<0.0001 (n=5).

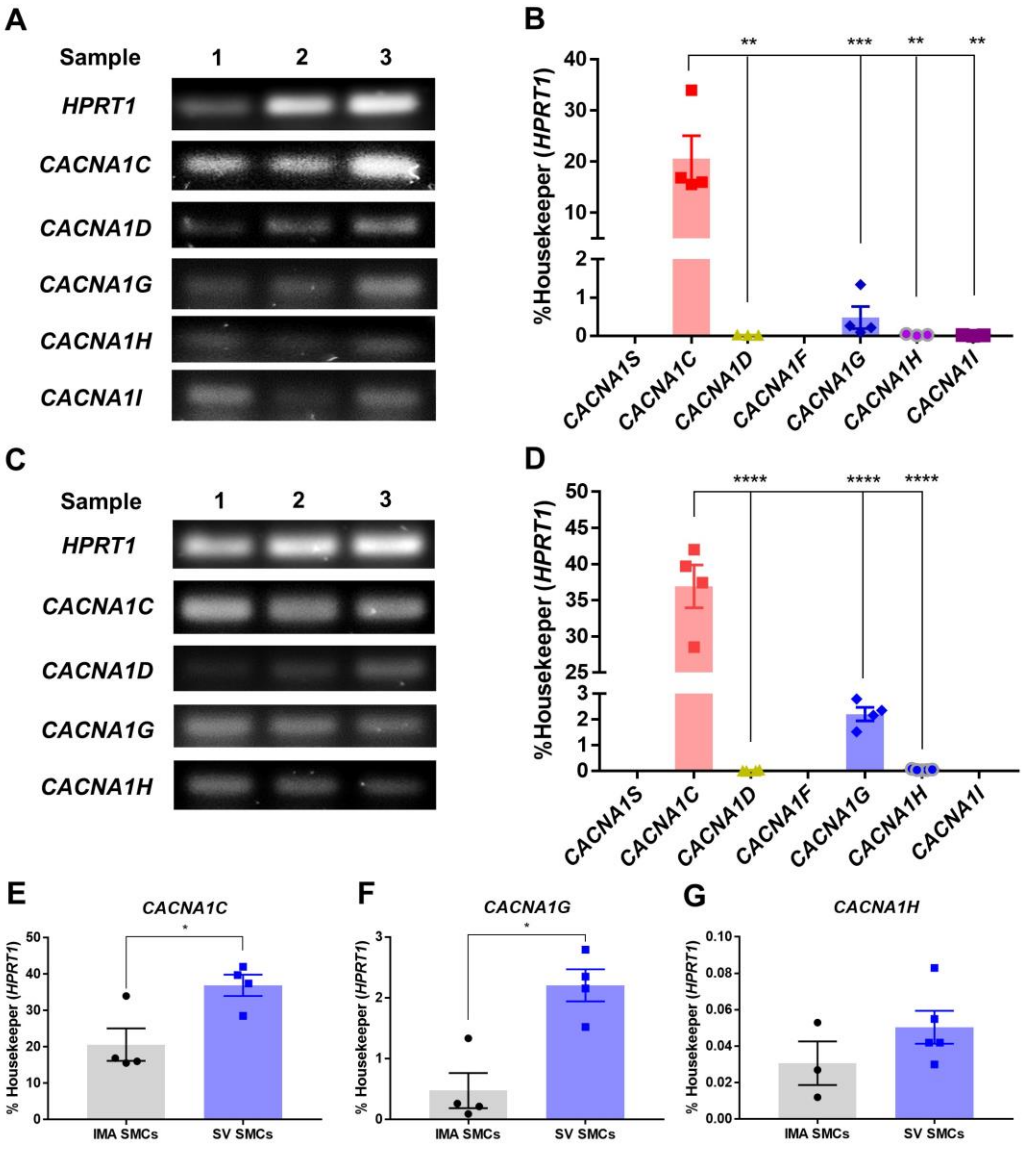

Figure 5.2 Differential expression of L- and T-type VGCCs genes in IMA and SV SMCs. (**A**) Agarose gels stained with SYBR safe to visualise the RT-PCR products corresponding to L-type (*CACNA1C*, *CACNA1D*) and T-type (*CACNA1G*, *CACNA1H*, *CACNA1I*) VGCCs genes in IMA. (**B**) Quantification of RT-PCR results exemplified in panel A. (**C**) Agarose gels stained with SYBR safe to visualise the RT-PCR products corresponding to L-type (*CACNA1C*, *CACNA1D*) and T-type (*CACNA1G*, *CACNA1H*) VGCCs genes in SV. (**D**) Quantification of RT-PCR results exemplified in panel C. (**E-G**) Bar graphs summarising the mRNA expression of *CACNA1C* (E), *CACNA1G* (F), and *CACNA1H* (G) in IMA and SV SMCs. In panels B, D and E-G data are presented as mean ± S.E.M., normalised to that of a housekeeping gene, *HPRT1*; Statistics performed using ANOVA with Sidak test (B, D) and student's t-test (E-G), *P<0.05, **P<0.01, ***P<0.001, ****P<0.0001 (n≥3).

The mRNA levels of *CACNA1C* and *CACNA1G* were markedly higher in SV than in IMA, while no significant differences were found for *CACNA1H* (Figure 5.2E-G).

5.2.2 Functional Activity and Expression of Kv7 channels in IMA and SV SMCs

Several studies showed that the application of a specific Kv7 channel inhibitor, XE991, inhibited the voltage-gated K^+ current in vascular myocytes from rodent and human visceral artery (Yeung and Greenwood, 2005; Mackie et al., 2008; Lee et al., 2020). We also reported that XE991 (10 µM) induced the Ca^{2+} oscillations in rat aortic A7r5 cells (Chapter 3, 4). Application of XE991 (10 µM) caused a prominent $[Ca^{2+}]_i$ transient in IMA (AUC: 89.49 ± 16.48, n=6; Figure 5.3A) while responses in SV SMCs were small to no response (AUC: 6.01 ± 6.89, n=5; significantly different from IMA, $p<0.0001$; Figure 5.3B, C). In IMA, the change of $[Ca^{2+}]_i$ was characterised as a rapid large-amplitude increase followed by a decline to a plateau value which was close to the basal level in IMA SMCs.

Previous research demonstrated the expression of the Kv7 channels in human VSMCs (Mackie et al., 2008; Ng et al., 2011) with *KCNQ1*, *KCNQ4* and *KCNQ5* being the major subunits (Greenwood and Ohya, 2009). To the best of our knowledge, there is no study relating to the expression of Kv7s in IMA and SV SMCs. In both cell types, we detected transcripts for *KCNQ3*, *KCNQ4* and *KCNQ5,* with *KCNQ5* being the most abundant (Figure 5.4A-D). Interestingly, there was no detectable expression of *KCNQ1* or *KCNQ2* in either cell type. The mRNA levels of *KCNQ5* were markedly higher in IMA than in SV SMCs, while no significant differences were found for *KCNQ3* and *KCNQ4* (Figure 5.4E-G).

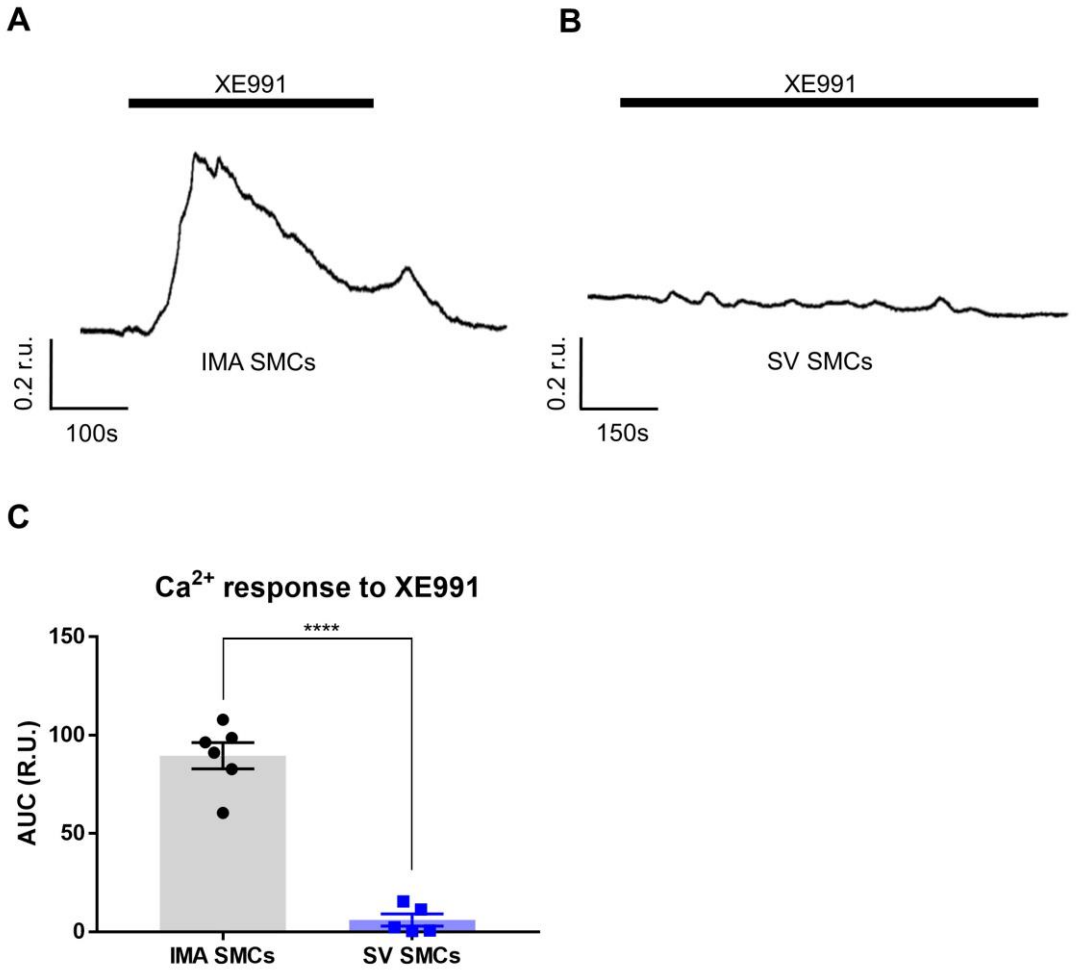

Figure 5.3 XE991 induces larger Ca^{2+} transients in IMA as compared to SV SMCs. (**A-B**) Representative example traces showing rises in $[Ca^{2+}]_i$ evoked by XE991 (10 µM; the application period is indicated by the solid bar). (**C**) Comparison of Ca^{2+} signal response induced by XE991 between IMA and SV SMCs. In panel C data are presented as mean ± S.E.M.; Statistics performed using unpaired student's t-test, ****P<0.0001 (n≥5).

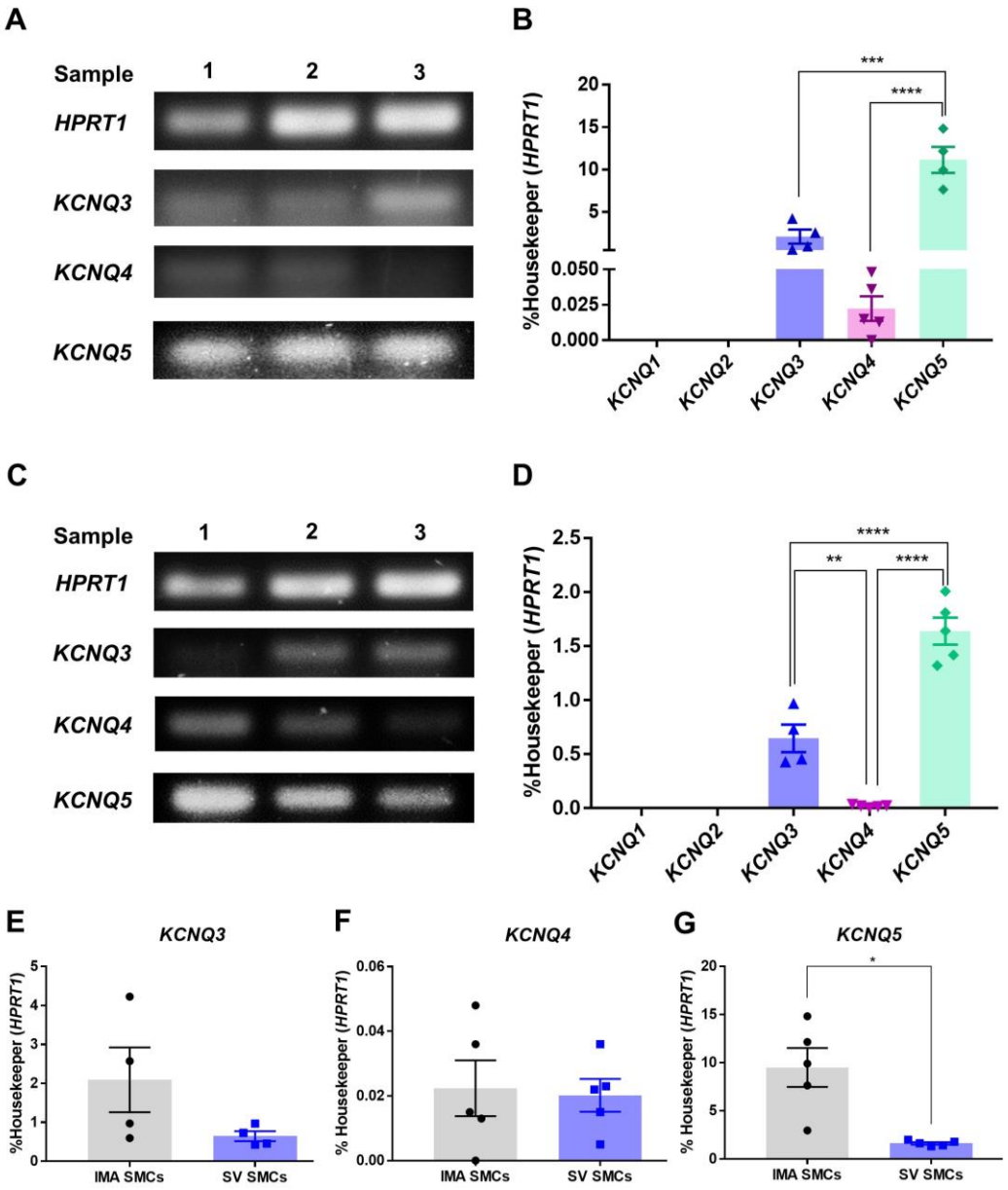

Figure 5.4 Differential expression of *KCNQ* genes in IMA and SV SMCs. (**A**) Agarose gels stained with SYBR safe to visualise the RT-PCR products of *KCNQ3*, *KCNQ4* and *KCNQ5* in IMA SMCs. (**B**) Quantification of RT-PCR results exemplified in panel A. (**C**) Agarose gels stained with SYBR safe to visualise the RT-PCR products of *KCNQ3*, *KCNQ4* and *KCNQ5* in SV SMCs. (**D**) Quantification of RT-PCR results exemplified in panel C. (**E-G**) Bar graphs summarising the mRNA expression of *KCNQ3* (E), *KCNQ4* (F), and *KCNQ5* (G) in IMA and SV SMCs. In panels B, D and E-G data are presented as mean ± S.E.M., normalised to that of a housekeeping gene, *HPRT1*; Statistics performed using ANOVA with Sidak test (B, D) and student's t-test (E-G), *P<0.05, **P<0.01, ***P<0.001, ****P<0.0001 (n≥4).

5.2.3 Effects of AVP on $[Ca^{2+}]_i$ in human IMA and SV SMCs

AVP is a hormone with the prominent vasoconstrictor effect, which acts in the vasculature via V1AR receptor, which is coupled through $G_{q/11}$ to PLC, and their activation induces vasoconstriction via the elevation of $[Ca^{2+}]_i$ (Henderson and Byron, 2007). Although the pathways leading to AVP-induced $[Ca^{2+}]_i$ are complex, one component in the AVP signalling cascade is likely to include the PLC-mediated Kv7 channel inhibition, depolarisation and VGCCs activation, as discussed and evidenced in rat A7r5 cells in Chapters 3 and 4. Indeed, in many types of excitable cells, $G_{q/11}$-PLC signalling cascade can regulate the excitability via suppression of Kv7 channels, which are positively regulated by PIP_2 and negatively regulated by Ca^{2+} and PKC (Mani et al., 2016; Mackie et al., 2008). We thus next tested how Kv7 channel activity affects AVP-induced Ca^{2+} signalling in human IMA and SV SMCs.

In IMA, AVP (100 pM) caused a sharp increase in $[Ca^{2+}]_i$; however, there were no oscillations (AUC: 16.75 ± 8.53, n=4; Figure 5.5A). Depolarisation with the inhibition of Kv7s by XE991 caused larger $[Ca^{2+}]_i$ elevation than that produced by AVP in IMA SMCs (Figure 5.5A; cf. Figure 5.3A). Retigabine applied 2 minutes before and during the administration of AVP almost completely abolished the AVP-induced increase of $[Ca^{2+}]_i$ in human IMA SMCs. Either nifedipine or NNC 55-0396 applied in a similar way also significantly reduced the $[Ca^{2+}]_i$ transients (Figure 5.5A-C), with retigabine being the most efficacious of the three compounds tested (AUC: 1.55 ± 0.36, n=5; Figure 5.5C).

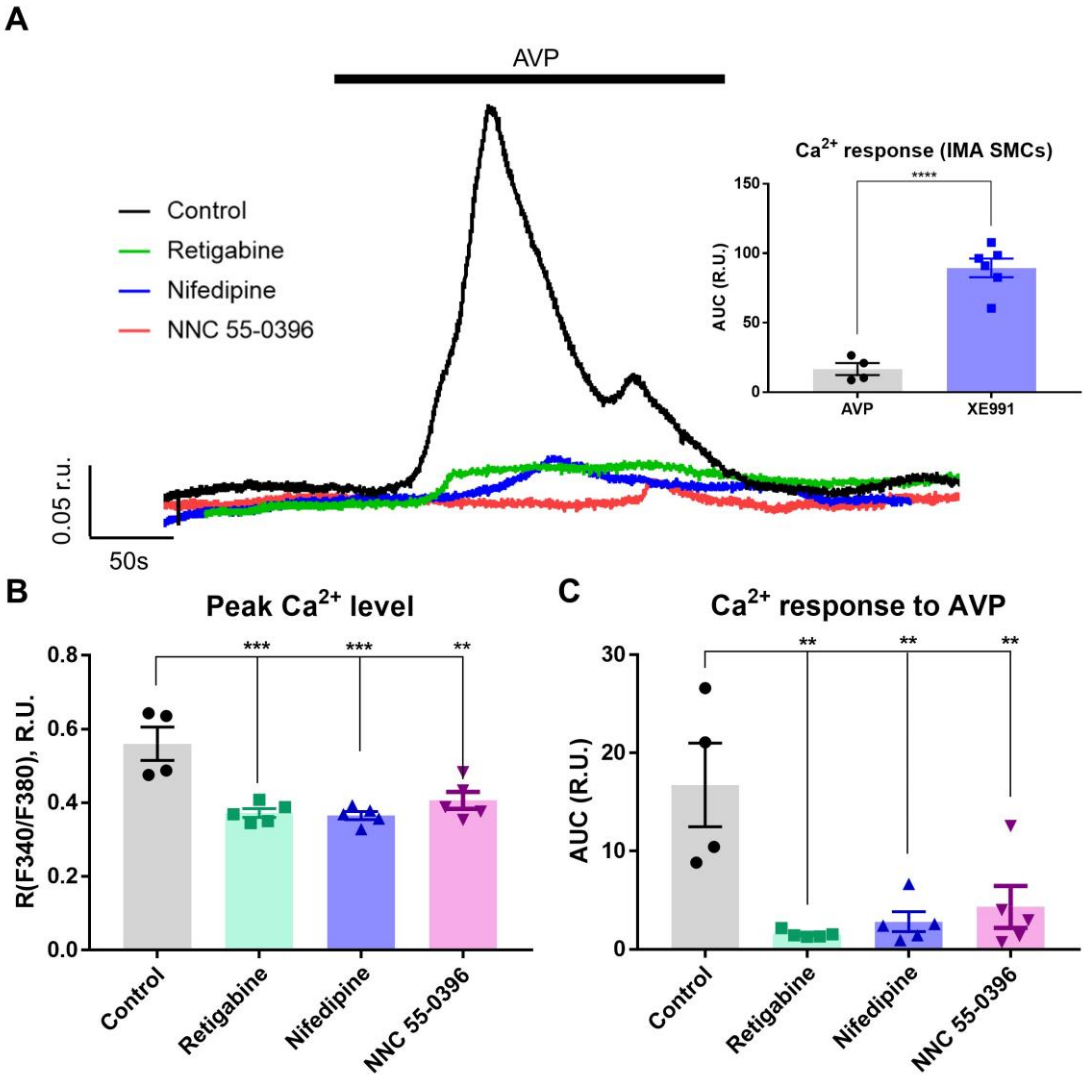

Figure 5.5 AVP-induced Ca^{2+} transients in IMA SMCs is reduced by Kv7 activator, L- and T-type Ca^{2+} channel blockers. (**A**) Representative example traces showing rises in $[Ca^{2+}]_i$ evoked by AVP (100 pM; the application period is indicated by the solid bar) in control conditions (black) or the presence of retigabine (10 μM; green), nifedipine (2 μM; blue) or NNC 55-0396 (3 μM; red), as indicated. Comparison of Ca^{2+} signal response induced by AVP and XE991 in IMA SMCs summarised in the inset on the right. (**B-C**) Bar graphs showing the peak Ca^{2+} level (B) and mean AUC of the response (C) to AVP. In panels data are presented as mean ± S.E.M.; Statistics performed using unpaired student's t-test (A) and ANOVA with Sidak test (B, C), **P<0.01, ***P<0.001, ****P<0.0001 (n≥4).

In contrast, AVP (100 pM and 10 nM) failed to produce Ca^{2+} response in SV SMCs (Figure 5.6A, B). A higher concentration of AVP (300 nM) was needed to produce a Ca^{2+} transient in SV SMCs (AUC: 12.56 ± 6.99, n=5; Figure 5.6C). Addition of retigabine, nifedipine or NNC 55-0396 significantly reduced the $[Ca^{2+}]_i$ transients in human SV SMCs (Figure 5.6C-E).

There was no significant difference in the degree of inhibition of AVP-evoked response of $[Ca^{2+}]_i$ between retigabine, nifedipine and NNC 55-0396 in either SMC type (Figure 5.5C, 5.6E, 5.7A), but retigabine exerted larger inhibition in IMA than that in SV (AUC of the AVP-induced Ca^{2+} transient in the presence of retigabine in IMA: 1.55 ± 0.36, n=5, vs. 2.91 ± 1.20, n=4 in SV; $p<0.05$; Figure 5.7B). Although the degree of inhibition of nifedipine and NNC 55-0396 was somewhat different between IMA and SV, there was no statistically significant difference between the groups (Figure 5.7C, D). Collectively, our data indicate that Kv7 channels are functional in human IMA and SV SMCs, especially in the former type. Pharmacological activation of Kv7 channels can effectively halt AVP-evoked Ca^{2+} signals in IMA SMCs and significantly reduce such signalling in SV SMCs.

5.2.4 Effects of Bradykinin on $[Ca^{2+}]_i$ in IMA SMCs

Bradykinin (BK) is a potent vasoactive peptide which, similarly to AVP, acts upon $G_{q/11}$-coupled receptors (B_1 and B_2 BK receptors) (Regoli and Barabe, 1980) and one of its known effectors is the Kv7 channel (Liu et al., 2010). Moreover, Kv7 channel activator, retigabine, was shown to offset the depolarising effect of BK in neurons (Linley et al., 2012). Having found a significant expression and function

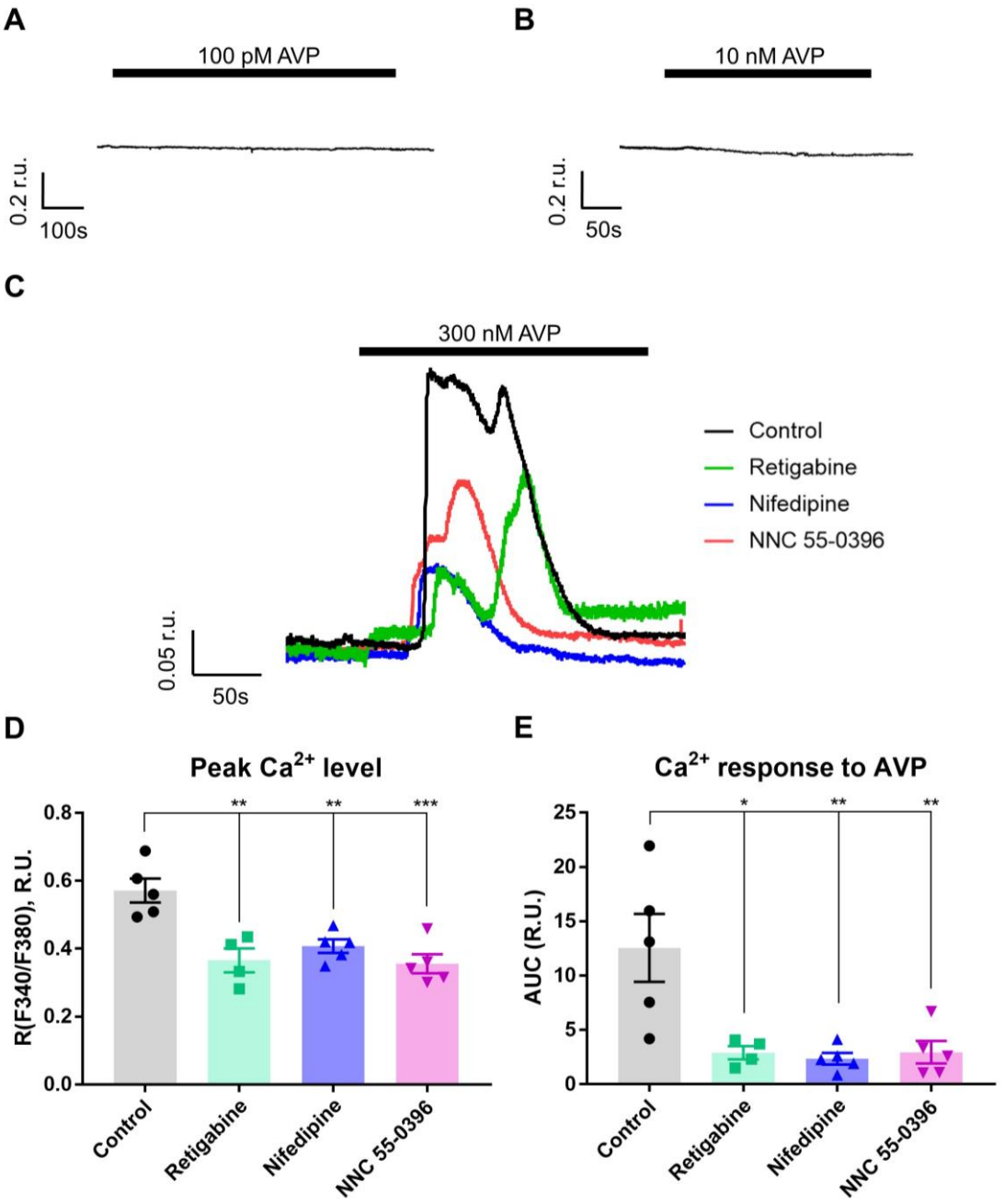

Figure 5.6 AVP-induced Ca^{2+} transients in SV SMCs. (**A-B**) Representative example traces showing the concentration-dependent effect of AVP (100 pM; A and 10 nM; B) in SV SMCs. (**C**) Representative example traces showing rises in $[Ca^{2+}]_i$ evoked by AVP (300 nM; the application period is indicated by the solid bar) in control conditions (black) or the presence of retigabine (10 μM; green), nifedipine (2 μM; blue) or NNC 55-0396 (3 μM; red), as indicated. (**D-E**) Bar graphs showing the peak Ca^{2+} level (D) and mean AUC of the response (E) to AVP. In panels D-E data are presented as mean ± S.E.M.; Statistics performed using ANOVA with Sidak test, *P<0.05, **P<0.01, ***P<0.001 (n≥4).

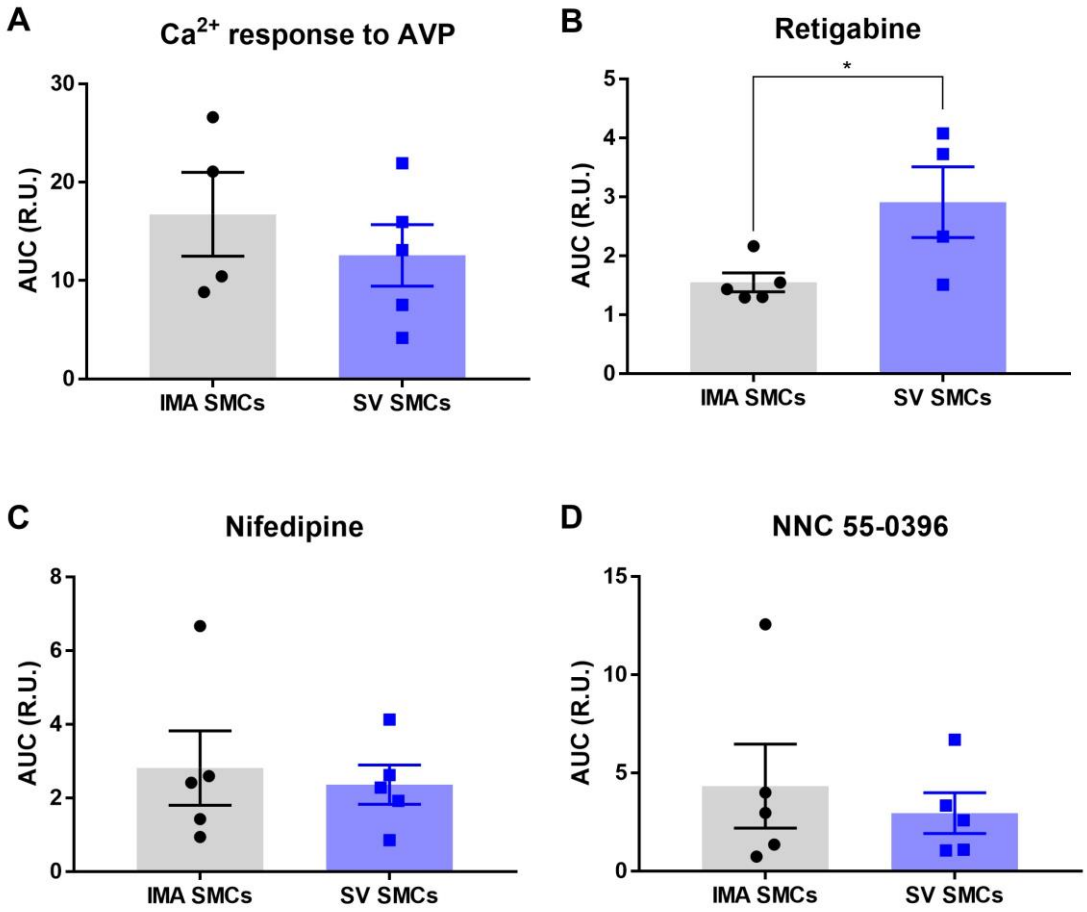

Figure 5.7 The effect of Kv7 activator, L- and T-type Ca^{2+} channel blockers on AVP-induced Ca^{2+} transients in IMA and SV SMCs. (**A-D**) Bar graphs showing the mean AUC of the response to AVP (100 pM in IMA, 300 nM in SV; A), after preapplication of retigabine (10 μM; B), nifedipine (2 μM; C) or NNC 55-0396 (3 μM; D). In panels A-D data are presented as mean ± S.E.M.; Statistics performed using paired/unpaired student's t-test, *P<0.05 (n≥4).

of Kv7 channels in primary human IMA and SV SMCs, their possible role in the modulation of BK-induced $[Ca^{2+}]_i$ responses were then investigated.

In the presence of extracellular Ca^{2+}, exposure of IMA SMCs to BK (250 nM) evoked a rapid transient rise of $[Ca^{2+}]_i$ followed by a slow decline (Figure 5.8A). We hypothesised that as in the case of AVP, this $[Ca^{2+}]_i$ transient may arise from i) IP_3-mediated ER Ca^{2+} release; ii) depolarisation-induced Ca^{2+} influx via VGCCs (Choi and Hwang, 2018). Furthermore, since BK inhibits Kv7 channels in neurons (Liu et al., 2010; Linley et al., 2008; Delmas and Brown, 2005; Gamper et al., 2004), it is logical to propose that a BK-induced Kv7 channel inhibition would be a major factor in the BK-induced depolarisation. In the next series of experiments, we investigated this potential mechanism. First, we tested the effect of retigabine on BK-induced $[Ca^{2+}]_i$ transients. Two minutes of pretreatment with retigabine (10 μM) followed by application of BK (250 nM) substantially decreased the $[Ca^{2+}]_i$ transient by about a half in IMA SMCs (AUC: 69.49 ± 18.15, n=5 to 36.06 ± 8.21, n=5, $p<0.05$; Figure 5.8A, B, E, F). BK-triggered $[Ca^{2+}]_i$ increase was also attenuated upon pretreatment of the L-type Ca^{2+} channel inhibitor, nifedipine (Figure 5.8C, E, F), but T-type Ca^{2+} channel inhibitor, NNC 55-0396 did not produce a significant effect in IMA SMCs (Figure 5.8D-F). Nifedipine significantly reduced the peak amplitude of Ca^{2+} transient, but the effect on AUC did not reach significance (AUC: 69.49 ± 18.15, n=5 vs. 60.71 ± 8.24 by nifedipine, n=5; Figure 5.8F). Only retigabine significantly attenuated both the peak amplitude of the BK-induced Ca^{2+} transient and AUC in IMA SMCs (Figure 5.8E, F).

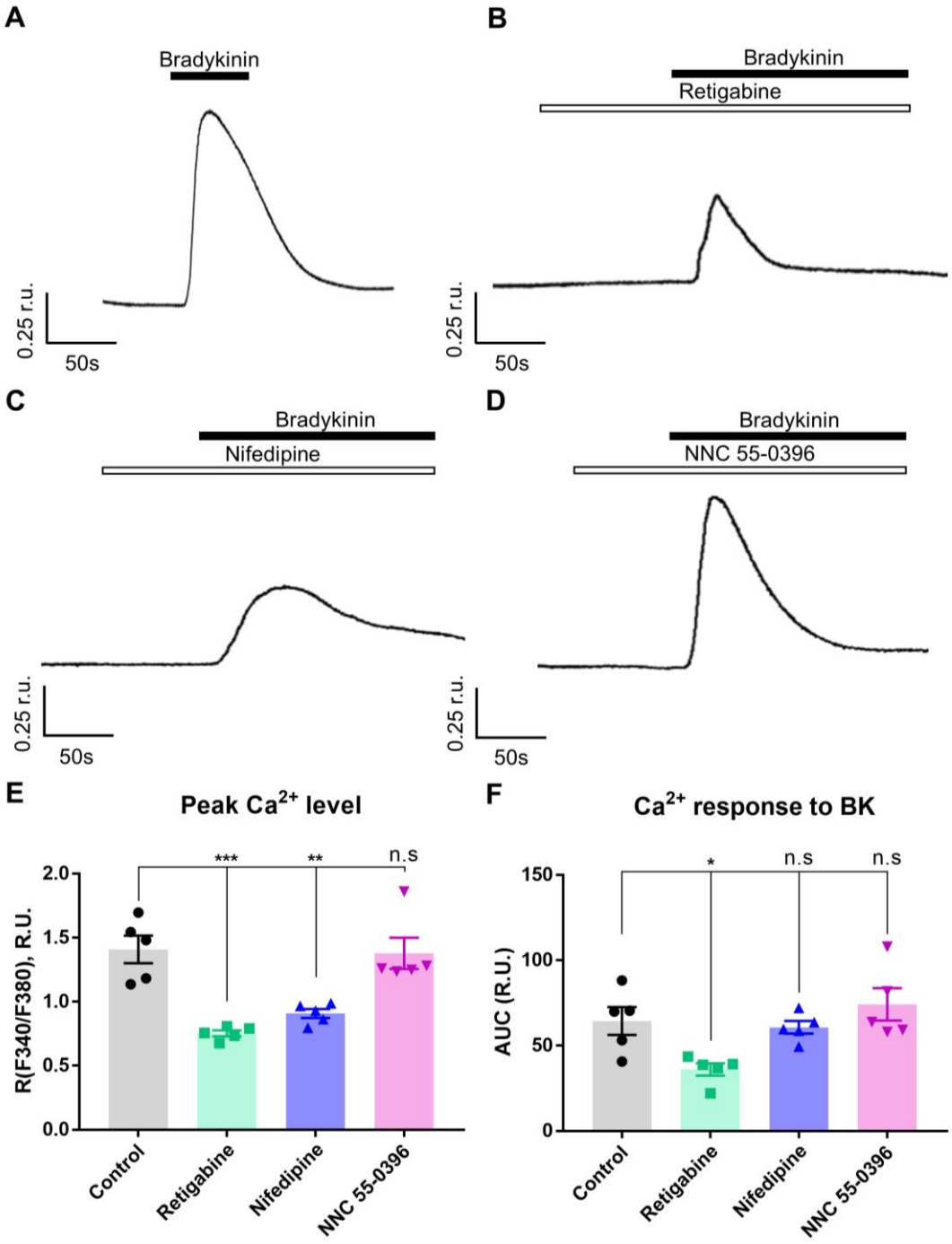

Figure 5.8 Retigabine attenuates BK-evoked Ca^{2+} transients in IMA SMCs. (**A-D**) Representative example traces showing rises in $[Ca^{2+}]_i$ induced by bradykinin (250 nM) in control conditions (A), in cells pretreated with retigabine (10 μM; B), nifedipine (2 μM; C) or NNC 55-0396 (3 μM; D), as indicated. (**E-F**) Bar graphs summarising the effects of retigabine, nifedipine or NNC 55-0396 on the peak Ca^{2+} level (E) and mean AUC (F) induced by BK. In panels E-F data are presented as mean ± S.E.M.; Statistics performed using ANOVA with Sidak test, n.s., not significant, *P<0.05, **P<0.01, ***P<0.001 (n=5).

Next, we performed FluoVolt imaging to investigate whether BK-induced increase of $[Ca^{2+}]_i$ via the change of E_m in IMA SMCs. BK (250 nM) evoked a rise in fluorescence, indicating the sustained depolarisation in IMA SMCs (Figure 5.9A). In contrast, the application of retigabine produced a decrease of FluoVolt fluorescence, indicative of hyperpolarisation. In the continuous presence of retigabine, BK was no longer able to depolarise the E_m (Figure 5.9B, C). Our findings indicate that the BK-induced depolarisation is likely due to the BK-induced inhibition of Kv7 channels. Therefore, a substantial component of the BK-mediated Ca^{2+} signalling is related to the VGCCs-mediated extracellular Ca^{2+} entry, which can be modulated with Kv7 activators in IMA SMCs.

5.2.5 Effects of Bradykinin on $[Ca^{2+}]_i$ in SV SMCs

We then analysed the effect of BK (250 nM) in SV SMCs. Similar to IMA SMCs, BK induced a prominent rise of $[Ca^{2+}]_i$, followed by a steady decline in SV SMCs (Figure 5.10A). However, the amplitude of BK-induced $[Ca^{2+}]_i$ transients in SV SMCs was significantly smaller than those in IMA (AUC: 69.49 ± 18.15, n=5 to 26.33 ± 8.72, n=6, $p<0.01$; Figure 5.10A). Interestingly, in contrast to the inhibiting effect of retigabine and nifedipine in IMA SMCs, the transient increase in $[Ca^{2+}]_i$ was not prevented by either drug, if anything, slightly higher transients were observed in SV SMCs (Figure 5.10B, C, E, F). NNC 55-0396 had no significant effect on the peak BK response and AUC of BK-induced $[Ca^{2+}]_i$ transients in SV SMCs (Figure 5.10D, E, F).

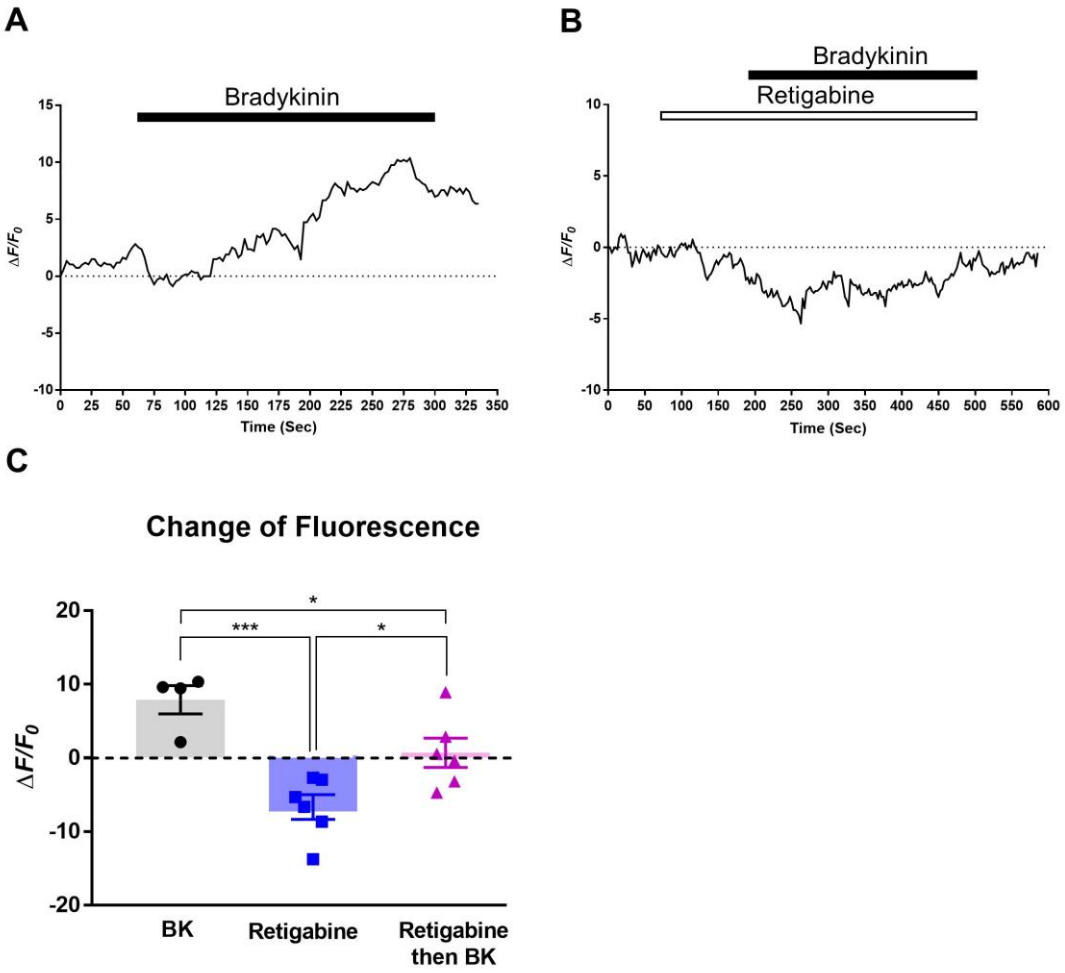

Figure 5.9 Bradykinin depolarises IMA SMCs, an effect opposed by the Kv7 channel potentiation. (**A-B**) Representative example traces showing the change of FluoVolt membrane potential recording (measured as $\Delta F/F_0$) during application of BK (250 nM), either alone (A) or after pre-application and still in the presence of retigabine (10 µM; B). The periods of drug application are indicated by horizontal bars. (**C**) Bar graph showing the percentage change in FuoVolt fluorescence in response to BK, retigabine and retigabine with BK. BK controls (grey bar) were performed on one group of cells, and the retigabine with subsequent application of BK (blue and purple bars, respectively) were performed on an independent group of cells. In panel C data are presented as mean ± S.E.M.; Statistics performed using ANOVA with Sidak test, *P<0.05, ***P<0.001 (n≥4).

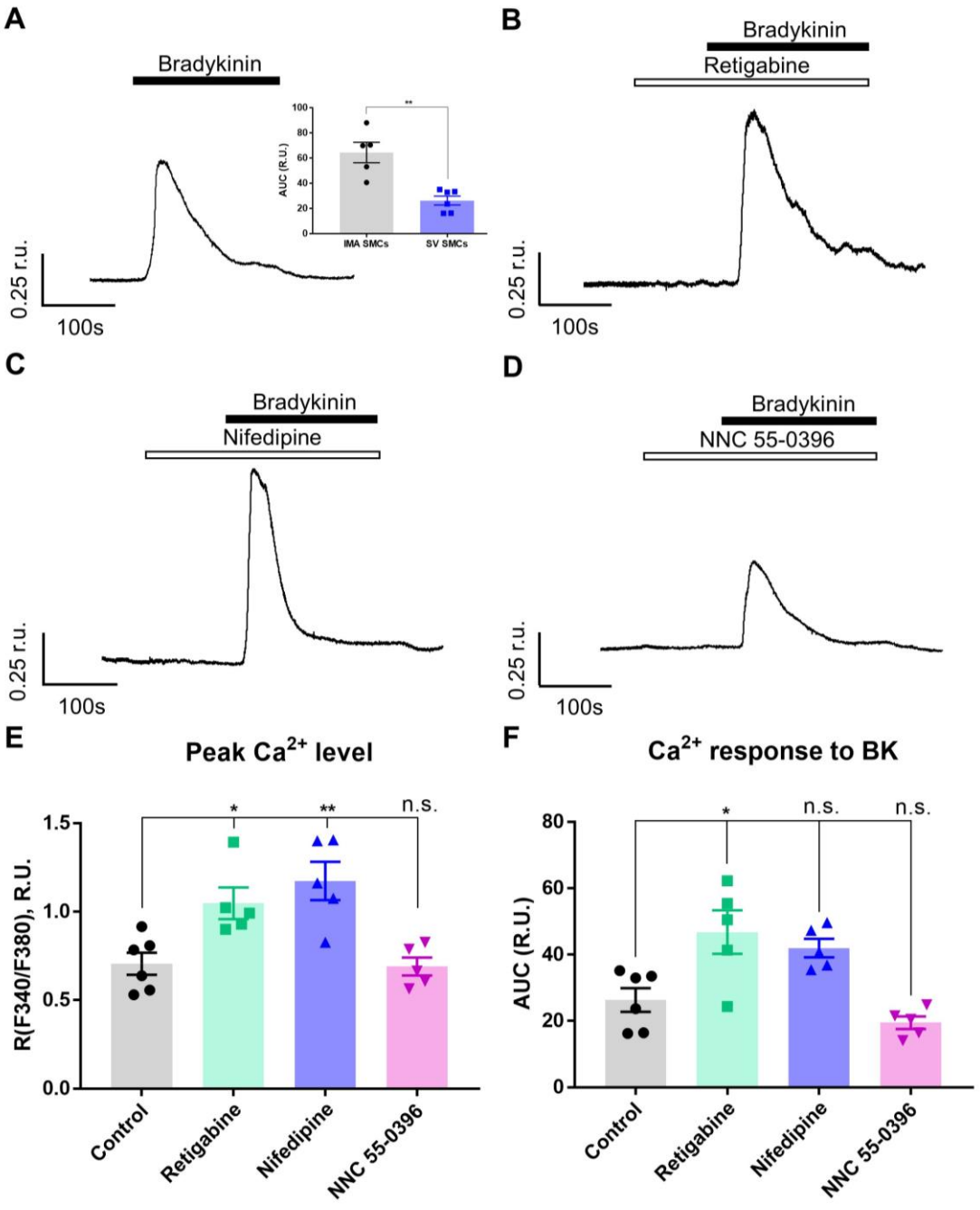

Figure 5.10 Retigabine does not attenuate BK-evoked Ca^{2+} transients in SV SMCs. (**A-D**) Representative example traces showing rises in $[Ca^{2+}]_i$ induced by BK (250 nM) in control conditions (the effects of BK in IMA and SV; summarised in the inset on the right) (A), after preapplication of retigabine (10 μM; B), nifedipine (2 μM; C) or NNC 55-0396 (3 μM; D), as indicated. (**E-F**) Bar graphs summarising the effects of retigabine, nifedipine or NNC 55-0396 on the peak Ca^{2+} level (E) and mean AUC (F) induced by BK. In panels E-F data are presented as mean ± S.E.M.; Statistics performed using ANOVA with Sidak test, n.s., not significant, *P<0.05, **P<0.01 (n≥5).

To further determine the association between Kv7 channels and BK-mediated Ca^{2+} signalling in SV SMCs, E_m was investigated in cells loaded with FluoVolt indicator. BK (250 nM) increased in fluorescence, consistent with E_m depolarisation in SV SMCs (Figure 5.11A). There was a steady rise in fluorescence during the BK application with partial recovery upon the washout. Interestingly, this depolarising effect of BK was not prevented in cells pretreated with retigabine (10 µM; Figure 5.11B). Retigabine did not produce a significant decrease of E_m in SV SMCs exposed to BK (Figure 5.11C). In line with the FluoVolt and mRNA expression data, the BK-induced Ca^{2+} signalling was reduced by the pretreatment of retigabine in IMA (Figure 5.8F), but not in SV SMCs (Figure 5.10F), suggesting that Kv7 channels are functionally active in IMA but much less so in SV SMCs.

Interestingly, while BK still induced depolarisation in SV SMCs (which was not significantly different from that observed in IMA SMCs), the BK-induced Ca^{2+} transients induced by this agonist in SV SMCs were much smaller in amplitude, as compared to these in IMA and were not prevented by the VGCC blockers (Figure 5.10), suggesting that these perhaps are formed by the Ca^{2+} release from the ER (although the contribution of other sources, such as CRAC or TRP channels cannot be excluded). The reason why VGCCs do not engage with the BK-induced depolarisation in SV at the moment are unknown and require further investigation. One potential mechanism could be in the lack of co-localisation of BK receptors and VGCCs in SV, as was found to be the case in sensory neurons (Jin et al., 2013).

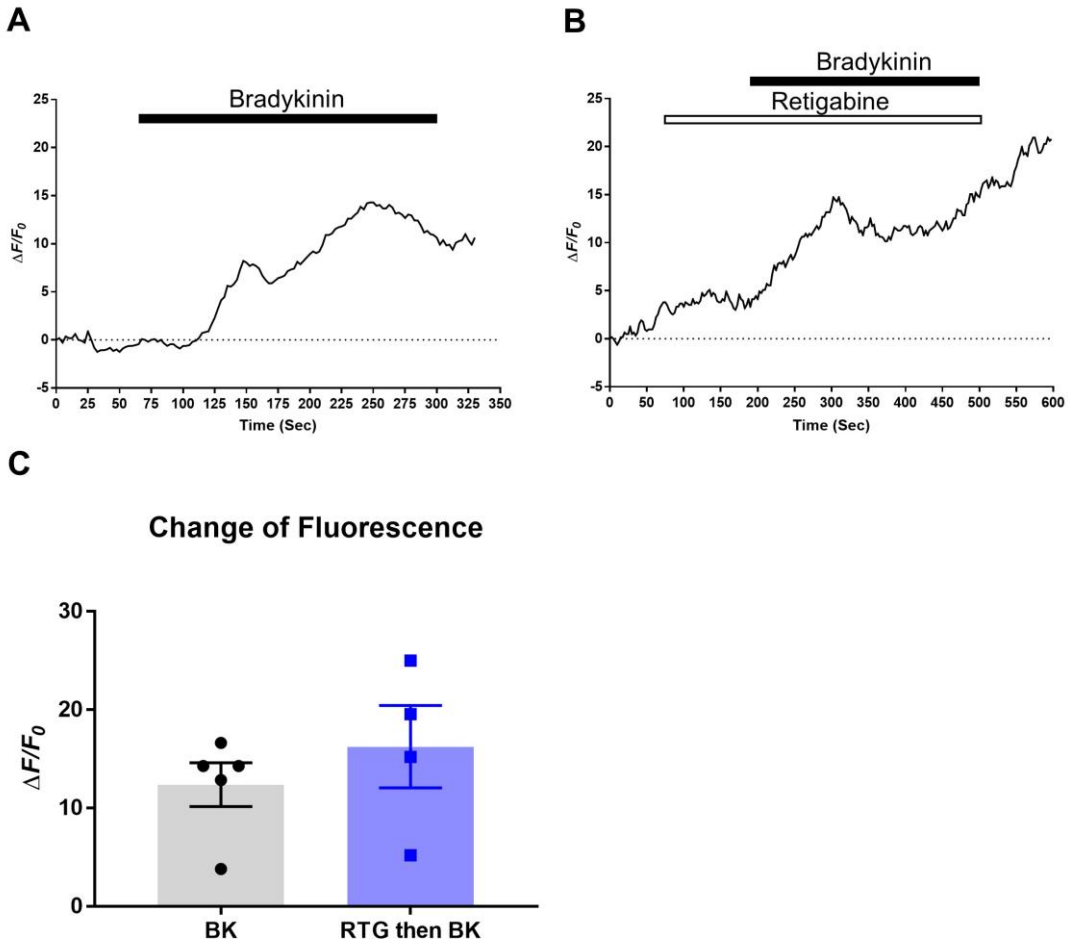

Figure 5.11 Limited effects of retigabine on BK-evoked depolarisation in SV SMCs. (**A-B**) Representative example traces showing the change of FluoVolt membrane potential recording (measured as $\Delta F/F_0$) during application of BK (250 nM) in control conditions (A) and after the preapplication of retigabine (10 µM; B), the periods indicated by horizontal bars. (**C**) Bar graph showing the percentage change in membrane potential to BK and the presence of retigabine. In panel C data are presented as mean ± S.E.M.; Statistics performed using unpaired student's t-test (n≥4).

5.3 Discussion

The present results identify Kv7 channels as an essential mechanism controlling Ca^{2+} homeostasis in human VSMCs and reveal several important differences between arterial and venous SMCs in this regard. First, we show that Kv7 channel inhibitor, XE991, induced a substantial increase of $[Ca^{2+}]_i$ in IMA but only negligible Ca^{2+} transients in SV SMCs, suggesting the tonic Kv7 channel activity plays a stronger role in limiting VGCC activity at resting conditions in IMA as compared to SV SMCs. These findings correlate well with a much higher level of expression of Kv7s in IMA as compared to SV SMCs.

Previous studies have shown that mRNA for *Kcnq1, 4* and *5* are readily detectable in rat mesenteric artery smooth muscles and mice portal vein (Mackie et al., 2008; Yeung et al., 2007). We showed that *Kcnq1, 4* and *5* are expressed in rat A7r5 cells (Chapter 3). Less information on *KCNQ* gene expression is available in human vasculature. *KCNQ4* was consistently found in mesenteric arteries with variable *KCNQ1, 3* and *5* expression, while *KCNQ2* was also undetectable (Ng et al., 2011). Kv7.1 and Kv7.5 distributed in the human carotid artery and subclavian vein (Oliveras et al., 2014). To our knowledge, there is no data on *KCNQ* gene expression for human IMA and SV SMCs in current literature. The analysis of mRNA expression revealed transcripts for *KCNQ3*, *KCNQ4* and *KCNQ5, but not KCNQ1 or KCNQ2*, with *KCNQ5* being the most abundant in both IMA and SV SMCs, but the level of all transcripts was about an order of magnitude lower in SV.

Our measurements of E_m using FluoVolt show that the activation of Kv7 channels with retigabine attenuated the BK-induced depolarisation in IMA, but not SV

SMCs. This is well-correlated with higher expression of *KCNQ5* in IMA than in SV SMCs. Accordingly, IMA SMCs are more reactive to Kv7 channel modulators than SV SMCs. It also could explain why retigabine has a limited effect on BK-induced Ca^{2+} transient in SV SMCs. The data obtained here in two primary human VSM cell types give a clear example of differential functional expression of Kv7 channels in SMCs of different blood vessel types.

Second, we observed that SV SMCs respond to the depolarisation with high extracellular K^+ buffer with much larger $[Ca^{2+}]_i$ transients than IMA SMCs. This correlated with higher expression levels of *CACNA1C* and *CACNA1G* in SV vs. IMA SMCs, an observation that could potentially explain higher Ca^{2+} transients in the SV. Even though the expression of *KCNQ* genes was lower in the latter cell type (as compared to IMA), there are other K^+ channels which contribute to high-K^+-induced depolarisation in SMCs, and if VGCCs are expressed at the higher levels in SV, this would explain larger Ca^{2+} influx. It has to be noted that either L- or T-type VGCC inhibitor attenuated the high-K^+-induced Ca^{2+} transients in IMA and SV SMCs to a similar degree.

Earlier, we identified that hypoxia decreased the expression of *Kcnq5* and increased the expression of *Cana1h* in rat aortic A7r5 cells (Chapter 4). Human SV SMCs experience lower pressure and oxygen levels than IMA SMCs within the body and, in broad agreement with this, SV-derived cells expressed less *KCNQ* transcripts and more of the VGCC-encoding genes. IMA and SV grafts have been performed in CABG surgery to treat atherosclerotic coronary artery disease. The predictor of long-term graft patency is the initial patency at one week after bypass surgery. SV grafts have higher closure rates than IMA grafts,

resulting frequently in angina, myocardial infarction, and heart failure (Goldman et al., 2004). The mechanisms for graft failure include thrombotic closure, neointimal hyperplasia, fibrosis, and the proliferation of SMCs (Guragai et al., 2017). Recently, impaired Kv7 channel activity has been found in renal, mesenteric, and coronary arteries from hypertensive rodent models (Jepps et al., 2011). The definitive mechanisms of graft failure remain challenging, and further studies are needed. Our results would indicate that the characteristics of the lower Kv7 channels activity and higher VGCCs expression in SV than IMA may be related to the patency via the modulation of Ca^{2+} signalling.

Third, IMA SMCs exhibited higher Kv7 channel activity compared with SV SMCs: XE991 did not induce a strong Ca^{2+} response in SV (as opposed to IMA) cells, suggesting low tonic activity of Kv7 in SV SMCs. Consistent with this, Kv7 activator, retigabine strongly suppressed GPCR-induced $[Ca^{2+}]_i$ transients in IMA but was much less efficacious in SV SMCs. Responses to BK were not reduced by retigabine in SV and responses to AVP were reduced, but to a lesser degree, as compared to IMA. In addition, compared to IMA SMCs, SV SMCs responded to much higher concentrations of AVP, which suggests either a lower density or sensitivity of AVP receptors in SV SMCs or weaker downstream signalling cascade; the latter is consistent with lower expression of Kv7s.

Fourth, there are marked differences in BK responses to IMA and SV SMCs. BK is a well-known inflammatory mediator that can cause acute pain and bronchoconstriction. Amongst its signalling mechanisms is the triggering the release of intracellular Ca^{2+} and the inhibition of Kv7 currents (Liu et al., 2010). Retigabine reduced the BK-induced $[Ca^{2+}]_i$ transients by about a half in IMA

SMCs, whereas nifedipine and NNC 55-0396 had no significant effect (Figure 5.8F). In contrast, in SV SMCs, neither of the drugs significantly reduced the BK-induced $[Ca^{2+}]_i$ transients with retigabine and nifedipine, producing some enhancement instead. The reason why nifedipine and retigabine produce an increase in BK-mediated Ca^{2+} transients in SV SMCs still require further investigation.

There are also marked differences in the Ca^{2+} responses induced by AVP and BK. In IMA SMCs, the AVP-induced $[Ca^{2+}]_i$ transients almost entirely depended on Ca^{2+} influx via VGCCs and were nearly abolished by either the VGCC inhibitors or retigabine-induced hyperpolarisation, while the BK-induced $[Ca^{2+}]_i$ raises had a mixed origin (that is, VGCC-dependent and VGCC-independent, both component amounting to about a half of the total $[Ca^{2+}]_i$ transient; Figure 5.8A, B, F). In SV SMCs, the AVP-induced $[Ca^{2+}]_i$ transients had mixed origin (VGCC-dependent and VGCC-independent), while the BK-induced $[Ca^{2+}]_i$ responses were almost entirely VGCC-independent. These physiological effects are likely to result from different Ca^{2+} signalling pathway in these two types of cells. Thus, the L-type Ca^{2+} channel blocker, nifedipine, did not significantly alter BK-induced effects in cultured human airway SMCs (Liu et al., 2007). Previous reports showed BK-induced Ca^{2+} signalling is dependent on the release of Ca^{2+} from IP_3-sensitive Ca^{2+} stores via activation of PLC, Ca^{2+}-induced Ca^{2+} release and/or the influx of extracellular Ca^{2+} through SOCE channel and also TRPC channels (Couture et al., 2001; Szteyn et al., 2015; Liu et al., 2010; Li et al., 2018). Some reports also showed that BK could stimulate L- and T-type VGCCs currents in heart cells (El-Bizri et al., 2003). Nonetheless, the molecular identities

of BK-mediated Ca^{2+} signalling pathways, especially in human VSMCs, are not yet fully understood.

AVP is released in response to stress or vasodilatory shock, and its main effect in the vasculature is vasoconstriction (Barrett et al., 2007). BK has a biphasic effect of inducing vasoconstriction at higher concentrations ($\geq 10^{-10}$ mol/L) and vasodilation with lower concentrations ($\leq 10^{-12}$ mol/L) (Regoli and Barabe, 1980; Bhoola et al., 1992). The role and mechanisms that BK-induced vasodilation is related to the release of NO, prostacyclin, and endothelium-derived hyperpolarising factors (Murphey et al., 2003). However, the mechanisms of vasoconstrictive action of high concentrations of BK are not fully understood (Zhang et al., 2015). Also, BK inhibits the Kv7-mediated currents, which results in the activation of VGCC-mediated Ca^{2+} influx coupled or uncoupled to Ca^{2+}-activated Cl^- current (Liu et al., 2010; Choi and Hwang, 2018). Both mobilisation of intracellular Ca^{2+} and influx of extracellular Ca^{2+} have been implicated in AVP- and BK-induced elevation of $[Ca^{2+}]_i$, but the relative contribution of both mechanisms may be different in various cell types (Yang et al., 1999).

A marked difference may exist in the coupling of the BK and AVP receptors to the Ca^{2+} signalling cascades in the IMA and SV SMCs. Both BK and AVP receptors in the VSMCs are coupled to $G_{q/11}$ and PLC, but it appears that BK receptors are coupled to ER Ca^{2+} release much better than the AVP receptors. One example of a similar dichotomy could be found in $G_{q/11}$ GPCR signalling in sympathetic neurons. Indeed, it is well demonstrated that among the four major $G_{q/11}$-coupled receptors in sympathetic neurons: muscarinic M1, bradykinin B2, angiotensin AT1 and purinergic P2Y receptors, stimulation of neither the M1 nor

AT1 receptors provoke IP_3-mediated $[Ca^{2+}]_i$ rises, whereas the B2 and P2Y receptors do. Nevertheless, stimulation of all four receptors induces robust PIP_2 hydrolysis (reviewed in (Hernandez et al., 2008; Gamper and Rohacs, 2012)). The difference in the ability to produce Ca^{2+} release could be due to the different microdomain localisation of the individual GPCR types and the proximity to the ER. However, this limitation would not affect the conclusion that Kv7 channels are essential in controlling Ca^{2+} signalling in human VSMCs.

Regardless of the specifics of the signalling cascades of individual GPCR in VSMs, our findings provide several vital conclusions: i) functional Kv7 channels are expressed in human VSMCs; ii) Kv7 channels would likely have much stronger control over arterial tone as compared to venous due to the higher expression of *KCNQ5* in the former cell type; iii) Kv7 channel activators would likely to have better efficacy in preventing vasospasm of arteries as compared to veins during surgical procedures.

5.4 Summary

- AVP and XE991 induced a large increase of $[Ca^{2+}]_i$ in primary human IMA SMCs.
- Kv7.5 mRNA transcript is the predominant Kv7 subunit in human IMA and SV SMCs.
- Retigabine effectively attenuated the Ca^{2+} transients induced in human arterial SMCs by AVP or BK.

Chapter 6

Conclusions

6.1 Principle findings

As discussed in the general introduction, Kv7 channels produce an outward K^+ current with characteristics that enable them to serve as powerful brakes against the excitation. Retigabine and its analogue, flupirtine, have been used clinically against some neuronal excitability disorders, such as epilepsy and pain (Yeung et al., 2007). Moreover, in rats with subarachnoid haemorrhage, retigabine attenuated the vasospasm in the basilar artery (Mani et al., 2013). These and other findings discussed in the introduction strongly suggest that Kv7 channels have physiological roles in regulating vascular tone and vasoconstriction (Mackie and Byron, 2008; Greenwood and Ohya, 2009; Ng et al., 2011). Yet, hitherto little is known about the roles of Kv7 channels in the regulation of $[Ca^{2+}]_i$ in SMCs. Ca^{2+} homeostasis is essential for the normal functioning of cells, and the mishandling of Ca^{2+} signalling has been suggested to result in vasoconstriction and proliferation in VSMCs. Until now, L-type VGCCs remain the primary targets of the Ca^{2+} channel blockers to treat cardiovascular diseases (Catterall et al., 2003), while T-type VGCC's role is also increasingly recognised (Cribbs, 2006). Better understanding the mechanisms of controlling $[Ca^{2+}]_i$ in the vasculature could potentially identify the novel treatment for cardiovascular diseases, even to pulmonary hypertension. Hence this thesis was undertaken to investigate the role of Kv7 channels on aspects of Ca^{2+} homeostasis in VSMCs.

In Chapter 3, we identified that direct (XE991) or GPCR-mediated (AVP) Kv7 channel inhibition triggers Ca^{2+} oscillations in rat A7r5 cells through L- and T-type VGCCs. These oscillations correlated well with E_m spikes and, hence, most likely reflect VGCC activation during action potential generation. We further identified Kv7.5 as a major Kv7 channel subunit in A7r5 cells: it has the highest mRNA and protein expression levels among all Kv7 channels tested. In addition, our recent electrophysiological experiments indicated low XE991 sensitivity of endogenous Kv7 channels in A7r5 cells (Tsai et al., 2020), which also points to Kv7.5, as this subunit has ~50 times lower XE991 sensitivity as compared to other Kv7 subunits (Schroeder et al., 2000; Wang et al., 2000; Søgaard et al., 2001). These findings identify that Kv7.5 is a potential target for Ca^{2+} modulation in VSMCs. We also discovered that the PLC-IP_3 signalling pathway is necessary for AVP- but not XE991-mediated Kv7 inhibition in A7r5 cells. Finally, we obtained some evidence that ER Ca^{2+} channels (IP_3Rs and RyRs) do contribute to AVP-mediated Ca^{2+} signalling in A7r5 cells. These findings are summarised in Figure 6.1.

In Chapter 4, we investigated the role of Kv7 channels in responses of the Ca^{2+} homeostasis to hypoxia. We found that hypoxic conditions resulted in the marked downregulation of Kv7.5 in A7r5 cells, an effect most likely mediated by HIF-1α. Yet, despite of the decreased abundance, Kv7 channel activity still influenced Ca^{2+} signalling in hypoxic rat A7r5 cells. Kv7 channel inhibition induced prolonged Ca^{2+} oscillation that lasted for much longer than in control cells. Retigabine still effectively attenuated the XE991 or AVP-induced repetitive Ca^{2+} oscillation in hypoxic cells. Hypoxia also resulted in marked upregulation of the Cav3.2 T-type Ca^{2+} channel, an effect likely mediated by HIF-2α.

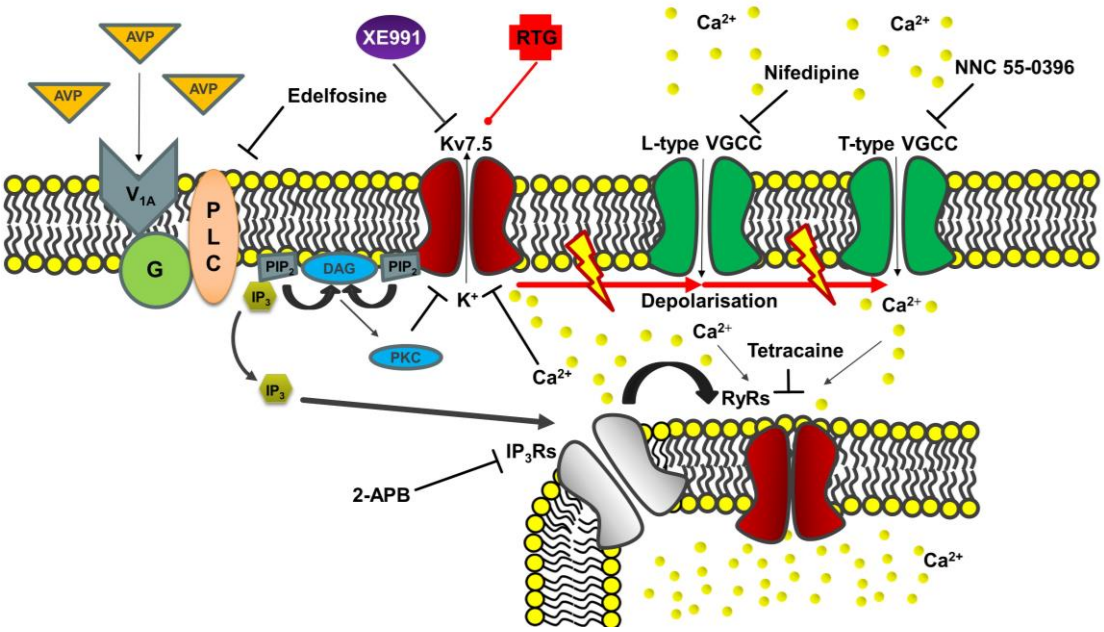

Figure 6.1 Schematic representation of the functional Kv7 role in the regulation of Ca^{2+} signalling in VSMCs. Direct (XE991) and GPCR-mediated (AVP) Kv7 channel inhibition increase the $[Ca^{2+}]_i$ via depolarisation to open both L- and T-type Ca^{2+} channels to generate Ca^{2+} oscillations. AVP can activate the V1A receptor to stimulate the PLC-IP_3 pathway and inhibit Kv7 channels by a combination of PIP_2 depletion, PKC activation and ER Ca^{2+} release.

AVP: vasopressin; DAG: diacylglycerol; G: G protein-coupled receptor; IP_3: inositol 1,4,5-trisphosphate; IP_3R: inositol 1,4,5-trisphosphate receptor; PIP_2: phosphatidylinositol 4,5-bisphosphate; PLC: phospholipase C; PKC: protein kinase C; RyR: ryanodine receptor; VGCC: voltage-gated Ca^{2+} channel; V_{1A}: vasopressin receptor 1A; 2-APB: 2-Aminoethyl diphenylborinate

Inhibition of IP_3Rs and RyRs reduced the AVP-induced enhancement $[Ca^{2+}]_i$ in the hypoxic cells as well, however, the effects were reduced compared to these in the normoxic controls, potentially suggesting lower Ca^{2+} load of the ER. Yet, the later results should be treated with caution due to the potential non-specific effects of ER Ca^{2+} channel inhibitors.

Finally, in Chapter 5, we investigated the physiological role of Kv7 channels in regulating $[Ca^{2+}]_i$ in primary human IMA and SV SMCs. The high expression and function of Kv7 channels critically determine the potency of the crucial regulator of $[Ca^{2+}]_i$ in IMA SMCs. As in the case of A7r5 cells, human VSMCs also displayed the highest levels of Kv7.5 among five Kv7 subunits, as well as the presence of L- and T-type VGCCs. Importantly, retigabine was found to be more efficacious than Ca^{2+} channels blockers to inhibit Ca^{2+} transients in IMA SMCs. T-type Ca^{2+} channels are expressed at higher levels in SV, as compared to IMA SMCs. The regional differences in O_2 demand may be responsible for different gene expressions of Kv7s and T-type Ca^{2+} channels to account for distinct Ca^{2+} signalling in different cell types.

6.2 Summary and clinical relevance

Membrane potential shift driven by electrical activity is critical for cell proliferation and differentiation. The ion channels, especially Kv7/KCNQ potassium channels, have been reported to regulate resting E_m in neurons and various blood vessels (Zhou et al., 2016; Greenwood and Ohya, 2009; Joshi et al., 2009; Ng et al., 2011; Mackie et al., 2008). However, the role of Kv7 channels on $[Ca^{2+}]_i$ in VSMCs is not well studied. The data presented in this thesis indicate that Kv7

channels may have important clinical implications in cardiovascular diseases. Retigabine or its more selective successors could have a potential in the containment of the AVP-related perioperative vasospasm, hypoxia-enhanced voltage-gated Ca^{2+} influx and vasoconstriction, as well as SCMs proliferation (Platoshyn et al., 2000). In the present study, we use both rat and human VSMCs to study the role and mechanism of Kv7s in $[Ca^{2+}]_i$ regulation. XE991 (direct) or $G\alpha_{q/11}$ receptor-mediated inhibition (AVP; indirect) leads to E_m depolarisation and promote Ca^{2+} oscillations via both L- and T-type VGCCs. The Kv7/Ca^{2+} channel signalling complex provides an important mechanism in regulating $[Ca^{2+}]_i$ in VSMCs. This feedback mechanism is evident from observations that the downregulation of Kv7.5 and upregulation of Cav3.2 T-type Ca^{2+} channels may be involved in the membrane-depolarisation-induced Ca^{2+} oscillations during hypoxia. The T-type Ca^{2+} channel is an important mediator of VSMC proliferation (Cribbs, 2006) and the new Cav3.x blocker (NNC 55-0396) was reported to be more selective (Huang et al., 2004) to have antiangiogenic activity (Kim et al., 2015). Reduced Kv currents, decreased E_m (depolarisation), and elevated $[Ca^{2+}]_i$ play a critical role in stimulating the proliferation of VSMCs and inducing PAH (Platoshyn et al., 2000). The activity of T-VGCCs is dependent on the resting E_m. Therefore, the ability of retigabine to restore the E_m and inactivate VGCCs could have beneficial effects over and above those of Ca^{2+} channel blockers. Kv7 activators would not only inhibit Ca^{2+} influx but also restore the electrical driving force for a range of ions that cross the cell membrane (Sedivy et al., 2015).

HIF transcription factors affect the ion channels expression and cellular response to hypoxia (Semenza, 2001; Hu et al., 2003; Hirota, 2020). We show that HIF-2α appears to regulate Cav3.2 T-type Ca^{2+} channel in hypoxic A7r5 cells while HIF-

1α was likely responsible for downregulation of Kv7.5. Recently, pharmacological inhibition of HIF-2α was reported as a possible novel therapeutic strategy for the treatment of vascular remodelling and right heart failure in patients with PAH (Dai et al., 2018). An understanding of the exact mechanism of both Kv7 and Cav3 channels by the HIF signalling pathway in SMCs is required in order to support the development of a therapy tailored to this endogenous pathway. Direct targeting of Kv7 and/or VGCC is also a viable strategy to normalise VSMC's activity in various pathological conditions, even when Kv7 expression is reduced (as evidenced by efficacy of retigabine to attenuate Ca^{2+} oscillations in hypoxic VSMCs). Moreover, it is conceivable that a single molecule could be developed which could simultaneously act as a Kv7 channel opener and T-type Ca^{2+} channel blocker. Thus, Kv7 channels are activated (Gao et al., 2017; Eid and Gurney, 2018), and T-type Ca^{2+} channels are inhibited by zinc (Huang et al., 2020; Traboulsie et al., 2007); there is also a similar pattern in the sensitivity of both channel types to ROS (Huang et al., 2016; Gamper et al., 2006). Hence there is appeared to be scope for tailoring pharmacology for simultaneous co-modulation of both channels in VSMCs.

6.3 Further work

All of the points mentioned above are fascinating and point to the use of Kv7 activators to normalise VSMC's function. Using these important findings as a basis for future studies may certainly offer potential pathways for therapeutic intervention. In terms of the direction for future work, it may be worthwhile to perform knock-out or knockdown of Kv7.5 in VSMCs and evaluate how would this impact AVP-induced Ca^{2+} signalling or effects of hypoxia.

The use of whole-cell patch-clamp electrophysiological recordings would provide further information about specific Kv7 or T-type VGCCs protein expression on the inhibition of Kv7s induced $[Ca^{2+}]_i$ and VGCC activity. The inclusion of electrophysiology data demonstrating the effect of Kv7s on VGCC activity in normoxic and hypoxic environments would allow a more definitive conclusion to be drawn. In addition, the availability of novel, more specific, Kv7 activators, e.g. GoSlo-SR compounds, will aid the verification of Kv7.4/7.5 effects in subsequent investigations (Zavaritskaya et al., 2020).

The limited data shown here regarding the potential involvement of HIF signalling on the activity of Kv7s and VGCCs warrants further investigation. While numerous hypoxia and HIF signalling studies have been performed, we still have little understanding of the differential roles that each HIFα protein plays. Relative to HIF-1α, there are not many studies related to HIF-2α in cardiovascular disorders (reviewed in (Lee et al., 2019)). Recent studies indicate that Ca^{2+} plays a key role in the hypoxic cellular response, and an increase of $[Ca^{2+}]_i$ was observed at least in part via the increase of T-type Ca^{2+} channels activity during hypoxia (Seta et al., 2004; Wan et al., 2013); therefore, exploration of the HIF transcription signalling pathway and their correlation between Kv7s and Ca^{2+} channels during hypoxia may help to elucidate the exact mechanism of Ca^{2+} modulation.

Finally, in this study, we reveal the importance of the Kv7s in the tight control of $[Ca^{2+}]_i$ using indirect inhibition via GPCRs ligands, AVP and BK. These ligands trigger $G_{q/11}$-PLC signalling cascade to inhibit Kv7 in multiple cell types (Liu et al., 2010; Yang et al., 1999; Mackie et al., 2008). Yet, there is another signalling

cascade associated with these GPCR: RhoA-mediated ROCK activation. This signalling cascade is known to be important in cardiovascular physiology (Loirand et al., 2006). It has been shown that hypoxia alters the expression and/or activity of RhoA/ROCK proteins and HIF-1α. (Turcotte et al., 2003). A recent report has demonstrated the inhibition of the RhoA/ROCK signalling pathway ameliorates hypoxic pulmonary hypertension via HIF-1α-dependent upregulation of TRPCs (Wang et al., 2019). However, the possible interaction between RhoA/ROCK and HIFα in VSMCs, and their roles in the regulation of Kv7 channels have not been studied in the present thesis. Therefore, the use of the Rho inhibitor (e.g. C3 transferase) and the ROCK inhibitor (e.g. fasudil) are the pertinent experiments to explore the role of RhoA/ROCK signalling (Gonzalez-Rodriguez et al., 2015). These studies will advance our current understanding of how Kv7 channels are regulated, how hypoxia regulates ion channel activity, and how Ca^{2+} overload is controlled in VSMCs.

6.4 Conclusion

Kv7.5 has tight control over the VGCCs activity and Ca^{2+} homeostasis in rat and human VSMCs. As regenerative activation of VGCCs in response to E_m depolarisation could cause excessive Ca^{2+} influx and inappropriate vasospasm, direct activation in response to myogenic depolarisation or be sensitive to extrinsic factors that modulate the myogenic response suggest that Kv7 channels may have precise control of this important physiological mechanism. Moreover, Kv7 channel activators may have the therapeutic advantage over the VGCC blockers as the former would not directly block excitation-contraction coupling. Our research provides a new perspective for understanding $[Ca^{2+}]_i$ as well as Kv7/KCNQ channel function in the vasculature. We also suggest Kv7.5 as a

target for the therapeutic control of vascular tone in cardiovascular diseases and hypoxia.

References

Abe, H., Semba, H. and Takeda, N. 2017. The roles of hypoxia signaling in the pathogenesis of cardiovascular diseases. *Journal of Atherosclerosis and Thrombosis.* **24**(9), pp.884-894.

Aboyans, V., Ricco, J.-B., Bartelink, M.-L.E., Björck, M., Brodmann, M., Cohnert, T., Collet, J.-P., Czerny, M., De Carlo, M. and Debus, S. 2018. 2017 ESC Guidelines on the Diagnosis and Treatment of Peripheral Arterial Diseases, in collaboration with the European Society for Vascular Surgery (ESVS) Document covering atherosclerotic disease of extracranial carotid and vertebral, mesenteric, renal, upper and lower extremity arteries Endorsed by: the European Stroke Organization (ESO) The Task Force for the Diagnosis and Treatment of Peripheral Arterial Diseases of the European Society of Cardiology (ESC) and of the European Society for Vascular Surgery (ESVS). *European Heart Journal.* **39**(9), pp.763-816.

Aley, P.K., Wilkinson, J.A., Bauer, C.C., Boyle, J.P., Porter, K.E. and Peers, C. 2008. Hypoxic remodelling of Ca^{2+} signalling in proliferating human arterial smooth muscle. *Molecular and Cellular Biochemistry.* **318**(1-2), pp.101-108.

Allbritton, N.L., Meyer, T. and Stryer, L. 1992. Range of messenger action of calcium-ion and inositol 1,4,5-trisphosphate. *Science.* **258**(5089), pp.1812-1815.

Alonso, M.T., Gajate, C., Mollinedo, F., Modolell, M., Alvarez, J. and García-Sancho, J. 1997. Dissociation of the effects of the antitumour ether lipid ET-18-OCH3 on cytosolic calcium and on apoptosis. *British Journal of Pharmacology.* **121**(7), pp.1364-1368.

Amberg, G.C. and Navedo, M.F. 2013. Calcium dynamics in vascular smooth muscle. *Microcirculation.* **20**(4), pp.281-289.

Amberg, G.C., Navedo, M.F., Nieves-Cintrón, M., Molkentin, J.D. and Santana, L.F. 2007. Calcium sparklets regulate local and global calcium in murine arterial smooth muscle. *The Journal of physiology.* **579**(Pt 1), pp.187-201.

Apostolova, E., Zagorchev, P., Kokova, V. and Peychev, L. 2017. Retigabine diminishes the effects of acetylcholine, adrenaline and adrenergic agonists on the spontaneous activity of guinea pig smooth muscle strips in vitro. *Autonomic Neuroscience-Basic & Clinical.* **203**, pp.51-57.

Appelhoff, R.J., Tian, Y.M., Raval, R.R., Turley, H., Harris, A.L., Pugh, C.W., Ratcliffe, P.J. and Gleadle, J.M. Differential function of the prolyl hydroxylases PHD1, PHD2, and PHD3 in the regulation of hypoxia-inducible factor. *The Journal of Biological Chemistry.* **279**(37), pp.38458-38465.

Archer, S.L., Souil, E., Dinh-Xuan, A.T., Schremmer, B., Mercier, J.C., El Yaagoubi, A., Nguyen-Huu, L., Reeve, H.L. and Hampl, V. 1998. Molecular identification of the role of voltage-gated K^+ channels, Kv1.5 and Kv2.1, in hypoxic pulmonary vasoconstriction and control of resting membrane potential in

rat pulmonary artery myocytes. *Journal of Clinical Investigation.* **101**(11), pp.2319-2330.

Ast, T. and Mootha, V.K. 2019. Oxygen and mammalian cell culture: are we repeating the experiment of Dr. Ox? *Nat Metab*. **1**(9), pp.858-860.

Bal, M., Zhang, J., Hernandez, C.C., Zaika, O. and Shapiro, M.S. 2010. Ca^{2+}/calmodulin disrupts AKAP79/150 interactions with KCNQ (M-Type) K^+ channels. *The Journal of neuroscience : the official journal of the Society for Neuroscience.* **30**(6), p2311.

Barhanin, J., Lesage, F., Guillemare, E., Fink, M., Lazdunski, M. and Romey, G. 1996. KvLQT1 and lsK (minK) proteins associate to form the I_{Ks} cardiac potassium current. *Nature.* **384**(6604), pp.78-80.

Barrett, L.K., Singer, M. and Clapp, L.H. 2007. Vasopressin: Mechanisms of action on the vasculature in health and in septic shock. *Critical Care Medicine.* **35**(1), pp.33-40.

Barrett, P.Q., Lu, H.-K., Colbran, R., Czernik, A. and Pancrazio, J.J. 2000. Stimulation of unitary T-type Ca^{2+} channel currents by calmodulin-dependent protein kinase II. American Journal of Physiology-Cell Physiology. **279**(6), pp.C1694-C1703.

Bayliss, W.M. 1902. On the local reactions of the arterial wall to changes of internal pressure. *The Journal of physiology.* **28**(3), pp.220-231.

Bean, B.P., Sturek, M., Puga, A. and Hermsmeyer, K. 1986. Calcium channels in muscle-cells isolated from rat mesenteric-arteries: modulation by dihydropyridine drugs. *Circulation Research.* **59**(2), pp.229-235.

Beaudry, M., Hidalgo, M., Launay, T., Bello, V. and Darribère, T. 2016. Regulation of myogenesis by environmental hypoxia. *Journal of cell science*. **129**(15), pp.2887-2896.

Becker, P.L. and Fay, F.S. 1987. Photobleaching of fura-2 and its effect on determination of calcium concentrations. *American Journal of Physiology-Cell Physiology.* **253**(4), pp.C613-C618.

Befani, C. and Liakos, P. 2018. The role of hypoxia-inducible factor-2 alpha in angiogenesis. *Journal of cellular physiology.* **233**(12), pp.9087-9098.

Bencze, M., Behuliak, M., Vavřínová, A. and Zicha, J. 2015. Broad-range TRP channel inhibitors (2-APB, flufenamic acid, SKF-96365) affect differently contraction of resistance and conduit femoral arteries of rat. *European Journal of Pharmacology.* **765**, pp.533-540.

Benham, C.D. and Tsien, R.W. 1987. Calcium-permeable channels in vascular smooth muscle: voltage-activated, receptor-operated, and leak channels. *Society of General Physiologists series*. **42**, pp.45-64.

Benjamin, E.J., Blaha, M.J., Chiuve, S.E., Cushman, M., Das, S.R., Deo, R., de Ferranti, S.D., Floyd, J., Fornage, M., Gillespie, C., Isasi, C.R., Jimenez, M.C., Jordan, L.C., Judd, S.E., Lackland, D., Lichtman, J.H., Lisabeth, L., Liu, S.M., Longenecker, C.T., Mackey, R.H., Matsushita, K., Mozaffarian, D., Mussolino, M.E., Nasir, K., Neumar, R.W., Palaniappan, L., Pandey, D.K., Thiagarajan, R.R., Reeves, M.J., Ritchey, M., Rodriguez, C.J., Roth, G.A., Rosamond, W.D., Sasson, C., Towfighi, A., Tsao, C.W., Turner, M.B., Virani, S.S., Voeks, J.H., Willey, J.Z., Wilkins, J.T., Wu, J.H.Y., Alger, H.M., Wong, S.S., Muntner, P., Amer Heart Assoc Stat, C. and Stroke Stat, S. 2017. Heart Disease and Stroke Statistics-2017 Update: A Report From the American Heart Association. *Circulation.* **135**(10), pp.E146-E603.

Bennett, D.L., Cheek, T.R., Berridge, M.J., DeSmedt, H., Parys, J.B., Missiaen, L. and Bootman, M.D. 1996. Expression and function of ryanodine receptors in nonexcitable cells. *The Journal of Biological Chemistry.* **271**(11), pp.6356-6362.

Berridge, M.J., Lipp, P. and Bootman, M.D. 2000. The versatility and universality of calcium signalling. *Nature reviews. Molecular cell biology.* **1**(1), pp.11-21.

Bezanilla, F. 2008. How membrane proteins sense voltage. *Nature reviews. Molecular cell biology.* **9**(4), pp.323-332.

Bezprozvanny, I.B., Ondrias, K., Kaftan, E., Stoyanovsky, D.A. and Ehrlich, B.E. 1993. Activation of the calcium release channel (ryanodine receptor) by heparin and other polyanions is calcium-dependent. *Molecular Biology of the Cell.* **4**(3), pp.347-352.

Bhoola, K.D., Figueroa, C.D. and Worthy, K. 1992. Bioregulation of kinins: kallikreins, kininogens, and kininases. *Pharmacological Reviews.* **44**(1), pp.1-80.

Blaustein, M.P. and Hamlyn, J.M. 1984. Sodium transport inhibition, cell calcium, and hypertension. The natriuretic hormone/Na^+-Ca^{2+} exchange/hypertension hypothesis. *American Journal of Medicine.* **77**(4A), pp.45-59.

Bootman, M.D., Collins, T.J., Peppiatt, C.M., Prothero, L.S., MacKenzie, L., De Smet, P., Travers, M., Tovey, S.C., Seo, J.T., Berridge, M.J., Ciccolini, F. and Lipp, P. 2001. Calcium signalling-an overview. *Seminars in Cell & Developmental Biology.* **12**(1), pp.3-10.

Borjesson, S.I. and Elinder, F. 2008. Structure, function, and modification of the voltage sensor in voltage-gated ion channels. *Cell Biochemistry and Biophysics.* **52**(3), pp.149-174.

Boycott, H.E., Dallas, M.L., Elies, J., Pettinger, L., Boyle, J.P., Scragg, J.L., Gamper, N. and Peers, C. 2013. Carbon monoxide inhibition of Cav3.2 T-type Ca^{2+} channels reveals tonic modulation by thioredoxin. *The FASEB Journal*. **27**(8), pp.3395-3407.

Bradford, M.M. 1976. A rapid and sensitive method for the quantitation of microgram quantities of protein utilizing the principle of protein-dye binding. *Analytical biochemistry.* **72**, pp.248-254.

Brayden, J.E. 2002. Functional roles of K_{ATP} channels in vascular smooth muscle. *Clinical and experimental pharmacology & physiology.* **29**(4), pp.312-316.

Brini, M. and Carafoli, E. 2009. Calcium pumps in health and disease. *Physiological Reviews.* **89**(4), pp.1341-1378.

Brini, M. and Carafoli, E. 2011. The plasma membrane Ca^{2+} ATPase and the plasma membrane sodium calcium exchanger cooperate in the regulation of cell calcium. *Cold Spring Harbor Perspectives in Biology.* **3**(2), pp.a004168.

Brown, I., Diederich, L., Good, M. E., DeLalio, L. J., Murphy, S. A., Cortese-Krott, M. M., Hall, J. L., Le, T. H. and Isakson, B. E. 2018. Vascular smooth muscle remodeling in conductive and resistance arteries in hypertension. *Arteriosclerosis Thrombosis and Vascular Biology.* **38**(9), pp.1969-1985.

Brown, M.J., Palmer, C.R., Castaigne, A., de Leeuw, P.W., Mancia, G., Rosenthal, T. and Ruilope, L.M. 2000. Morbidity and mortality in patients randomised to double-blind treatment with a long-acting calcium-channel blocker or diuretic in the International Nifedipine GITS study: Intervention as a Goal in Hypertension Treatment (INSIGHT). *Lancet.* **356**(9227), pp.366-372.

Brueggemann, L.I., Mackie, A.R., Cribbs, L.L., Freda, J., Tripathi, A., Majetschak, M. and Byron, K.L. 2014. Differential protein kinase C-dependent modulation of Kv7.4 and Kv7.5 subunits of vascular Kv7 channels. *The Journal of Biological Chemistry.* **289**(4), pp.2099-2111.

Brueggemann, L.I., Mackie, A.R., Martin, J.L., Cribbs, L.L. and Byron, K.L. 2011. Diclofenac distinguishes among homomeric and heteromeric potassium channels composed of KCNQ4 and KCNQ5 Subunits. *Molecular Pharmacology.* **79**(1), pp.10-23.

Brueggemann, L.I., Moran, C.J., Barakat, J.A., Yeh, J.Z., Cribbs, L.L. and Byron, K.L. 2007. Vasopressin stimulates action potential firing by protein kinase C-dependent inhibition of KCNQ5 in A7r5 rat aortic smooth muscle cells. *American Journal of Physiology. Heart and Circulatory Physiology*. **292**(3), pp.H1352-1363.

Busse, R., Fleming, I. and Hecker, M. 1993. Signal transduction in endothelium-dependent vasodilatation. *European Heart Journal.* **14**, pp.2-9.

Byron, K.L. 1996. Vasopressin stimulates Ca^{2+} spiking activity in A7r5 vascular smooth muscle cells via activation of phospholipase A_2. *Circulation Research.* **78**(5), pp.813-820.

Byron, K.L. and Brueggemann, L.I. 2018. Kv7 potassium channels as signal transduction intermediates in the control of microvascular tone. *Microcirculation.* **25**(1), pp.e12419.

Capiod, T. 2011. Cell proliferation, calcium influx and calcium channels. *Biochimie.* **93**(12), pp.2075-2079.

Catterall, W.A. 2011. Voltage-gated calcium channels. *Cold Spring Harbor Perspectives in Biology.* **3**(8), pp.a003947.

Catterall, W.A., Perez-Reyes, E., Snutch, T.P. and Striessnig, J. 2005. International Union of Pharmacology. XLVIII. Nomenclature and structure-function relationships of voltage-gated calcium channels. *Pharmacological Reviews.* **57**(4), pp.411-425.

Catterall, W.A., Striessnig, J., Snutch, T.P. and Perez-Reyes, E. 2003. International Union of Pharmacology. XL. Compendium of voltage-gated ion channels: Calcium channels. *Pharmacological Reviews.* **55**(4), pp.579-581.

Chadha, P.S., Jepps, T.A., Carr, G., Stott, J.B., Zhu, H.L., Cole, W.C. and Greenwood, I.A. 2014. Contribution of Kv7.4/kv7.5 heteromers to intrinsic and calcitonin gene-related peptide-induced cerebral reactivity. *Arteriosclerosis, Thrombosis, and Vascular Biology.* **34**(4), pp.887-893.

Chang, A., Abderemane-Ali, F., Hura, G.L., Rossen, N.D., Gate, R.E. and Minor, D.L. 2018. A calmodulin C-lobe Ca^{2+}-dependent switch governs Kv7 channel function. *Neuron.* **97**(4), pp.836-852.

Chen, X., Li, W., Hiett, S.C. and Obukhov, A.G. 2016. Novel roles for Kv7 channels in shaping histamine-induced contractions and bradykinin-dependent relaxations in pig coronary arteries. *PLoS One*. **11**(2), pe0148569.

Cheng, H., Lederer, W.J. and Cannell, M.B. 1993. Calcium sparks: elementary events underlying excitation-contraction coupling in heart muscle. *Science.* **262**(5134), pp.740-744.

Cheng, K.T., Liu, X., Ong, H.L., Swaim, W. and Ambudkar, I.S. 2011. Local Ca^{2+} entry via Orai1 regulates plasma membrane recruitment of TRPC1 and controls cytosolic Ca^{2+} signals required for specific cell functions. *PLoS Biology.* **9**(3), pp.e1001025.

Cheung, K.H., Shineman, D., Müller, M., Cárdenas, C., Mei, L., Yang, J., Tomita, T., Iwatsubo, T., Lee, V.M. and Foskett, J.K. 2008. Mechanism of Ca^{2+} disruption in Alzheimer's disease by presenilin regulation of $InsP_3$ receptor channel gating. *Neuron.* **58**(6), pp.871-883.

Choi, S.I. and Hwang, S.W. 2018. Depolarizing effectors of bradykinin signaling in nociceptor excitation in pain perception. *Biomolecules & Therapeutics.* **26**(3), pp.255-267.

Colton, C.K. and Zhu, M.X. 2007. 2-Aminoethoxydiphenyl borate as a common activator of TRPV1, TRPV2, and TRPV3 channels. *Handbook of experimental pharmacology.* (179), pp.173-187.

Cool, C.D., Groshong, S.D., Oakey, J. and Voelkel, N.F. 2005. Pulmonary hypertension: Cellular and molecular mechanisms. *Chest.* **128**(6), pp.565S-571S.

Coppock, E.A., Martens, J.R. and Tamkun, M.M. 2001. Molecular basis of hypoxia-induced pulmonary vasoconstriction: role of voltage-gated K^+ channels.

American Journal of Physiology-Lung Cellular and Molecular Physiology. **281**(1), pp.L1-L12.

Couture, R., Harrisson, M., Vianna, R.M. and Cloutier, F. 2001. Kinin receptors in pain and inflammation. *European Journal of Pharmacology.* **429**(1-3), pp.161-176.

Covello, K.L., Kehler, J., Yu, H., Gordan, J.D., Arsham, A.M., Hu, C.J., Labosky, P.A., Simon, M.C. and Keith, B. 2006. HIF-2α regulates Oct-4: effects of hypoxia on stem cell function, embryonic development, and tumor growth. *Genes & Development.* **20**(5), pp.557-570.

Cox, R.H. 2005. Molecular determinants of voltage-gated potassium currents in vascular smooth muscle. *Cell Biochemistry and Biophysics.* **42**(2), pp.167-195.

Cribbs, L.L. 2006. T-type Ca^{2+} channels in vascular smooth muscle: Multiple functions. *Cell Calcium.* **40**(2), pp.221-230.

Csernoch, L., Szentesi, P., Sárközi, S., Szegedi, C., Jona, I. and Kovács, L. 1999. Effects of tetracaine on sarcoplasmic calcium release in mammalian skeletal muscle fibres. *The Journal of physiology.* **515**(Pt 3), pp.843-857.

Curtis, T.M., Tumelty, J., Stewart, M.T., Arora, A.R., Lai, F.A., McGahon, M.K., Scholfield, C.N. and McGeown, J.G. 2008. Modification of smooth muscle Ca^{2+}-sparks by tetracaine: evidence for sequential RyR activation. *Cell Calcium.* **43**(2), pp.142-154.

Dai, Z., Zhu, M.M., Peng, Y., Machireddy, N., Evans, C.E., Machado, R., Zhang, X. and Zhao, Y.Y. 2018. Therapeutic targeting of vascular remodeling and right heart failure in pulmonary arterial hypertension with a HIF-2α Inhibitor. *American Journal of Respiratory and Critical Care Medicine.* **198**(11), pp.1423-1434.

Dallas, M.L., Scragg, J.L. and Peers, C. 2009. Inhibition of L-type Ca^{2+} channels by carbon monoxide. Adv Exp Med Biol. **648**, pp.89-95.

Del Toro, R., Levitsky, K.L., Lopez-Barneo, J. and Chiara, M.D. 2003. Induction of T-type calcium channel gene expression by chronic hypoxia. *The Journal of Biological Chemistry.* **278**(25), pp.22316-22324.

del Valle-Rodríguez, A., López-Barneo, J. and Ureña, J. 2003. Ca^{2+} channel-sarcoplasmic reticulum coupling: a mechanism of arterial myocyte contraction without Ca^{2+} influx. *The EMBO Journal.* **22**(17), pp.4337-4345.

Delmas, P. and Brown, D.A. 2005. Pathways modulating neural KCNQ/M (Kv7) potassium channels. *Nature Reviews Neuroscience.* **6**(11), pp.850-862.

Deng, M., Deng, L. and Xue, Y. 2012. MAP kinase-mediated and MLCK-independent phosphorylation of MLC20 in smooth muscle cells. *Current Basic and Pathological Approaches to the Function of Muscle Cells and Tissues - From Molecules to Humans.*

Dogan, M.F., Yildiz, O., Arslan, S.O. and Ulusoy, K.G. 2019. Potassium channels in vascular smooth muscle: a pathophysiological and pharmacological perspective. *Fundamental & clinical pharmacology.* **33**(5), pp.504-523.

Dray, A. and Perkins, M. 1993. Bradykinin and inflammatory pain. *Trends in Neurosciences.* **16**(3), pp.99-104.

Du, X. and Gamper, N. 2013. Potassium channels in peripheral pain pathways: expression, function and therapeutic potential. *Current neuropharmacology.* **11**(6), pp.621-640.

Du, X., Hao, H., Gigout, S., Huang, D., Yang, Y., Li, L., Wang, C., Sundt, D., Jaffe, D.B., Zhang, H. and Gamper, N. 2014. Control of somatic membrane potential in nociceptive neurons and its implications for peripheral nociceptive transmission. *Pain.* **155**(11), pp.2306-2322.

Duckles, Hayley (2013) The vascular smooth muscle T-type Ca^{2+} channel: An anti-proliferative target for heme oxygenase-1. PhD thesis, University of Leeds.

Duckles, H., Boycott, H.E., Al-Owais, M.M., Elies, J., Johnson, E., Dallas, M.L., Porter, K.E., Giuntini, F., Boyle, J.P., Scragg, J.L. and Peers, C. 2015. Heme oxygenase-1 regulates cell proliferation via carbon monoxide-mediated inhibition of T-type Ca^{2+} channels. *Pflugers Archiv : European journal of physiology*. **467**(2), pp.415-427.

Dulak, J., Deshane, J., Jozkowicz, A. and Agarwal, A. 2008. Heme Oxygenase-1 and Carbon Monoxide in Vascular Pathobiology. *Circulation*. **117**(2), pp.231-241.

Duscher, D., Januszyk, M., Maan, Z.N., Whittam, A.J., Hu, M.S., Walmsley, G.G., Dong, Y., Khong, S.M., Longaker, M.T. and Gurtner, G.C. 2017. Comparison of the hydroxylase Inhibitor dimethyloxalylglycine and the iron chelator deferoxamine in diabetic and aged wound healing. *Plastic and reconstructive surgery.* **139**(3), pp.695e-706e.

Eagleton, M.J., Bishop, P.D., Bena, J.F., Nassoiy, S.P., Clair, D.G., Kashyap, V.S. and Ouriel, K. 2008. Calcium channel blockers and angiotensin-converting enzyme inhibitors may be associated with altered atherosclerotic plaque size and morphology. *Vascular.* **16**(3), pp.171-178.

Earley, S. and Brayden, J.E. 2015. Transient receptor potential channels in the vasculature. *Physiological Reviews.* **95**(2), pp.645-690.

Eid, B.G. and Gurney, A.M. 2018. Zinc pyrithione activates K^+ channels and hyperpolarizes the membrane of rat pulmonary artery smooth muscle cells. *PLoS One.* **13**(2), pp.e0192699.

Ekberg, J., Schuetz, F., Boase, N.A., Conroy, S.J., Manning, J., Kumar, S., Poronnik, P. and Adams, D.J. 2007. Regulation of the voltage-gated K^+ channels KCNQ2/3 and KCNQ3/5 by ubiquitination. Novel role for Nedd4-2. *The Journal of Biological Chemistry.* **282**(16), pp.12135-12142.

El-Bizri, N., Bkaily, G., Wang, S.M., Jacques, D., Regoli, D., D'Orleans-Juste, P. and Sukarieh, R. 2003. Bradykinin induced a positive chronotropic effect via stimulation of T- and L-type calcium currents in heart cells. *Canadian Journal of Physiology and Pharmacology.* **81**(3), pp.247-258.

Elies, J., Scragg, J.L., Boyle, J.P., Gamper, N. and Peers, C. 2016. Regulation of the T-type Ca^{2+} channel Cav3.2 by hydrogen sulfide: emerging controversies concerning the role of H_2S in nociception. *The Journal of Physiology*. **594**(15), pp.4119-4129.

Epstein, A.C., Gleadle, J.M., McNeill, L.A., Hewitson, K.S., O'Rourke, J., Mole, D.R., Mukherji, M., Metzen, E., Wilson, M.I., Dhanda, A., Tian, Y.M., Masson, N., Hamilton, D.L., Jaakkola, P., Barstead, R., Hodgkin, J., Maxwell, P.H., Pugh, C.W., Schofield, C.J. and Ratcliffe, P.J. 2001. C. elegans EGL-9 and mammalian homologs define a family of dioxygenases that regulate HIF by prolyl hydroxylation. *Cell*. **107**(1), pp.43-54.

Ertel, E.A., Campbell, K.P., Harpold, M.M., Hofmann, F., Mori, Y., Perez-Reyes, E., Schwartz, A., Snutch, T.P., Tanabe, T., Birnbaumer, L., Tsien, R.W. and Catterall, W.A. 2000. Nomenclature of voltage-gated calcium channels. *Neuron.* **25**(3), pp.533-535.

Evans, A.M., Osipenko, O.N. and Gurney, A.M. 1996. Properties of a novel K^+ current that is active at resting potential in rabbit pulmonary artery smooth muscle cells. *Journal of Physiology-London.* **496**(2), pp.407-420.

Fauconnier, J., Roberge, S., Saint, N. and Lacampagne, A. 2013. Type 2 ryanodine receptor: a novel therapeutic target in myocardial ischemia/reperfusion. *Pharmacology & Therapeutics*. **138**(3), pp.323-332.

Fedorova, M., Kuleva, N. and Hoffmann, R. 2010. Identification of cysteine, methionine and tryptophan residues of actin oxidized in vivo during oxidative stress. *Journal of Proteome Research.* **9**(3), pp.1598-1609.

Fernández-Tenorio, M., González-Rodríguez, P., Porras, C., Castellano, A., Moosmang, S., Hofmann, F., Ureña, J. and López-Barneo, J. 2010. Short communication: genetic ablation of L-type Ca^{2+} channels abolishes depolarization-induced Ca^{2+} release in arterial smooth muscle. *Circulation Research.* **106**(7), pp.1285-1289.

Fleischmann, B.K., Murray, R.K. and Kotlikoff, M.I. 1994. Voltage window for sustained elevation of cytosolic calcium in smooth muscle cells. *Proceedings of the National Academy of Sciences of the United States of America.* **91**(25), pp.11914-11918.

Forsythe, J.A., Jiang, B.H., Iyer, N.V., Agani, F., Leung, S.W., Koos, R.D. and Semenza, G.L. 1996. Activation of vascular endothelial growth factor gene transcription by hypoxia-inducible factor 1. *Molecular and Cellular Biology.* **16**(9), pp.4604-4613.

Foskett, J.K., White, C., Cheung, K.H. and Mak, D.O. 2007. Inositol trisphosphate receptor Ca^{2+} release channels. *Physiological Reviews.* **87**(2), pp.593-658.

Fosmo, A.L. and Skraastad, Ø.B. 2017. The Kv7 Channel and Cardiovascular Risk Factors. *Frontiers in cardiovascular medicine.* **4**, pp.75-75.

Gamper, N., and Shapiro, M.S. 2015. *KCNQ Channels. Handbook of Ion Channels, In: Zheng J, Trudeau, M.C ed* (CRC Press, Boca Raton, FL). pp.275-306.

Gamper, N., and Shapiro, M.S. 2003. Calmodulin mediates Ca^{2+}-dependent modulation of M-type K^+ channels. *The Journal of General Physiology.* **122**(1), pp.17-31.

Gamper, N., Li, Y. and Shapiro, M.S. 2005. Structural requirements for differential sensitivity of KCNQ K^+ channels to modulation by Ca^{2+}/calmodulin. *Molecular Biology of the Cell.* **16**(8), pp.3538-3551.

Gamper, N., Reznikov, V., Yamada, Y., Yang, J. and Shapiro, M.S. 2004. Phosphatidylinositol 4,5-bisphosphate signals underlie receptor-specific $G_{q/11}$-mediated modulation of N-type Ca^{2+} channels. *The Journal of neuroscience : the official journal of the Society for Neuroscience.* **24**(48), pp.10980-10992.

Gamper, N. and Rohacs, T. 2012. Phosphoinositide sensitivity of ion channels, a functional perspective. *Phosphoinositides II: The Diverse Biological Functions.* Springer, pp.289-333.

Gamper, N. and Shapiro, M.S. 2007. Target-specific PIP_2 signalling: how might it work? *The Journal of physiology.* **582**(Pt 3), pp.967-975.

Gamper, N., Zaika, O., Li, Y., Martin, P., Hernandez, C.C., Perez, M.R., Wang, A.Y., Jaffe, D.B. and Shapiro, M.S. 2006. Oxidative modification of M-type K^+ channels as a mechanism of cytoprotective neuronal silencing. *The EMBO Journal.* **25**(20), pp.4996-5004.

Gao, H., Boillat, A., Huang, D., Liang, C., Peers, C. and Gamper, N. 2017. Intracellular zinc activates KCNQ channels by reducing their dependence on phosphatidylinositol 4,5-bisphosphate. *Proceedings of the National Academy of Sciences of the United States of America.* **114**(31), pp.E6410-E6419.

Gao, Y. 2017. Intracellular Ca^{2+} Regulation. In: Gao, Y. ed. *Biology of Vascular Smooth Muscle: Vasoconstriction and Dilatation.* Singapore: Springer Singapore, pp.139-154.

Gerhard-Herman, M.D., Gornik, H.L., Barrett, C., Barshes, N.R., Corriere, M.A., Drachman, D.E., Fleisher, L.A., Fowkes, F.G., Hamburg, N.M., Kinlay, S., Lookstein, R., Misra, S., Mureebe, L., Olin, J.W., Patel, R.A., Regensteiner, J.G., Schanzer, A., Shishehbor, M.H., Stewart, K.J., Treat-Jacobson, D. and Walsh, M.E. 2017. 2016 AHA/ACC Guideline on the Management of Patients With Lower Extremity Peripheral Artery Disease: A Report of the American College of Cardiology/American Heart Association Task Force on Clinical Practice Guidelines. *Circulation.* **135**(12), pp.e726-e779.

Ghosh, D., Syed, A.U., Prada, M.P., Nystoriak, M.A., Santana, L.F., Nieves-Cintrón, M. and Navedo, M.F. 2017. Calcium channels in vascular smooth muscle. *Advances in Pharmacology (San Diego, Calif.).* **78**, pp.49-87.

Giachini, F. R., Lima, V. V., Filgueira, F. P., Dorrance, A. M., Carvalho, M. H., Fortes, Z. B., Webb, R. C. and Tostes, R. C. 2012. STIM 1/Orai 1 contributes to sex differences in vascular responses to calcium in spontaneously hypertensive rats. *Clinical Science.* **122**(5-6), pp.215-226.

Goldman, S., Zadina, K., Moritz, T., Ovitt, T., Sethi, G., Copeland, J.G., Thottapurathu, L., Krasnicka, B., Ellis, N., Anderson, R.J. and Henderson, W. 2004. Long-term patency of saphenous vein and left internal mammary artery grafts after coronary artery bypass surgery: results from a Department of Veterans Affairs Cooperative Study. *Journal of the American College of Cardiology.* **44**(11), pp.2149-2156.

Gollasch, M., Haase, H., Ried, C., Lindschau, C., Morano, I., Luft, F.C. and Haller, H. 1998. L-type calcium channel expression depends on the differentiated state of vascular smooth muscle cells. *The FASEB Journal*. **12**(7), pp.593-601.

Golovina, V. A., Platoshyn, O., Bailey, C. L., Wang, J., Limsuwan, A., Sweeney, M., Rubin, L. J., & Yuan, J. X. 2001. Upregulated TRP and enhanced capacitative Ca^{2+} entry in human pulmonary artery myocytes during proliferation. *American Journal of Physiology-Heart and Circulatory Physiology.* **280**(2), pp.H746-H755.

Gonzalez-Rodriguez, P., Falcon, D., Castro, M.J., Urena, J., Lopez-Barneo, J. and Castellano, A. 2015. Hypoxic induction of T-type Ca^{2+} channels in rat cardiac myocytes: role of HIF-1 and RhoA/ROCK signalling. *Journal of Physiology-London.* **593**(21), pp.4729-4745.

Gordienko, D.V. and Bolton, T.B. 2002. Crosstalk between ryanodine receptors and IP_3 receptors as a factor shaping spontaneous Ca^{2+}-release events in rabbit portal vein myocytes. *The Journal of physiology*. 542(Pt 3), pp.743-762.

Goulopoulou, S. and Webb, R.C. 2014. Symphony of vascular contraction: how smooth muscle cells lose harmony to signal increased vascular resistance in hypertension. *Hypertension.* **63**(3), pp.E33-E39.

Greene, D.L., Kang, S. and Hoshi, N. 2017. XE991 and Linopirdine Are State-Dependent Inhibitors for Kv7/KCNQ Channels that Favor Activated Single Subunits. *The Journal of Pharmacology and Experimental Therapeutics*. **362**(1), pp.177-185.

Greenwood, I.A. and Ohya, S. 2009. New tricks for old dogs: KCNQ expression and role in smooth muscle. *British Journal of Pharmacology.* **156**(8), pp.1196-1203.

Grynkiewicz, G., Poenie, M. and Tsien, R.Y. 1985. A new generation of Ca^{2+} indicators with greatly improved fluorescence properties. *The Journal of Biological Chemistry.* **260**(6), pp.3440-3450.

Guan, Z., Baty, J.J., Zhang, S., Remedies, C.E. and Inscho, E.W. 2019. Rho kinase inhibitors reduce voltage-dependent Ca^{2+} channel signaling in aortic and renal microvascular smooth muscle cells. *American journal of physiology. Renal Physiology.* **317**(5), pp.F1132-F1141.

Guragai, N., Rampal, U., Vasudev, R., Patel, H., Joshi, M.B. and Shamoon, F. 2017. A rare case of late onset saphenous vein graft spasm. *Journal of Community Hospital Internal Medicine Perspectives.* **7**(5), pp.332-335.

Gurkoff, G.G., Shahlaie, K., Lyeth, B.G. and Berman, R.F. 2017. Chapter 11 - Voltage-Gated Calcium Channel Blockers for the Treatment of Traumatic Brain Injury. *In: Heidenreich, K.A. ed. New Therapeutics for Traumatic Brain Injury. San Diego: Academic Press*, pp.179-197.

Gutman, G.A., Chandy, K.G., Adelman, J.P., Aiyar, J., Bayliss, D.A., Clapham, D.E., Covarriubias, M., Desir, G.V., Furuichi, K., Ganetzky, B., Garcia, M.L., Grissmer, S., Jan, L.Y., Karschin, A., Kim, D., Kuperschmidt, S., Kurachi, Y., Lazdunski, M., Lesage, F., Lester, H.A., McKinnon, D., Nichols, C.G., O'Kelly, I., Robbins, J., Robertson, G.A., Rudy, B., Sanguinetti, M., Seino, S., Stuehmer, W., Tamkun, M.M., Vandenberg, C.A., Wei, A., Wulff, H. and Wymore, R.S. 2003. International Union of Pharmacology. XLI. Compendium of voltage-gated ion channels: Potassium channels. *Pharmacological Reviews.* **55**(4), pp.583-586.

Haick, J.M. and Byron, K.L. 2016. Novel treatment strategies for smooth muscle disorders: Targeting Kv7 potassium channels. *Pharmacology & Therapeutics.* **165**, pp.14-25.

Hammond, E.M., Asselin, M.C., Forster, D., O'Connor, J.P.B., Senra, J.M. and Williams, K.J. 2014. The meaning, measurement and modification of hypoxia in the laboratory and the clinic. *Clinical Oncology.* **26**(5), pp.277-288.

Hara, S., Hamada, J., Kobayashi, C., Kondo, Y. and Imura, N. 2001. Expression and characterization of hypoxia-inducible factor (HIF)-3α in human kidney: Suppression of HIF-mediated gene expression by HIF-3α. *Biochemical and Biophysical Research Communications.* **287**(4), pp.808-813.

Harraz, O.F., Abd El-Rahman, R.R., Bigdely-Shamloo, K., Wilson, S.M., Brett, S.E., Romero, M., Gonzales, A.L., Earley, S., Vigmond, E.J., Nygren, A., Menon, B.K., Mufti, R.E., Watson, T., Starreveld, Y., Furstenhaupt, T., Muellerleile, P.R., Kurjiaka, D.T., Kyle, B.D., Braun, A.P. and Welsh, D.G. 2014. Cav3.2 channels and the induction of negative feedback in cerebral arteries. *Circulation Research.* **115**(7), pp.650-661.

Harraz, O.F. and Welsh, D.G. 2013. Protein kinase A regulation of T-type Ca^{2+} channels in rat cerebral arterial smooth muscle. *Journal of Cell Science.* **126**(13), pp.2944-2954.

Harris, S.K., Roos, M.G. and Landry, G.J. 2016. Statin use in patients with peripheral arterial disease. *Journal of Vascular Surgery.* **64**(6), pp.1881-1888.

Henderson, K.K. and Byron, K.L. 2007. Vasopressin-induced vasoconstriction: two concentration-dependent signaling pathways. *Journal of Applied Physiology.* **102**(4), pp.1402-1409.

Hering, S., Beyl, S., Stary, A., Kudrnac, M., Hohaus, A., Guy, H.R. and Timin, E. 2008. Pore stability and gating in voltage-activated calcium channels. *Channels (Austin, Tex.)*. **2**(2), pp.61-69.

Hernandez, C.C., Zaika, O., Tolstykh, G.P. and Shapiro, M.S. 2008. Regulation of neural KCNQ channels: Signalling pathways, structural motifs and functional implications. *Journal of Physiology-London.* **586**(7), pp.1811-1821.

Hilgers, R.H. and Webb, R.C. 2005. Molecular aspects of arterial smooth muscle contraction: Focus on Rho. *Experimental Biology and Medicine.* **230**(11), pp.829-835.

Hirota, K. 2020. Basic biology of hypoxic responses mediated by the transcription factor HIFs and its implication for medicine. *Biomedicines.* **8**(2), pp.32.

Hoeper, M.M., Ghofrani, H.A., Grunig, E., Klose, H., Olschewski, H. and Rosenkranz, S. 2017. Pulmonary Hypertension. *Deutsches Arzteblatt International.* **114**(5), pp.73-83.

Hofnagel, O., Luechtenborg, B., Eschert, H., Weissen-Plenz, G., Severs, N.J. and Robenek, H. 2006. Pravastatin inhibits expression of lectin-like oxidized low-density lipoprotein receptor-1 (LOX-1) in watanabe heritable hyperlipidemic rabbits - A new pleiotropic effect of statins. *Arteriosclerosis Thrombosis and Vascular Biology.* **26**(3), pp.604-610.

Hofnagel, O., Luechtenborg, B., Stolle, K., Lorkowski, S., Eschert, H., Plenz, G. and Robenek, H. 2004. Proinflammatory cytokines regulate LOX-1 expression in vascular smooth muscle cells. *Arteriosclerosis Thrombosis and Vascular Biology.* **24**(10), pp.1789-1795.

Hong, Z.G., Weir, E.K., Nelson, D.P. and Olschewski, A. 2004. Subacute hypoxia decreases voltage-activated potassium channel expression and function in pulmonary artery myocytes. *American Journal of Respiratory Cell and Molecular Biology.* **31**(3), pp.337-343.

Horowitz, L.F., Hirdes, W., Suh, B.C., Hilgemann, D.W., Mackie, K. and Hille, B. 2005. Phospholipase C in living cells: activation, inhibition, Ca^{2+} requirement, and regulation of M current. *The Journal of General Physiology.* **126**(3), p243.

Hoshi, N., Zhang, J.S., Omaki, M., Takeuchi, T., Yokoyama, S., Wanaverbecq, N., Langeberg, L.K., Yoneda, Y., Scott, J.D., Brown, D.A. and Higashida, H. 2003. AKAP150 signaling complex promotes suppression of the M-current by muscarinic agonists. *Nature Neuroscience.* **6**(6), pp.564-571.

Hoth, M. and Penner, R. 1992. Depletion of intracellular calcium stores activates a calcium current in mast cells. *Nature.* **355**(6358), pp.353-356.

Howard, R.J., Clark, K.A., Holton, J.M. and Minor, D.L. 2007. Structural insight into KCNQ (Kv7) channel assembly and channelopathy. *Neuron.* **53**(5), pp.663-675.

Howitt, L., Kuo, I.Y., Ellis, A., Chaston, D.J., Shin, H.S., Hansen, P.B. and Hill, C.E. 2013. Chronic deficit in nitric oxide elicits oxidative stress and augments T-type calcium-channel contribution to vascular tone of rodent arteries and arterioles. *Cardiovascular Research.* **98**(3), pp.449-457.

Hu, C.J., Wang, L.Y., Chodosh, L.A., Keith, B. and Simon, M.C. 2003. Differential roles of hypoxia-inducible factor 1α (HIF-1α) and HIF-2α in hypoxic gene regulation. *Molecular and Cellular Biology.* **23**(24), pp.9361-9374.

Hu, J., Discher, D.J., Bishopric, N.H. and Webster, K.A. 1998. Hypoxia regulates expression of the endothelin-1 gene through a proximal hypoxia-inducible factor-1 binding site on the antisense strand. *Biochemical and Biophysical Research Communications.* **245**(3), pp.894-899.

Huang, D., Huang, S., Gao, H., Liu, Y., Qi, J., Chen, P., Wang, C., Scragg, J.L., Vakurov, A., Peers, C., Du, X., Zhang, H. and Gamper, N. 2016. Redox-dependent modulation of T-type Ca^{2+} channels in sensory neurons contributes to acute anti-nociceptive effect of substance P. *Antioxidants & Redox Signaling.* **25**(5), pp.233-251.

Huang, D., Shi, S., Liang, C., Zhang, X., Du, X., An, H., Peers, C., Zhang, H. and Gamper, N. 2020. Delineating an extracellular redox-sensitive module in T-type Ca^{2+} channels. *The Journal of Biological Chemistry.* **295**(18), pp.6177-6186.

Huang, L., Keyser, B.M., Tagmose, T.M., Hansen, J.B., Taylor, J.T., Zhuang, H., Zhang, M., Ragsdale, D.S. and Li, M. 2004. NNC 55-0396 [(1S,2S)-2-(2-(N-[(3-benzimidazol-2-yl)propyl]-N-methylamino)ethyl)-6-fluoro-1,2,3,4-tetrahydro-1-isopropyl-2-naphtyl cyclopropanecarboxylate dihydrochloride]: a new selective inhibitor of T-type calcium channels. *The Journal of Pharmacology and Experimental Therapeutics.* **309**(1), pp.193-199.

Hughes, A.D. 1995. Calcium channels in vascular smooth muscle cells. *Journal of Vascular Research.* **32**(6), pp.353-370.

Huguenard, J.R. and Prince, D.A. 1994. Intrathalamic rhythmicity studied in vitro: nominal T-current modulation causes robust antioscillatory effects. *The Journal of neuroscience : the official journal of the Society for Neuroscience.* **14**(9), p5485.

Hulme, J.T., Coppock, E.A., Felipe, A., Martens, J.R. and Tamkun, M.M. 1999. Oxygen sensitivity of cloned voltage-gated K^+ channels expressed in the pulmonary vasculature. *Circulation Research.* **85**(6), pp.489-497.

Iannotti, F.A., Panza, E., Barrese, V., Viggiano, D., Soldovieri, M.V. and Taglialatela, M. 2010. Expression, Localization, and Pharmacological Role of Kv7 Potassium Channels in Skeletal Muscle Proliferation, Differentiation, and Survival after Myotoxic Insults. *Journal of Pharmacology and Experimental Therapeutics*. **332**(3), pp.811-820.

Iftinca, M., Hamid, J., Chen, L., Varela, D., Tadayonnejad, R., Altier, C., Turner, R.W. and Zamponi, G.W. 2007. Regulation of T-type calcium channels by Rho-associated kinase. *Nature Neuroscience.* **10**(7), pp.854-860.

Injarabian, L., Scherlinger, M., Devin, A., Ransac, S., Lykkesfeldt, J. and Marteyn, B.S. 2020. Ascorbate maintains a low plasma oxygen level. *Scientific Reports*. **10**(1), p10659.

Ivan, M., Kondo, K., Yang, H.F., Kim, W., Valiando, J., Ohh, M., Salic, A., Asara, J.M., Lane, W.S. and Kaelin, W.G. 2001. HIFα targeted for VHL-mediated destruction by proline hydroxylation: Implications for O_2 sensing. *Science.* **292**(5516), pp.464-468.

Iwai, M., Michikawa, T., Bosanac, I., Ikura, M. and Mikoshiba, K. 2007. Molecular basis of the isoform-specific ligand-binding affinity of inositol 1,4,5-trisphosphate receptors. *The Journal of Biological Chemistry.* **282**(17), pp.12755-12764.

Jaakkola, P., Mole, D.R., Tian, Y.M., Wilson, M.I., Gielbert, J., Gaskell, S.J., von Kriegsheim, A., Hebestreit, H.F., Mukherji, M., Schofield, C.J., Maxwell, P.H., Pugh, C.W. and Ratcliffe, P.J. 2001. Targeting of HIF-α to the von Hippel-Lindau ubiquitylation complex by O_2-regulated prolyl hydroxylation. *Science.* **292**(5516), pp.468-472.

Jackson, W.F. 2018. Kv channels and the regulation of vascular smooth muscle tone. *Microcirculation.* **25**(1), pe12421.

Jacob, M., Chappell, D. and Becker, B.F. 2016. Regulation of blood flow and volume exchange across the microcirculation. *Critical Care.* **20**(1), p319.

Jagger, J.H., Porter, V.A., Lederer, W.J. and Nelson, M.T. 2000. Calcium sparks in smooth muscle. *American Journal of Physiology-Cell Physiology.* **278**(4), pp. C235-C256.

Jain, S., Maltepe, E., Lu, M.M., Simon, C. and Bradfield, C.A. 1998. Expression of ARNT, ARNT2, HIF1α, HIF2α and Ah receptor mRNAs in the developing mouse. *Mechanisms of Development.* **73**(1), pp.117-123.

Jensen, H.S., Callø, K., Jespersen, T., Jensen, B.S. and Olesen, S.P. 2005. The KCNQ5 potassium channel from mouse: a broadly expressed M-current like potassium channel modulated by zinc, pH, and volume changes. *Brain research. Molecular brain research.* **139**(1), pp.52-62.

Jentsch, T.J. 2000. Neuronal KCNQ potassium channels: Physiology and role in disease. *Nature Reviews Neuroscience.* **1**(1), pp.21-30.

Jepps, T.A., Chadha, P.S., Davis, A.J., Harhun, M.I., Cockerill, G.W., Olesen, S.P., Hansen, R.S. and Greenwood, I.A. 2011. Downregulation of Kv7.4 channel activity in primary and secondary hypertension. *Circulation.* **124**(5), pp.602-611.

Jepps, T.A., Olesen, S.P. and Greenwood, I.A. 2013. One man's side effect is another man's therapeutic opportunity: targeting Kv7 channels in smooth muscle disorders. *British journal of pharmacology*. **168**(1), pp.19-27.

Jespersen, T., Membrez, M., Nicolas, C.S., Pitard, B., Staub, O., Olesen, S.P., Baró, I. and Abriel, H. 2007. The KCNQ1 potassium channel is down-regulated by ubiquitylating enzymes of the Nedd4/Nedd4-like family. *Cardiovascular Research.* **74**(1), pp.64-74.

Jin, X., Shah, S., Liu, Y., Zhang, H., Lees, M., Fu, Z., Lippiat, J.D., Beech, D.J., Sivaprasadarao, A., Baldwin, S.A., Zhang, H. and Gamper, N. 2013. Activation of the Cl^- channel ANO1 by localized calcium signals in nociceptive sensory neurons requires coupling with the IP_3 receptor. *Science signaling.* **6**(290), ra73.

Jin, Z.G. and Berk, B.C. 2004. SOXF: Redox mediators of vascular smooth muscle cell growth. *Heart.* **90**(5), pp.488-490.

Joshi, S., Balan, P. and Gurney, A.M. 2006. Pulmonary vasoconstrictor action of KCNQ potassium channel blockers. *Respiratory Research.* **7**(1), p31.

Joshi, S., Sedivy, V., Hodyc, D., Herget, J. and Gurney, A.M. 2009. KCNQ modulators reveal a key role for KCNQ potassium channels in regulating the tone of rat pulmonary artery smooth muscle. *Journal of Pharmacology and Experimental Therapeutics.* **329**(1), pp.368-376.

Kawaguchi, A., Sato, M., Kimura, M., Yamazaki, T., Yamamoto, H., Tazaki, M., Ichinohe, T. and Shibukawa, Y. 2015. Functional expression of bradykinin B_1 and B_2 receptors in neonatal rat trigeminal ganglion neurons. *Frontiers in Cellular Neuroscience*. **9**(229).

Ke, Q.D. and Costa, M. 2006. Hypoxia-inducible factor-1 (HIF-1). *Molecular Pharmacology.* **70**(5), pp.1469-1480.

Keith, B., Johnson, R.S. and Simon, M.C. 2011. HIF1α and HIF2α: Sibling rivalry in hypoxic tumour growth and progression. *Nature reviews. Cancer.* **12**(1), pp.9-22.

Kennedy, E., Hakimjavadi, R., Greene, C., Mooney, C.J., Fitzpatrick, E., Collins, L.E., Loscher, C.E., Guha, S., Morrow, D., Redmond, E.M. and Cahill, P.A. 2014. Embryonic rat vascular smooth muscle cells revisited - a model for neonatal, neointimal SMC or differentiated vascular stem cells? *Vascular cell*. **6**(1), pp.6.

Khalil, R., Lodge, N., Saida, K. and Vanbreemen, C. 1987. Mechanism of calcium activation in vascular smooth muscle. *Journal of Hypertension.* **5**, pp.S5-S15.

Khalil, R.A. and Vanbreemen, C. 1988. Sustained contraction of vascular smooth muscle: calcium influx or C-kinase activation? *Journal of Pharmacology and Experimental Therapeutics.* **244**(2), pp.537-542.

Kharade, S.V., Sonkusare, S.K., Srivastava, A.K., Thakali, K.M., Fletcher, T.W., Rhee, S.W. and Rusch, N.J. 2013. The β3 subunit contributes to vascular calcium

channel upregulation and hypertension in angiotensin II-infused C57BL/6 Mice. *Hypertension.* **61**(1), pp.137-142.

Kim, D., Song, I., Keum, S., Lee, T., Jeong, M.J., Kim, S.S., McEnery, M.W. and Shin, H.S. 2001. Lack of the burst firing of thalamocortical relay neurons and resistance to absence seizures in mice lacking α_{1G} T-type Ca^{2+} channels. *Neuron.* **31**(1), pp35-45.

Kim, K.H., Kim, D., Park, J.Y., Jung, H.J., Cho, Y.H., Kim, H.K., Han, J., Choi, K.Y. and Kwon, H.J. 2015. NNC 55-0396, a T-type Ca^{2+} channel inhibitor, inhibits angiogenesis via suppression of hypoxia-inducible factor-1α signal transduction. *Journal of Molecular Medicine.* **93**(5), pp.499-509.

Kim, W.Y., Perera, S., Zhou, B., Carretero, J., Yeh, J.J., Heathcote, S.A., Jackson, A.L., Nikolinakos, P., Ospina, B., Naumov, G., Brandstetter, K.A., Weigman, V.J., Zaghlul, S., Hayes, D.N., Padera, R.F., Heymach, J.V., Kung, A.L., Sharpless, N.E., Kaelin, W.G., Jr. and Wong, K.K. 2009. HIF2α cooperates with RAS to promote lung tumorigenesis in mice. *The Journal of Clinical Investigation.* **119**(8), pp.2160-2170.

Kimes, B.W. and Brandt, B.L. 1976. Characterization of two putative smooth muscle cell lines from rat thoracic aorta. *Experimental Cell Research.* **98**(2), pp.349-366.

Kitamura, K. and Yamazaki, J. 2001. Chloride channels and their functional roles in smooth muscle tone in the vasculature. *Japanese Journal of Pharmacology.* **85**(4), pp.351-357.

Klöckner, U., Lee, J.H., Cribbs, L.L., Daud, A., Hescheler, J., Pereverzev, A., Perez-Reyes, E. and Schneider, T. 1999. Comparison of the Ca^{2+} currents induced by expression of three cloned α1 subunits, α1G, α1H and α1I, of low-voltage-activated T-type Ca^{2+} channels. *The European Journal of Neuroscience.* **11**(12), pp.4171-4178.

Klugbauer, N., Lacinova, L., Marais, E., Hobom, M. and Hofmann, F. 1999. Molecular diversity of the calcium channel α2δ subunit. *Journal of Neuroscience.* **19**(2), pp.684-691.

Köhler, R., Kaistha, B.P. and Wulff, H. 2010. Vascular K_{Ca}-channels as therapeutic targets in hypertension and restenosis disease. *Expert Opinion on Therapeutic Targets.* **14**(2), pp.143-155.

Komai, H. and McDowell, T.S. 2001. Local anesthetic inhibition of voltage-activated potassium currents in rat dorsal root ganglion neurons. *Anesthesiology.* **94**(6), pp.1089-1095.

Kraus, R.L., Li, Y., Gregan, Y., Gotter, A.L., Uebele, V.N., Fox, S.V., Doran, S.M., Barrow, J.C., Yang, Z.-Q., Reger, T.S., Koblan, K.S. and Renger, J.J. 2010. In vitro characterization of T-type calcium channel antagonist TTA-A2 and in vivo effects on arousal in mice. *Journal of Pharmacology and Experimental Therapeutics.* **335**(2), pp.409-417.

Kubisch, C., Schroeder, B.C., Friedrich, T., Lütjohann, B., El-Amraoui, A., Marlin, S., Petit, C. and Jentsch, T.J. 1999. KCNQ4, a Novel Potassium Channel Expressed in Sensory Outer Hair Cells, Is Mutated in Dominant Deafness. *Cell*. **96**(3), pp.437-446.

Kuhr, F.K., Smith, K.A., Song, M.Y., Levitan, I. and Yuan, J.X. 2012. New mechanisms of pulmonary arterial hypertension: Role of Ca^{2+} signaling. *American Journal of Physiology-Heart and Circulatory Physiology.* **302**(8), pp.H1546-H1562.

Kuo, I.Y.T., Wölfle, S.E. and Hill, C.E. 2011. T-type calcium channels and vascular function: the new kid on the block? *The Journal of physiology*. **589**(Pt 4), pp.783-795.

Labrousse-Arias, D., Castillo-González, R., Rogers, N.M., Torres-Capelli, M., Barreira, B., Aragonés, J., Cogolludo, Á., Isenberg, J.S. and Calzada, M.J. 2016. HIF-2α-mediated induction of pulmonary thrombospondin-1 contributes to hypoxia-driven vascular remodelling and vasoconstriction. *Cardiovascular Research.* **109**(1), pp.115-130.

Lai, N., Lu, W. and Wang, J. 2015. Ca^{2+} and ion channels in hypoxia-mediated pulmonary hypertension. *International Journal of Clinical and Experimental Pathology.* **8**(2), pp.1081-1092.

Lanner, J.T., Georgiou, D.K., Joshi, A.D. and Hamilton, S.L. 2010. Ryanodine receptors: Structure, expression, molecular details, and function in calcium release. *Cold Spring Harbor Perspectives in Biology.* **2**(11), pp.a003996.

Large, W.A. 2002. Receptor-operated Ca^{2+}-permeable nonselective cation channels in vascular smooth muscle: A Physiologic perspective. *Journal of Cardiovascular Electrophysiology.* **13**(5), pp.493-501.

Lee, J., Kim, D. and Shin, H.S. 2004. Lack of delta waves and sleep disturbances during non-rapid eye movement sleep in mice lacking alpha1G-subunit of T-type calcium channels. *Proceedings of the National Academy of Sciences of the United States of America.* **101**(52), pp.18195-18199.

Lee, J.H., Chae, M.R., Kang, S.J., Sung, H.H., Han, D.H., So, I., Park, J.K. and Lee, S.W. 2020. Characterization and functional roles of KCNQ-encoded voltage-gated potassium (Kv7) channels in human corpus cavernosum smooth muscle. *Pflugers Archiv : European Journal of Physiology.* **472**(1), pp.89-102.

Lee, J.W., Ko, J., Ju, C. and Eltzschig, H.K. 2019. Hypoxia signaling in human diseases and therapeutic targets. *Experimental & Molecular Medicine.* **51**(6), pp.1-13.

Lee, P.J., Jiang, B.H., Chin, B.Y., Iyer, N.V., Alam, J., Semenza, G.L. and Choi, A.M. 1997. Hypoxia-inducible factor-1 mediates transcriptional activation of the heme oxygenase-1 gene in response to hypoxia. *The Journal of Biological Chemistry.* **272**(9), pp.5375-5381.

Li, G., Che, H., Wu, W.Y., Jie, L.J., Xiao, G.S., Wang, Y. and Li, G.R. 2018. Bradykinin-mediated Ca^{2+} signalling regulates cell growth and mobility in human cardiac c-Kit^{+} progenitor cells. *Journal of Cellular and Molecular Medicine.* **22**(10), pp.4688-4699.

Li, M., Hansen, J.B., Huang, L., Keyser, B.M. and Taylor, J.T. 2005. Towards selective antagonists of T-type calcium channels: Design, characterization and potential applications of NNC 55-0396. *Cardiovascular Drug Reviews.* **23**(2), pp.173-196.

Li, Y., Gamper, N., Hilgemann, D.W. and Shapiro, M.S. 2005. Regulation of Kv7 (KCNQ) K^{+} channel open probability by phosphatidylinositol 4,5-bisphosphate. *Journal of Neuroscience.* **25**(43), pp.9825-9835.

Lim, S. and Park, S. 2014. Role of vascular smooth muscle cell in the inflammation of atherosclerosis. *BMB Reports.* **47**(1), pp.1-7.

Linley, J.E., Pettinger, L., Huang, D.Y. and Gamper, N. 2012. M channel enhancers and physiological M channel block. *Journal of Physiology-London.* **590**(4), pp.793-807.

Linley, J.E., Rose, K., Patil, M., Robertson, B., Akopian, A.N. and Gamper, N. 2008. Inhibition of M current in sensory neurons by exogenous proteases: a signaling pathway mediating inflammatory nociception. *The Journal of neuroscience : the official journal of the Society for Neuroscience.* **28**(44), pp.11240-11249.

Lipskaia, L., del Monte, F., Capiod, T., Yacoubi, S., Hadri, L., Hours, M., Hajjar, R.J. and Lompré, A.-M. 2005. Sarco/endoplasmic reticulum Ca^{2+}-ATPase gene transfer reduces vascular smooth muscle cell proliferation and neointima formation in the rat. *Circulation Research.* **97**(5), pp.488-495.

Liu, B., Freyer, A.M. and Hall, I.P. 2007. Bradykinin activates calcium-dependent potassium channels in cultured human airway smooth muscle cells. *American journal of physiology. Lung Cellular and Molecular Physiology.* **292**(4), pp.L898-907.

Liu, B.Y., Linley, J.E., Du, X.N., Zhang, X., Ooi, L., Zhang, H.L. and Gamper, N. 2010. The acute nociceptive signals induced by bradykinin in rat sensory neurons are mediated by inhibition of M-type K^{+} channels and activation of Ca^{2+}-activated Cl^{-} channels. *The Journal of Clinical Investigation.* **120**(4), pp.1240-1252.

Liu, J., Ren, Y.G., Kang, L. and Zhang, L.H. 2014. Oxidized low-density lipoprotein increases the proliferation and migration of human coronary artery smooth muscle cells through the upregulation of osteopontin. *International Journal of Molecular Medicine.* **33**(5), pp.1341-1347.

Liu, Z.W. and Khalil, R.A. 2018. Evolving mechanisms of vascular smooth muscle contraction highlight key targets in vascular disease. *Biochemical Pharmacology.* **153**, pp.91-122.

Livak, K.J. and Schmittgen, T.D. 2001. Analysis of relative gene expression data using real-time quantitative PCR and the $2^{-\Delta\Delta CT}$ Method. *Methods.* **25**(4), pp.402-408.

Loirand, G., Guérin, P. and Pacaud, P. 2006. Rho kinases in cardiovascular physiology and pathophysiology. *Circulation Research.* **98**(3), pp.322-334.

Lopez-Barneo, J., del Toro, R., Levitsky, K.L., Chiara, M.D. and Ortega-Saenz, P. 2004. Regulation of oxygen sensing by ion channels. *Journal of Applied Physiology.* **96**(3), pp.1187-1195.

Lu, W., Kang, J., Hu, K., Tang, S., Zhou, X., Xu, L., Li, Y. and Yu, S. 2017. The role of the Nox4-derived ROS-mediated RhoA/Rho kinase pathway in rat hypertension induced by chronic intermittent hypoxia. *Sleep Breath.* **21**(3), pp.667-677.

Lu, Y., Hanna, S.T., Tang, G. and Wang, R. 2002. Contributions of Kv1.2, Kv1.5 and Kv2.1 subunits to the native delayed rectifier K^+ current in rat mesenteric artery smooth muscle cells. *Life Sciences.* **71**(12), pp.1465-1473.

Lusis, A.J. 2000. Atherosclerosis. *Nature.* **407**(6801), pp.233-241.

Mackie, A.R., Brueggemann, L.I., Henderson, K.K., Shiels, A.J., Cribbs, L.L., Scrogin, K.E. and Byron, K.L. 2008. Vascular KCNQ potassium channels as novel targets for the control of mesenteric artery constriction by vasopressin, based on studies in single cells, pressurized arteries, and in vivo measurements of mesenteric vascular resistance. *Journal of Pharmacology and Experimental Therapeutics.* **325**(2), pp.475-483.

Mackie, A.R. and Byron, K.L. 2008. Cardiovascular KCNQ (Kv7) Potassium Channels: Physiological Regulators and New Targets for Therapeutic Intervention. *Molecular Pharmacology.* **74**(5), pp.1171-1179.

Mahon, P.C., Hirota, K. and Semenza, G.L. 2001. FIH-1: a novel protein that interacts with HIF-1α and VHL to mediate repression of HIF-1 transcriptional activity. *Genes & Development.* **15**(20), pp.2675-2686.

Main, M.J., Cryan, J.E., Dupere, J.R.B., Cox, B., Clare, J.J. and Burbidge, S.A. 2000. Modulation of KCNQ2/3 potassium channels by the novel anticonvulsant retigabine. *Molecular Pharmacology.* **58**(2), pp.253-262.

Makino, Y., Cao, R.H., Svensson, K., Bertilsson, G.R., Asman, M., Tanaka, H., Cao, Y.H., Berkenstam, A. and Poellinger, L. 2001. Inhibitory PAS domain protein is a negative regulator of hypoxia-inducible gene expression. *Nature.* **414**(6863), pp.550-554.

Maljevic, S. and Lerche, H. 2014. Potassium channel genes and benign familial neonatal epilepsy. *Progress in brain research*. **213**, pp.17-53.

Mandl, M. and Depping, R. 2014. Hypoxia-inducible aryl hydrocarbon receptor nuclear translocator (ARNT) (HIF-1β): is it a rare Exception? *Molecular Medicine.* **20**, pp.215-220.

Mangoni, M.E., Traboulsie, A., Leoni, A.L., Couette, B., Marger, L., Le Quang, K., Kupfer, E., Cohen-Solal, A., Vilar, J., Shin, H.S., Escande, D., Charpentier, F., Nargeot, J. and Lory, P. 2006. Bradycardia and slowing of the atrioventricular conduction in mice lacking Cav3.1/α_{1G} T-type calcium channels. *Circulation Research.* **98**(11), pp.1422-1430.

Mani, B.K., Brueggemann, L.I., Cribbs, L.L. and Byron, K.L. 2009. Opposite regulation of KCNQ5 and TRPC6 channels contributes to vasopressin-stimulated calcium spiking responses in A7r5 vascular smooth muscle cells. *Cell Calcium.* **45**(4), pp.400-411.

Mani, B.K., Brueggemann, L.I., Cribbs, L.L. and Byron, K.L. 2011. Activation of vascular KCNQ (Kv7) potassium channels reverses spasmogen-induced constrictor responses in rat basilar artery. *British Journal of Pharmacology.* **164**(2), pp.237-249.

Mani, B.K., O'Dowd, J., Kumar, L., Brueggemann, L.I., Ross, M. and Byron, K.L. 2013. Vascular KCNQ (Kv7) potassium channels as common signaling intermediates and therapeutic targets in cerebral vasospasm. *Journal of Cardiovascular Pharmacology.* **61**(1), pp.51-62.

Mani, B.K., Robakowski, C., Brueggemann, L.I., Cribbs, L.L., Tripathi, A., Majetschak, M. and Byron, K.L. 2016. Kv7.5 potassium channel subunits are the primary targets for PKA-dependent enhancement of vascular smooth muscle Kv7 currents. *Molecular Pharmacology.* **89**(3), pp.323-334.

Marrion, N.V. 1997. Control of M-current. *Annual Review of Physiology.* **59**, pp.483-504.

Martinsen, A., Baeyens, N., Yerna, X. and Morel, N. 2012. Rho kinase regulation of vasopressin-induced calcium entry in vascular smooth muscle cell: Comparison between rat isolated aorta and cultured aortic cells. *Cell Calcium.* **52**(6), pp.413-421.

Martinsen, A., Dessy, C. and Morel, N. 2014. Regulation of calcium channels in smooth muscle: new insights into the role of myosin light chain kinase. *Channels (Austin, Tex.).* **8**(5), pp.402-413.

Maruyama, T., Kanaji, T., Nakade, S., Kanno, T. and Mikoshiba, K. 1997. 2APB, 2-aminoethoxydiphenyl borate, a membrane-penetrable modulator of Ins(1,4,5)P_3-induced Ca^{2+} release. *Journal of Biochemistry.* **122**(3), pp.498-505.

Mason, R.P. 2002. Mechanisms of plaque stabilization for the dihydropyridine calcium channel blocker amlodipine: review of the evidence. *Atherosclerosis.* **165**(2), pp.191-199.

Maxwell, P.H., Wiesener, M.S., Chang, G.W., Clifford, S.C., Vaux, E.C., Cockman, M.E., Wykoff, C.C., Pugh, C.W., Maher, E.R. and Ratcliffe, P.J. 1999. The tumour suppressor protein VHL targets hypoxia-inducible factors for oxygen-dependent proteolysis. *Nature.* **399**(6733), pp.271-275.

Mayet, J. and Hughes, A. 2003. Cardiac and vascular pathophysiology in hypertension. *Heart (British Cardiac Society).* **89**(9), pp.1104-1109.

Mignen, O., Brink, C., Enfissi, A., Nadkarni, A., Shuttleworth, T.J., Giovannucci, D.R. and Capiod, T. 2005. Carboxyamidotriazole-induced inhibition of mitochondrial calcium import blocks capacitative calcium entry and cell proliferation in HEK-293 cells. *Journal of Cell Science*. **118**(Pt 23), pp.5615-5623.

Miller, E.W., Lin, J.Y., Frady, E.P., Steinbach, P.A., Kristan, W.B. and Tsien, R.Y. 2012. Optically monitoring voltage in neurons by photo-induced electron transfer through molecular wires. *Proceedings of the National Academy of Sciences of the United States of America*. **109**(6), pp.2114-2119.

Moosmang, S., Schulla, V., Welling, A., Feil, R., Feil, S., Wegener, J.W., Hofmann, F. and Klugbauer, N. 2003. Dominant role of smooth muscle L-type calcium channel Cav1.2 for blood pressure regulation. *The EMBO Journal.* **22**(22), pp.6027-6034.

Morales-Cano, D., Moreno, L., Barreira, B., Briones, A.M., Pandolfi, R., Moral-Sanz, J., Callejo, M., Mondejar-Parreño, G., Cortijo, J., Salaices, M., Duarte, J., Perez-Vizcaino, F. and Cogolludo, A. 2016. Activation of PPARβ/δ prevents hyperglycaemia-induced impairment of Kv7 channels and cAMP-mediated relaxation in rat coronary arteries. *Clin Sci (Lond)*. **130**(20), pp.1823-1836.

Morales-Cano, D., Moreno, L., Barreira, B., Pandolfi, R., Chamorro, V., Jimenez, R., Villamor, E., Duarte, J., Perez-Vizcaino, F. and Cogolludo, A. 2015. Kv7 channels critically determine coronary artery reactivity: Left-right differences and down-regulation by hyperglycaemia. *Cardiovascular Research.* **106**(1), pp.98-108.

Morecroft, I., Murray, A., Nilsen, M., Gurney, A.M. and MacLean, M.R. 2009. Treatment with the Kv7 potassium channel activator flupirtine is beneficial in two independent mouse models of pulmonary hypertension. *British Journal of Pharmacology.* **157**(7), pp.1241-1249.

Morin, T.J. and Kobertz, W.R. 2008. Counting membrane-embedded KCNE β-subunits in functioning K^+ channel complexes. *Proceedings of the National Academy of Sciences of the United States of America.* **105**(5), pp.1478-1482.

Moudgil, R., Michelakis, E.D. and Archer, S.L. 2006. The role of K^+ channels in determining pulmonary vascular tone, oxygen sensing, cell proliferation, and apoptosis: Implications in hypoxic pulmonary vasoconstriction and pulmonary arterial hypertension. *Microcirculation.* **13**(8), pp.615-632.

Mozaffarian, D., Benjamin, E.J., Go, A.S., Arnett, D.K., Blaha, M.J., Cushman, M., Das, S.R., de Ferranti, S., Despres, J.P., Fullerton, H.J., Howard, V.J., Huffman, M.D., Isasi, C.R., Jimenez, M.C., Judd, S.E., Kissela, B.M., Lichtman, J.H., Lisabeth, L.D., Liu, S.M., Mackey, R.H., Magid, D.J., McGuire, D.K., Mohler, E.R., Moy, C.S., Muntner, P., Mussolino, M.E., Nasir, K., Neumar, R.W., Nichol, G., Palaniappan, L., Pandey, D.K., Reeves, M.J., Rodriguez, C.J., Rosamond, W., Sorlie, P.D., Stein, J., Towfighi, A., Turan, T.N., Virani, S.S., Woo, D., Yeh, R.W., Turner, M.B., Amer Heart Assoc Stat, C. and Stroke Stat, S. 2016. Heart

Disease and Stroke Statistics-2016 Update A Report From the American Heart Association. *Circulation.* **133**(4), pp.E38-E360.

Murphey, L., Vaughan, D. and Brown, N. 2003. Contribution of bradykinin to the cardioprotective effects of ACE inhibitors. *European Heart Journal Supplements.* **5**(suppl A), pp.A37-A41.

Narayanan, D., Adebiyi, A. and Jaggar, J.H. 2012. Inositol trisphosphate receptors in smooth muscle cells. *American Journal of Physiology-Heart and Circulatory Physiology.* **302**(11), pp.H2190-H2210.

Navedo, M.F., Nieves-Cintrón, M., Amberg, G.C., Yuan, C., Votaw, V.S., Lederer, W.J., McKnight, G.S. and Santana, L.F. 2008. AKAP150 is required for stuttering persistent Ca^{2+} sparklets and angiotensin II-induced hypertension. *Circulation Research.* **102**(2), pp.e1-e11.

Nelson, M.T., Joksovic, P.M., Su, P., Kang, H.-W., Van Deusen, A., Baumgart, J.P., David, L.S., Snutch, T.P., Barrett, P.Q., Lee, J.-H., Zorumski, C.F., Perez-Reyes, E. and Todorovic, S.M. 2007. Molecular mechanisms of subtype-specific inhibition of neuronal T-type calcium channels by ascorbate. *The Journal of neuroscience : the official journal of the Society for Neuroscience.* **27**(46), pp.12577-12583.

Nelson, M.T., Patlak, J.B., Worley, J.F. and Standen, N.B. 1990. Calcium channels, potassium channels, and voltage dependence of arterial smooth muscle tone. *American Journal of Physiology.* **259**(1), pp.C3-C18.

Nelson, M.T. and Quayle, J.M. 1995. Physiological roles and properties of potassium channels in arterial smooth muscle. *American Journal of Physiology-Cell Physiology.* **268**(4), pp.C799-C822.

Ng, F.L., Davis, A.J., Jepps, T.A., Harhun, M.I., Yeung, S.Y., Wan, A., Reddy, M., Melville, D., Nardi, A., Khong, T.K. and Greenwood, I.A. 2011. Expression and function of the K^+ channel KCNQ genes in human arteries. *British Journal of Pharmacology.* **162**(1), pp.42-53.

Nguyen, E.K., Koval, O.M., Noble, P., Broadhurst, K., Allamargot, C., Wu, M., Strack, S., Thiel, W.H. and Grumbach, I.M. 2018. CaMKII (Ca^{2+}/Calmodulin-Dependent Kinase II) in mitochondria of smooth muscle cells controls mitochondrial mobility, migration, and neointima formation. *Arteriosclerosis Thrombosis and Vascular Biology.* **38**(6), pp.1333-1345.

Nixon, G.F., Mignery, G.A. and Somlyo, A.V. 1994. Immunogold localization of inositol 1,4,5-trisphosphate receptors and characterization of ultrastructural features of the sarcoplasmic reticulum in phasic and tonic smooth muscle. *Journal of Muscle Research and Cell Motility.* **15**(6), pp.682-700.

Nowycky, M.C., Fox, A.P. and Tsien, R.W. 1985. Three types of neuronal calcium channel with different calcium agonist sensitivity. *Nature.* **316**(6027), pp.440-443.

Nwasokwa, O.N. 1995. Coronary artery bypass graft disease. *Annals of Internal Medicine.* **123**(7), pp.528-545.

Ohya, S., Asakura, K., Muraki, K., Watanabe, M. and Imaizumi, Y. 2002. Molecular and functional characterization of ERG, KCNQ, and KCNE subtypes in rat stomach smooth muscle. *American Journal of Physiology-Gastrointestinal and Liver Physiology.* **282**(2), pp.G277-G287.

Ohya, S., Sergeant, G.P., Greenwood, I.A. and Horowitz, B. 2003. Molecular variants of KCNQ channels expressed in murine portal vein myocytes - A role in delayed rectifier current. *Circulation Research.* **92**(9), pp.1016-1023.

Okunande, G.W., Miller, M.L., Pyne, G.J., Sutliff, R.L., O'Connor, K.T., Neumann, J.C., Andringa, A., Miller, D.A., Prasad, V., Doetschman, T., Paul, R.J. and Shull, G.E. 2004. Targeted ablation of plasma membrane Ca^{2+}-ATPase (PMCA) 1 and 4 indicates a major housekeeping function for PMCA1 and a critical role in hyperactivated sperm motility and male fertility for PMCA4. *The Journal of Biological Chemistry.* **279**(32), pp.33742-33750.

Oliveras, A., Roura-Ferrer, M., Solé, L., Cruz, A.d.l., Prieto, A., Etxebarria, A., Manils, J., Morales-Cano, D., Condom, E., Soler, C., Cogolludo, A., Valenzuela, C., Villarroel, A., Comes, N. and Felipe, A. 2014. Functional assembly of Kv7.1/Kv7.5 channels with emerging properties on vascular muscle physiology. *Arteriosclerosis, Thrombosis, and Vascular Biology.* **34**(7), pp.1522-1530.

Oza, N.B., Schwartz, J.H., Goud, H.D. and Levinsky, N.G. 1990. Rat aortic smooth muscle cells in culture express kallikrein, kininogen, and bradykininase activity. *The Journal of Clinical Investigation.* **85**(2), pp.597-600.

Palmer, L.A., Semenza, G.L., Stoler, M.H. and Johns, R.A. 1998. Hypoxia induces type II NOS gene expression in pulmonary artery endothelial cells via HIF-1. *American Journal of Physiology-Lung Cellular and Molecular Physiology.* **274**(2), pp.L212-L219.

Pan, Z., Kao, T., Horvath, Z., Lemos, J., Sul, J.Y., Cranstoun, S.D., Bennett, V., Scherer, S.S. and Cooper, E.C. 2006. A common ankyrin-G-based mechanism retains KCNQ and Na_v channels at electrically active domains of the axon. *The Journal of neuroscience : the official journal of the Society for Neuroscience.* **26**(10), pp.2599-2613.

Paredes, R.M., Etzler, J.C., Watts, L.T., Zheng, W. and Lechleiter, J.D. 2008. Chemical calcium indicators. *Methods.* **46**(3), pp.143-151.

Park, J., Werley, C.A., Venkatachalam, V., Kralj, J.M., Dib-Hajj, S.D., Waxman, S.G. and Cohen, A.E. 2013. Screening fluorescent voltage indicators with spontaneously spiking HEK cells. *PLoS One.* **8**(12), pp.e85221.

Park, W. S., Han, J. and Earm, Y. E. 2008. Physiological role of inward rectifier K^+ channels in vascular smooth muscle cells. *Pflugers Archiv : European Journal of Physiology.* **457**(1), pp.137-147.

Pasterkamp, G., de Kleijn, D.P.V. and Borst, C. 2000. Arterial remodeling in atherosclerosis, restenosis and after alteration of blood flow: potential

mechanisms and clinical implications. *Cardiovascular Research.* **45**(4), pp.843-852.

Patel, A.J., Lazdunski, M. and Honore, E. 1997. Kv2.1/Kv9.3, a novel ATP-dependent delayed-rectifier K^+ channel in oxygen-sensitive pulmonary artery myocytes. *The EMBO Journal.* **16**(22), pp.6615-6625.

Peers, C. 2002. Hypoxic regulation of ion channel function and expression. *Experimental Physiology.* **87**(4), pp.413-422.

Peers, C., Bauer, C.C., Boyle, J.P., Scragg, J.L. and Dallas, M.L. 2012. Modulation of ion channels by hydrogen sulfide. *Antioxid Redox Signal*. **17**(1), pp.95-105.

Perez-Reyes, E. 2003. Molecular physiology of low-voltage-activated T-type calcium channels. *Physiological Reviews.* **83**(1), pp.117-161.

Perez-Reyes, E. 2006. Molecular characterization of T-type calcium channels. *Cell Calcium.* **40**(2), pp.89-96.

Perez-Reyes, E., Cribbs, L.L., Daud, A., Lacerda, A.E., Barclay, J., Williamson, M.P., Fox, M., Rees, M. and Lee, J.H. 1998. Molecular characterization of a neuronal low-voltage-activated T-type calcium channel. *Nature.* **391**(6670), pp.896-900.

Perez-Reyes, E. and Lee, J.H. 2014. Ins and outs of T-channel structure function. *Pflugers Archiv : European Journal of Physiology.* **466**(4), pp.627-633.

Platoshyn, O., Golovina, V.A., Bailey, C.L., Limsuwan, A., Krick, S., Juhaszova, M., Seiden, J.E., Rubin, L.J. and Yuan, J.X. 2000. Sustained membrane depolarization and pulmonary artery smooth muscle cell proliferation. *American Journal of Physiology. Cell Physiology.* **279**(5), pp.C1540-1549.

Poburko, D., Lee, C.H. and van Breemen, C. 2004. Vascular smooth muscle mitochondria at the cross roads of Ca^{2+} regulation. *Cell Calcium.* **35**(6), pp.509-521.

Poburko, D., Liao, C.H., van Breemen, C. and Demaurex, N. 2009. Mitochondrial regulation of sarcoplasmic reticulum Ca^{2+} content in vascular smooth muscle cells. *Circulation Research.* **104**(1), pp.104-112.

Porter, K.E., Naik, J., Turner, N.A., Dickinson, T., Thompson, M.M. and London, N.J. 2002. Simvastatin inhibits human saphenous vein neointima formation via inhibition of smooth muscle cell proliferation and migration. *Journal of Vascular Surgery.* **36**(1), pp.150-157.

Powis, G., Seewald, M.J., Gratas, C., Melder, D., Riebow, J. and Modest, E.J. 1992. Selective inhibition of phosphatidylinositol phospholipase C by cytotoxic ether lipid analogues. *Cancer Research*. **52**(10), pp.2835-2840.

Prabhakar, N.R. 2012. Carbon monoxide (CO) and hydrogen sulfide (H_2S) in hypoxic sensing by the carotid body. Respiratory physiology & neurobiology. **184**(2), pp.165-169.

Pugh, C.W. and Ratcliffe, P.J. 2003. Regulation of angiogenesis by hypoxia: role of the HIF system. *Nature Medicine.* **9**(6), pp.677-684.

Raidoo, D.M. and Bhoola, K.D. 1998. Pathophysiology of the kallikrein-kinin system in mammalian nervous tissue. *Pharmacology & Therapeutics.* **79**(2), pp.105-127.

Ray, J.B., Arab, S., Deng, Y., Liu, P., Penn, L., Courtman, D.W. and Ward, M.E. 2008. Oxygen regulation of arterial smooth muscle cell proliferation and survival. *American journal of physiology. Heart and circulatory physiology*. **294**(2), pp.H839-852.

Regoli, D. and Barabe, J. 1980. Pharmacology of bradykinin and related kinins. *Pharmacological Reviews.* **32**(1), pp.1-46.

Robbins, J. 2001. KCNQ potassium channels: physiology, pathophysiology, and pharmacology. *Pharmacology & Therapeutics.* **90**(1), pp.1-19.

Roos, J., DiGregorio, P.J., Yeromin, A.V., Ohlsen, K., Lioudyno, M., Zhang, S.Y., Safrina, O., Kozak, J.A., Wagner, S.L., Cahalan, M.D., Velicelebi, G. and Stauderman, K.A. 2005. STIM1, an essential and conserved component of store-operated Ca^{2+} channel function. *Journal of Cell Biology.* **169**(3), pp.435-445.

Rundfeldt, C. 1997. The new anticonvulsant retigabine (D-23129) acts as an opener of K^+ channels in neuronal cells. *European Journal of Pharmacology.* **336**(2-3), pp.243-249.

Salamanca, D.A. and Khalil, R.A. 2005. Protein kinase C isoforms as specific targets for modulation of vascular smooth muscle function in hypertension. *Biochemical Pharmacology.* **70**(11), pp.1537-1547.

Sanguinetti, M.C., Curran, M.E., Zou, A., Shen, J., Specter, P.S., Atkinson, D.L. and Keating, M.T. 1996. Coassembly of K_VLQT1 and minK (IsK) proteins to form cardiac I_{KS} potassium channel. *Nature.* **384**(6604), pp.80-83.

Scheuermann, T.H., Li, Q., Ma, H.W., Key, J., Zhang, L., Chen, R., Garcia, J.A., Naidoo, J., Longgood, J., Frantz, D.E., Tambar, U.K., Gardner, K.H. and Bruick, R.K. 2013. Allosteric inhibition of hypoxia inducible factor-2 with small molecules. *Nature chemical biology.* **9**(4), pp.271-276.

Schroeder, B.C., Hechenberger, M., Weinreich, F., Kubisch, C. and Jentsch, T.J. 2000. KCNQ5, a novel potassium channel broadly expressed in brain, mediates M-type currents. *The Journal of Biological Chemistry.* **275**(31), pp.24089-24095.

Schuh, K., Uldrijan, S., Telkamp, M., Rothlein, N. and Neyses, L. 2001. The plasmamembrane calmodulin-dependent calcium pump: a major regulator of nitric oxide synthase I. *Journal of Cell Biology.* **155**(2), pp.201-205.

Scragg, J.L., Dallas, M.L. and Peers, C. 2007. Molecular requirements for L-type Ca^{2+} channel blockade by testosterone. *Cell Calcium*. **42**(1), pp.11-15.

Sears, J.E., Hoppe, G., Ebrahem, Q. and Anand-Apte, B. 2008. Prolyl hydroxylase inhibition during hyperoxia prevents oxygen-induced retinopathy. *Proceedings of the National Academy of Sciences of the United States of America*. **10**5(50), pp.19898-19903.

Sedivy, V., Joshi, S., Ghaly, Y., Mizera, R., Zaloudikova, M., Brennan, S., Novotna, J., Herget, J. and Gurney, A.M. 2015. Role of Kv7 channels in responses of the pulmonary circulation to hypoxia. *American journal of physiology. Lung Cellular and Molecular Physiology.* **308**(1), pp.L48-57.

Sellak, H., Zhou, C., Liu, B., Chen, H., Lincoln, T.M. and Wu, S. 2014. Transcriptional regulation of α1H T-type calcium channel under hypoxia. *American Journal of Physiology. Cell Physiology.* **307**(7), pp.C648-656.

Semenza, G.L. 2000. HIF-1: mediator of physiological and pathophysiological responses to hypoxia. *Journal of Applied Physiology.* **88**(4), pp.1474-1480.

Semenza, G.L. 2001. HIF-1 and mechanisms of hypoxia sensing. *Current Opinion in Cell Biology.* **13**(2), pp.167-171.

Semenza, G.L. 2003. Targeting HIF-1 for cancer therapy. *Nature Reviews. Cancer.* **3**(10), pp.721-732.

Semenza, G.L. 2009. Regulation of oxygen homeostasis by hypoxia-inducible factor 1. *Physiology (Bethesda).* **24**, pp.97-106.

Semenza, G.L. 2010. Defining the role of hypoxia-inducible factor 1 in cancer biology and therapeutics. *Oncogene.* **29**(5), pp.625-634.

Semenza, G.L., Nejfelt, M.K., Chi, S.M. and Antonarakis, S.E. 1991. Hypoxia-inducible nuclear factors bind to an enhancer element located 3' to the human erythropoietin gene. *Proceedings of the National Academy of Sciences of the United States of America.* **88**(13), pp.5680-5684.

Semenza, G.L., Roth, P.H., Fang, H.M. and Wang, G.L. 1994. Transcriptional regulation of genes encoding glycolytic enzymes by hypoxia-inducible factor 1. *The Journal of Biological Chemistry.* **269**(38), pp.23757-23763.

Senatore, A. and Spafford, J.D. 2015. Physiology and Pathology of Voltage-Gated T-Type Calcium Channels. In: Schaffer, S.W. and Li, M. eds. *T-type Calcium Channels in Basic and Clinical Science.* Vienna: Springer Vienna, pp.3-17.

Seta, K.A., Yuan, Y., Spicer, Z., Lu, G., Bedard, J., Ferguson, T.K., Pathrose, P., Cole-Strauss, A., Kaufhold, A. and Millhorn, D.E. 2004. The role of calcium in hypoxia-induced signal transduction and gene expression. *Cell Calcium.* **36**(3-4), pp.331-340.

Shimoda, L.A. and Polak, J. 2011. Hypoxia. 4. Hypoxia and ion channel function. *American Journal of Physiology-Cell Physiology.* **300**(5), pp.C951-C967.

Simonneau, G., Robbins, I.M., Beghetti, M., Channick, R.N., Delcroix, M., Denton, C.P., Elliott, C.G., Gaine, S.P., Gladwin, M.T., Jing, Z.C., Krowka, M.J., Langleben, D., Nakanishi, N. and Souza, R. 2009. Updated clinical classification of pulmonary hypertension. *Journal of the American College of Cardiology.* **54**(1), pp.S43-S54.

Smani, T., Hernández, A., Ureña, J., Castellano, A.G., Franco-Obregón, A., Ordoñez, A. and López-Barneo, J. 2002. Reduction of Ca^{2+} channel activity by hypoxia in human and porcine coronary myocytes. *Cardiovascular Research.* **53**(1), pp.97-104.

Soboloff, J., Spassova, M., Xu, W., He, L.P., Cuesta, N. and Gill, D.L. 2005. Role of endogenous TRPC6 channels in Ca^{2+} signal generation in A7r5 smooth muscle cells. *The Journal of Biological Chemistry.* **280**(48), pp.39786-39794.

Søgaard, R., Ljungstrøm, T., Pedersen, K.A., Olesen, S.P. and Jensen, B.S. 2001. KCNQ4 channels expressed in mammalian cells: functional characteristics and pharmacology. *American Journal of Physiology. Cell Physiology.* **280**(4), pp.C859-866.

Soldovieri, M.V., Miceli, F. and Taglialatela, M. 2011. Driving with no brakes: Molecular pathophysiology of Kv7 potassium channels. *Physiology.* **26**(5), pp.365-376.

Sowter, H.M., Raval, R., Moore, J., Ratcliffe, P.J. and Harris, A.L. 2003. Predominant role of hypoxia-inducible transcription factor (Hif)-1α versus Hif-2α in regulation of the transcriptional response to hypoxia. *Cancer Research.* **63**(19), pp.6130-6134.

Stott, J.B., Jepps, T.A. and Greenwood, I.A. 2014. Kv7 potassium channels: a new therapeutic target in smooth muscle disorders. *Drug discovery today.* **19**(4), pp.413-424.

Striessnig, J., Ortner, N.J. and Pinggera, A. 2015. Pharmacology of L-type calcium channels: novel drugs for old targets? *Current Molecular Pharmacology.* **8**(2), pp.110-122.

Suh, B.C. and Hille, B. 2002. Recovery from muscarinic modulation of M current channels requires phosphatidylinositol 4,5-bisphosphate synthesis. *Neuron.* **35**(3), pp.507-520.

Sun, Y.Y. and Chen, X.P. 2011. Ox-LDL-induced LOX-1 expression in vascular smooth muscle cells: role of reactive oxygen species. *Fundamental & Clinical Pharmacology.* **25**(5), pp.572-579.

Swärd, K., Dreja, K., Lindqvist, A., Persson, E., & Hellstrand, P. 2002. Influence of mitochondrial inhibition on global and local $[Ca^{2+}]_i$ in rat tail artery. *Circulation Research.* **90**(7), pp.792-799.

Szewczyk, M.M., Davis, K.A., Samson, S.E., Simpson, F., Rangachari, P.K. and Grover, A.K. 2007. Ca^{2+}-pumps and Na^{+}-Ca^{2+}-exchangers in coronary artery endothelium versus smooth muscle. *Journal of Cellular and Molecular Medicine.* **11**(1), pp.129-138.

Szteyn, K., Gomez, R., Berg, K.A. and Jeske, N.A. 2015. Divergence in endothelin-1- and bradykinin-activated store-operated calcium entry in afferent sensory neurons. *ASN neuro.* **7**(2), p1759091415578714.

Tasker, P.N., Taylor, C.W. and Nixon, G.F. 2000. Expression and distribution of $InsP_3$ receptor subtypes in proliferating vascular smooth muscle cells. *Biochemical and Biophysical Research Communications.* **273**(3), pp.907-912.

Tatulian, L., Delmas, P., Abogadie, F.C. and Brown, D.A. 2001. Activation of expressed KCNQ potassium currents and native neuronal M-type potassium currents by the anti-convulsant drug retigabine. *Journal of Neuroscience.* **21**(15), pp.5535-5545.

Thuesen, A.D., Lyngso, K.S., Rasmussen, L., Stubbe, J., Skott, O., Poulsen, F.R., Pedersen, C.B., Rasmussen, L.M. and Hansen, P.B.L. 2017. P/Q-type and T-type voltage-gated calcium channels are involved in the contraction of mammary and brain blood vessels from hypertensive patients. *Acta Physiologica.* **219**(3), pp.640-651.

Tobelaim, W.S., Dvir, M., Lebel, G., Cui, M., Buki, T., Peretz, A., Marom, M., Haitin, Y., Logothetis, D.E., Hirsch, J.A. and Attali, B. 2017. Ca^{2+}-Calmodulin and PIP_2 interactions at the proximal C-terminus of Kv7 channels. *Channels.* **11**(6), pp.686-695.

Toescu, E.C. 2004. Hypoxia sensing and pathways of cytosolic Ca^{2+} increases. *Cell calcium.* **36**(3-4), pp.187-199.

Touyz, R.M., Alves-Lopes, R., Rios, F.J., Camargo, L.L., Anagnostopoulou, A., Arner, A. and Montezano, A.C. 2018. Vascular smooth muscle contraction in hypertension. *Cardiovascular Research.* **114**(4), pp.529-539.

Touyz, R.M. and Briones, A.M. 2011. Reactive oxygen species and vascular biology: implications in human hypertension. *Hypertension Research.* **34**(1), pp.5-14.

Traboulsie, A., Chemin, J., Chevalier, M., Quignard, J.-F., Nargeot, J. and Lory, P. 2007. Subunit-specific modulation of T-type calcium channels by zinc. *The Journal of physiology.* **578**(Pt 1), pp.159-171.

Tringham, E., Powell, K.L., Cain, S.M., Kuplast, K., Mezeyova, J., Weerapura, M., Eduljee, C., Jiang, X., Smith, P., Morrison, J.-L., Jones, N.C., Braine, E., Rind, G., Fee-Maki, M., Parker, D., Pajouhesh, H., Parmar, M., O'Brien, T.J. and Snutch, T.P. 2012. T-type calcium channel blockers that attenuate thalamic burst firing and suppress absence seizures. *Science Translational Medicine.* **4**(121), pp.121ra119.

Tsai, Y.M., Jones, F., Mullen, P., Porter, K.E., Steele, D., Peers, C. and Gamper, N. (2020). Vascular Kv7 channels control intracellular Ca^{2+} dynamics in smooth muscle. *Cell Calcium.* **92**, pp.102283.

Tsien, R.W., Lipscombe, D., Madison, D.V., Bley, K.R. and Fox, A.P. 1988. Multiple types of neuronal calcium channels and their selective modulation. *Trends in Neurosciences.* **11**(10), pp.431-438.

Turcotte, S., Desrosiers, R.R. and Béliveau, R. 2003. HIF-1α mRNA and protein upregulation involves Rho GTPase expression during hypoxia in renal cell carcinoma. *Journal of Cell Science.* **116**(Pt 11), pp.2247-2260.

Tykocki, N.R., Boerman, E.M. and Jackson, W.F. 2017. Smooth muscle ion channels and regulation of vascular tone in resistance arteries and arterioles. *Comprehensive Physiology.* **7**(2), pp.485-581.

Uchida, K., Miyauchi, H., Furuichi, T., Michikawa, T. and Mikoshiba, K. 2003. Critical regions for activation gating of the inositol 1,4,5-trisphosphate receptor. *The Journal of Biological Chemistry.* **278**(19), pp.16551-16560.

Ureña, J., Franco-Obregón, A. and López-Barneo, J. 1996. Contrasting effects of hypoxia on cytosolic Ca^{2+} spikes in conduit and resistance myocytes of the rabbit pulmonary artery. *The Journal of physiology.* **496**(Pt 1), pp.103-109.

Vaithianathan, T., Narayanan, D., Asuncion-Chin, M.T., Jeyakumar, L.H., Liu, J., Fleischer, S., Jaggar, J.H. and Dopico, A.M. 2010. Subtype identification and functional characterization of ryanodine receptors in rat cerebral artery myocytes. *American Journal of Physiology. Cell Physiology.* **299**(2), pp.C264-278.

Vallot, O., Combettes, L., Jourdon, P., Inamo, J., Marty, I., Claret, M. and Lompre, A.M. 2000. Intracellular Ca^{2+} handling in vascular smooth muscle cells is affected by proliferation. *Arteriosclerosis Thrombosis and Vascular Biology.* **20**(5), pp.1225-1235.

VanBavel, E., Sorop, O., Andreasen, D., Pfaffendorf, M. and Jensen, B.L. 2002. Role of T-type calcium channels in myogenic tone of skeletal muscle resistance arteries. *American Journal of Physiology-Heart and Circulatory Physiology.* **283**(6), pp.H2239-H2243.

Vangheluwe, P., Raeymaekers, L., Dode, L. and Wuytack, F. 2005. Modulating sarco(endo)plasmic reticulum Ca^{2+} ATPase2 (SERCA2) activity: cell biological implications. *Cell Calcium.* **38**(3-4), pp.291-302.

Visa, A., Shaikh, S., Alza, L., Herreros, J. and Canti, C. 2019. The hard-to-close window of T-type calcium channels. *Trends in Molecular Medicine.* **25**(7), pp.571-584.

Wan, J., Yamamura, A., Zimnicka, A.M., Voiriot, G., Smith, K.A., Tang, H., Ayon, R.J., Choudhury, M.S., Ko, E.A., Wang, J., Wang, C., Makino, A. and Yuan, J.X. 2013. Chronic hypoxia selectively enhances L- and T-type voltage-dependent Ca^{2+} channel activity in pulmonary artery by upregulating Cav1.2 and Cav3.2.

American journal of physiology. Lung Cellular and Molecular Physiology. **305**(2), pp.L154-164.

Wang, G.L. and Semenza, G.L. 1995. Purification and characterization of hypoxia-inducible factor 1. *The Journal of Biological Chemistry.* **270**(3), pp.1230-1237.

Wang, H.S., Brown, B.S., McKinnon, D. and Cohen, I.S. 2000. Molecular basis for differential sensitivity of KCNQ and I_{Ks} channels to the cognitive enhancer XE991. *Molecular pharmacology.* **57**(6), pp.1218-1223.

Wang, H.S., Pan, Z., Shi, W., Brown, B.S., Wymore, R.S., Cohen, I.S., Dixon, J.E. and McKinnon, D. 1998. KCNQ2 and KCNQ3 potassium channel subunits: molecular correlates of the M-channel. *Science.* **282**(5395), pp.1890-1893.

Wang, J., Juhaszova, M., Rubin, L.J. and Yuan, X.J. 1997. Hypoxia inhibits gene expression of voltage-gated K^+ channel alpha subunits in pulmonary artery smooth muscle cells. *Journal of Clinical Investigation.* **100**(9), pp.2347-2353.

Wang, V., Davis, D.A., Haque, M., Huang, L.E. and Yarchoan, R. 2005. Differential gene up-regulation by hypoxia-inducible factor-1α and hypoxia-inducible factor-2α in HEK293T cells. *Cancer research.* **65**(8), pp.3299-3306.

Wang, X.Y., Mo, D., Tian, W., Liu, X.X., Zhou, Y.G., Sun, Y., Feng, Y.D., Xiao, X., Hao, X.W., Zhang, H.N., Li, C., Cao, W. and Li, X.Q. 2019. Inhibition of RhoA/ROCK signaling pathway ameliorates hypoxic pulmonary hypertension via HIF-1α-dependent functional TRPC channels. *Toxicology and Applied Pharmacology.* **369**, pp.60-72.

Wei, W., Floten, H.S. and He, G.W. 2002. Interaction between vasodilators and vasopressin in internal mammary artery and clinical significance. *Annals of Thoracic Surgery.* **73**(2), pp.516-522.

Weir, E.K. and Olschewski, A. 2006. Role of ion channels in acute and chronic responses of the pulmonary vasculature to hypoxia. *Cardiovascular Research.* **71**(4), pp.630-641.

Wenger, R.H. 2002. Cellular adaptation to hypoxia: O_2-sensing protein hydroxylases, hypoxia-inducible transcription factors, and O_2-regulated gene expression. *FASEB Journal.* **16**(10), pp.1151-1162.

Westcott, E.B., Goodwin, E.L., Segal, S.S. and Jackson, W.F. 2012. Function and expression of ryanodine receptors and inositol 1,4,5-trisphosphate receptors in smooth muscle cells of murine feed arteries and arterioles. *The Journal of physiology.* **590**(8), pp.1849-1869.

Wiedmann, F., Schmidt, C., Lugenbiel, P., Staudacher, I., Rahm, A.K., Seyler, C., Schweizer, P.A., Katus, H.A. and Thomas, D. 2016. Therapeutic targeting of two-pore-domain potassium (K_{2P}) channels in the cardiovascular system. *Clinical science (London, England : 1979).* **130**(9), pp.643-650.

Wiesener, M.S., Jürgensen, J.S., Rosenberger, C., Scholze, C.K., Hörstrup, J.H., Warnecke, C., Mandriota, S., Bechmann, I., Frei, U.A., Pugh, C.W., Ratcliffe, P.J., Bachmann, S., Maxwell, P.H. and Eckardt, K.U. 2003. Widespread hypoxia-inducible expression of HIF-2α in distinct cell populations of different organs. *FASEB Journal.* **17**(2), pp.271-273.

Winegar, B.D., Kelly, R. and Lansman, J.B. 1991. Block of current through single calcium channels by Fe, Co, and Ni. Location of the transition metal binding site in the pore. *The Journal of General Physiology.* **97**(2), pp.351-367.

Woodsome, T.P., Eto, M., Everett, A., Brautigan, D.L. and Kitazawa, T. 2001. Expression of CPI-17 and myosin phosphatase correlates with Ca^{2+} sensitivity of protein kinase C-induced contraction in rabbit smooth muscle. *Journal of Physiology-London.* **535**(2), pp.553-564.

Wu, K.D., Bungard, D. and Lytton, J. 2001. Regulation of SERCA Ca^{2+} pump expression by cytoplasmic Ca^{2+} in vascular smooth muscle cells. *American Journal of Physiology. Cell Physiology.* **280**(4), pp.C843-851.

Wulff, H., Castle, N.A. and Pardo, L.A. 2009. Voltage-gated potassium channels as therapeutic targets. *Nature Reviews Drug Discovery.* **8**(12), pp.982-1001.

Wuttke, T.V., Seebohm, G., Bail, S., Maljevic, S. and Lerche, H. 2005. The new anticonvulsant retigabine favors voltage-dependent opening of the Kv7.2 (KCNQ2) channel by binding to its activation gate. *Molecular Pharmacology*. **67**(4), pp.1009-1017.

Xu, X., Ali, S., Li, Y., Yu, H., Zhang, M., Lu, J. and Xu, T. 2016. 2-Aminoethoxydiphenyl Borate Potentiates CRAC Current by Directly Dilating the Pore of Open Orai1. *Scientific Reports.* **6**(1), p29304.

Yadav, V.R., Song, T., Mei, L., Joseph, L., Zheng, Y.M. and Wang, Y.X. 2018. PLCγ1-PKCε-IP_3R1 signaling plays an important role in hypoxia-induced calcium response in pulmonary artery smooth muscle cells. *American journal of physiology. Lung Cellular and Molecular Physiology.* **314**(5), pp.L724-735.

Yang, C.M., Tsai, Y.J., Pan, S.L., Wu, W.B., Wang, C.C., Lee, Y.S., Lin, C.C., Huang, S.C.M. and Chiu, C.T. 1999. Pharmacological and functional characterization of bradykinin receptors in rat cultured vascular smooth muscle cells. *Cellular Signalling.* **11**(12), pp.853-862.

Yang, X.R., Lin, M.J., Yip, K.P., Jeyakumar, L.H., Fleischer, S., Leung, G.P. and Sham, J.S. 2005. Multiple ryanodine receptor subtypes and heterogeneous ryanodine receptor-gated Ca^{2+} stores in pulmonary arterial smooth muscle cells. *American journal of physiology. Lung Cellular and Molecular Physiology.* **289**(2), pp.L338-348.

Yeung, S.Y. and Greenwood, I.A. 2005. Electrophysiological and functional effects of the KCNQ channel blocker XE991 on murine portal vein smooth muscle cells. *British Journal of Pharmacology.* **146**(4), pp.585-595.

Yeung, S.Y., Pucovsky, V., Moffatt, J.D., Saldanha, L., Schwake, M., Ohya, S. and Greenwood, I.A. 2007. Molecular expression and pharmacological identification of a role for Kv7 channels in murine vascular reactivity. *British Journal of Pharmacology.* **151**(6), pp.758-770.

Yimin, H., Xiaoyu, L., Yuping, H., Weiyan, L. and Ning, L. 2013. The effect of vasopressin on the hemodynamics in CABG patients. *Journal of Cardiothoracic Surgery.* **8**, pp.49-49.

Yip, K.P. and Sham, J.S. 2011. Mechanisms of vasopressin-induced intracellular Ca^{2+} oscillations in rat inner medullary collecting duct. *American journal of physiology. Renal Physiology.* **300**(2), pp.F540-548.

Yoshii, T., Iwai, M., Li, Z., Chen, R., Ide, A., Fukunaga, S., Oshita, A., Mogi, M., Higaki, J. and Horiuchi, M. 2006. Regression of atherosclerosis by amlodipine via anti-inflammatory and anti-oxidative stress actions. *Hypertension Research.* **29**(6), pp.457-466.

Yuan, J.P., Kim, M.S., Zeng, W., Shin, D.M., Huang, G., Worley, P.F. and Muallem, S. 2009. TRPC channels as STIM1-regulated SOCs. *Channels (Austin).* **3**(4), pp.221-225.

Yuan, J.X. 2001. Oxygen-sensitive K^+ channel(s): where and what? *American Journal of Physiology-Lung Cellular and Molecular Physiology.* **281**(6), pp.L1345-L1349.

Yuan, Q., Bleiziffer, O., Boos, A.M., Sun, J.M., Brandl, A., Beier, J.P., Arkudas, A., Schmitz, M., Kneser, U. and Horch, R.E. 2014. PHDs inhibitor DMOG promotes the vascularization process in the AV loop by HIF-1α up-regulation and the preliminary discussion on its kinetics in rat. *BMC Biotechnology.* **14**(1), p112

Yuan, X.J. 1995. Voltage-gated K^+ currents regulate resting membrane potential and $[Ca^{2+}]_i$ in pulmonary arterial myocytes. *Circulation Research.* **77**(2), pp.370-378.

Zalk, R., Clarke, O.B., des Georges, A., Grassucci, R.A., Reiken, S., Mancia, F., Hendrickson, W.A., Frank, J. and Marks, A.R. 2015. Structure of a mammalian ryanodine receptor. *Nature.* **517**(7532), pp.44-49.

Zavaritskaya, O., Dudem, S., Ma, D., Rabab, K.E., Albrecht, S., Tsvetkov, D., Kassmann, M., Thornbury, K., Mladenov, M., Kammermeier, C., Sergeant, G., Mullins, N., Wouappi, O., Wurm, H., Kannt, A., Gollasch, M., Hollywood, M.A. and Schubert, R. 2020. Vasodilation of rat skeletal muscle arteries by the novel BK channel opener GoSlo is mediated by the simultaneous activation of BK and Kv 7 channels. *British Journal of Pharmacology.* **177**(5), pp.1164-1186.

Zhang, D.X. and Gutterman, D.D. 2019. Myocardin and Kv1 Channels. Arteriosclerosis, Thrombosis, and Vascular Biology. **39**(12), pp.2454-2456.

Zhang, H., Craciun, L.C., Mirshahi, T., Rohács, T., Lopes, C.M., Jin, T. and Logothetis, D.E. 2003. PIP_2 activates KCNQ channels, and its hydrolysis underlies receptor-mediated inhibition of M currents. *Neuron.* **37**(6), pp.963-975.

Zhang, J., Bal, M., Bierbower, S., Zaika, O. and Shapiro, M.S. 2011. AKAP79/150 signal complexes in G-protein modulation of neuronal ion channels. *The Journal of neuroscience : the official journal of the Society for Neuroscience.* **31**(19), p7199.

Zhang, J., Yang, G.M., Zhu, Y., Peng, X.Y., Liu, L.M. and Li, T. 2015. Bradykinin induces vascular contraction after hemorrhagic shock in rats. *Journal of Surgical Research.* **193**(1), pp.334-343.

Zhang, S.L., Yu, Y., Roos, J., Kozak, J.A., Deerinck, T.J., Ellisman, M.H., Stauderman, K.A. and Cahalan, M.D. 2005. STIM1 is a Ca^{2+} sensor that activates CRAC channels and migrates from the Ca^{2+} store to the plasma membrane. *Nature.* **437**(7060), pp.902-905.

Zhang, W. and Trebak, M. 2011. STIM1 and Orai1: Novel targets for vascular diseases? *Science China-Life Sciences.* **54**(8), pp.780-785.

Zhao, J., Du, F., Shen, G., Zheng, F. and Xu, B. 2015. The role of hypoxia-inducible factor-2 in digestive system cancers. *Cell Death & Disease.* **6**(1), pp.e1600-e1600.

Zholos, A. 2010. Pharmacology of transient receptor potential melastatin channels in the vasculature. *British journal of pharmacology*. **159**(8), pp.1559-1571.

Zhong, X.Z., Harhun, M.I., Olesen, S.P., Ohya, S., Moffatt, J.D., Cole, W.C. and Greenwood, I.A. 2010. Participation of KCNQ (Kv7) potassium channels in myogenic control of cerebral arterial diameter. *The Journal of physiology.* **588**(Pt 17), pp.3277-3293.

Zhou, N., Huang, S., Li, L., Huang, D., Yan, Y., Du, X. and Zhang, H. 2016. Suppression of Kv7/KCNQ potassium channel enhances neuronal differentiation of PC12 cells. *Neuroscience.* **333**, pp.356-367.